

Departamento de Física Teórica y del Cosmos
Universidad de Granada



Collider Implications of Heavy Fermions in Models with Extra Dimensions

Adrián Carmona Bermúdez

Ph.D. Advisors:
Francisco del Águila Giménez
José Santiago Pérez

– May 2012 –

Editor: Editorial de la Universidad de Granada
Autor: Adrián Carmona Bermúdez
D.L.: GR 203-2013
ISBN: 978-84-9028-286-1

Departamento de Física Teórica y del Cosmos
Universidad de Granada



Implicaciones en Colisionadores de Fermiones Pesados en Modelos con Dimensiones Extras

Adrián Carmona Bermúdez

Directores:
Francisco del Águila Giménez
José Santiago Pérez

– Mayo 2012–

D. Francisco del Águila Giménez, Catedrático de Universidad, y D. José Santiago Pérez, Profesor Titular de Universidad,

CERTIFICA: que la presente memoria, *Collider Implications of Heavy Fermions in Models with Extra Dimensions (Implicaciones en Colisionadores de Fermiones Pesados en Modelos con Dimensiones Extras)*, ha sido realizada por D. Adrián Carmona Bermúdez bajo su dirección en el Departamento de Física Teórica y del Cosmos, así como que éste ha disfrutado de estancias en el extranjero, durante un periodo superior a tres meses, tanto en el Departamento de Física Teórica de la Universidad de Oxford (Reino Unido) como en la división teórica de Fermilab (EEUU).

Granada, 23 de Mayo de 2012

Fdo: Francisco del Águila Giménez

José Santiago Pérez

Contents

Introduction	1
Introducción	5
1 The Standard Model and Experimental Constraints	9
1.1 The Standard Model of Particle Physics	9
1.2 Massive Neutrinos	12
1.2.1 Neutrino Oscillations	13
1.2.2 Experiments	15
1.3 The Standard Model as an Effective Theory	25
1.3.1 Precision Tests of the Standard Model	26
1.3.2 Constraints on New Physics	29
2 Models with Warped Extra Dimensions	35
2.1 Randall-Sundrum Models	36
2.1.1 Higgs Boson	37
2.1.2 Gauge Bosons	39
2.1.3 Fermions	43
2.2 Non-Custodial Models	48
2.2.1 Bulk Bosons	49
2.2.2 Bulk Fermions	50
2.2.3 Electroweak Constraints	53
2.2.4 Phenomenological Implications	61
2.3 Gauge-Higgs Unification Models	63
2.4 Higgsless Models	67
3 Collider Implications of Top Compositeness	71
3.1 The $t\bar{t}$ Forward-Backward Asymmetry	72
3.2 A Realistic Higgsless Model	74
3.3 Stealth Gluons	80
3.4 Third Generation Quark Excitations	83
3.4.1 $W^+W^-b\bar{b}$ Channel	83
3.4.2 $Zt\bar{t}$ Channel	87
3.4.3 $Zb\bar{b}$ Channel	88
3.5 Light Quark Excitations	90
3.5.1 $Zq\bar{q}$ Channel	90
3.5.2 $Wq\bar{q}'$ Channel	90
3.6 Higgs Decays	91
3.6.1 Low Energy Phase	93
3.6.2 High Energy Phase	94
3.6.3 Results	95

4 A Holographic Higgs Model of Lepton Masses and Mixings	97
4.1 The Model	98
4.2 The Leptonic Spectrum	101
4.2.1 Lepton Spectrum in the Zero Mode Approximation	102
4.2.2 Inclusion of Massive Kaluza-Klein Modes	105
4.2.3 Exact Higgs Treatment	106
4.3 Higher Order Effects	107
4.4 Electroweak and Flavor Constraints	110
4.5 Tau Custodians at the LHC	114
4.6 Analysis	116
4.7 Updated Results	119
Conclusions	121
Conclusiones	123
Appendices	125
A Group Theory Summary	125
A.1 A_4 Representations	125
A.2 $SO(5)$ Generators in the Fundamental Representation	126
List of figures	127
List of tables	133
Bibliography	137

Introduction

Since Glashow, Weinberg and Salam laid the cornerstone of the Standard Model of particle physics in the late sixties, its experimental confirmation has reached an impressive level. With the exception of the sector responsible for the electroweak symmetry breaking, whose study motivated the construction of the Large Hadron Collider at CERN, all the particles and force carriers predicted by the model have already been discovered. In particular, the electroweak precision data measured at different experiments have successfully tested the model to the quantum level. Nevertheless, there are still some important questions in particle physics which can not be properly explained within the Standard Model and have prompted a large number of its extensions. For instance, the observed pattern of fermion masses and mixing angles, the huge hierarchy existing between the characteristic scales of the electroweak and the gravitational interactions, the light Higgs mass despite its quadratic sensitivity to any other scale in the model (the *hierarchy problem*) or the tiny neutrino masses needed to explain the observation of neutrino oscillations are some relevant features which are difficult to address in the framework of the Standard Model. All these facts suggest us to consider the Standard Model as an effective theory of nature which needs to be completed with some more fundamental theory at energies above some cut-off scale Λ . Trying to discover some of the missing pieces in this puzzle, the Large Hadron Collider is for the very first time exploring a completely new region of energy. With its projected 14 TeV of center of mass energy and its current run at 8 TeV, the CERN collider is trying to unravel the precise mechanism of electroweak symmetry breaking in the hunting for the Higgs boson. Moreover, due to the high energy of the collisions taking place and the large accelerator instant luminosity, the Large Hadron Collider is also an ideal top factory.

In an attempt to solve the hierarchy problem appearing in the standard realization of the electroweak symmetry breaking, different models extend the Standard Model with new fermion and gauge boson resonances. As fermions with larger Yukawa couplings to the Higgs field feel more than any other one the electroweak symmetry breaking, the study of the third generation (both in the lepton and quark sectors) is the best way to determine the precise mechanism working in the Higgs sector and/or any possible new physics fixing the hierarchy problem. Besides, as the implications of the third generation in the electroweak symmetry breaking are best revealed in a full-fledged theory of flavor, we can expect to obtain also some information on the observed spectrum of fermion masses and mixing angles (the *flavor puzzle*). For these reasons, we will consider in this Thesis the framework of models with warped extra dimensions (and their four-dimensional strongly coupled duals), which are a very compelling extension of the Standard Model addressing at the same time the hierarchy problem and the flavor puzzle, through the collider implications of third generation fermions and their Kaluza-Klein excitations.

In Chapter 1 we will briefly introduce the Standard Model of the strong and electroweak interactions. This will allow us to fix some of the notation used through this Thesis. Then, we will also discuss neutrino oscillations and review the main experiments leading to the current bounds on the neutrino spectrum and the different lepton mixing angles.

We will present the general framework of models with a warped extra dimension in Chapter 2. In these models, the fundamental scale of the theory (usually of the order of the Planck mass) is red-shifted by the warp factor to a few TeV on the infrared brane, where the Higgs boson is localized. This allows us to explain the smallness of the electroweak scale in relation to the Plank

mass in terms of the curvature and size of the extra dimension. Moreover, promoting fermions (and gauge bosons) to bulk fields and localizing them differently along the extra dimension, we obtain naturally hierarchical masses and mixing angles, similar to the ones observed in the quark sector. Starting from the five-dimensional action we will obtain the general equations of motion and boundary conditions fulfilled by the Kaluza-Klein expansions of these bulk fermions and gauge bosons. We will consider the cases of a boundary and a bulk Higgs. Then, we will study a recently suggested generalization of the AdS₅ background, where conformality is strongly deformed near the infrared brane. For the first time, we analyze the effect of bulk fermions on electroweak precision observables in this framework, once the top and bottom masses are reproduced [1]. The rest of the chapter is devoted to review some other relevant models with warped extra dimensions which will be used in this Thesis. In particular, we will present the general setup of gauge-Higgs unification models, where the Higgs boson arises from the scalar component of a five-dimensional gauge field, and Higgsless models, where the electroweak symmetry is broken by boundary conditions.

As fermion masses in models with warped extra dimensions are given by the overlaps with the infrared localized Higgs sector, third generation quarks (and specially the top) have sizable couplings to the Kaluza-Klein excitations, which are also localized towards the same brane. Couplings of gauge boson resonances to light quarks are much smaller and can be naturally axial-vector in the allowed region of the parameter space. Besides, in the case of Higgsless models, the first resonances have to be lighter than ~ 1 TeV to unitarize the elastic scattering of longitudinally polarized gauge bosons. Therefore, these models can provide a light axigluon with large couplings to the top quark and its Kaluza-Klein vector-like excitations. We consider this scenario in Chapter 3, focusing on top related searches. Top quark properties are rather well known experimentally, although there are still some of them which are poorly measured (as the V_{tb} matrix element or the $Zt\bar{t}$ coupling). Its mass is known with an accuracy of less than 1% and is in quite good agreement with electroweak precision data through radiative corrections. The Tevatron and the Large Hadron Collider have observed electroweak single top quark production, from where V_{tb} is extracted (although still with a limited precision). Also, the $t\bar{t}$ production cross section and its invariant mass distribution have also been measured at the two accelerators. The results obtained in both cases are consistent with the Standard Model predictions. However, CDF and DØ experiments at Fermilab have found a $(2-3)\sigma$ discrepancy with the Standard Model expectation for the $t\bar{t}$ forward-backward asymmetry. The subsequent CDF claim that this deviation with the Standard Model prediction increased for invariant masses above 450 GeV, triggered a large number of Standard Model extensions trying to accommodate the observed value. The large value of the asymmetry as well as the apparent absence of new physics footprints on the rest of top measurements suggest that a light massive gluon like the one previously mentioned, with small-close to axial couplings to the light quarks and sizable couplings to the right-handed top, could fit all the pieces together. We will show in this chapter that this is indeed the case, provided that new heavy vector-like quarks are present (thus making the resonance a *stealth gluon*) [2-4]. We will study, in a benchmark model, the phenomenology of these new channels when fermion excitations decay to a electroweak gauge boson and a Standard Model quark. Finally, we will consider also decays into a Higgs boson and a standard quark in the framework of minimal composite Higgs models [5, 6].

Unlike the quark case, lepton mixing angles are not hierarchical but they can also be accommodated in the framework of models with warped extra dimensions. One interesting possibility is to use a discrete symmetry on the lepton sector accounting for the mismatch between the charged lepton and neutrino mass matrices responsible for the observed non-hierarchical mixing angles. The discrete A_4 symmetry is one of the most appealing examples. Four dimensional models with this global symmetry can predict a tri-bimaximal mixing pattern at leading order. In Chapter 4 we will implement it for the first time in gauge-Higgs unification models [7]. In principle, and contrary to the top quark, the τ lepton should not be so sensitive to the new physics due to its smaller mass. Nevertheless, we will show that due to the presence of the A_4 symmetry there is an extra suppression on the lepton Yukawa couplings making the right-handed τ more composite

than naively expected from its mass. One interesting consequence in these models is the presence of new light vector-like doublets, with masses as low as few hundreds of GeV, large couplings to the τ and a very characteristic collider phenomenology. We will perform a detailed analysis of the collider phenomenology of these light resonances and compute the Large Hadron Collider reach for them [8].

The main results of this Ph. D. Thesis are summarized in the Conclusions. Finally, in an appendix we briefly review the relevant group theory properties needed for the analysis of the model of lepton masses and mixings discussed in Chapter 4.

Although not directly connected with the phenomenological study presented in this Thesis, and therefore not included here, I have also computed the dimension 6 effective Lagrangian arising from the tree level integration of an arbitrary number of bulk fermions in models with warped extra dimensions for an arbitrary background [9]. What can be used in definite extra-dimensional models, as those studied here, for a more accurate prediction of their indirect phenomenological implications. I have also collaborated in the elaboration of the proceedings of Ref. [10].

Introducción

Desde que Glashow, Weinberg y Salam establecieran los pilares del Modelo Estándar de física de partículas a finales de los años sesenta, su confirmación experimental ha alcanzado un nivel impresionante. Con la excepción del sector responsable de la ruptura de la simetría electrodébil, cuyo estudio ha motivado la construcción del Gran Colisionador de Hadrones en el CERN, todas las partículas de materia y mediadoras de fuerza predichas por el modelo han sido ya descubiertas. En particular, los datos de precisión electrodébiles medidos en diferentes experimentos han confirmado con éxito el modelo a nivel cuántico. Sin embargo, todavía hay algunas cuestiones importantes en la física de partículas que no pueden ser explicadas adecuadamente en el Modelo Estándar y que han conducido a un número importante de sus extensiones. Por ejemplo, el patrón observado de masas de fermiones y ángulos de mezcla, la enorme jerarquía existente entre las escalas características de las interacciones electrodébil y gravitatoria, la ligera masa del Higgs a pesar de su sensibilidad cuadrática a cualquier otra escala presente en el modelo (el *problema de las jerarquías*) o las diminutas masas de neutrinos necesarias para explicar la observación de oscilaciones de neutrinos son algunos de los aspectos relevantes que difícilmente pueden abordarse en el marco del Modelo Estándar. Todos estos hechos sugieren que consideremos al Modelo Estándar como una teoría efectiva de la naturaleza que debe ser completada con alguna teoría más fundamental a energías superiores a cierta escala Λ . Tratando de descubrir algunas de las piezas que faltan en este puzzle, el Gran Colisionador de Hadrones está explorando por vez primera un rango de energías completamente nuevo. Con una energía de centro de masas proyectada de 14 TeV y una actual de 8 TeV, el colisionador del CERN está tratando de desentrañar el mecanismo preciso de ruptura espontánea de simetría en la caza del bosón de Higgs. Por otro lado, debido a las altas energías de las colisiones que tienen lugar y la gran luminosidad instantánea del acelerador, el Gran Colisionador de Hadrones es también una fábrica ideal de quarks *top*.

En un intento por resolver el problema de la jerarquías que aparece en la realización estándar de la ruptura de la simetría electrodébil, diferentes modelos extienden el Modelo Estándar con nuevas resonancias de fermiones y bosones de *gauge*. Como los fermiones con mayor acoplamiento de Yukawa al bosón de Higgs sienten más que cualquier otro la ruptura de la simetría electrodébil, el estudio de la tercera generación (tanto en el sector leptónico como en el de quarks) es la mejor manera de determinar el mecanismo exacto operando en el sector de Higgs y/o cualquier posible nueva física resolviendo el problema de las jerarquías. Además, como las implicaciones de la tercera generación en la ruptura de la simetría electrodébil se muestran mejor en una teoría completa de sabor, podemos esperar obtener también alguna información sobre el espectro observado de masas de fermiones y ángulos de mezcla (el *puzzle de sabor*). Por estas razones, en esta Tesis vamos a considerar el marco general de los modelos con dimensiones adicionales curvas (así como sus modelos duales cuatro-dimensionales fuertemente acoplados), que son una extensión muy convincente del Modelo Estándar arreglando al mismo tiempo el problema de la jerarquías y el puzzle de sabor, a través de las implicaciones en colisionadores de la tercera generación y sus excitaciones de Kaluza-Klein.

En el Capítulo 1 introduciremos brevemente el Modelo Estándar de las interacciones fuerte y electrodébil. Esto nos permitirá establecer parte de la notación utilizada a lo largo de esta Tesis. Después, consideraremos también las oscilaciones de neutrinos y revisaremos algunos de los experimentos principales que han conducido a los límites actuales para las masas de los neutrinos

y los diferente ángulos de mezcla leptónicos.

Presentaremos el marco general de los modelos con una dimensión adicional curva en el Capítulo 2. En estos modelos, la escala fundamental de la teoría (que suele ser del orden de la masa de Planck) es reducida exponencialmente por el factor de curvatura de la dimensión extra a unos pocos TeV en la membrana infrarroja, donde se encuentra localizado el bosón de Higgs. Esto nos permite explicar la pequeñez de la escala electrodébil en relación a la masa Plank en términos de la curvatura y el tamaño de la dimensión extra. Por otra parte, dejando que fermiones (y bosones de *gauge*) se propaguen por la dimension adicional y localizándolos en distintos lugares de ella, se obtienen de forma natural masas y ángulos de mezcla jerárquicos, como los observados en el sector de quarks. A partir de la acción cinco-dimensional obtendremos las ecuaciones generales de movimiento y las condiciones de contorno satisfechas por las expansiones de Kaluza-Klein de fermiones y bosones de *gauge*. Consideraremos los casos de un Higgs cinco-dimensional y localizado en la membrana. A continuación, estudiaremos una generalización de estos modelos sugerida recientemente, donde la métrica AdS_5 es deformada cerca de la membrana infrarroja. Por primera vez, analizamos en este marco el efecto de los fermiones cinco-dimensionales en los observables de precisión electrodébiles, una vez reproducidas las masas de los quarks *top* y *bottom* [1]. El resto del capítulo está dedicado a revisar algunos modelos relevantes con dimensiones adicionales curvas que se utilizarán en esta Tesis. En particular, presentaremos la estructura general de los modelos de unificación *gauge*-Higgs, donde el bosón de Higgs se identifica con la componente escalar de un campo de *gauge* cinco-dimensional, y los modelos sin Higgs, donde la ruptura de la simetría electrodébil se realiza mediante condiciones de contorno.

Como las masas de los fermiones en modelos con dimensiones adicionales curvas vienen dadas por el solapamiento con el sector de Higgs, localizado en el infrarrojo, los quarks de la tercera generación (y en especial el *top*) tienen acoplamientos importantes a las excitaciones de Kaluza-Klein, que también se encuentran localizadas en la misma membrana. Los acoplamientos de las resonancias de los bosones de *gauge* a los quarks ligeros son mucho más pequeños y pueden ser de forma natural axiales en la región permitida del espacio de parámetros. Además, en el caso de los modelos sin Higgs, las primeras resonancias deben ser más ligeras que ~ 1 TeV para unitarizar la dispersión elástica de bosones de *gauge* polarizados longitudinalmente. Por lo tanto, estos modelos pueden proporcionar un gluon axial ligero con grandes acoplamientos con el quark *top* y sus excitaciones de Kaluza-Klein vectoriales. Consideramos este escenario en el Capítulo 3, centrándonos en búsquedas relacionadas con el *top*. Los propiedades del quark *top* son bastante bien conocidas desde el punto de vista experimental, aunque todavía hay algunas que no están bien medidas (como el elemento de matriz V_{tb} o el acoplamiento $Zt\bar{t}$). Su masa es conocida con una precisión de mejor que el 1% y concuerda bastante bien con los datos de precisión electrodébil a través de las correcciones radiativas. El Tevatron y el Gran Colisionador de Hadrones han observado producción sencilla electrodébil de quarks *top*, de donde se extrae V_{tb} (aunque todavía con una precisión limitada). Además, la sección eficaz de producción de $t\bar{t}$ y su distribución de masa invariante también se han medido en los dos aceleradores. Los resultados obtenidos en ambos casos son consistentes con las predicciones del Modelo Estándar. Sin embargo, los experimentos CDF y DØ en Fermilab han encontrado una discrepancia de $(2 - 3)\sigma$ con el resultado esperado por parte del Modelo Estándar para la asimetría angular de $t\bar{t}$. La posterior afirmación de CDF de que la desviación con la predicción estándar en dicha asimetría crecía para masas invariantes superiores a 450 GeV, provocó un gran número de extensiones del Modelo Estándar intentando reproducir el valor observado. El gran tamaño de la asimetría, así como la aparente ausencia de huella de nueva física en el resto de medidas, sugieren que un gluón masivo ligero como el mencionado anteriormente, con acoplamientos pequeños casi axiales a los quarks ligeros y grandes a la componente a derechas del quark *top*, podría hacer encajar todas las piezas. Mostraremos en este capítulo que esto es así, a condición de que nuevos quarks vectoriales pesados estén presentes (haciendo de la resonancia un *gluon sigiloso*) [2-4]. Estudiaremos, en un modelo de referencia, la fenomenología de estos nuevos canales, cuando las excitaciones fermiónicas se desintegran en un bosón de *gauge* electrodébil y un

quark del Modelo Estándar. Por último, consideraremos también desintegraciones en un bosón de Higgs y un quark estándar en el marco de modelos minimales de Higgs compuesto [5, 6].

A diferencia del caso de quarks, los ángulos de mezcla leptónicos no son jerárquicos, aunque también pueden ser acomodados en el marco de los modelos con dimensiones adicionales curvas. Una posibilidad interesante es utilizar una simetría discreta en el sector leptónico que de cuenta de la falta de alineamiento existente entre la matriz de masa de los leptones cargados y la de los neutrinos, responsable de los ángulos de mezcla no jerárquicos observados. La simetría discreta A_4 es uno de los ejemplos más atractivos. Modelos cuatro-dimensionales con esta simetría global pueden predecir un patrón de mezcla de tri-bimaximal a primer orden. En el Capítulo 4 lo implementaremos por vez primera en el caso de modelos de unificación *gauge*-Higgs [7]. En principio, y a diferencia del quark *top*, el leptón τ no debería ser tan sensible a la nueva física debido a su menor masa. Sin embargo, mostraremos que debido a la presencia de la simetría A_4 existe una supresión adicional en los acoplamientos de Yukawa leptónicos que hacen al τ a derechas más compuesto de lo que ingenuamente se esperaba de su masa. Una consecuencia interesante en estos modelos es la presencia de nuevos dobletes vectoriales, con masas de unos cientos de GeV, grandes acoplamientos al leptón τ y una fenomenología en colisionadores de estas resonancias ligeras y calcularemos el alcance del Gran Colisionador de Hadrones para encontrarlas [8].

Los principales resultados de esta Tesis Doctoral se resumen en las conclusiones. Finalmente, revisaremos brevemente en un apéndice la teoría de grupos relevante necesaria para el análisis del modelo de masas y mezclas de leptones analizado en el Capítulo 4.

A pesar de no estar directamente relacionado con el estudio fenomenológico presentado en esta Tesis, y por lo tanto no incluido en la misma, también he calculado el Lagrangiano efectivo de dimensión 6 obtenido tras la integración a nivel árbol de un número arbitrario de fermiones cinco-dimensionales, en modelos con dimensiones adicionales curvas para un fondo arbitrario [9]. Lo que se puede utilizar en determinados modelos extra-dimensionales, como los aquí estudiados, para una predicción más precisa de sus implicaciones fenomenológicas indirectas. También colaboré en la elaboración de las actas de la Ref. [10].

1

The Standard Model and Experimental Constraints

1.1 The Standard Model of Particle Physics

The Standard Model (SM) of particle physics [12–14] is a renormalizable non-abelian gauge theory based on the local symmetry group $SU(3)_C \otimes SU(2)_L \otimes U(1)_Y$. The exchange of gauge bosons transforming in the adjoint representation of the strong ($\{G_\mu^a, a = 1, 2, \dots, 8\}$), weak ($\{W_\mu^I, I = 1, 2, 3\}$) and hypercharge (B_μ) groups describe the different interactions included in the SM. Below the electroweak (EW) scale $v \sim 246$ GeV this gauge group is spontaneously broken to $SU(3)_C \otimes U(1)_Q$ by the *vacuum expectation value* (vev) of a complex scalar field, the Higgs field H [15–18], with gauge quantum numbers $(SU(3), SU(2))_{U(1)} = (\mathbf{1}, \mathbf{2})_{1/2}$. The fermion sector of the theory is chiral with respect to the EW gauge group $SU(2)_L \otimes U(1)_Y$ with left-handed (LH) irreducible representation (irrep) of the Lorentz group transforming as doublets of $SU(2)_L$ and right-handed (RH) irreps as $SU(2)_L$ singlets. Moreover, the matter content of the theory is organized in a three-fold generation (or family) structure with identical gauge quantum numbers. We show in Table 1.1 the field content and gauge quantum numbers of one of these fermion generations.

$q_L = \begin{pmatrix} u_L \\ d_L \end{pmatrix}$	u_R	d_R	$l_L = \begin{pmatrix} \nu_L \\ e_L \end{pmatrix}$	e_R
$(\mathbf{3}, \mathbf{2})_{1/6}$	$(\mathbf{3}, \mathbf{1})_{2/3}$	$(\mathbf{3}, \mathbf{1})_{-1/3}$	$(\mathbf{1}, \mathbf{2})_{-1/2}$	$(\mathbf{1}, \mathbf{1})_{-1}$

Table 1.1: Gauge quantum numbers and chirality of one generation of SM fermions.

The SM Lagrangian is the following

$$\begin{aligned}
\mathcal{L}_{\text{SM}} &= -\frac{1}{4} \{G_{\mu\nu}^a G_a^{\mu\nu} + W_{\mu\nu}^I W_I^{\mu\nu} + B_{\mu\nu} B^{\mu\nu}\} \\
&+ \bar{q}_i i \not{D} q_i + \bar{u}_i i \not{D} u_i + \bar{d}_i i \not{D} d_i + \bar{l}_i i \not{D} l_i + \bar{e}_i i \not{D} e_i \\
&+ (D_\mu H)^\dagger (D^\mu H) - \lambda (H^\dagger H - v^2/2)^2 \\
&- \left[\lambda_{ij}^u \bar{q}_i u_j \tilde{H} + \lambda_{ij}^d \bar{q}_i d_j H + \lambda_{ij}^e \bar{l}_i e_j H + \text{h.c.} \right], \tag{1.1}
\end{aligned}$$

where, from now on, repeated indices imply summation unless otherwise stated, a and I are gauge indices and the Latin subscripts $i, j = 1, 2, 3$ are used to denote different families. The covariant derivative reads

$$D_\mu = \partial_\mu - ig_s \frac{\lambda_a}{2} G_\mu^a - ig \frac{\sigma_I}{2} W_\mu^I - ig' Y B_\mu, \tag{1.2}$$

where g_s, g and g' are the $SU(3)_C, SU(2)_L$ and $U(1)_Y$ gauge constants, respectively, while λ_a (σ_I) are the Gell-Mann (Pauli) matrices. We have also introduced the hypercharge $-1/2$ scalar doublet $\tilde{H} = i\sigma_2 H^*$. The field strength tensors of the different gauge groups are

$$G_{\mu\nu}^a = \partial_\mu G_\nu^a - \partial_\nu G_\mu^a - g_s f_{bc}^a G_\mu^b G_\nu^c, \tag{1.3}$$

$$W_{\mu\nu}^I = \partial_\mu W_\nu^I - \partial_\nu W_\mu^I - g \epsilon_{JK}^I W_\mu^J W_\nu^K, \tag{1.4}$$

$$B_{\mu\nu} = \partial_\mu B_\nu - \partial_\nu B_\mu, \tag{1.5}$$

where f_{bc}^a and ϵ_{JK}^I are the $SU(3)_C$ and $SU(2)_L$ structure constants, respectively,

$$\left[\frac{\lambda_b}{2}, \frac{\lambda_c}{2} \right] = i f_{bc}^a \frac{\lambda_a}{2}, \quad \left[\frac{\sigma_J}{2}, \frac{\sigma_K}{2} \right] = i \epsilon_{JK}^I \frac{\sigma_I}{2}. \tag{1.6}$$

As mentioned before, the Higgs doublet H is responsible for the spontaneous symmetry breaking (SSB) of the theory below the EW scale

$$SU(2)_L \otimes U(1)_Y \xrightarrow{\text{SSB}} U(1)_Q, \tag{1.7}$$

where $Q = T_3 + Y = \sigma_3/2 + Y$ is the electric charge generator. It can be expanded around its vev

$$\langle H \rangle = \frac{1}{\sqrt{2}} \begin{pmatrix} 0 \\ v \end{pmatrix}, \tag{1.8}$$

in the following way

$$H(x) = e^{i\sigma \cdot \theta(x)/v} \frac{1}{\sqrt{2}} \begin{pmatrix} 0 \\ v + h(x) \end{pmatrix}, \tag{1.9}$$

where $\theta^i(x)$, $i = 1, 2, 3$ are the massless would-be Nambu-Goldstone bosons (NGB) corresponding to each broken generator [19, 20] and $h(x)$ is the physical Higgs boson. The latter is the only physical degree of freedom added to the theory as it is evident in the unitary gauge, in which the NGB $\theta^i(x)$ are gauged away and become the longitudinal components of the massive gauge bosons W_μ^\pm and Z_μ ,

$$H(x) \xrightarrow{\text{Unitary Gauge}} e^{-i\sigma \cdot \theta(x)/v} H(x) = \frac{1}{\sqrt{2}} \begin{pmatrix} 0 \\ v + h(x) \end{pmatrix}. \tag{1.10}$$

The scalar kinetic term give rise to masses for all the EW gauge bosons except the combination coupled to the electric charge, the photon A_μ ,

$$(D_\mu H)^\dagger (D^\mu H) = M_W^2 W_\mu^+ W^{-\mu} + \frac{1}{2} M_Z^2 Z_\mu Z^\mu + \dots \tag{1.11}$$

In the above expression we have defined

$$W_\mu^\pm = \frac{1}{\sqrt{2}} (W_\mu^1 \mp iW_\mu^2), \quad (1.12)$$

and

$$Z_\mu = -\sin\theta_W B_\mu + \cos\theta_W W_\mu^3, \quad (1.13)$$

$$A_\mu = \cos\theta_W B_\mu + \sin\theta_W W_\mu^3. \quad (1.14)$$

The mixing between the different neutral gauge bosons is given by the Weinberg angle θ_W , defined by $\tan\theta_W = g'/g$, while the different masses for the EW gauge bosons are

$$M_W = \frac{v}{2}g, \quad (1.15)$$

$$M_Z = \frac{v}{2}\sqrt{g^2 + g'^2} = \frac{M_W}{\cos\theta_W}, \quad (1.16)$$

$$M_A = 0. \quad (1.17)$$

The scalar vev also gives masses to the fermions through the Yukawa couplings

$$-\mathcal{L}_{\text{mass}} = \mathcal{M}_{ij}^u \bar{u}_{iL} u_{jR} + \mathcal{M}_{ij}^d \bar{d}_{iL} d_{jR} + \mathcal{M}_{ij}^e \bar{e}_{iL} e_{jR} + \text{h.c.}, \quad (1.18)$$

where the mass matrices are given by $\mathcal{M}^{u,d,e} = \frac{v}{\sqrt{2}} \lambda_{ij}^{u,d,e}$. In order to go to the physical basis we make the following redefinitions,

$$u_{iL} \rightarrow (\mathcal{U}_L^u)_{ij} u_{jL}, \quad u_{iR} \rightarrow (\mathcal{U}_R^u)_{ij} u_{jR}, \quad (1.19)$$

$$d_{iL} \rightarrow (\mathcal{U}_L^d)_{ij} d_{jL}, \quad d_{iR} \rightarrow (\mathcal{U}_R^d)_{ij} d_{jR}, \quad (1.20)$$

$$e_{iL} \rightarrow (\mathcal{U}_L^e)_{ij} e_{jL}, \quad e_{iR} \rightarrow (\mathcal{U}_R^e)_{ij} e_{jR}, \quad (1.21)$$

where $\mathcal{U}_L^{u,d,e}$ and $\mathcal{U}_R^{u,d,e}$ are unitary matrices satisfying

$$(\mathcal{U}_L^u)^\dagger \mathcal{M}^u \mathcal{U}_R^u = \text{diag}(m_u, m_c, m_t), \quad (1.22)$$

$$(\mathcal{U}_L^d)^\dagger \mathcal{M}^d \mathcal{U}_R^d = \text{diag}(m_d, m_s, m_b), \quad (1.23)$$

$$(\mathcal{U}_L^e)^\dagger \mathcal{M}^e \mathcal{U}_R^e = \text{diag}(m_e, m_\mu, m_\tau), \quad (1.24)$$

with all masses real and positive. These rotations do not introduce any mixing in the neutral sector due to the Glashow-Iliopoulos-Maiani (GIM) mechanism [21], since the neutral gauge couplings are universal and they just involve fermions with opposite quantum numbers. Nevertheless, this mechanism is not present in the charged sector, where the gauge couplings link different T_L^3 fermion eigenstates, and the above rotations give rise to mixing terms between different quark families

$$\mathcal{L}^W = \frac{g}{\sqrt{2}} \{ W_\mu^+ [\bar{u}_{iL} \mathbf{V}_{ij} d_{jL} + \bar{\nu}_{iL} e_{jL}] + \text{h.c.} \}, \quad (1.25)$$

parametrized by the Cabbibo-Kobayashi-Maskawa mixing matrix (CKM) $\mathbf{V} = (\mathcal{U}_L^u)^\dagger \mathcal{U}_L^d$ [22, 23]. In the lepton sector, there is no such mixing between families because, since there are no RH neutrinos, we have reabsorbed the matrix \mathcal{U}_L^e that would have appeared from the rotation of e_{iL} by a redefinition of ν_{iL}

$$\nu_{iL} \rightarrow (\mathcal{U}_L^e)_{ij} \nu_{jL}. \quad (1.26)$$

The fermion couplings to the Z_μ gauge boson are given by

$$\mathcal{L}^Z = \frac{g}{2\cos\theta_W} (\bar{u}_{iL} \gamma^\mu u_{iL} + \bar{\nu}_{iL} \gamma^\mu \nu_{iL} - \bar{d}_{iL} \gamma^\mu d_{iL} - \bar{e}_{iL} \gamma^\mu e_{iL} - 2\sin^2\theta_W J_{em}^\mu) Z_\mu, \quad (1.27)$$

while the couplings to the photon A_μ read

$$\mathcal{L}^A = eJ_{em}^\mu A_\mu, \quad (1.28)$$

with $e = gg'/\sqrt{g^2 + g'^2}$ the electric charge and J_{em}^μ the electromagnetic current

$$J_{em}^\mu = \sum_\psi Q_\psi \bar{\psi} \gamma^\mu \psi, \quad (1.29)$$

where ψ runs over all the SM fermions.

Finally, we should mention that, leaving aside the Yukawa part of the Lagrangian, there is a global $U(3)^5$ symmetry corresponding to the different family rotations that leave the Lagrangian invariant. Once we consider the Yukawa couplings that give rise to the fermion masses this is not longer true. Nevertheless, not all the $U(3)^5$ is broken by these couplings and there is an accidental global symmetry left

$$G_{\text{SM}}^{\text{global}} = U(1)_B \otimes U(1)_{L_e} \otimes U(1)_{L_\mu} \otimes U(1)_{L_\tau}. \quad (1.30)$$

In the above expression, $U(1)_B$ is the baryon number symmetry, under which the (anti)quarks have charge $B = (-)1/3$ and the leptons are singlets, and $U(1)_{L_e, L_\mu, L_\tau}$ are the different lepton flavor symmetries, with $L_i = (-)1$ for (anti)leptons of the i -th family and zero otherwise. Due to quantum anomalies, the only symmetry that remains exact at the quantum level is the combination of baryon and lepton numbers $U(1)_{B-L}$, with $L = L_e + L_\mu + L_\tau$ the total lepton number.

1.2 Massive Neutrinos

Neutrino oscillation experiments over the last decades have proven that neutrinos are massive and non degenerate. Neutrino masses could arise in principle from radiative corrections. However, in the SM, this is not possible because the only mass term compatible with the gauge group that can be constructed using SM fields is $\bar{l}l^c$, which violates the total lepton number by two units. As mentioned before, $U(1)_{B-L}$ is an exact symmetry of the theory even at the quantum level so operators violating this symmetry can not appear through radiative corrections.

Therefore, in order to consider massive neutrinos we should go beyond the SM (BSM). That means either to enlarge the local symmetry group $SU(3)_C \otimes SU(2)_L \otimes U(1)_Y$, to extend the matter content of the theory or to give up renormalizability. Throughout this thesis we will develop all of these possibilities. We will extend the SM gauge group adding new matter content with an arbitrary number of RH neutrinos ν_{iR} , singlets under the enlarged gauge group, and we will consider our theory as an effective field theory (EFT) at low energies with non-renormalizable mass terms violating lepton number.

In any case, the existence of non-degenerate massive neutrinos will imply that the charged currents (CC), which are diagonal in the lepton sector of the SM, should include flavor changing terms as the matrix from the rotation of e_{iL} can no longer be absorbed through a convenient redefinition of the LH neutrinos. Thereby, we obtain

$$\mathcal{L}^W \supset \frac{g}{\sqrt{2}} (\bar{e}_{iL} \gamma^\mu \mathbf{U}_{ij} \nu_{jL} W_\mu^- + \text{h.c.}), \quad (1.31)$$

with $\mathbf{U} = (\mathcal{U}_L^e)^\dagger \mathcal{U}_L^\nu$ the Pontecorvo-Nakagawa-Maki-Sakata (PMNS) matrix [25–27] and \mathcal{U}_L^ν the rotation for the LH neutrino ν_{iL} that diagonalizes the neutrino mass matrix,

$$\nu_{iL} \rightarrow (\mathcal{U}_L^\nu)_{ij} \nu_{jL}. \quad (1.32)$$

The PMNS matrix can be parametrized conveniently writing

$$\begin{pmatrix} 1 & 0 & 0 \\ 0 & c_{23} & s_{23} \\ 0 & -s_{23} & c_{23} \end{pmatrix} \cdot \begin{pmatrix} c_{13} & 0 & s_{13}e^{-i\delta_{CP}} \\ 0 & 1 & 0 \\ -s_{13}e^{i\delta_{CP}} & 0 & c_{13} \end{pmatrix} \cdot \begin{pmatrix} c_{12} & s_{12} & 0 \\ -s_{12} & c_{12} & 0 \\ 0 & 0 & 1 \end{pmatrix} \cdot \begin{pmatrix} e^{i\eta_1} & 0 & 0 \\ 0 & e^{i\eta_2} & 0 \\ 0 & 0 & 1 \end{pmatrix},$$

where $c_{ij} = \cos \theta_{ij}$ and $s_{ij} = \sin \theta_{ij}$. Without loss of generality, we can take θ_{ij} to lie in the first quadrant, $\theta_{ij} \in [0, \pi/2]$, and the phases $\delta_{CP}, \eta_i \in [0, 2\pi]$. In the case of three Dirac neutrinos, the Majorana phases η_1 y η_2 can be absorbed in the RH neutrino definition ν_{iR} . In this case, the PMNS reads

$$\mathbf{U} = \begin{pmatrix} c_{12}c_{13} & s_{12}c_{13} & s_{13}e^{-i\delta_{CP}} \\ -s_{12}c_{23} - c_{12}s_{13}s_{23}e^{i\delta_{CP}} & c_{12}c_{23} - s_{12}s_{13}s_{23}e^{i\delta_{CP}} & c_{13}s_{23} \\ s_{12}s_{23} - c_{12}s_{13}c_{23}e^{i\delta_{CP}} & -c_{12}s_{23} - s_{12}s_{13}c_{23}e^{i\delta_{CP}} & c_{13}c_{23} \end{pmatrix}. \quad (1.33)$$

1.2.1 Neutrino Oscillations

In what follows, we will use Greek subscripts $\alpha = e, \mu, \tau$ to denote the current eigenstates $\{|\nu_\alpha\rangle, \alpha = e, \mu, \tau\}$ produced in a weak interaction. In general they will be linear combinations of the neutrino mass eigenstates,

$$|\nu_\alpha\rangle = \sum_i \mathbf{U}_{\alpha i}^* |\nu_i\rangle, \quad (1.34)$$

where we have used Latin indices $i = 1, 2, 3$ for the mass eigenstates and, as usual, \mathbf{U} stands for the PMNS mixing matrix.

A current eigenstate $|\nu_\alpha\rangle$, created in a weak interaction at $t_0 = 0$, will evolve after a time t as

$$|\nu_\alpha(t)\rangle = \sum_i \mathbf{U}_{\alpha i}^* |\nu_i(t)\rangle, \quad (1.35)$$

where the time evolution of the mass eigenstates is given by

$$|\nu_i(t)\rangle = e^{-iHt} |\nu_i(0)\rangle, \quad H = \sqrt{\mathbf{P}^2 + M^2}, \quad (1.36)$$

and¹

$$\langle \nu_i(0) | H | \nu_j(0) \rangle \approx p_i \delta_{ij} + \frac{m_i^2}{2p_i} \delta_{ij} \approx p \delta_{ij} + \frac{m_i}{2E} \delta_{ij}, \quad p_i \approx p \approx E. \quad (1.37)$$

It can be detected through the process $\nu_\alpha(t)N \rightarrow e_\beta N'$ with a probability

$$\begin{aligned} P_{\alpha\beta} = P(\nu_\alpha \rightarrow \nu_\beta) &= |\langle \nu_\beta | \nu_\alpha(t) \rangle|^2 = \left| \sum_{ij} \mathbf{U}_{\beta j} \mathbf{U}_{\alpha i}^* \langle \nu_j | \nu_i(t) \rangle \right|^2 = \left| \sum_i \mathbf{U}_{\beta i} \mathbf{U}_{\alpha i}^* e^{-im_i^2 L/2E} \right|^2 \\ &= \sum_{ij} \mathbf{U}_{\beta j}^* \mathbf{U}_{\alpha j} \mathbf{U}_{\beta i} \mathbf{U}_{\alpha i}^* e^{-i\Delta m_{ij}^2 L/2E}, \end{aligned} \quad (1.38)$$

where we have defined $\Delta m_{ij}^2 = m_i^2 - m_j^2$ and used that, for relativistic neutrinos, $t \approx L$. We can split the sum $\sum_{ij} = \sum_{i=j} + \sum_{i>j} + \sum_{i<j}$ and use the unitarity of \mathbf{U} to write

$$\begin{aligned} \sum_{i=j} \mathbf{U}_{\beta j}^* \mathbf{U}_{\alpha j} \mathbf{U}_{\beta i} \mathbf{U}_{\alpha i}^* &= \left(\sum_j \mathbf{U}_{\beta j}^* \mathbf{U}_{\alpha j} \right) \left(\sum_i \mathbf{U}_{\beta i} \mathbf{U}_{\alpha i}^* \right) - \sum_{i \neq j} \mathbf{U}_{\beta j}^* \mathbf{U}_{\alpha j} \mathbf{U}_{\beta i} \mathbf{U}_{\alpha i}^* \\ &= \delta_{\alpha\beta} - 2 \sum_{i>j} \text{Re} [\mathbf{U}_{\beta j}^* \mathbf{U}_{\alpha j} \mathbf{U}_{\beta i} \mathbf{U}_{\alpha i}^*]. \end{aligned} \quad (1.39)$$

¹We assume here that neutrinos are created with a definite momentum rather than a definite energy. However, both cases lead to the same result [28].

Analogously,

$$\begin{aligned}
\sum_{i \neq j} \mathbf{U}_{\beta j}^* \mathbf{U}_{\alpha j} \mathbf{U}_{\beta i} \mathbf{U}_{\alpha i}^* e^{-i\Delta m_{ij}^2 L/2E} &= 2 \sum_{i>j} \text{Re} \left[\mathbf{U}_{\beta j}^* \mathbf{U}_{\alpha j} \mathbf{U}_{\beta i} \mathbf{U}_{\alpha i}^* e^{-i\Delta m_{ij}^2 L/2E} \right] \\
&= 2 \sum_{i>j} \text{Re} \left[\mathbf{U}_{\beta j}^* \mathbf{U}_{\alpha j} \mathbf{U}_{\beta i} \mathbf{U}_{\alpha i}^* \right] \cos \Delta m_{ij}^2 L/2E \\
&+ 2 \sum_{i>j} \text{Im} \left[\mathbf{U}_{\beta j}^* \mathbf{U}_{\alpha j} \mathbf{U}_{\beta i} \mathbf{U}_{\alpha i}^* \right] \sin \Delta m_{ij}^2 L/2E. \quad (1.40)
\end{aligned}$$

Using the above expressions we can write the oscillation probability as follows

$$\begin{aligned}
P_{\alpha\beta} = \delta_{\alpha\beta} &- 4 \sum_{i>j} \text{Re} \left[\mathbf{U}_{\beta j}^* \mathbf{U}_{\alpha j} \mathbf{U}_{\beta i} \mathbf{U}_{\alpha i}^* \right] \sin^2 \left(\frac{\Delta m_{ij}^2 L}{4E} \right) \\
&+ 2 \sum_{i>j} \text{Im} \left[\mathbf{U}_{\beta j}^* \mathbf{U}_{\alpha j} \mathbf{U}_{\beta i} \mathbf{U}_{\alpha i}^* \right] \sin \left(\frac{\Delta m_{ij}^2 L}{2E} \right). \quad (1.41)
\end{aligned}$$

The corresponding probability for antineutrinos $\bar{P}_{\alpha\beta} = P(\bar{\nu}_\alpha \rightarrow \bar{\nu}_\beta)$ can be obtained from $P_{\alpha\beta}$ taking into account that the process $\bar{\nu}_\alpha \rightarrow \bar{\nu}_\beta$ is the CPT transformed of $\nu_\beta \rightarrow \nu_\alpha$. Therefore, imposing CPT invariance, we obtain

$$\bar{P}_{\alpha\beta} = P(\bar{\nu}_\alpha \rightarrow \bar{\nu}_\beta) = P(\nu_\beta \rightarrow \nu_\alpha) = P_{\beta\alpha}. \quad (1.42)$$

On the other hand, (1.41) implies that

$$P(\nu_\beta \rightarrow \nu_\alpha; \mathbf{U}) = P(\nu_\alpha \rightarrow \nu_\beta; \mathbf{U}^*). \quad (1.43)$$

Thereby, in the case of CPT invariance, this probability reads

$$\begin{aligned}
\bar{P}_{\alpha\beta} = \delta_{\alpha\beta} &- 4 \sum_{i>j} \text{Re} \left[\mathbf{U}_{\beta j}^* \mathbf{U}_{\alpha j} \mathbf{U}_{\beta i} \mathbf{U}_{\alpha i}^* \right] \sin^2 \left(\frac{\Delta m_{ij}^2 L}{4E} \right) \\
&- 2 \sum_{i>j} \text{Im} \left[\mathbf{U}_{\beta j}^* \mathbf{U}_{\alpha j} \mathbf{U}_{\beta i} \mathbf{U}_{\alpha i}^* \right] \sin \left(\frac{\Delta m_{ij}^2 L}{2E} \right). \quad (1.44)
\end{aligned}$$

A complex PMNS mixing matrix \mathbf{U} will lead in general to $P(\bar{\nu}_\alpha \rightarrow \bar{\nu}_\beta) \neq P(\nu_\alpha \rightarrow \nu_\beta)$, a leptonic evidence of CP violation (CPV) since both processes are related by a CP transformation. Nevertheless, we can check that the two possible Majorana phases η_1 and η_2 cancel out in $\mathbf{U}_{\beta j}^* \mathbf{U}_{\alpha j} \mathbf{U}_{\beta i} \mathbf{U}_{\alpha i}^*$, making $\delta_{CP} \neq 0$ the only possible source of CPV observation in neutrino oscillations. Therefore, as $e^{-i\delta_{CP}}$ always appears in the PMNS matrix multiplied by $\sin \theta_{13}$, it becomes crucial to measure accurately θ_{13} and determine whether it is zero or not.

The two most significant parameters characterizing a neutrino oscillation experiment are the typical neutrino energy E and the source-detector distance L . In general, neutrino beams are not monochromatic and the detectors have a finite energy resolution. Therefore, the experiments are actually sensitive to the average probability

$$\begin{aligned}
\langle P_{\alpha\beta} \rangle &= \frac{\int dE \frac{d\Phi}{dE} \sigma(E) P_{\alpha\beta}(E) \sigma(E)}{\int dE \frac{d\Phi}{dE} \sigma(E) \epsilon(E)} = \delta_{\alpha\beta} - 4 \sum_{i>j} \text{Re} \left[\mathbf{U}_{\beta j} \mathbf{U}_{\alpha j}^* \mathbf{U}_{\beta i}^* \mathbf{U}_{\alpha i} \right] \left\langle \sin^2 \left(\frac{\Delta m_{ij}^2 L}{4E} \right) \right\rangle \\
&+ 2 \sum_{i>j} \text{Im} \left[\mathbf{U}_{\beta j} \mathbf{U}_{\alpha j}^* \mathbf{U}_{\beta i}^* \mathbf{U}_{\alpha i} \right] \left\langle \sin \left(\frac{\Delta m_{ij}^2 L}{2E} \right) \right\rangle, \quad (1.45)
\end{aligned}$$

where Φ is the neutrino flux, σ is the detection cross section and $\epsilon(E)$ is the detector efficiency. To be sensitive to Δm_{ij}^2 , a neutrino oscillation experiment must be designed in such a way that $E/L \simeq \Delta m_{ij}^2$. The typical values of E and L for different neutrino sources and the corresponding ranges of accessible Δm_{ij}^2 are summarized in Table 1.2.

Experiment		L (m)	E (MeV)	Δm^2 (eV ²)
Reactor	SBL	$10^2 - 10^3$	1	$10^{-2} - 10^{-3}$
	LBL	$10^4 - 10^5$		$10^{-4} - 10^{-5}$
Accelerator	SBL	10^2	$10^3 - 10^4$	> 0.1
	LBL	$10^5 - 10^6$	10^4	$10^{-2} - 10^{-3}$
Atmospheric		$10^4 - 10^7$	$10^2 - 10^5$	$10^{-1} - 10^{-4}$
Solar		10^{10}	1	10^{-10}

Table 1.2: Orders of magnitude of Δm^2 values which can be probed in different experiments. SBL (LBL) stands for *short (long) baseline*. Table taken from [29].

In certain regions of the parameter space it is possible to consider only two mass eigenstates ν_i and two flavors ν_α . If so, the mixing matrix reads

$$\mathbf{U} = \begin{pmatrix} \cos \theta & \sin \theta \\ -\sin \theta & \cos \theta \end{pmatrix}, \quad (1.46)$$

where we have disregarded the Majorana phase, because these experiments are not sensitive to it. In this case there is only one mass splitting Δm^2 and the probability becomes

$$P_{\alpha\beta} = \delta_{\alpha\beta} - (2\delta_{\alpha\beta} - 1) \sin^2 2\theta \sin^2 \left(\frac{\Delta m^2 L}{4E} \right). \quad (1.47)$$

When neutrinos propagate through dense matter, they interact differently depending on the neutrino flavor. In particular, only electron neutrinos can exchange a W with matter electrons while all the different flavor neutrinos will exchange a Z boson with an ambient electron, proton, or neutron. Therefore, the above probabilities will be modified, giving rise to the Mikheev-Smirnov-Wolfenstein (MSW) effect [30, 31]. In the two flavor case, $\sin^2 2\theta$ and Δm^2 must be replaced by

$$\Delta m_M^2 = \Delta m^2 \sqrt{\sin^2 2\theta + (\cos 2\theta - A/\Delta m^2)^2}, \quad (1.48)$$

$$\sin^2 2\theta_M = \frac{\sin^2 2\theta}{\sin^2 2\theta + (\cos 2\theta - A/\Delta m^2)^2}, \quad (1.49)$$

where $A = \pm 2\sqrt{2}G_F E N_e$, with G_F the Fermi constant, N_e the electron density and the plus (minus) sign corresponding to the (anti) neutrino case. We should notice that, as we can see from the above equations, the importance of matter effects grows with the neutrino energy E . On the other hand, if $\cos 2\theta \simeq A/\Delta m^2$, then $\sin^2 2\theta_M$ will be near its maximum value, corresponding to $\theta_M \simeq \pi/4$. This is known as the *large mixing angle* (LMA) MSW effect and actually happens in the case of solar neutrino oscillations.

1.2.2 Experiments

Solar Neutrinos Electron neutrinos ν_e are produced in the Sun as a product of the nuclear reactions which generate the solar energy. They originate mainly from the three reactions that

form part of the proton-proton chain: $p + p \rightarrow d + e^+ + \nu_e$ (pp neutrinos), $e^- + {}^7\text{Be} \rightarrow {}^7\text{Li} + \nu_e$ (beryllium neutrinos) and ${}^8\text{B} \rightarrow {}^8\text{Be}^* + e^+ + \nu_e$ (boron neutrinos). In Fig. 1.1 we show the solar neutrino flux as predicted by the Solar Standard Model (SSM) [32]. The flux for the pp neutrinos is by far the largest one but their energy is quite small $E < 0.42$ MeV; the flux for the beryllium neutrinos is sizable and almost monochromatic, with an energy width of 2 keV which is characteristic of the temperature of the Sun core; while the boron neutrinos have a small flux but with energies going beyond 10 MeV.

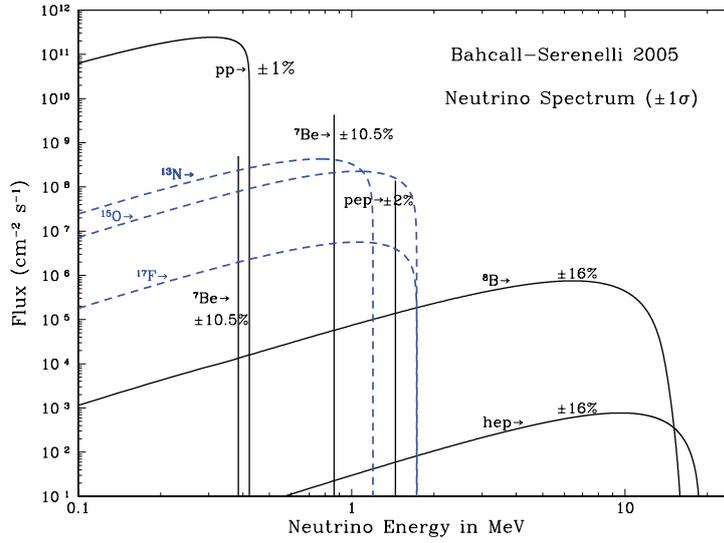


Figure 1.1: Solar neutrino flux predicted by the SSM [32]. Figure taken from John Bahcall's web site, [33].

Several solar neutrino experiments like Homestake [34], GALLEX [35], GNO [36], SAGE [37], Kamiokande [38], Super-Kamiokande [39, 40], . . . , found a deficit of the observed ν_e 's with respect to the SSM prediction. The existence of a discrepancy of $\sim 2-5\sigma$ with respect to the predicted SSM value gave rise to the *solar neutrino problem* (SNP). Moreover, all these results were incompatible with either standard or nonstandard solar model predictions. However, they were in agreement with the neutrino oscillation hypothesis in the (ν_1, ν_2) sector.

The Sudbury Neutrino Observatory (SNO) experiment gave a direct proof that solar ν_e actually change flavor. It can detect neutrinos through three types of processes:

- Elastic scattering (ES), $\nu_\alpha + e^- \rightarrow \nu_\alpha + e^-$, $\alpha = e, \mu, \tau$. If we call Φ_α , $\alpha = e, \mu, \tau$ the different neutrino fluxes reaching the Earth, the ES measurement gives $\Phi_{\text{ES}} = \Phi_e + 0.155(\Phi_\mu + \Phi_\tau)$.
- CC interactions, $\nu_e + d \rightarrow p + p + e^-$, only involving electron neutrinos ν_e and determining $\Phi_{\text{CC}} = \Phi_e$.
- Neutral currents (NC) interactions, $\nu_\alpha + d \rightarrow p + n + \nu_\alpha$, $\alpha = e, \mu, \tau$. They are equally sensitive to all three neutrino flavors $\Phi_{\text{NC}} = \Phi_e + \Phi_\mu + \Phi_\tau$.

If solar ν_e 's oscillate, the averaged survival probability at the Earth will be given by $\langle P_{ee} \rangle = \Phi_{\text{CC}}/\Phi_{\text{NC}}$. SNO proved that about two thirds of the solar neutrinos change their flavor to ν_μ, ν_τ in their travel to the Earth, obtaining $P_{ee} \sim 1/3$ in its energy range. We show in Figure 1.2 the fluxes $\Phi_{\mu\tau} = \Phi_\mu + \Phi_\tau$ and Φ_e measured by SNO [41].

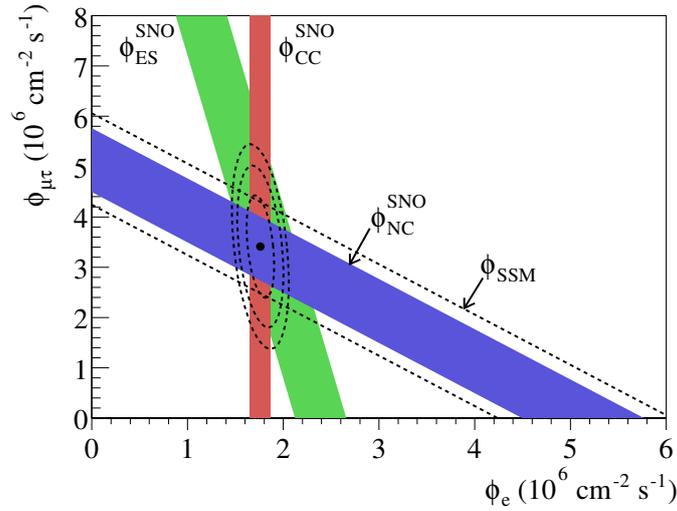


Figure 1.2: Electron and muon/tau neutrino flux by SNO [41]. The intercept of these bands with the axes represent the $\pm 1\sigma$ uncertainties.

The Borexino experiment [42] was designed to measure the ${}^7\text{Be}$ ν_e line through elastic interactions. We can therefore constrain the electron neutrino survival probability at energies $E < 1$ MeV where the matter effects in the Sun are negligible. It can also measure boron neutrinos at higher energies, $E = 5$ MeV, where the matter effects are dominant. We show in Figure 1.3 the obtained electron neutrino ν_e survival probability, compared with the LMA MSW prediction.

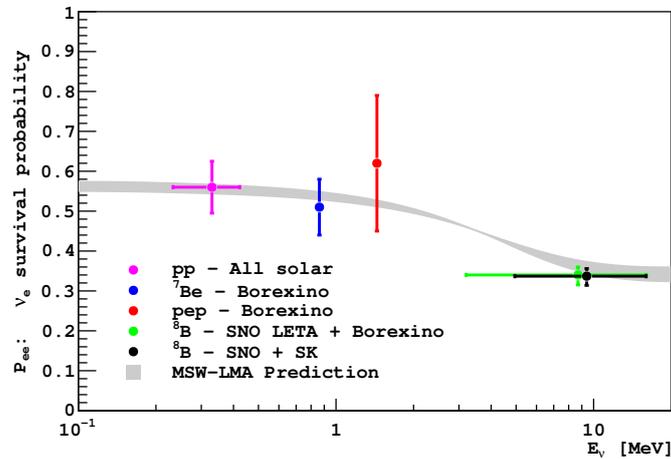


Figure 1.3: Global experimental constraints on the low energy solar P_{ee} . For the ${}^7\text{Be}$ point, the inner (red) error bars show the experimental uncertainty, while the outer (blue) error bars show the total (experimental + SSM) uncertainty. The remaining points were obtained following the procedure described in [43]. The green points are calculated without using the Borexino data. The LMA MSW prediction is also shown for comparison; the band defines the 1σ range of the mixing parameter estimate in [44], which does not include the current result. Figure extracted from [42].

Atmospheric Neutrinos The interaction of cosmic rays with nitrogen and oxygen atoms present in the Earth's atmosphere produce pions and some kaons decaying in electron and muon neutrinos and anti-neutrinos:

$$\begin{aligned} \text{cosmic ray} + \text{nucleon} &\rightarrow \pi^\pm(K^\pm) + X \\ \pi^\pm(K^\pm) &\rightarrow \mu^\pm + \nu_\mu(\bar{\nu}_\mu) \\ \mu^\pm &\rightarrow e^\pm + \nu_e(\bar{\nu}_e) + \bar{\nu}_\mu(\nu_\mu). \end{aligned} \quad (1.50)$$

Without neutrino oscillations, we would naively expect a flavor ratio

$$R_{\mu/e} = \frac{N(\nu_\mu) + N(\bar{\nu}_\mu)}{N(\nu_e) + N(\bar{\nu}_e)} \sim 2 \quad (1.51)$$

of muon neutrino events to electron neutrino events. However, the theoretical computation of this ratio in each experiment is more complicated and the different experiments present this ratio in relation to the MonteCarlo (MC) theoretical expectation $R_{\mu/e}/R_{\mu/e}^{MC}$. The water Cherenkov detectors IMB [49] and Kamiokande detected a flavor ratio smaller than the expected by MC simulations, $R_{\mu/e}/R_{\mu/e}^{MC} \sim 0.6$, leading to the *atmospheric neutrino anomaly*. The case for this anomaly became much stronger with the increase of statistics by Super-Kamiokande (SK) [50]. SK divides the events into several subsamples according to the visible energy in the event. They are classified as fully-contained (FC) if all the energy is deposited inside the inner detector, or as partially-contained (PC) if there are through-going muons of higher energies depositing energy in the outer region. Furthermore, the FC events are subdivided into sub-GeV events if the total visible energy $E_v < 1.33$ GeV and multi-GeV events when $E_v > 1.33$ GeV. The SK experiment found

$$R_{\mu/e}^{\text{sub-GeV}}/R_{\mu/e}^{MC} = 0.658 \pm 0.016 \pm 0.035, \quad (1.52)$$

$$R_{\mu/e}^{\text{multi-GeV+PC}}/R_{\mu/e}^{MC} = 0.702_{-0.030}^{+0.032} \pm 0.101. \quad (1.53)$$

Moreover, SK measured the zenith-angle distribution for the different events, see Fig 1.4, where $\cos\theta = 1$ refers to downward particles and $\cos\theta = -1$ corresponds to upward events. While the various electron neutrino distributions are consistent with expectations, the distributions for muon neutrinos presented a zenith-angle dependence deficit. This fact was in agreement with the hypothesis of a $\nu_\mu \rightarrow \nu_\tau$ oscillation with a subdominant contribution from $\nu_\mu \rightarrow \nu_e$. As matter effects are related to ν_e , we can furthermore interpret the data in terms of vacuum oscillation between ν_μ and ν_τ , for which the main parameters are θ_{23} and Δm_{32}^2 . In this case, the oscillation probability is given by Eq. (1.47):

$$P(\nu_\mu \rightarrow \nu_\tau) = \sin^2 2\theta_{23} \sin^2 \left(\frac{\Delta m_{32}^2 L}{4E} \right). \quad (1.54)$$

The SK results lead to $\sin^2 2\theta_{23} > 0.92$ and $1.5 \times 10^{-3} \text{ eV}^2 < |\Delta m_{32}^2| < 3.4 \times 10^{-3} \text{ eV}^2$ at 90% Confidence Level (CL).

Reactor Neutrinos Nuclear reactors produce electron anti-neutrino $\bar{\nu}_e$ beams with $E_\nu \sim \text{MeV}$. As a consequence of its low energy, the only charged leptons which can be produced through the CC are electrons. If the $\bar{\nu}_e$ changed flavor, its CC interaction could not be observed. This is the reason why reactor experiments are disappearance experiments. Several reactor experiments with relatively short baselines did not find any evidence of $\bar{\nu}_e$ oscillation: Gosgen [51], Krasnoyarsk [52], Bugey [52], CHOOZ [53] and Palo Verde [54]. However, the Kamioka Liquid-scintillator Anti-Neutrino Detector (KamLAND) [55] – with an average travel distance of ~ 200 km and a neutrino

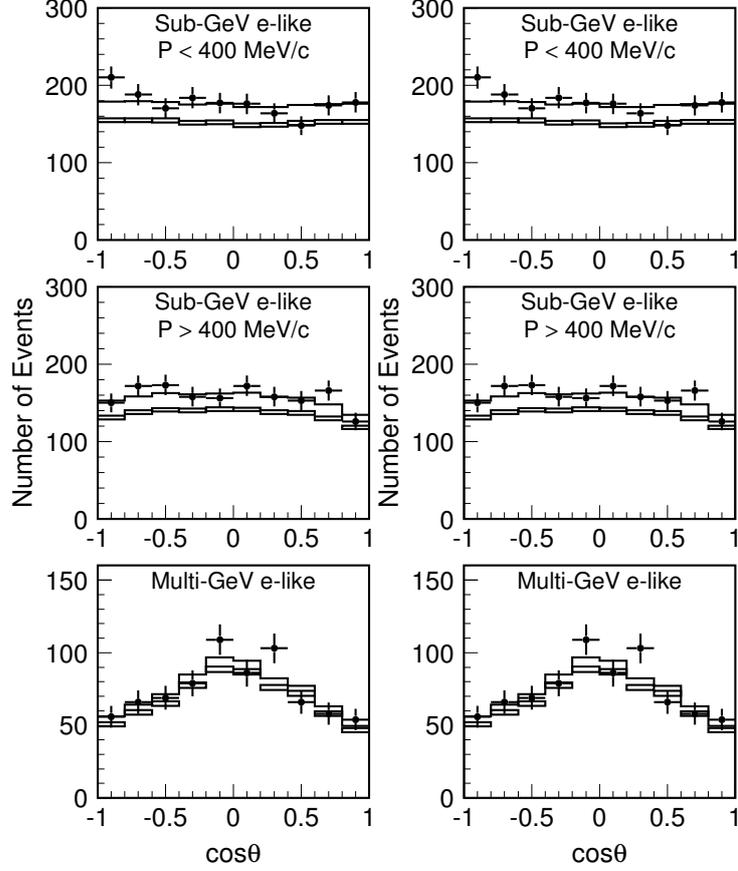


Figure 1.4: The zenith angle distribution for fully-contained 1-ring events, multi-ring events, partially-contained events and upward muons from SK experiment [50]. The points show the data, box histograms show the non-oscillated MC events and the lines show the best-fit expectations for $\nu_\mu \leftrightarrow \nu_\tau$ oscillations with $\sin^2 2\theta_{23} = 1.00$ and $|\Delta m_{32}^2| = 2.1 \times 10^{-3} \text{ eV}^2$. The best-fit expectation is corrected by the 39 systematic error terms, while the correction is not made for the non-oscillated MC events. The height of the boxes shows the statistical error of the MC.

beam energy $E \sim \text{MeV}$ – clearly observed the oscillation pattern in the survival probability, see Fig. 1.5.

For the length scales relevant to reactor neutrino oscillation at KamLAND and the *large mixing angle* (LMA) MSW solution for the solar neutrino oscillations, the dependence on the larger $\nu_1 - \nu_3$ mass splitting (as we will see later $|\Delta m_{31}^2| \sim |\Delta m_{32}^2| \gg \Delta m_{21}^2$, with the convention that $m_2 > m_1$) averages out and the P_{ee} survival probability can be approximated by [56]

$$P(\bar{\nu}_e \rightarrow \bar{\nu}_e) \approx (1 - 2\sin^2 \theta_{13}) \tilde{P}^{2\nu}(\bar{\nu}_e \rightarrow \bar{\nu}_e), \quad (1.55)$$

where we have also used that, as we will see later, $\theta_{13} \ll 1$. In the case of reactor neutrinos at KamLAND [55]

$$\tilde{P}^{2\nu}(\bar{\nu}_e \rightarrow \bar{\nu}_e) = 1 - \sin^2 2\theta_{12}^M \sin^2 \left(\frac{\Delta m_{21M}^2 L}{4E} \right), \quad (1.56)$$

where Δm_{21M}^2 and $\sin^2 2\theta_{12}^M$ are the corresponding MSW modified parameters given by Eqs. (1.48)

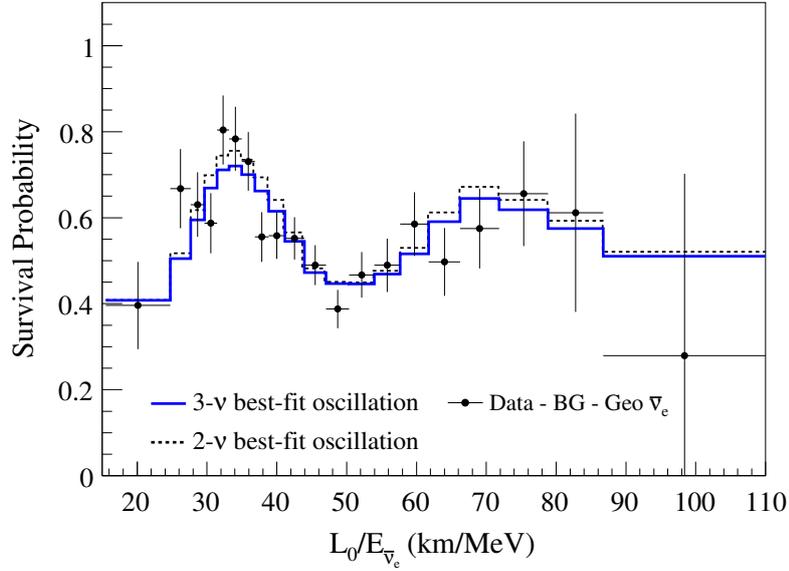


Figure 1.5: Ratio of the observed $\bar{\nu}_e$ spectrum to the expectation for no-oscillation versus L_0/E for the KamLAND data [55]. $L_0 = 180$ km is the flux-weighted average reactor baseline. The 2- ν and 3- ν histograms are the expected distributions based on the best-fit parameter values from the two- and three-flavor unbinned maximum-likelihood analysis of the KamLAND data.

and (1.49), with $A = -2\sqrt{2}G_F\tilde{N}_eE$ and $\tilde{N}_e = N_e \cos^2 \theta_{13}$. We show in Figs. 1.6 and 1.7 the distinct KamLAND fits for θ_{12}, θ_{13} and Δm_{21}^2 .

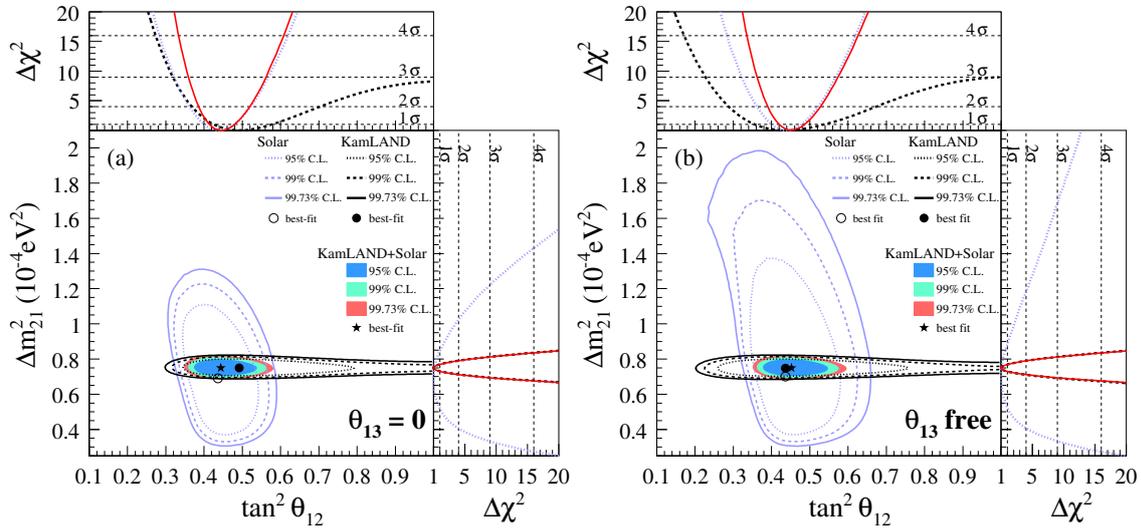


Figure 1.6: Allowed regions projected in the $(\tan^2 \theta_{12}, \Delta m_{21}^2)$ plane, for solar and KamLAND data from (a) the two-flavor oscillation analysis ($\theta_{13} = 0$) and (b) the three-flavor oscillation analysis, where θ_{13} is a free parameter. The shaded regions are from the combined analysis of the solar and KamLAND data. The side panels show the $\Delta\chi^2$ profiles projected onto the $\tan^2 \theta_{12}$ and Δm_{21}^2 axes. Figure extracted from [55].

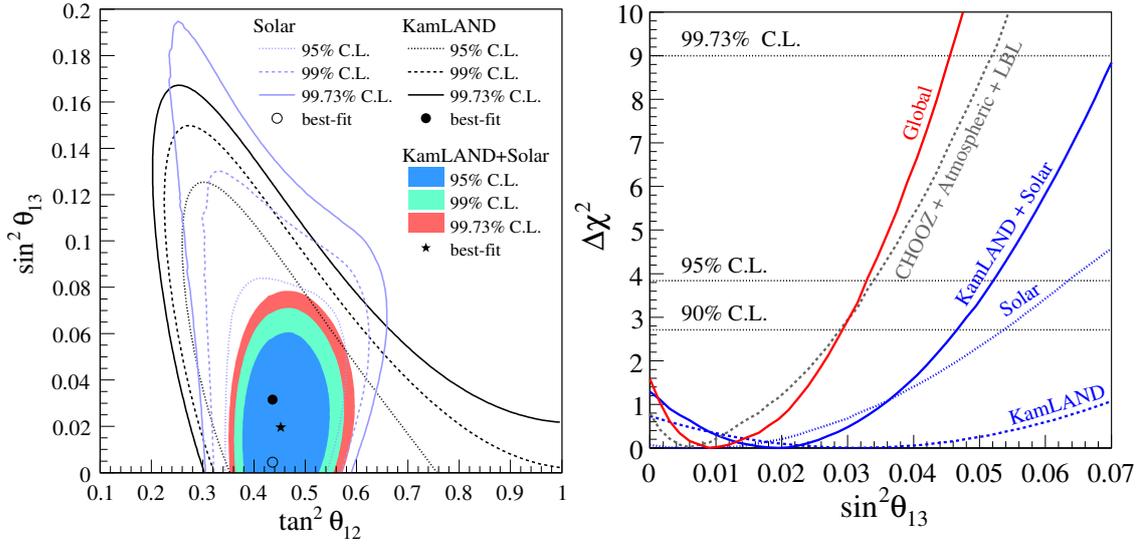


Figure 1.7: Left: Allowed regions from the solar and KamLAND data projected in the $(\tan^2 \theta_{12}, \sin^2 \theta_{13})$ plane for the three-flavor analysis. Right: $\Delta\chi^2$ -profiles projected onto the $\sin^2 \theta_{13}$ axis for different combinations of the oscillation data floating the undisplayed parameters ($\tan^2 \theta_{12}, \Delta m_{21}^2$). Figure extracted from [55].

Recently, there has been a lot of interest to measure θ_{13} using nuclear reactors since, as we have mentioned before, determining accurately its value is very important to measure a possible CPV in the lepton sector. Examples of this are the Double-Chooz [57] and Daya Bay [58] experiments, both with electron antineutrinos $\bar{\nu}_e$ of $E < 9$ MeV traveling a distance of $L \sim 1 - 2$ km before reaching the detector. With these orders of magnitude, the survival probability is given by [56]

$$P(\bar{\nu}_e \rightarrow \bar{\nu}_e) \approx 1 - \sin^2 2\theta_{13} \left(\frac{\Delta m_{\text{atm}}^2 L}{4E} \right), \quad (1.57)$$

where we have neglected matter effects and Δm_{atm}^2 is the *atmospheric* squared-mass difference. Assuming that $m_1 < m_2$, we can consider two possibilities: $m_2 < m_3$ or *normal hierarchy* and $m_2 > m_3$ or *inverted hierarchy*, see Fig. 1.8. In the first case $\Delta m_{\text{atm}}^2 = \Delta m_{31}^2$ while in the second one $\Delta m_{\text{atm}}^2 = \Delta m_{23}^2$.

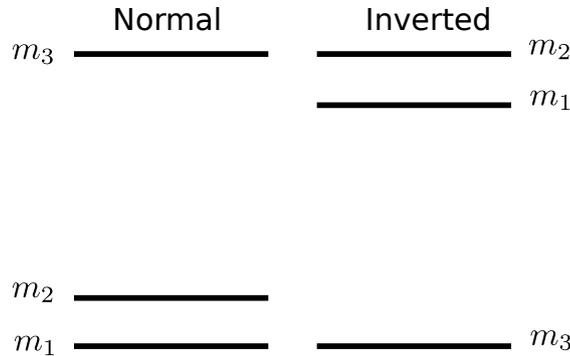


Figure 1.8: Normal and inverted hierarchy for the neutrino spectrum.

The Double-Chooz experiment finds [57]

$$0.017 < \sin^2 2\theta_{13} < 0.16, \quad \text{at 90\% CL}, \quad (1.58)$$

excluding the no oscillation hypothesis at the 94% CL. On the other hand, the Daya Bay experiment finds [58]

$$\sin^2 2\theta_{13} = 0.092 \pm 0.016 \text{ (stat)} \pm 0.005 \text{ (syst)}, \quad (1.59)$$

excluding a vanishing θ_{13} angle at 5.2σ . Besides, the RENO experiment [59] has recently measured the θ_{13} angle with a significance of 4.9σ , obtaining at 1σ

$$\sin^2 2\theta_{13} = 0.113 \pm 0.013 \text{ (stat)} \pm 0.019 \text{ (syst)}, \quad (1.60)$$

which is in agreement with the values above.

Accelerator Neutrinos Usually, in accelerator neutrino experiments, the neutrino beam is produced through the decay of pions (and some kaons) coming from the scattering of accelerated protons on a fixed target:

$$\begin{aligned} p + \text{target} &\rightarrow \pi^\pm + X \\ \pi^\pm &\rightarrow \mu^\pm + \nu_\mu(\bar{\nu}_\mu) \\ \mu_\pm &\rightarrow e^\pm + \nu_e(\bar{\nu}_e) + \bar{\nu}_\mu(\nu_\mu). \end{aligned} \quad (1.61)$$

The final composition of the neutrino beam as well as its beam energy are established through the selection of the sign of the decaying π^\pm and by stopping the muons in the beam line.

The K2K [60] experiment used a nearly pure ν_μ beam of energy $E \sim 1.4$ GeV, with SK being the far detector at a distance $L \sim 250$ km. They obtained for Δm_{atm}^2

$$1.9 \times 10^{-3} \text{eV}^2 < \Delta m_{\text{atm}}^2 < 3.5 \times 10^{-3} \text{eV}^2 \quad \text{at 90\%CL}, \quad (1.62)$$

the first terrestrial confirmation of atmospheric neutrino oscillation parameters. MINOS [61] and T2K [62] experiments estimate θ_{13} by measuring the ν_e appearance probability in a nearly pure ν_μ beam,

$$P(\nu_\mu \rightarrow \nu_e) \approx \sin^2 \theta_{23} \sin^2 2\theta_{13} \sin^2 \left(\frac{\Delta m_{32}^2 L}{4E} \right). \quad (1.63)$$

We show in Fig. 1.9 the confidence levels for $\sin^2 2\theta_{13}$ obtained by T2K with the 90% CL upper bound from Double-Chooz and MINOS.

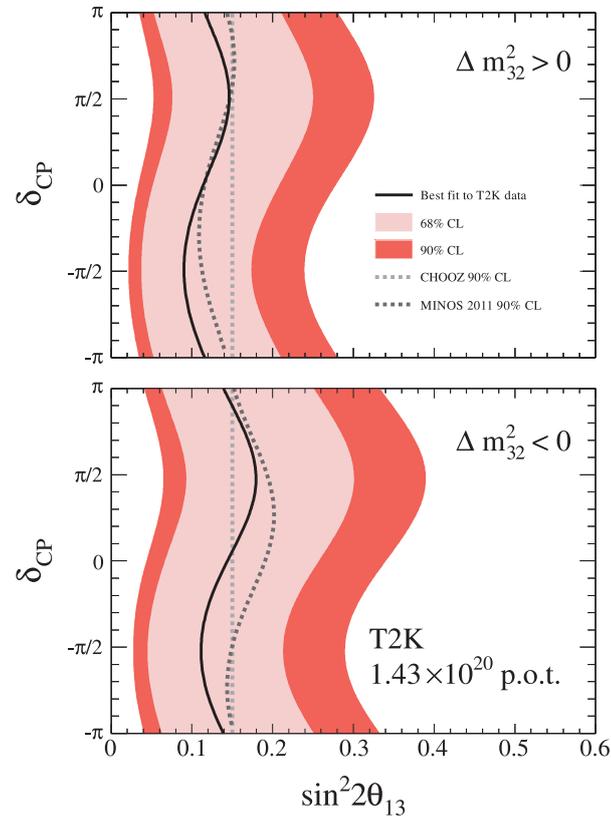


Figure 1.9: Confidence intervals for $\sin^2 2\theta_{13}$ for the normal mass hierarchy (upper) and inverted hierarchy (lower) as a function of the CP violation parameter δ_{CP} . The 90% CL upper limits from Double-CHOOZ and MINOS are shown by the dashed lines. The shaded regions show the T2K 68% and 90% CL intervals, and the solid line shows the T2K best fit. Figure extracted from [63].

Overview The best-fit values and allowed 1, 2 and 3σ ranges for the mass mixing parameters are presented in Table 1.3. We also show in Fig. 1.10 the different bounds on the neutrino mixing angles.

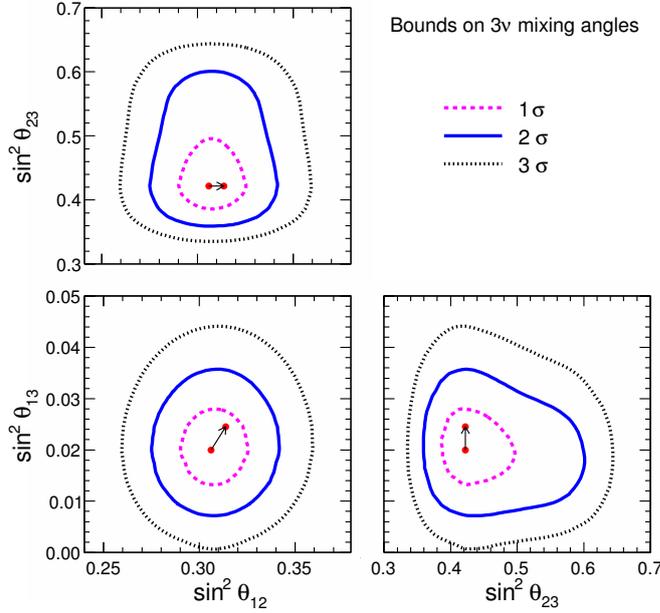


Figure 1.10: Global 3ν analysis: Joint contours at 1, 2 and 3σ ($\Delta\chi^2 = 1, 4$ and 9) for couples of $\sin^2 \theta_{ij}$ parameters, assuming old reactor neutrino fluxes. For new reactor fluxes, the best fits (and, to a large extent, also the contours) are shifted as indicated by the arrows [64].

Parameter	$\delta m^2 / 10^{-5} \text{ eV}^2$	$\sin^2 \theta_{12}$	$\sin^2 \theta_{13}$	$\sin^2 \theta_{23}$	$\Delta m^2 / 10^{-3} \text{ eV}^2$
Best fit	7.58	0.306 (0.312)	0.021 (0.025)	0.42	2.35
1σ range	7.32 – 7.80	0.291 – 0.324 (0.296 – 0.329)	0.013 – 0.028 (0.018 – 0.032)	0.39 – 0.50	2.26 – 2.47
2σ range	7.16 – 7.99	0.275 – 0.342 (0.280 – 0.347)	0.008 – 0.036 (0.012 – 0.041)	0.36 – 0.60	2.17 – 2.57
3σ range	6.99 – 8.18	0.259 – 0.359 (0.265 – 0.364)	0.001 – 0.044 (0.005 – 0.050)	0.34 – 0.64	2.06 – 2.67

Table 1.3: Results of the global 3ν oscillation analysis, in terms of best-fit values and allowed 1, 2 and 3σ ranges for the mass-mixing parameters, assuming old reactor neutrino fluxes. The corresponding best fits and ranges for the new reactor fluxes are shown in parentheses [64].

1.3 The Standard Model as an Effective Theory

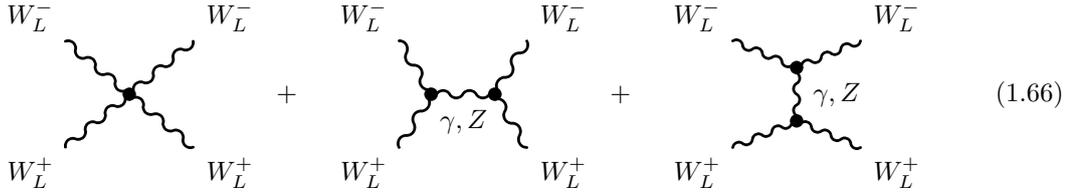
As mentioned before, electroweak symmetry breaking (EWSB) by the Higgs mechanism provides masses to the different fermions and also to the W^\pm and Z gauge bosons, as it is required by experiments. The Higgs scalar also plays an important role in the SM as an ultraviolet (UV) moderator of the longitudinal W^\pm and Z scattering. In principle, in order to give masses to the EW gauge bosons W^\pm and Z we just need three degrees of freedom that will become their longitudinal polarizations. Therefore, we could write down for instance a non-linear representation of the EWSB $SU(2)_L \otimes U(1)_Y \rightarrow U(1)_Q$ using just the three would-be NGB $\theta^i(x)$

$$\Sigma = \exp(i\sigma \cdot \theta(x)/(\sqrt{2}v)), \quad (1.64)$$

where the kinetic term for the Goldstones would give a mass to the corresponding EW gauge bosons

$$\mathcal{L}_\Sigma = \frac{v^2}{2} \text{Tr} [(D_\mu \Sigma)^\dagger (D^\mu \Sigma)] = M_W^2 W_\mu^+ W^{-\mu} + \frac{1}{2} M_Z^2 Z_\mu Z^\mu + \dots \quad (1.65)$$

This minimal scenario is somehow problematic because it has a divergent UV behavior for the longitudinal W^\pm and Z scattering. For the sake of concreteness, let us consider just the charged case, since the neutral one is completely analogous. The following tree level diagrams

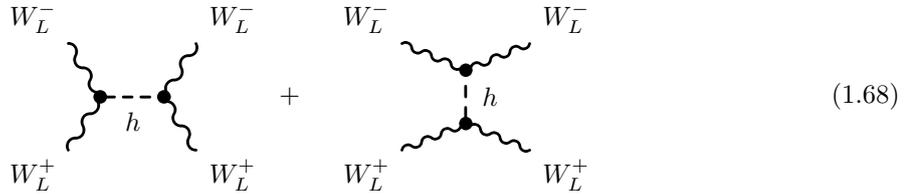


$$(1.66)$$

lead to

$$\mathcal{M}(W_L^+ W_L^- \rightarrow W_L^+ W_L^-) = \frac{g^2}{4M_W^2}(s+t). \quad (1.67)$$

This E^2 dependence means in particular that the unitarity of the theory is violated at some scale $\Lambda_{\text{unit}} \lesssim 700$ GeV. In the SM that does not happen because the scalar Higgs contributions stabilizes this UV behavior [65]. In particular, we need to add to the above diagrams the following ones



$$(1.68)$$

resulting in the following amplitude

$$\mathcal{M}(W_L^+ W_L^- \rightarrow W_L^+ W_L^-) = -\frac{g^2}{4M_W^2} m_h^2 \left[\frac{s}{s-m_h^2} + \frac{t}{t-m_h^2} \right], \quad (1.69)$$

which no longer grows at high energies.

However, the elementary nature of the Higgs boson scalar makes the realization of EWSB problematic in the SM. The reason is that the mass of an elementary scalar develops a quadratic

sensitivity to any new scale in the UV at the quantum level. In particular, the leading radiative contributions to the SM Higgs mass are

$$h \text{---} \text{---} \text{---} \text{---} = h \text{---} \text{---} \text{---} \text{---} + \text{---} \text{---} \text{---} \text{---} + \text{---} \text{---} \text{---} \text{---} + \dots, \quad (1.70)$$

resulting in the following corrections to the squared Higgs mass

$$\delta m_h^2 = (2M_W^2 + M_Z^2 + m_h^2 - 4m_t) \frac{3G_F \Lambda^2}{16\sqrt{2}\pi^2}, \quad (1.71)$$

where Λ is the effective cut-off scale of the theory, above which the SM is not longer valid. We know that, at least, above the Planck scale, $M_{\text{Pl}} \sim 10^{16}$ GeV, gravity becomes strongly coupled and we must include it in the theory. This quadratic sensitivity to the SM cut-off constitutes the so called hierarchy problem and it is the main motivation for physics BSM around the TeV scale to stabilize the EW scale.

On the other hand, as a description of current experimental data, the SM has proven to be extremely successful. In particular, the electroweak precision tests (EWPT), with a precision in many cases at the 1‰ level, have tested successfully the model to the level of quantum corrections. Next, we will discuss how successful the SM is in a quantitative way and, at the same time, we will consider how to test models of new physics (NP) against current experimental data.

1.3.1 Precision Tests of the Standard Model

The gauge sector corresponding to the EW group $SU(2)_L \otimes U(1)_Y$ and the Higgs sector of the SM have four independent parameters, g , g' , v and the quartic coupling λ . If we add the fermion sector, we should include a large number of new parameters, the Yukawa couplings. Regarding precision tests of the SM we can neglect all the Yukawa couplings except for that of the top, λ_{tt}^u , the only one which is relevant excluding flavor and very small parameters. Therefore, leaving aside the strong gauge sector, the SM has five independent relevant parameters,

$$g, g', v, \lambda_{tt}^u, \lambda, \quad (1.72)$$

in terms of which, we can obtain definite predictions for any precision observable. One could trade these parameters by the observables that have been experimentally measured with the best precision, usually,

$$M_Z, G_F, \alpha, m_t, m_h, \quad (1.73)$$

with $\alpha = e^2/(4\pi)$ the electromagnetic coupling constant. The Higgs mass has not been measured yet, but we have some serious hints from the Large Hadron Collider (LHC) searches as we will see below. Anyway, the fact that we have not found it yet means that it is heavy, which in turns implies that λ is large. Thus, we cannot neglect it as it can give important corrections to EW observables at the radiative level, due to the extreme accuracy of the experimental data. We can then express, in the context of the SM, all other observables in terms of these five and compare these predictions with experimental data.

The main experimental tests of the SM come from low energy (mainly violating experiments, e^+e^- scattering at and around the Z pole leptons off nucleons) scattering data, precision CP, P or flavour – Large Electron-Positron collider (LEP) and Stanford Linear Collider (SLAC) –, e^+e^- scattering above the Z pole, up to energies ~ 200 GeV (LEP2), Tevatron data ($p\bar{p}$ collider at 1.96

TeV center of mass energy) and also LHC data (pp collider at 7 TeV center of mass energy at the moment), which are already imposing stringent constraints on the Higgs mass m_h .

The SM predictions have been computed to at least one loop and a comparison with experimental data results in an excellent fit, see [44] and Table 1.4.

Quantity	Value	Standard Model	Pull
M_Z [GeV]	91.1876 ± 0.0021	91.1874 ± 0.0021	0.1
Γ_Z [GeV]	2.4952 ± 0.0023	2.4954 ± 0.0009	-0.1
$\Gamma(\text{had})$ [GeV]	1.7444 ± 0.0020	1.7418 ± 0.0009	—
$\Gamma(\text{inv})$ [MeV]	499.0 ± 1.5	501.69 ± 0.07	—
$\Gamma(\ell^+\ell^-)$ [MeV]	83.984 ± 0.086	84.005 ± 0.015	—
σ_{had} [nb]	41.541 ± 0.037	41.484 ± 0.008	1.5
R_e	20.804 ± 0.050	20.735 ± 0.010	1.4
R_μ	20.785 ± 0.033	20.735 ± 0.010	1.5
R_τ	20.764 ± 0.045	20.780 ± 0.010	-0.4
R_b	0.21629 ± 0.00066	0.21578 ± 0.00005	0.8
R_c	0.1721 ± 0.0030	0.17224 ± 0.00003	0.0
$A_{FB}^{(0,e)}$	0.0145 ± 0.0025	0.01633 ± 0.00021	-0.7
$A_{FB}^{(0,\mu)}$	0.0169 ± 0.0013		0.4
$A_{FB}^{(0,\tau)}$	0.0188 ± 0.0017		1.5
$A_{FB}^{(0,b)}$	0.0992 ± 0.0016	0.1034 ± 0.0007	-2.7
$A_{FB}^{(0,c)}$	0.0706 ± 0.0035	0.0739 ± 0.0005	-0.9
$A_{FB}^{(0,s)}$	0.0976 ± 0.0114	0.1035 ± 0.0007	-0.6
$\bar{s}_\ell^2(A_{FB}^{(0,q)})$	0.2324 ± 0.0012	0.23146 ± 0.00012	0.8
	0.2316 ± 0.0018		
A_e	0.15138 ± 0.00216	0.1475 ± 0.0010	1.8
	0.1544 ± 0.0060		1.1
	0.1498 ± 0.0049		0.5
A_μ	0.142 ± 0.015		-0.4
A_τ	0.136 ± 0.015		-0.8
	0.1439 ± 0.0043		-0.8
A_b	0.923 ± 0.020	0.9348 ± 0.0001	-0.6
A_c	0.670 ± 0.027	0.6680 ± 0.0004	0.1
A_s	0.895 ± 0.091	0.9357 ± 0.0001	-0.4

Table 1.4: Principal Z pole observables and their SM predictions. The first $\bar{s}_\ell^2(A_{FB}^{(0,q)})$ value is the effective angle extracted from the hadronic charge asymmetry while the second is the combined lepton asymmetry from CDF [45] and D0 [46]. The three values of A_e are (i) from A_{LR} for hadronic final states [47]; (ii) from A_{LR} for leptonic final states and from polarized Bhabba scattering [48]; and (iii) from the angular distribution of the τ polarization. The two A_τ values are from SLD and the total τ polarization, respectively. Table extracted from [44].

We should notice that the the Z pole observables are measured typically at $\lesssim 1\%$ level, fully probing the quantum structure of the SM which is of order $\sim 1/16\pi^2 \sim 1\%$. On the other hand, there are some observables that show some discrepancy with the SM, like the total hadronic cross section at the Z pole, σ_{had} (pull=+1.5), and the forward-backward asymmetry of $e^+e^- \rightarrow b\bar{b}$ at the Z pole, $A_{FB}^{(0,b)}$ (pull=-2.7). We could see this *bottom anomaly* as a hint of the presence of NP strongly coupled to the third quark family. Nevertheless, this is not straightforward as the other observable that is also sensitive to the b couplings to the Z , $R_b \equiv \Gamma(b\bar{b})/\Gamma(\text{had})$, is in agreement with the SM prediction (pull=+0.8).

The quadratic dependence on m_t of some observables strongly constraints the top mass. The obtained result agrees very well with direct measurements at Tevatron, although the latest measurements of m_t and M_W at the Tevatron start to show some tension [66]. On the other hand, the dependence on the Higgs mass is only logarithmic, leading to a much weaker sensitivity. Nevertheless, experimental data is so precise that a bound on the SM Higgs mass can be put [66]

$$m_h \leq 145 \text{ GeV}, \quad (\text{from EWPT plus direct searches at 95\% CL in the SM}). \quad (1.74)$$

It is important however to stress that this bound only applies to the SM Higgs. One could have a heavier Higgs whose effects on EW precision observables are compensated by some NP.

Finally, we must say that e^+e^- scattering above the Z pole mass (LEP2) is also an important constraint for the SM because its smaller precision ($\sim 10^{-2}$ relative precision) is compensated by a gain in energy, $\sqrt{s} \leq 209 \text{ GeV}$.

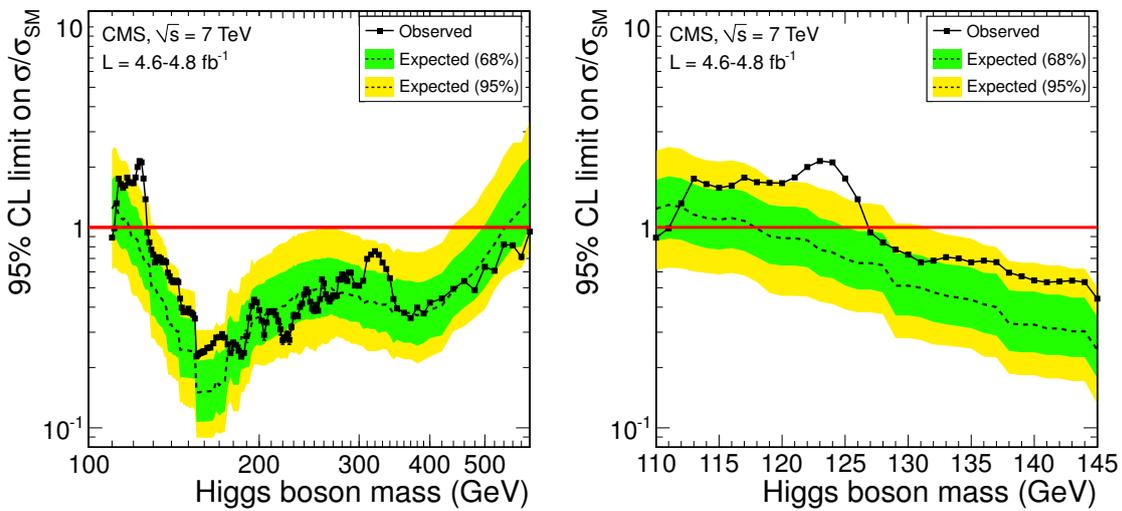


Figure 1.11: CMS 95% CL upper limits on $\sigma/\sigma_{\text{SM}}$ for the SM Higgs boson hypothesis as a function of the Higgs boson mass in the range 110–600 GeV (left) and 110–145 GeV (right). The observed values as a function of mass are shown by the solid line. The dashed line indicates the expected median of results for the no Higgs hypothesis, while the green (dark) and yellow (light) bands indicate the ranges that are expected to contain 68% and 95% of all observed excursions from the median, respectively. Figure taken from [68].

Other important constraints come from the recent Higgs searches at the LHC, which in a relatively short period of time have set bounds on the SM Higgs mass far more stringent than those coming from Tevatron [67], see Fig. 1.11. In particular, analysis from CMS [68], corresponding to an integrated luminosity of $4.6 - 4.8 \text{ fb}^{-1}$, exclude the SM Higgs boson at 95% CL in the range of mass 127 – 600 GeV whereas the ATLAS [69] experiment excludes the ranges 112.9 – 115.5 GeV, 131–238 GeV and 251–466 GeV at 95% CL using an integrated luminosity of 4.9 fb^{-1} .

There is also a lower bound for the Higgs mass coming from LEP [70] and several nuclear experiments like SINDRUM [71], the CERN-Edinburghh-Mainz-Orsay-Pisa-Siegen collaboration [72], CLEO [73] and CUSB [74]

$$m_h \geq 114.4 \text{ GeV} \quad (\text{for a SM Higgs at 95\% CL}), \quad (1.75)$$

All these limits are just for the SM Higgs. In particular, non-SM Higgses can be lighter than the above limit, see [75] for a recent review, although there is a model-independent limit $m_h \geq 82 \text{ GeV}$.

1.3.2 Constraints on New Physics

As we have just seen, the agreement between the SM and experimental data is extraordinary. Therefore, it is natural to assume that the NP should be a small correction to the SM. In principle, for each extension of the SM, with its new parameters, we could compute all precision observables in terms of them. A fit to the EW precision observables will then decide whether the particular model is excluded or it is compatible with current data. There is however another possibility of doing this study using effective Lagrangians. In this way, we can do the analysis for a completely general extension of the SM (with some mild assumptions) and perform the comparison with experiment. This will put bounds on the coefficients of the different operators appearing in the Effective Lagrangian (EL). We then only need to compute the values of such coefficients in our particular model and will automatically know the constraints on the model.

The main idea behind the effective description is that, at some particular energy, at which we are doing an observation (experiment), the details of physics at much higher energies (shorter distances) are irrelevant for the description of the observation. More precisely, if we consider a renormalizable quantum field theory with light and heavy fields, ϕ and Φ , respectively,

$$\mathcal{L}(\phi, \Phi) = \mathcal{L}_l(\phi) + \mathcal{L}_h(\Phi) + \mathcal{L}_{lh}(\phi, \Phi), \quad (1.76)$$

and Λ the mass scale of the heavy fields, for processes at energy $E \ll \Lambda$ we can integrate out the heavy degrees of freedom Φ obtaining an EL $\mathcal{L}_{\text{eff}}(\phi)$, which just depend on the light fields ϕ ,

$$\exp\left(i \int d^4x \mathcal{L}_{\text{eff}}(\phi)\right) = \int \mathcal{D}\phi|_{p>\Lambda} \mathcal{D}\Phi \exp\left(i \int d^4x \mathcal{L}(\phi, \Phi)\right). \quad (1.77)$$

The EL can be expressed, in general, by an infinite expansion of operators built with the low energy degrees of freedom and preserving the relevant symmetries at this scale,

$$\mathcal{L}_{\text{eff}}(\phi) = \sum_d \mathcal{L}_d = \sum_d \sum_i \alpha_i^{(d)} \mathcal{O}_i^{(d)}, \quad (1.78)$$

where \mathcal{L}_d is the sum of all operators with mass dimension d , $[\mathcal{O}_i^{(d)}] = d$. In D space-time dimensions the Lagrangian has mass dimension D . Thus, the coefficients of the expansion have $[\alpha^{(d)}] = D - d$. In particular, for $D = 4$, we have that the coefficients have mass dimension $[\alpha^{(d)}] = 4 - d$, which is negative for all operators of dimension higher than four.

It may look impossible to do any physics with a Lagrangian that has an infinite number of terms. However, it is not the case because we are limited by the experimental precision of the observables we are interested in. Therefore, we do not need an infinite precision in our calculations. Moreover, we should recall that the coefficient of operators with dimension higher than D have negative mass dimension and are therefore suppressed by the cut-off scale Λ . Thus, operators of higher dimensions will be suppressed by increasing powers of E/Λ , with $E \ll \Lambda$. This allows us to cut the sum in d in Eq. (1.78), keeping a finite number of operators (as the number of possible operators of a given dimension d , built with a finite number of fields, is finite). Furthermore, we can reduce the number of operators involved using the fact that operators which are related by the classical equations of motion are redundant [76]. This means that, two operators that are related by the classical equation of motion give the same physics, even including quantum effects, and we only need to consider one of them in Eq. (1.78).

Another possible issue of EL could be the non-renormalizability of the theory, as we have coefficients with negative mass dimensions. This means that an infinite number of counterterms will be required to renormalize the theory. However, as we are limited by the experimental precision of our observables, we can neglect higher order counterterms which are irrelevant for the experimental predictions.

Due to the excellent agreement between the SM and experimental data, a very natural choice of relevant degrees of freedom and symmetries are those of the SM. The choice is whether we keep

the Higgs boson or we work in the non-linear sigma model representation of the SM presented before. In both cases it is easy to compute the first few terms of the EL. For instance, assuming the SM with the Higgs boson in the linear representation, there is only one allowed operator of dimension five, assuming lepton number violation [77]

$$\mathcal{L}_5 = \frac{a^{(5)}}{\Lambda} \epsilon_{ij} \epsilon_{kl} \bar{l}_R^i H^j H^l l_L^k + \text{h.c.}, \quad (1.79)$$

which gives a Majorana mass to neutrinos. Given the smallness of such masses, it is natural to assume approximate lepton and baryon number conservation as did W. Buchmüller and D. Wyler when they classified all possible non-redundant operators of dimension six [78]. The total number of such operators, up to flavour indices, is 81. One can then take these 81 operators and study their effects on EWPT. Such an exercise has been recently performed by several groups [79–81].

Oblique Corrections

We can consider a simplifying assumption in order to have a smaller set of parameters. Following [82], we can assume that NP is *universal* in the following sense. We assume that there are some gauge boson fields \bar{W}_μ^I and \bar{B}_μ to which the light fermions couple as they do to the SM gauge bosons,

$$\mathcal{L} = -g \bar{W}_\mu^I J_I^\mu - g' \bar{B}_\mu J_Y^\mu + \dots, \quad (1.80)$$

with

$$J_I^\mu = \sum_f \psi_L^f \frac{\sigma^I}{2} \gamma^\mu \psi_L^f, \quad J_Y^\mu = \sum_f \psi^f Y_f \gamma^\mu \psi^f, \quad (1.81)$$

and the sum running over all light fermions in the SM.

We should notice that these interpolating gauge fields are not necessarily the SM gauge bosons and will usually have a component of NP. The important feature, that is the very definition of these interpolating fields (and of the universality of NP) is that the only gauge interactions – apart from quantum chromodynamics (QCD) – of the light fermions is the one given in Eq. (1.80). We will also assume that the scale of NP Λ is far enough above the relevant energies that we can safely expand in powers of energy (or momentum). Finally we will just assume unbroken QED (and in particular electric charge conservation). With these assumptions all effects of NP relevant for EWPT can be encoded in the self-energies of the interpolating fields.

In principle, we can split these self-energies in two parts, one arising from local tree level corrections from NP and another that contains all loop corrections from the SM fields,

$$\Pi^{\mu\nu} = \Pi_{\text{NP-tree}}^{\mu\nu} + \Pi_{\text{SM-loop}}^{\mu\nu}. \quad (1.82)$$

Here, we are just interested in the first term of the above expression,

$$\Pi_{\text{NP-tree}}^{\mu\nu} = [\] \eta^{\mu\nu} + [\] \frac{p^\mu p^\nu}{p^2}, \quad (1.83)$$

which accounts for NP tree level corrections. Moreover, we can keep only the terms proportional to $\eta^{\mu\nu}$ in the two point function, as the terms proportional to the external momenta $p^\mu p^\nu$ will vanish or be negligible when contracted with conserved currents or currents built with light fermions. Thus, the most general, $U(1)_Q$ gauge invariant, universal Lagrangian reads

$$\mathcal{L} = -\bar{W}^+ \Pi_{+-}(p^2) \bar{W}^- - \frac{1}{2} \bar{W}^3 \Pi_{33}(p^2) \bar{W}^3 - \bar{W}^3 \Pi_{3B}(p^2) \bar{B} - \frac{1}{2} \bar{B} \Pi_{BB}(p^2) \bar{B}, \quad (1.84)$$

where we have not explicitly written the vector indices that are contracted with $\eta^{\mu\nu}$. Furthermore, the assumption $p \ll \Lambda$ allows us to truncate the momentum Taylor series of the two point functions,

$$\Pi(p^2) = \Pi(0) + p^2 \Pi'(0) + \frac{1}{2} (p^2)^2 \Pi''(0) + \dots, \quad (1.85)$$

where we have kept only operators of dimension six or lower. Thus, assuming we can keep only up to dimension six operators, we have $3 \times 4 = 12$ independent coefficients (the two point function and the first two derivatives at $p^2 = 0$ for each of the four combinations). However, not all of those are independent. First, three of these coefficients can be removed by canonically normalizing the fields. This corresponds to the determination of g , g' and v in the SM,

$$\begin{aligned} \Pi'_{+-}(0) &= \Pi'_{BB}(0) = 1, \\ \Pi_{+-}(0) &= -M_W^2 = -(80.425 \text{ GeV})^2. \end{aligned} \quad (1.86)$$

The remaining 9 parameters are not yet fully independent. The reason is that we have not yet required that $U(1)_Q$ is unbroken (other than electric charge conservation). Imposing conservation of the $U(1)$ group generated by $Q = T_3 + Y$ we obtain the following two consistency conditions

$$\begin{aligned} g'^2 \Pi_{33} + g^2 \Pi_{BB} + 2gg' \Pi_{3B} &= 0, \\ g \Pi_{BB} + g' \Pi_{3B} &= 0. \end{aligned} \quad (1.87)$$

We are therefore left with $7 = 12 - 3 - 2$ coefficients that parametrize any new universal physics beyond the SM. A smart choice of these seven independent parameters is given in Table 1.5. These coefficients are related to the Peskin-Takeuchi S, T, U parameters [83] by

$$S = 4s_W^2 \hat{S} / \alpha_{em}, \quad T = \hat{T} / \alpha_{em}, \quad U = -4s_W^2 \hat{U} / \alpha_{em}. \quad (1.88)$$

Coefficients	Dim. 6 operator	$SU(2)_C$	$SU(2)_L$	Dim. 6 contribution
$\hat{S} = \frac{g}{g'} \frac{\Pi'_{3B}(0)}{\Pi'_{+-}(0)}$	$\frac{\alpha_{\hat{S}}}{\Lambda^2} (H^\dagger \sigma^I H) W_{\mu\nu}^I B^{\mu\nu}$	+	-	$\hat{S} = 2 \frac{g}{g'} \alpha_{\hat{S}} \frac{v^2}{\Lambda^2}$
$\hat{T} = \frac{\Pi_{33}(0) - \Pi_{+-}(0)}{-\Pi_{+-}(0)}$	$\frac{\alpha_{\hat{T}}}{\Lambda^2} H^\dagger D_\mu H ^2$	-	-	$\hat{T} = -\alpha_{\hat{T}} \frac{v^2}{\Lambda^2}$
$\hat{U} = \frac{\Pi'_{+-}(0) - \Pi'_{33}(0)}{\Pi'_{+-}(0)}$	Dim. 8	-	-	
$V = \frac{-\Pi_{+-}(0)}{2} \left(\frac{\Pi''_{33}(0) - \Pi''_{+-}(0)}{\Pi'_{+-}(0)} \right)$	Dim. 10	-	-	
$X = \frac{-\Pi_{+-}(0)}{2\Pi'_{+-}(0)} \frac{\Pi''_{3B}(0)}{\sqrt{\Pi'_{+-}(0)\Pi'_{BB}(0)}}$	Dim. 8	+	-	
$Y = \frac{-\Pi_{+-}(0)}{2\Pi'_{+-}(0)} \frac{\Pi''_{BB}(0)}{\Pi'_{BB}(0)}$	$\frac{\alpha_Y}{\Lambda^2} (\partial_\rho B_{\mu\nu})^2$	+	+	$Y = -4\alpha_Y \frac{M_W^2}{\Lambda^2}$
$W = \frac{-\Pi_{+-}(0)}{2\Pi'_{+-}(0)} \frac{\Pi''_{33}(0)}{\Pi'_{+-}(0)}$	$\frac{\alpha_W}{\Lambda^2} (D_\rho W_{\mu\nu}^I)^2$	+	+	$W = -4\alpha_W \frac{M_W^2}{\Lambda^2}$

Table 1.5: Coefficients of the most general Lagrangian of new universal physics BSM. The expressions below are also valid when the normalization conditions, Eq. (1.86), have not been imposed. We also show the contribution to these coefficients from the corresponding dimension 6 operators. Table adapted from [82].

We have also shown in Table 1.5 which $SU(2)_L \otimes U(1)_Y$ -invariant dimension 6 operator (assuming a fundamental Higgs) generates the corresponding operator and whether they preserve or

violate custodial symmetry and $SU(2)_L$ symmetry, as well as their contributions to the corresponding coefficients. From the dimension of the different operators we can see that there is a hierarchy between the different coefficients,

$$\hat{U} \sim \frac{M_W^2}{\Lambda^2} \hat{T}, \quad V \sim \frac{M_W^4}{\Lambda^4} \hat{T}, \quad X \sim \frac{M_W^2}{\Lambda^2} \hat{S}, \quad (1.89)$$

where we have assumed that operators preserving/breaking the same groups of symmetries are generated at a similar scale. Thus, in models with new universal physics, there are four oblique parameters that fully parametrize corrections to EWPT,

$$\hat{S}, \hat{T}, W, Y. \quad (1.90)$$

In particular, we have that, for universal physics, \hat{T} is related to the ρ parameter,

$$\rho = 1 + \hat{T}, \quad \text{Universal physics.} \quad (1.91)$$

This could be expected from the fact that \hat{T} is the only of the four parameters that violates custodial symmetry. A fit to these four coefficients was performed in [82] with the result shown in Table 1.6. We can see that these four coefficients must be $\lesssim 10^{-3}$. One interesting remark is that is actually LEP2 (less precise but higher energies) which allows us for an independent determination of the four parameters, see Fig. 1.12, not independently constrained by LEP. It should be noted also that the result of the fit depends on the Higgs mass. The reason is the logarithmic dependence of the different coefficients (mainly \hat{S} and \hat{T}) on the Higgs mass.

Fit	$10^3 \hat{S}$	$10^3 \hat{T}$	$10^3 W$	$10^3 Y$
115 GeV Higgs	0.0 ± 1.3	0.1 ± 0.9	0.1 ± 1.2	-0.4 ± 0.8
800 GeV Higgs	-0.9 ± 1.3	2.1 ± 1.0	0.0 ± 1.2	-0.2 ± 0.8

Table 1.6: Fit to universal corrections to the SM [82].

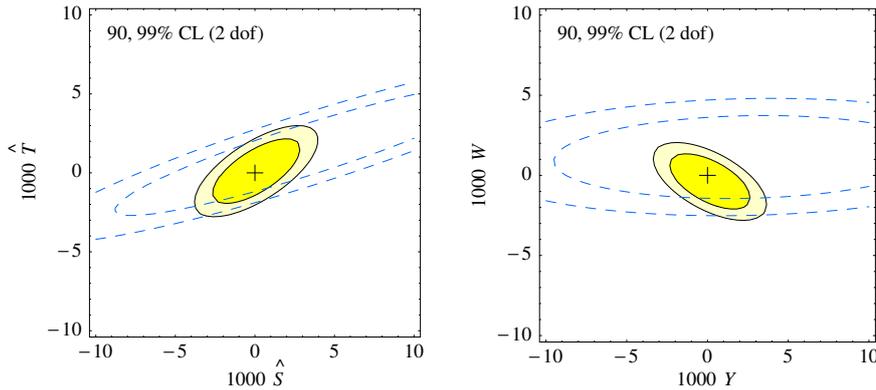


Figure 1.12: Allowed values at 90, 99% CL of (\hat{S}, \hat{T}) (for generic W, Y) and of (W, Y) (for generic \hat{S}, \hat{T}) with $m_h = 115$ GeV. The dashed lines show the weaker constraints obtained by the EWPT alone. Figure extracted from [82].

The leading top mass dependence of these four oblique parameters is quadratic, and represents a nice example of non-applicability of the decoupling theorem. The dependence on the Higgs mass is only logarithmic as implied by the screening theorem [84],

$$\hat{S} = \frac{G_F M_W^2}{12\sqrt{2}\pi^2} \ln\left(\frac{m_h^2}{m_{h,\text{ref}}^2}\right) + \dots, \quad \hat{T} = -\frac{3G_F M_W^2 g'^2}{4\sqrt{2}\pi^2 g^2} \ln\left(\frac{m_h^2}{m_{h,\text{ref}}^2}\right) + \dots \quad (1.92)$$

Non-Oblique Corrections

In general, NP will not only lead to corrections to the oblique parameters mentioned before. There may be also non-universal corrections to the light observables which can not be encoded in these parameters, like the SM one-loop corrections to the $Zb_L\bar{b}_L$ vertex,

$$\text{Diagram 1} + \text{Diagram 2} + \text{Diagram 3} \quad (1.93)$$

where we have just written some of the non-universal one-loop corrections which are present. In some cases, we can consider that the mixing between the oblique parameters and these non-universal corrections is small and treat them separately. Nevertheless, in general this will not be the case and we should compute the general EL arising without further assumptions.

Another example of non-oblique corrections are the flavor violating (FV) operators. In particular, a wide range of BSM models present *flavor changing neutral currents* (FCNC) with flavor off-diagonal couplings to the Z boson and/or the scalar Higgs h . These flavor changing couplings are absent in the SM due to the GIM mechanism and are extremely constrained by experiments. Some of these constraints come from $\Delta F = 2$ processes in the quark sector like $K^0 - \bar{K}^0$, $B_d - \bar{B}_d$ or $B_s - \bar{B}_s$ mixing [85, 86]. Other are due to $\Delta F = 1$ processes like nuclear $\mu - e$ conversion [87], tri-lepton decays as $\mu \rightarrow 3e$ or $\tau \rightarrow 3e$ [44] or radiative decays like $b \rightarrow s\gamma$ [88], $\tau \rightarrow \mu\gamma$ and $\mu \rightarrow e\gamma$ [89, 90].

The most general EL parametrizing the $\Delta F = 2$ processes in the quark sector reads [85]

$$\mathcal{L}_{\text{eff}}^{\Delta F=2} = \mathcal{L}_{\text{eff}}^{\Delta S=2} + \mathcal{L}_{\text{eff}}^{\Delta C=2} + \mathcal{L}_{\text{eff}}^{\Delta B=2}, \quad (1.94)$$

where

$$\begin{aligned} -\mathcal{L}_{\text{eff}}^{\Delta S=2} &= \sum_{i=1}^5 \frac{\alpha_i^{sd}}{\Lambda^2} \mathcal{O}_i^{sd} + \sum_{i=1}^3 \frac{\tilde{\alpha}_i^{sd}}{\Lambda^2} \tilde{\mathcal{O}}_i^{sd}, \\ -\mathcal{L}_{\text{eff}}^{\Delta C=2} &= \sum_{i=1}^5 \frac{\alpha_i^{cu}}{\Lambda^2} \mathcal{O}_i^{cu} + \sum_{i=1}^3 \frac{\tilde{\alpha}_i^{cu}}{\Lambda^2} \tilde{\mathcal{O}}_i^{cu}, \\ -\mathcal{L}_{\text{eff}}^{\Delta B=2} &= \sum_{i=1}^5 \frac{\alpha_i^{bq}}{\Lambda^2} \mathcal{O}_i^{bq} + \sum_{i=1}^3 \frac{\tilde{\alpha}_i^{bq}}{\Lambda^2} \tilde{\mathcal{O}}_i^{bq}, \end{aligned} \quad (1.95)$$

with $q = d(s)$ for $B_{d(s)} - \bar{B}_{d(s)}$ mixing and

$$\begin{aligned}
\mathcal{O}_1^{q_i q_j} &= \bar{q}_{jL}^\alpha \gamma_\mu q_{iL}^\alpha \bar{q}_{jL}^\beta \gamma^\mu q_{iL}^\beta, \\
\mathcal{O}_2^{q_i q_j} &= \bar{q}_{jR}^\alpha q_{iL}^\alpha \bar{q}_{jR}^\beta q_{iL}^\beta, \\
\mathcal{O}_3^{q_i q_j} &= \bar{q}_{jR}^\alpha q_{iL}^\beta \bar{q}_{jR}^\beta q_{iL}^\alpha, \\
\mathcal{O}_4^{q_i q_j} &= \bar{q}_{jR}^\alpha q_{iL}^\alpha \bar{q}_{jL}^\beta q_{iR}^\beta, \\
\mathcal{O}_5^{q_i q_j} &= \bar{q}_{jR}^\alpha q_{iL}^\beta \bar{q}_{jL}^\beta q_{iR}^\alpha.
\end{aligned} \tag{1.96}$$

In the above expressions α, β are colour indices. The operators $\tilde{\mathcal{O}}_{1,2,3}^{q_i, q_j}$ are obtained from $\mathcal{O}_{1,2,3}^{q_i, q_j}$ by the exchange $L \leftrightarrow R$. We show in Table 1.7 [86] the bounds on some relevant operators coming from flavor experiments. The most stringent bounds come from the K^0 sector and in particular from the mass difference Δm_K and the CP violating parameter ϵ_K . There are also important constraints coming from the CP violating observables in $D^0 - \bar{D}^0$ mixing.

Operator	Bounds on Λ in TeV ($\alpha_i = 1$)		Bounds on α_i ($\Lambda = 1$ TeV)		Observables
	Re	Im	Re	Im	
$(\bar{s}_L \gamma^\mu d_L)^2$	9.8×10^2	1.6×10^4	9.0×10^{-7}	3.4×10^{-9}	$\Delta m_K; \epsilon_K$
$(\bar{s}_R d_L)(\bar{s}_L d_R)$	1.8×10^4	3.2×10^5	6.9×10^{-9}	2.6×10^{-11}	$\Delta m_K; \epsilon_K$
$(\bar{c}_L \gamma^\mu u_L)^2$	1.2×10^3	2.9×10^3	5.6×10^{-7}	1.0×10^{-7}	$\Delta m_D; q/p , H_D$
$(\bar{c}_R u_L)(\bar{c}_L u_R)$	6.2×10^3	1.5×10^4	5.7×10^{-8}	1.1×10^{-8}	$\Delta m_D; q/p , H_D$
$(\bar{b}_L \gamma^\mu d_L)^2$	5.1×10^2	9.3×10^2	3.3×10^{-6}	1.0×10^{-6}	$\Delta m_{B_d}; S_{\psi K_S}$
$(\bar{b}_R d_L)(\bar{b}_L d_R)$	1.9×10^3	3.6×10^3	5.6×10^{-7}	1.7×10^{-7}	$\Delta m_{B_d}; S_{\psi K_S}$
$(\bar{b}_L \gamma^\mu s_L)^2$		1.1×10^2		7.6×10^{-5}	Δm_{B_s}
$(\bar{b}_R s_L)(\bar{b}_L s_R)$		3.7×10^2		1.3×10^{-5}	Δm_{B_s}

Table 1.7: Bounds on representative dimension-six $\Delta F = 2$ operators. Observables related to CP violation are separated from the CP conserving ones with semicolons. In the B_s system we only quote a bound on the absolute value of the NP amplitude derived from Δm_{B_s} , see Ref. [86].

We also show in Table 1.8 bounds on some *lepton flavor violating* (LFV) processes.

Process	Value at 90% CL	Ref.	Process	Value at 90% CL	Ref.
$\text{BR}(\mu^- \rightarrow e^- e^+ e^-)$	$< 1.0 \times 10^{-12}$	[44]	$\text{BR}(\tau^- \rightarrow \mu^- \mu^+ \mu^-)$	$< 2.1 \times 10^{-8}$	[44]
$\text{BR}(\tau^- \rightarrow e^- e^+ e^-)$	$< 2.7 \times 10^{-8}$	[44]	$\text{BR}(\mu^- \rightarrow e^- \gamma)$	$< 2.4 \times 10^{-12}$	[90]
$\text{BR}(\tau^- \rightarrow e^- \mu^+ \mu^-)$	$< 2.7 \times 10^{-8}$	[44]	$\text{BR}(\tau^- \rightarrow e^- \gamma)$	$< 3.3 \times 10^{-8}$	[44]
$\text{BR}(\tau^- \rightarrow e^+ \mu^- \mu^-)$	$< 1.7 \times 10^{-8}$	[44]	$\text{BR}(\tau^- \rightarrow \mu^- \gamma)$	$< 4.4 \times 10^{-8}$	[44]
$\text{BR}(\tau^- \rightarrow \mu^- e^+ e^-)$	$< 1.8 \times 10^{-8}$	[44]	B_{conv}	$< 6.1 \times 10^{-13}$	[91]
$\text{BR}(\tau^- \rightarrow \mu^+ e^- e^-)$	$< 1.5 \times 10^{-8}$	[44]			

Table 1.8: Upper bounds at 90 % CL on some LFV processes with their corresponding references. μ^+ and τ^+ decay modes are charge conjugates of the modes above. B_{conv} is the branching ratio for $\mu - e$ conversion.

2

Models with Warped Extra Dimensions

The SM has proven to be a very successful model and provides an extremely solid framework to reproduce and understand the current data. Nevertheless, there are still some important questions in particle physics that the model seems unable to answer. Thereby, the origin of neutrino masses, the large hierarchy between the EW and Planck scales as well as between the different fermion masses or the precise mechanism of EWSB are, to mention a few, questions which can be accommodated but not properly explained within the SM. As we mentioned in the previous chapter, we can consider it as an effective low energy theory to be completed at higher energies by a more fundamental theory which will account for these unexplained facts.

Models with warped extra dimensions (WED) provide an elegant framework to explain some of these issues. They provide a solution to the hierarchy problem [93] and, allowing gauge bosons [94,95] and fermions [96] to propagate through the bulk, they can also explain in geometrical terms the hierarchy existing between the different fermion masses. Indeed, different five dimensional (5D) fermion masses produce distinct localizations of fermions along the extra dimension, naturally leading to a hierarchical pattern of masses and mixing angles [96], like the one observed in the quark sector. The mixing angles in the lepton sector are not hierarchical but, as it was shown in [97], it is also possible to accommodate them within this setup [98]. Another possibility is to incorporate a discrete symmetry in the lepton sector [99–101], leading to non-hierarchical mixing angles as observed experimentally.

Nevertheless, in the basic framework of WED, there is still some tension between the preferred scale of NP by the solution of the hierarchy problem and by the EWPT [102] and flavor data [85, 86, 103–109]. The hierarchy problem points to a NP scale of the order of the EW scale, whereas the experimental constraints mentioned before push this scale to $\mathcal{O}(10)$ TeV or more. Enlarging the bulk gauge group and the particle content to incorporate the custodial symmetry $SO(4)$ [110–115] allows us to alleviate the constraints from EWPT and from some flavor data. Other possible ways to mitigate the constraints arising from the EWPT consist of introducing large brane kinetic terms for the gauge bosons [117, 118] or modifying the 5D anti de Sitter (AdS_5) background near the infrared (IR) brane [119–122]. Combining any of these options with flavor symmetries we can reduce the NP scale to $\mathcal{O}(3)$ TeV, within the reach of the LHC and with a relaxed *small hierarchy problem* [123].

We can go one step further in this process and pull down the cut-off scale to $\mathcal{O}(1)$ TeV in Higgsless models [124–132], where the elastic scattering of gauge bosons is unitarized summing

up the whole Kaluza-Klein (KK) tower of gauge bosons and EWSB is achieved by boundary conditions. Other possible realization of the EWSB in WED is given by models of gauge-Higgs unification (GHU) [133–137], where the Higgs doublet is identified with the massless KK mode of the scalar component of some 5D gauge fields. As we will see later, in terms of the AdS/conformal field theory (CFT) correspondence [138], that means that the Higgs boson arises as a pseudo-NGB of a spontaneously broken approximate symmetry; explaining thereby the small hierarchy between the Higgs mass and the NP scale.

We begin this chapter introducing the general Randall-Sundrum (RS) model and describing the KK expansion for fermions and gauge bosons when they propagate in the bulk. We will consider the cases of a brane localized and a bulk Higgs. In Section 2.2 we analyze the more general case introduced in [119, 120] where the AdS₅ warp factor is modified in the vicinity of the IR brane, reducing the contributions to the T and S parameters. We study for the first time the effect of bulk fermions on EW precision observables in this model with WED and no custodial symmetry [1]. We find that the top-quark mass, together with the corrections to the $Zb_L\bar{b}_L$ vertex and the one-loop contribution to the T parameter, which is finite, impose important constraints that single out a well defined region of parameter space. New massive vector bosons can be as light as ~ 1.5 TeV and have large couplings to the t_R quark, and suppressed couplings to t_L , b_L and to the lighter quarks. We discuss the implications for searches of models with WED at the LHC. In Section 2.3 we present the GHU models, explaining their precise mechanism of EWSB and how the Higgs boson gets a mass through quantum corrections, both in the AdS₅ case and in the dual picture. Finally, in Section 2.4 we consider the Higgsless case, explaining how we can break the EW symmetry, give masses to the different fermions and unitarize the elastic scattering of longitudinal gauge bosons without introducing a Higgs scalar.

We should remark that, although most of this chapter is a review of models and tools well known in the framework of WED and which will be used throughout this Thesis, the content of Section 2.2 is part of the Thesis research and was published in [1].

2.1 Randall-Sundrum Models

Let us consider the following 5D spacetime

$$\mathcal{M}_4 \times \mathcal{I}, \quad (2.1)$$

where \mathcal{M}_4 is the usual four dimensional (4D) Minkowski spacetime and \mathcal{I} is an extra spatial dimension compactified on an interval. In particular, we take an slice of AdS₅ with metric

$$ds^2 = g_{MN}dx^M dx^N = a(z)^2 (dx^\mu dx^\nu \eta_{\mu\nu} - dz^2), \quad a(z) = \frac{R}{z}, \quad (2.2)$$

and $R \leq z \leq R'$, where $R \sim M_{\text{Pl}}^{-1}$ and $R' \sim \text{TeV}^{-1}$ are the location of the UV and IR brane, respectively. In general, we use Latin capital letters $M, N, \dots \in \{0, 1, 2, 3, 5\}$ for the 5D manifold indices and small letters $a, b, \dots \in \{0, 1, 2, 3, 5\}$ for those of the tangent space, with

$$g^{MN} = e_a^M \eta^{ab} e_b^N, \quad \eta^{ab} = \text{diag}(1, -1, -1, -1, -1), \quad (2.3)$$

and $e_a^M = z/R$ the 5D *fünfbein*. Greek letters μ, ν, \dots will refer both to the first four components in the 5D manifold or the associated tangent space, i.e., $\mu, \nu, \dots \in \{0, 1, 2, 3\}$.

The size of \mathcal{I} can be stabilized *à la Goldberger & Wise* [139–141], introducing a new scalar field which breaks the conformal symmetry and gives the radion a finite mass, the scalar field associated with the fluctuations of this size. In general, the mass of the radion depends on the stabilization mechanism but, generically, it is expected to be the lightest particle in a normal RS setup [142]. The study of its phenomenology can be found in the literature [143–147] so we will leave it aside for the rest of this thesis.

2.1.1 Higgs Boson

In the original RS setup [93] the Higgs boson was localized, with the rest of gauge bosons and fermions, on the IR brane

$$\begin{aligned}\mathcal{S}_H &= \int d^4x \int_R^{R'} dz \delta(z - R') \sqrt{g_{IR}} [(D_\mu H)^\dagger (D_\nu H) g^{\mu\nu} - V(H)] \\ &= \int d^4x a(R')^2 [(D_\mu H)^\dagger (D_\nu H) \eta^{\mu\nu} - a(R')^2 V(H)],\end{aligned}\quad (2.4)$$

where $g_{IR} = \det(g_{\mu\nu}(z = R')) = (a(R'))^8$ is the determinant of the brane induced metric tensor. To obtain canonically normalized scalar kinetic term, we make the following redefinition of the Higgs doublet

$$H(x) \rightarrow a(R')^{-1} H(x) = \left(\frac{R'}{R}\right) H(x).\quad (2.5)$$

In particular, the Higgs vev is red-shifted to the TeV scale by the warp factor

$$v_{\text{new}} = \left(\frac{R}{R'}\right) v_{\text{old}} \sim \left(\frac{R}{R'}\right) M_{\text{Pl}} \sim \text{TeV},\quad (2.6)$$

explaining in terms of the extra-dimensional curvature the huge hierarchy between the EW and the Planck scales.

Alternatively, the Higgs boson can be promoted to a bulk field [148, 149], provided it is localized close enough towards the IR brane to solve the hierarchy problem. In the mixed position/space picture, where we have Fourier transformed the four extended dimensions, the relevant part of the Higgs action reads [149]

$$\begin{aligned}\mathcal{S}_H &= \int \frac{d^4p}{(2\pi)^4} \int_R^{R'} dz a(z)^3 \left[p^2 H^\dagger H - (\partial_z H)^\dagger (\partial_z H) - a(z)^2 \frac{\mu^2}{R^2} (H^\dagger H) + \dots \right] \\ &- \int \frac{d^4p}{(2\pi)^4} \int_R^{R'} dz [V_{\text{UV}}(H) \delta(z - R) + V_{\text{IR}}(H) \delta(z - R')],\end{aligned}\quad (2.7)$$

where ... stand for terms involving other fields and

$$V_{\text{UV}} = a(R)^4 m_{\text{UV}} (H^\dagger H),\quad (2.8)$$

$$V_{\text{IR}} = a(R')^4 \frac{\lambda R^2}{2} \left(H^\dagger H - \frac{v_{\text{IR}}^2}{2} \right)^2,\quad (2.9)$$

are the UV and IR brane localized potentials, respectively. We have written a quartic coupling only on the IR brane in order to trigger the EWSB precisely there. Using integration by parts and commuting δ and ∂_z , we obtain the following expression for the action variation

$$\begin{aligned}\delta\mathcal{S}_H &= \int \frac{d^4p}{(2\pi)^4} \int_R^{R'} dz a(z)^3 \delta H^\dagger \left(p^2 H + a(z)^{-3} \partial_z a(z)^3 \partial_z H - a(z)^2 \frac{\mu^2}{R^2} H \right) \\ &- \int \frac{d^4p}{(2\pi)^4} \int_R^{R'} dz \delta(z - R') \delta H^\dagger \left(a(z)^3 \partial_z H + \frac{\partial}{\partial H^\dagger} V_{\text{IR}} \right) \\ &+ \int \frac{d^4p}{(2\pi)^4} \int_R^{R'} dz \delta(z - R) \delta H^\dagger \left(a(z)^3 \partial_z H - \frac{\partial}{\partial H^\dagger} V_{\text{UV}} \right) + \text{h.c.}\end{aligned}\quad (2.10)$$

Asking for a stationary action, $\delta\mathcal{S}_H = 0$, we obtain the following equations

$$\left(p^2 + a(z)^{-3}\partial_z a(z)^3\partial_z - a(z)^2\frac{\mu^2}{R^2}\right)H(x, z) = 0, \quad (2.11)$$

$$a(z)^3\partial_z H(x, z) + \frac{\partial}{\partial H^\dagger}V_{\text{IR}}\Big|_{z=R'} = 0, \quad (2.12)$$

$$a(z)^3\partial_z H(x, z) - \frac{\partial}{\partial H^\dagger}V_{\text{UV}}\Big|_{z=R} = 0, \quad (2.13)$$

corresponding to the Higgs doublet equations of motion and boundary conditions. For $p_\nu = 0$ and an $SU(2)_L \otimes U(1)_Y \rightarrow U(1)_Q$ breaking pattern,

$$\langle H(x, z) \rangle = \frac{v(z)}{\sqrt{2}} \begin{pmatrix} 0 \\ 1 \end{pmatrix}, \quad (2.14)$$

the solutions of the bulk equation of motion (2.11) read

$$v(z) = a\left(\frac{z}{R}\right)^{2+\beta} + b\left(\frac{z}{R}\right)^{2-\beta}, \quad (2.15)$$

with $\beta = \sqrt{4 + \mu^2}$. Eq. (2.13) implies a relationship between the coefficients a and b

$$\frac{b}{a} = -\frac{2 + \beta - m_{\text{UV}}R}{2 - \beta - m_{\text{UV}}R}. \quad (2.16)$$

For the sake of simplicity, let us consider

$$m_{\text{UV}} = \frac{2 + \beta}{R}, \quad (2.17)$$

$$v(z) = a\left(\frac{z}{R}\right)^{2+\beta}. \quad (2.18)$$

In this case, Eq. (2.12) implies

$$v(z) = \frac{1}{R^{3/2}} \left(R^3 v_{\text{TeV}}^2 - \frac{2(2 + \beta)}{\lambda} \right)^{1/2} \left(\frac{z}{R'} \right)^{2+\beta}. \quad (2.19)$$

This particular choice of m_{UV} is not essential to solve the hierarchy problem because the general solution of Eq. (2.15) grows faster towards the IR brane, provided that $\beta \geq 0$. This was just a particular choice to make the solutions more transparent. Defining

$$v_4^2 = \int_R^{R'} dz \left(\frac{R}{z} \right)^3 v^2(z) = \frac{1}{R'^2} \left(R^3 v_{\text{TeV}}^2 - \frac{2(2 + \beta)}{\lambda} \right) \frac{1 - (R/R')^{2+2\beta}}{2(1 + \beta)}, \quad (2.20)$$

we can write

$$v(z) = \sqrt{\frac{2(1 + \beta)}{R^3 (1 - (R/R')^{2+2\beta})}} v_4 R' \left(\frac{z}{R'} \right)^{2+\beta}. \quad (2.21)$$

Expanding now the 5D Higgs doublet around the 5D vev $v(z)$

$$H(x, z) = e^{i\sigma \cdot \theta(x, z)/v(z)} \frac{1}{\sqrt{2}} \begin{pmatrix} 0 \\ v(z) + h(x, z) \end{pmatrix}, \quad (2.22)$$

we can compute the action to quadratic order in $h(x, z)$,

$$\begin{aligned} \mathcal{S}_h &= \int d^4x \int_R^{R'} dz a(z)^3 \left\{ \frac{1}{2} (\partial_\mu h)^2 - \frac{1}{2} (\partial_z h + \partial_z v)^2 - \frac{1}{2} \frac{\mu^2}{z^2} (h + v)^2 \right\} \\ &- \int d^4x \int_R^{R'} dz \left\{ \frac{1}{2} a(R)^4 m_{\text{UV}} (v + h)^2 \delta(z - R) + a(R')^4 \frac{\lambda R^2}{8} \left[(v^4 - 2v^2 v_{\text{IR}}^2 + v_{\text{IR}}^4) \right. \right. \\ &\quad \left. \left. + 4v (v^2 - v_{\text{IR}}^2) h + 2 (3v^2 - v_{\text{IR}}^2) h^2 \right] \delta(z - R') \right\}. \end{aligned} \quad (2.23)$$

Making an expansion in KK modes

$$h(x, z) = \sum_n f_n^h(z) h^{(n)}(x), \quad (2.24)$$

and using the Klein-Gordon equation for $h^{(n)}(x)$,

$$(\partial^2 + m_n^2) h^{(n)}(x) = 0, \quad (2.25)$$

we obtain the equations of motion and boundary conditions for the different KK mode profiles

$$\left(a(z)^{-3} \partial_z a(z)^3 \partial_z + m_n^2 - a(z)^2 \frac{\mu^2}{R^2} \right) f_n^h(z) = 0, \quad (2.26)$$

$$\partial_z f_n^h(z) - a(R) m_{\text{UV}} f_n^h(z) \Big|_{z=R} = 0, \quad (2.27)$$

$$\partial_z f_n^h(z) + a(R') m_{\text{IR}} f_n^h(z) \Big|_{z=R'} = 0, \quad (2.28)$$

where we have imposed $\delta \mathcal{S}_h = 0$ and used the equation of motion and boundary conditions for $v(z)$. In the above equations we have defined

$$m_{\text{IR}} = \frac{1}{R} [\lambda R^3 v^2(R') - (2 + \beta)]. \quad (2.29)$$

In general, we will identify $h^{(1)}(x)$ with the Higgs scalar. Comparing the equations of motion and boundary conditions for $v(z)$ and $f_n^h(z)$ we can see that, leaving aside the mass term m_n^2 , both profiles satisfy the same bulk equation and boundary condition on the UV brane. In particular, in the case of a light Higgs, i.e., $m_1 R' \ll 1$, both functions will be approximately proportional and the *vacuum expectation value* will be carried mostly by the first KK excitation $h^{(1)}(z)$,

$$f_1^h(z) = \frac{v(z)}{v_4} \left(1 + \mathcal{O} \left(\frac{m_h^2 z^2}{1 + \beta} \right) \right). \quad (2.30)$$

2.1.2 Gauge Bosons

Let us consider the action for a 5D gauge boson $A_M(x, z)$ with brane localized scalars $\phi_i(x)$ in the case of a $U(1)$ bulk gauge group¹ [124, 130],

$$\mathcal{S}_G = \int d^4x \int_R^{R'} dz \sqrt{g} \left\{ -\frac{1}{4} F_{MP} F_{NQ} g^{MN} g^{PQ} \right\} + \mathcal{S}_{\text{IR}} + \mathcal{S}_{\text{UV}}, \quad (2.31)$$

¹It is quite straightforward to generalize this case for more sophisticated non-abelian models.

where

$$\mathcal{S}_{UV} = \int d^4x \int_R^{R'} dz \sqrt{g_{UV}} \delta(z-R) \left\{ (D_\mu \phi_1)^\dagger (D_\nu \phi_1) g^{\mu\nu} - \lambda_1 \left(\phi_1^\dagger \phi_1 - \frac{1}{2} v_1^2 \right)^2 \right\}, \quad (2.32)$$

$$\mathcal{S}_{IR} = \int d^4x \int_R^{R'} dz \sqrt{g_{IR}} \delta(z-R') \left\{ (D_\mu \phi_2)^\dagger (D_\nu \phi_2) g^{\mu\nu} - \lambda_2 \left(\phi_2^\dagger \phi_2 - \frac{1}{2} v_2^2 \right)^2 \right\}. \quad (2.33)$$

In the above expressions,

$$g_{UV} = \det(g_{\mu\nu}(z=R)) = (a(R))^8, \quad g = \det(g_{MN}) = (a(z))^{10}, \quad (2.34)$$

while $F_{MN} = \partial_M A_N(x, z) - \partial_N A_M(x, z)$ and $D_M = \partial_M - ig_5 A_M(x, z)$ are the 5D field strength tensor and covariant derivative, respectively. The potential for the brane localized scalars will induce non-vanishing vev's breaking $U(1)$ at both branes

$$\phi_i(x) = \frac{1}{\sqrt{2}} (v_i + h_i(x)) e^{i\pi_i(x)/v_i}, \quad i = 1, 2. \quad (2.35)$$

After some algebra we obtain, to quadratic order in the fields,

$$\begin{aligned} \mathcal{S}_G = & \int d^4x \int dz a(z) \left\{ -\frac{1}{4} F_{\mu\nu} F^{\mu\nu} + \frac{1}{2} (\partial_\mu A_5) (\partial^\mu A_5) + \frac{1}{2} (\partial_z A_\mu) (\partial_z A^\mu) \right. \\ & \left. - \partial_\mu A^\mu a(z)^{-1} \partial_z (a(z) A_5) \right\} + \mathcal{S}_{UV} + \mathcal{S}_{IR}, \end{aligned} \quad (2.36)$$

where

$$\mathcal{S}_{UV} = \int d^4x \left\{ -a(z) A_5 (\partial_\mu A^\mu) + \frac{1}{2} [(\partial_\mu h_1)^2 + (\partial_\mu \pi_1 - g_5 v_1 A_\mu)^2] - \lambda_1 v_1^2 h_1^2 \right\}_{z=R}, \quad (2.37)$$

$$\mathcal{S}_{IR} = \int d^4x \left\{ +a(z) A_5 (\partial_\mu A^\mu) + \frac{1}{2} [(\partial_\mu h_2)^2 + (\partial_\mu \pi_2 - g_5 v_2 A_\mu)^2] - \lambda_2 v_2^2 h_2^2 \right\}_{z=R'}. \quad (2.38)$$

In these equations we have denoted

$$F^{\mu\nu} = F_{\alpha\beta} \eta^{\alpha\mu} \eta^{\beta\nu}, \quad \partial^\nu = \partial_\mu \eta^{\mu\nu}, \quad A^\nu = A_\mu \eta^{\mu\nu}, \quad (2.39)$$

and we have made the following transformations

$$\phi_1(x) \rightarrow a(R)^{-1} \phi_1(x) = a(R)^{-1} \frac{1}{\sqrt{2}} (v_1 + h_1(x)) e^{i\pi_1(x)/v_1}, \quad (2.40)$$

$$\phi_2(x) \rightarrow a(R')^{-1} \phi_2(x) = a(R')^{-1} \frac{1}{\sqrt{2}} (v_2 + h_2(x)) e^{i\pi_2(x)/v_2}, \quad (2.41)$$

to obtain canonically normalized scalar kinetic terms. To get rid of the mixing between the gauge field A_μ and the scalars A_5, π_1 and π_2 we introduce the following gauge-fixing term

$$\begin{aligned} \mathcal{S}_{GF} = & - \int d^4x \int_R^{R'} dz \frac{1}{2\xi} a(z) [\partial_\mu A^\mu - \xi a(z)^{-1} \partial_z (a(z) A_5)]^2 \\ & - \int d^4x \frac{1}{2\xi_1} [\partial_\mu A^\mu + \xi_1 (g_5 v_1 \pi_1 - a(z) A_5)]^2 \Big|_{z=R} \\ & - \int d^4x \frac{1}{2\xi_2} [\partial_\mu A^\mu + \xi_2 (g_5 v_2 \pi_2 + a(z) A_5)]^2 \Big|_{z=R'}. \end{aligned} \quad (2.42)$$

The variation of the whole action, $\delta\mathcal{S}_{G+GF} = \delta\mathcal{S}_G + \delta\mathcal{S}_{GF}$, to quadratic order in the fields A_μ, A_5 and $\pi_{1,2}$, reads

$$\begin{aligned}\delta\mathcal{S}_{G+GF} &= \int d^4x \int dz a(z) \delta A_\mu \left[(\partial^2 - a(z)^{-1} \partial_z a(z) \partial_z) \eta^{\mu\nu} - \left(1 - \frac{1}{\xi}\right) \partial^\mu \partial^\nu \right] A_\nu \\ &+ \int d^4x \int dz a(z) \delta A_5 \left[-\partial^2 + \xi \partial_z a(z)^{-1} \partial_z a(z) \right] A_5 + \delta\hat{\mathcal{S}}_{UV} + \delta\hat{\mathcal{S}}_{IR},\end{aligned}\quad (2.43)$$

where we have defined

$$\begin{aligned}\delta\hat{\mathcal{S}}_{UV} &= \int d^4x a(R) \delta A_\mu \left[(-\partial_z + g_5^2 v_1^2 a(z)^{-1}) \eta^{\mu\nu} + \frac{1}{\xi_1} a(z)^{-1} \partial^\mu \partial^\nu \right] A_\nu \Big|_{z=R} \\ &+ \int d^4x a(R) \left\{ \delta A_5 \left[(-\xi_1 a(z) + \xi a(z)^{-1} \partial_z a(z)) A_5 + \xi_1 g_5 v_1 \pi \right] \right. \\ &+ \left. \delta\pi \left[(-a(z)^{-1} \partial^2 - \xi_1 g_5^2 v_1^2 a(z)^{-1}) \pi + \xi_1 g_5 v_1 A_5 \right] \right\} \Big|_{z=R},\end{aligned}\quad (2.44)$$

$$\begin{aligned}\delta\hat{\mathcal{S}}_{IR} &= \int d^4x a(R') \delta A_\mu \left[(+\partial_z + g_5^2 v_2^2 a(z)^{-1}) \eta^{\mu\nu} + \frac{1}{\xi_2} a(z)^{-1} \partial^\mu \partial^\nu \right] A_\nu \Big|_{z=R'} \\ &+ \int d^4x a(R') \left\{ \delta A_5 \left[(-\xi_2 a(z) - \xi a(z)^{-1} \partial_z a(z)) A_5 - \xi_2 g_5 v_2 \pi \right] \right. \\ &+ \left. \delta\pi \left[(-a(z)^{-1} \partial^2 - \xi_2 g_5^2 v_2^2 a(z)^{-1}) \pi - \xi_2 g_5 v_2 A_5 \right] \right\} \Big|_{z=R'}.\end{aligned}\quad (2.45)$$

Asking for a stationary action, $\delta\mathcal{S}_{G+GF} = 0$, we obtain the equations of motion and boundary conditions for the different fields. In the case of $A_\mu(x, z)$, we get

$$\left[(\partial^2 - a(z)^{-1} \partial_z a(z) \partial_z) \eta^{\mu\nu} - \left(1 - \frac{1}{\xi}\right) \partial^\mu \partial^\nu \right] A_\nu(x, z) = 0, \quad (2.46)$$

$$\left[(-\partial_z + g_5^2 v_1^2 a(z)^{-1}) \eta^{\mu\nu} + \frac{1}{\xi_1} a(z)^{-1} \partial^\mu \partial^\nu \right] A_\nu(x, z) \Big|_{z=R} = 0, \quad (2.47)$$

$$\left[(+\partial_z + g_5^2 v_2^2 a(z)^{-1}) \eta^{\mu\nu} + \frac{1}{\xi_2} a(z)^{-1} \partial^\mu \partial^\nu \right] A_\nu(x, z) \Big|_{z=R'} = 0, \quad (2.48)$$

while for $A_5(x, z)$ they read

$$[-\partial^2 + \xi \partial_z a(z)^{-1} \partial_z a(z)] A_5(x, z) = 0, \quad (2.49)$$

$$\left(-a(z) + \frac{\xi}{\xi_1} a(z)^{-1} \partial_z a(z) \right) A_5(x, z) \Big|_{z=R} + g_5 v_1 \pi_1(x) = 0, \quad (2.50)$$

$$\left(-a(z) - \frac{\xi}{\xi_2} a(z)^{-1} \partial_z a(z) \right) A_5(x, z) \Big|_{z=R'} - g_5 v_2 \pi_2(x) = 0. \quad (2.51)$$

The boundary conditions for $A_5(x, z)$ are mixed with the brane equations of motion for $\pi_{1,2}(x)$

$$\left(-\frac{1}{\xi_1} \partial^2 - g_5^2 v_1^2 \right) \pi_1(x) + g_5 v_1 a(z) A_5(x, z) \Big|_{z=R} = 0, \quad (2.52)$$

$$\left(-\frac{1}{\xi_2} \partial^2 - g_5^2 v_2^2 \right) \pi_2(x) - g_5 v_2 a(z) A_5(x, z) \Big|_{z=R'} = 0. \quad (2.53)$$

If we decompose the 5D fields in KK modes

$$A_\mu(x, z) = \sum_n f_n^V(z) A_\mu^{(n)}(x), \quad A_5(x, z) = \sum_n f_n^S(z) A_5^{(n)}(x), \quad (2.54)$$

and we use the 4D equations of motion

$$\left[(\partial^2 + m_n^2) \eta^{\mu\nu} - \left(1 - \frac{1}{\xi} \right) \partial^\mu \partial^\nu \right] A_\mu^{(n)}(x) = 0, \quad (2.55)$$

$$[\partial^2 + \tilde{m}_n^2] A_5^{(n)}(x) = 0, \quad (2.56)$$

we can obtain the equations fulfilled by the 5D profiles. We have introduced m_n and \tilde{m}_n , the masses of the KK gauge bosons $A_\mu^{(n)}(x)$ and the scalar fields living in a combination of $A_5^{(n)}(x)$, $\pi_1(x)$ and $\pi_2(x)$, respectively. In the unitary gauge, where ξ, ξ_1 and $\xi_2 \rightarrow \infty$, we get for $f_n^V(z)$

$$[a(z)m_n^2 + \partial_z a(z) \partial_z] f_n^V(z) = 0, \quad (2.57)$$

$$[\partial_z - g_5^2 v_1^2 a^{-1}(z)] f_n^V(z) \Big|_{z=R} = 0, \quad (2.58)$$

$$[\partial_z + g_5^2 v_2^2 a^{-1}(z)] f_n^V(z) \Big|_{z=R'} = 0. \quad (2.59)$$

In the case of $f_n^S(z)$, we obtain, for arbitrary values of ξ, ξ_1 and ξ_2 ,

$$\left[\frac{\tilde{m}_n^2}{\xi} + \partial_z a(z)^{-1} \partial_z a(z) \right] f_n^S(z) = 0, \quad (2.60)$$

$$\left[a(z) \frac{\xi_1}{\xi} \frac{\tilde{m}_n^2/\xi_1}{\tilde{m}_n^2/\xi_1 - g_5^2 v_1^2} - a(z)^{-1} \partial_z a(z) \right] f_n^S(z) \Big|_{z=R} = 0, \quad (2.61)$$

$$\left[a(z) \frac{\xi_2}{\xi} \frac{\tilde{m}_n^2/\xi_2}{\tilde{m}_n^2/\xi_2 - g_5^2 v_2^2} + a(z)^{-1} \partial_z a(z) \right] f_n^S(z) \Big|_{z=R'} = 0. \quad (2.62)$$

In the unitary gauge, all the massive modes of $A_5(x, z)$ become non-physical, providing the longitudinal components of the massive KK tower. In this case, we should just consider the vector part of the 5D gauge field, $A_\mu(x, z)$, forgetting about $A_5(x, z)$ except for a possible massless mode, with a profile satisfying

$$\partial_z a(z)^{-1} \partial_z a(z) f_0^S(z) = 0, \quad (2.63)$$

and

$$\partial_z a(z) f_0^S(z) \Big|_{z=R, R'} = 0, \quad (2.64)$$

for $v_{1,2} \neq 0$, and

$$f_0^S(z) \Big|_{z=R, R'} = 0, \quad (2.65)$$

in other case, where we have taken the limit $\xi_{1,2} \rightarrow \infty$ before taking the limit $\xi \rightarrow \infty$.

The solutions to Eq. (2.57) are given by

$$f_n^V(z) = A_n a(z)^{-1} [J_1(m_n z) + B_n Y_1(m_n z)], \quad (2.66)$$

where the overall constant A_n is determined by the orthonormality condition

$$\int_R^{R'} dz a(z) f_n^V(z) f_m^V(z) = \delta_{nm}. \quad (2.67)$$

The boundary condition on the IR brane determines $B_n = -\tilde{J}_1^{IR}/\tilde{Y}_1^{IR}$, where

$$\tilde{J}_1^{UV,IR} = m_n a(z)^{-1} J_0(m_n z) \pm g_5^2 v_{1,2}^2 a(z)^{-2} J_1(m_n z) \Big|_{z=R, R'}, \quad (2.68)$$

$$\tilde{Y}_1^{UV,IR} = m_n a(z)^{-1} Y_0(m_n z) \pm g_5^2 v_{1,2}^2 a(z)^{-2} Y_1(m_n z) \Big|_{z=R, R'}. \quad (2.69)$$

On the other hand, the corresponding boundary condition on the UV will lead to the eigenvalue equation

$$\tilde{J}_1^{UV} \tilde{Y}_1^{IR} - \tilde{Y}_1^{UV} \tilde{J}_1^{IR}, \quad (2.70)$$

whose roots will determine the KK masses m_n .

2.1.3 Fermions

One important remark that should be made is that, in the 5D case, fermions are vector-like. This is due to the fact that the spinorial representation of the 5D Lorentz group is irreducible, with different 4D chiralities or Weyl spinors being connected through Lorentz transformations. Indeed, we can check that the 5D chirality matrix $\bar{\Gamma}$, which splits the spinorial representation in possible smaller irreps, is proportional to the identity. Let us first consider the 5D Clifford algebra

$$\{\Gamma^M, \Gamma^N\} = 2g^{MN}\mathbf{1}, \quad (2.71)$$

where the Γ matrices in the AdS_5 space are obtained from the ones living in the tangent space, $\Gamma^M = e_a^M \Gamma^a$. On the other hand, the 5D chirality matrix is defined by $\bar{\Gamma} = i\sqrt{-i}\Gamma^0\Gamma^1\Gamma^2\Gamma^3\Gamma^5$. It can be shown that we just have two different possibilities for Γ^5 ,

$$\Gamma^5 = \pm\Gamma^0\Gamma^1\Gamma^2\Gamma^3, \quad (2.72)$$

leading to $\bar{\Gamma} = \mp i\sqrt{-i}\mathbf{1}$, as mentioned before. That means that it is meaningless to talk about chirality from a 5D point of view. Nevertheless, as we will see later, it is still worth talking about LH and RH fermions from the 4D standpoint.

Taking into account that $\Gamma^0, \dots, \Gamma^3$ satisfy also the 4D Clifford algebra, whose representations are unique up to similarity transformations, we can obtain the possible representations for the 5D case

$$\Gamma^\mu = \gamma^\mu, \quad \mu = 0, 1, \dots, 4, \quad \Gamma^5 = \pm i\gamma_5, \quad (2.73)$$

where γ^μ 's are the usual Dirac matrices

$$\gamma^\mu = \begin{pmatrix} 0 & \sigma^\mu \\ \bar{\sigma}^\mu & 0 \end{pmatrix}, \quad \sigma^\mu = (\mathbf{1}_2, \sigma^i), \quad \bar{\sigma}^\mu = (\mathbf{1}_2, -\sigma^i), \quad (2.74)$$

and $\gamma_5 = i\gamma^0\gamma^1\gamma^2\gamma^3$. For the sake of definiteness, between the two possible options for Γ^5 , we will choose $\Gamma^5 = -i\gamma_5$ in such a way that $\Gamma^a \in \{\gamma^\mu, -i\gamma_5\}$.

In principle, it might seem impossible to produce a 4D chiral spectrum from a 5D theory, due to its vector-like character. However, the compactification of the extra dimension on \mathcal{I} breaks down the 5D Lorentz invariance, leading to massless KK modes for one of the 4D chiralities if the fermion boundary conditions are the appropriate ones. That means that, in order to reproduce the SM spectrum, we will need at least one 5D field for each of the SM chiral fermions.

Let us consider a number N_f of bulk fermions $\psi^k(x, z)$, with $k \in \mathbb{N}(N_f) = \{1, 2, \dots, N_f\}$. The relevant part of the action reads

$$\mathcal{S} = \int d^4x \int_R^{R'} dz a(z)^5 \left(\frac{i}{2} \left[\bar{\psi}^k e_a^M \Gamma^a \mathcal{D}_M \psi^k - (\mathcal{D}_M \psi^k)^\dagger \Gamma^0 e_a^M \Gamma^a \psi^k \right] - M_k \bar{\psi}^k \psi^k \right) + \mathcal{S}_{\text{bd}}, \quad (2.75)$$

where \mathcal{S}_{bd} denotes any possible boundary term, \mathcal{D}_M is the covariant derivative

$$\mathcal{D}_M = \partial_M - \frac{i}{2} \omega_M^{ab} \Sigma_{ab} = \partial_M + \frac{1}{8} \omega_M^{ab} [\Gamma_a, \Gamma_b], \quad (2.76)$$

and ω_M^{ab} is the spin connection

$$\omega_M^{ab} = \frac{1}{2} g^{RP} e_R^{[a} \partial_{[M} e_p^{b]} + \frac{1}{4} g^{RP} g^{TS} e_R^{[a} e_T^{b]} \partial_{[S} e_P^c] e_M^d \eta_{cd}. \quad (2.77)$$

The fermion bulk masses M_k can be taken diagonal without loss of generality.

After some algebra and integrations by parts, the action becomes

$$\mathcal{S} = \int d^4x \int_R^{R'} dz a(z)^4 \bar{\psi}^k \left[i\not{\partial} + \left(\partial_z + 2 \frac{a'(z)}{a(z)} \right) \gamma_5 - a(z) M_k \right] \psi^k + \hat{\mathcal{S}}_{\text{bd}}, \quad (2.78)$$

where

$$\hat{\mathcal{S}}_{\text{bd}} = \mathcal{S}_{\text{bd}} - \frac{1}{2} \left[a(z)^4 \bar{\psi}^k \gamma_5 \psi^k \right]_R^{R'}. \quad (2.79)$$

Imposing to the action to be stationary, i.e. $\delta\mathcal{S} = 0$, we obtain the bulk equations of motion,

$$\left[i\not{\partial} + \left(\partial_z + 2 \frac{a'(z)}{a(z)} \right) \gamma_5 - \frac{c_k}{z} \right] \psi^k = 0, \quad (2.80)$$

and boundary conditions

$$\left[a(z)^4 \left(\delta\bar{\psi}^k \gamma_5 \psi^k + \bar{\psi}^k \gamma_5 \delta\psi^k \right) \right]_R^{R'} = 0, \quad (2.81)$$

where we have defined $c_k = M_k R$ and assumed that $\mathcal{S}_{\text{bd}} = 0$. To proceed further we need to specify boundary conditions satisfying (2.81). Normally, at each endpoint, we impose Dirichlet boundary condition for one of the two 4D chiralities $P_{L,R} \psi^k(x, z)$. The boundary condition for the opposite chirality will be given by evaluating the bulk equation of motion on the corresponding brane. Following the usual notation, a Dirichlet boundary condition for the RH component is denoted by $[+]$, whereas $[-]$ denotes a Dirichlet boundary condition for the LH chirality. In the general case \mathcal{S}_{bd} will be non zero, leading to a redefinition of the fermion boundary conditions considered before [126]. Let us first analyze the case of an IR localized Dirac mass term

$$\mathcal{S}_{\text{bd}} = - \int d^4x \int_R^{R'} dz a(z)^4 \theta_{ij} \bar{\psi}_L^i \psi_R^j \delta(z - R') + \text{h.c.}, \quad (2.82)$$

where i and j run over the $\mathbb{N}(N_f)$ subsets \mathcal{J}_L and \mathcal{J}_R , respectively, with $\mathcal{J}_L \cap \mathcal{J}_R \neq \emptyset$. For simplicity, we take the fields ψ_R^i and ψ_L^j satisfying Dirichlet boundary conditions on the IR brane. In order to get the new boundary condition we will push the localized brane term at a distance ϵ away from the boundary, which implies the presence of a δ -function in the bulk equations of motion

$$i\not{\partial} \psi_L^i + \partial_z \psi_R^i - \frac{c_i + 2}{z} \psi_R^i - \theta_{ij} \delta(z - R' + \epsilon) \psi_R^j = 0, \quad (2.83)$$

$$i\not{\partial} \psi_R^j - \partial_z \psi_L^j - \frac{c_j - 2}{z} \psi_L^j - \theta_{ij}^* \delta(z - R' + \epsilon) \psi_L^i = 0. \quad (2.84)$$

Integrating these equations around $R' - \epsilon$ and using the previous boundary condition on the IR brane, we obtain the new ones

$$\psi_R^i(x, R') + \theta_{ij} \psi_R^j(x, R') = 0, \quad (2.85)$$

$$\psi_L^j(x, R') - \theta_{ij}^* \psi_L^i(x, R') = 0. \quad (2.86)$$

Notice that the limit $\theta_{ij} \rightarrow \infty$ is equivalent to flip the corresponding boundary conditions, $[+] \leftrightarrow [-]$, for the different fields. It is straightforward to deduce the UV case from this one. For instance, a Dirac mass term on the UV brane

$$\mathcal{S}_{\text{bd}} = - \int d^4x \int_R^{R'} dz a(z)^4 \theta_{ij} \bar{\psi}_L^i \psi_R^j \delta(z - R) + \text{h.c.}, \quad (2.87)$$

will lead to the following boundary conditions

$$\psi_R^i(x, R) - \theta_{ij} \psi_R^j(x, R) = 0, \quad (2.88)$$

$$\psi_L^j(x, R) + \theta_{ij}^* \psi_L^i(x, R) = 0. \quad (2.89)$$

Analogously, we can analyze the effect of a Majorana boundary term for bulk fields that are singlets under the corresponding gauge group. For instance, the following UV (IR) Majorana mass term

$$\mathcal{S}_{\text{bd}} = -\frac{1}{2} \int d^4x \int_R^{R'} dz a(z)^4 \theta_{ij} \bar{\psi}_R^{ic} \psi_R^j \delta(z - R^{(\prime)}) + \text{h.c.}, \quad (2.90)$$

where \mathcal{J}_L and \mathcal{J}_R are equal and θ_{ij} symmetric, leads to

$$\psi_R^{jc}(x, R^{(\prime)}) \pm \theta_{ij}^* \psi_R^{ic}(x, R^{(\prime)}) = 0. \quad (2.91)$$

Once we have computed the modified boundary conditions, we can proceed with the KK decomposition of the bulk fields. Let us consider first the case of Dirac fields, where the 5D fermion fields can be expanded as follows

$$\psi_L^k(x, z) = \sum_n f_{iL}^{(n)k}(z) \psi_L^{(n)l}(x), \quad \psi_R^k(x, z) = \sum_n f_{iR}^{(n)k}(z) \psi_R^{(n)l}(x), \quad (2.92)$$

where $k, l \in \mathbb{N}(N_f)$. In principle, before turning on possible brane mass terms, each bulk field $\psi_{L,R}^k(x, z)$ will have an independent infinite tower of KK modes. The effect of non-diagonal brane mass terms would be the mixing of the corresponding KK towers, with the rest of them being still independent. Nevertheless, leaving aside possible massless or *zero* modes, we can rearrange the infinite KK towers to eliminate the extra index l , see Fig. (2.1),

$$\psi_L^k(x, z) = f_{iL}^{(0)k}(z) \psi_L^{(0)l}(x) + \sum_{n \geq 1} f_L^{(n)k}(z) \psi_L^{(n)}(x), \quad (2.93)$$

$$\psi_R^k(x, z) = f_{iR}^{(0)k}(z) \psi_R^{(0)l}(x) + \sum_{n \geq 1} f_R^{(n)k}(z) \psi_R^{(n)}(x), \quad (2.94)$$

where in the above equations, $f_{iL}^{(0)k}(z) \neq 0 \Rightarrow f_{iR}^{(0)k}(z) = 0$ and *vice versa*.

If we introduce these expansions in the bulk equations of motion and impose that the 4D fields satisfy Dirac equations

$$i\cancel{\partial} \psi_L^{(n)}(x) - m_n \psi_R^{(n)}(x) = 0, \quad i\cancel{\partial} \psi_R^{(n)}(x) - m_n \psi_L^{(n)}(x) = 0, \quad (2.95)$$

we obtain

$$\mathcal{O}_{\pm c_k} f_{L,R}^{(n)k}(z) = \pm m_n f_{R,L}^{(n)k}(z), \quad \mathcal{O}_c = \partial_z - \frac{2-c}{z}. \quad (2.96)$$

For possible zero modes, if the boundary conditions allow their presence, the bulk equations are already decoupled and are thus easy to solve, leading to

$$f_{iR}^{(0)k}(z) = A_{kl} \left(\frac{z}{R}\right)^{c_k+2}, \quad \text{or} \quad f_{iL}^{(0)k}(z) = B_{kl} \left(\frac{z}{R}\right)^{c_k-2}, \quad (2.97)$$

where repeated indices do not sum. For the sake of simplicity, let us assume a UV mass term like (2.87) with $\mathcal{J}_L = \{k_1\}$, $\mathcal{J}_R = \{k_2\} \subset \mathbb{N}(N_f)$, $\psi^{k_1}[+, +]$, and $\psi^{k_2}[-, +]$, where the first sign

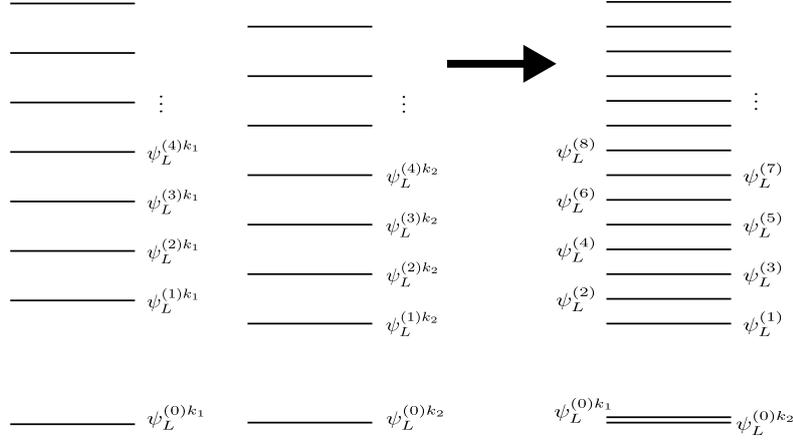


Figure 2.1: Rearrangement of KK towers mixed up through boundary conditions. We represent the different KK eigenstates, with bigger values in the y-axis meaning bigger KK masses.

corresponds to the boundary condition at the UV brane and the second one at the IR brane. The modified UV boundary conditions read

$$\psi_R^{k_1}(x, R) - \theta_{12}\psi_R^{k_2}(x, R) = 0, \quad (2.98)$$

$$\psi_L^{k_2}(x, R) + \theta_{12}^*\psi_L^{k_1}(x, R) = 0, \quad (2.99)$$

whereas the IR ones are still the same,

$$\psi_R^{k_1}(x, R') = \psi_R^{k_2}(x, R') = 0. \quad (2.100)$$

These boundary conditions allow a zero mode for the LH component

$$\psi_L^{k_1}(x, z) = A_{k_1 l} \left(\frac{z}{R}\right)^{c_{k_1}-2} \psi_L^{(0)l}(x) + \dots, \quad (2.101)$$

$$\psi_L^{k_2}(x, z) = A_{k_2 l} \left(\frac{z}{R}\right)^{c_{k_2}-2} \psi_L^{(0)l}(x) + \dots, \quad (2.102)$$

where $l \in \mathcal{J}_L \cup \mathcal{J}_R$. Requiring these functions to satisfy (2.99), we get

$$A_{k_2 l} = -\theta_{12}^* A_{k_1 l}, \quad \forall l \in \{k_1, k_2\}. \quad (2.103)$$

Finally, we can determine $A_{k_1 l}$ imposing canonically normalized kinetic terms, i.e.

$$\sum_{l \in \mathcal{J}_L \cup \mathcal{J}_R} \int_R^{R'} dz \left(\frac{R}{z}\right)^4 \bar{\psi}_L^{(0)l}(x) i \not{\partial} \psi_L^{(0)l}(x, z) = \sum_{l \in \mathcal{J}_L \cup \mathcal{J}_R} \bar{\psi}_L^{(0)l}(x) i \not{\partial} \psi_L^{(0)l}(x) + \dots \quad (2.104)$$

where \dots stands for terms arising from massive KK modes. Note that if we had mixed bulk fields $[+, +]$ and $[-, -]$ instead of the previous ones, the zero-modes present in the absence of brane masses would be no longer present. These two massless modes will become the LH and RH components of a new massive KK excitation. In fact, this is a 5D mechanism to give masses to the different fermions without the help of the Higgs scalar [126].

In the case of bulk fields which are not mixed through boundary conditions, we just have one constant which can be obtained through the normalization condition,

$$f_L^{(0)k}(z) = \sqrt{\frac{1-2c_k}{R((R'/R)^{1-2c_k}-1)}} \left(\frac{z}{R}\right)^{2-c_k}, \quad f_R^{(0)k}(z) = \sqrt{\frac{1+2c_k}{R((R'/R)^{1+2c_k}-1)}} \left(\frac{z}{R}\right)^{2+c_k}. \quad (2.105)$$

The LH zero mode corresponds to a chiral fermion exponentially localized towards the UV (IR) brane for $c_k > 1/2$ ($c_k < 1/2$), while the physical profile is flat for $c = 1/2$. For the RH case, the same applies making the substitution $c \rightarrow -c$.

For massive modes, we need to solve the following equations

$$[\mathcal{O}_{-c_k} \mathcal{O}_{c_k} + m_n^2] f_L^{(n)k}(z) = 0, \quad (2.106)$$

$$[\mathcal{O}_{c_k} \mathcal{O}_{-c_k} + m_n^2] f_R^{(n)k}(z) = 0, \quad (2.107)$$

which lead to

$$f_L^{(n)k}(z) = A_{nk} a(z)^{-5/2} (J_{c_k+1/2}(m_n z) + B_{nk} Y_{c_k+1/2}(m_n z)), \quad (2.108)$$

$$f_R^{(n)k}(z) = A_{nk} a(z)^{-5/2} (J_{c_k-1/2}(m_n z) + B_{nk} Y_{c_k-1/2}(m_n z)), \quad (2.109)$$

where we have used that, due the equations (2.96), the constants accompanying the Bessel functions J and Y are equal for both $f_L^{(n)k}$ and $f_R^{(n)k}$. Imposing the boundary conditions at both branes we will obtain an homogeneous system of $2 \times N_f$ linear equations with $2 \times N_f$ unknowns $\{A_{nk}, B_{nk}\}$. Requiring that the determinant of this system of equations vanishes, so that we get a non-trivial solution, will lead to an eigenvalue equation for m_n . At the end of the day, there will be an overall factor which can be determined by the normalization condition used above.

We will analyze now the case in which a brane Majorana mass term like (2.90) has been added. For the sake of simplicity, let us consider just one bulk field. The expansion is therefore

$$\psi_L(x, z) = \sum_n f_L^{(n)}(z) \psi_R^{(n)c}(x), \quad \psi_R(x, z) = \sum_n f_R^{(n)}(z) \psi_R^{(n)}(x), \quad (2.110)$$

where the 4D fields must obey a Majorana equation

$$i \not{\partial} \psi_R^{(n)}(x) - m_n^* \psi_R^{(n)c}(x) = 0. \quad (2.111)$$

Together with the bulk equations of motion, these equations lead to the following expressions

$$\mathcal{O}_c f_L^{(n)}(z) = m_n^* f_R^{(n)}(z), \quad \mathcal{O}_{-c} f_R^{(n)}(z) = -m_n f_L^{(n)}(z), \quad (2.112)$$

whose solutions are,

$$f_L^{(n)}(z) = A_n a(z)^{-5/2} (J_{c+1/2}(|m_n|z) + B_n Y_{c+1/2}(|m_n|z)), \quad (2.113)$$

$$f_R^{(n)}(z) = A_n a(z)^{-5/2} \frac{m_n}{|m_n|} (J_{c-1/2}(|m_n|z) + B_n Y_{c-1/2}(|m_n|z)). \quad (2.114)$$

The brane Majorana mass term produces a boundary condition mixing $f_L^{(n)}$ and $f_R^{(n)*}$. If θ_{ij} is real, m_n will be also real and the linear system resulting from imposing the boundary conditions will factorize into two simpler ones; one for the real parts of the unknowns, and another one for their imaginary parts (obtained changing the sign of θ_{ij}).

Up to now, in all this study, we have ignored Yukawa couplings and the effect of EWSB due to the Higgs vev. In general, if we consider the bulk equations of motion after SSB, the Higgs vev will couple the equations corresponding to bulk fields related by a Yukawa mass term. In

most cases these equations are impossible to solve. In this cases, it is customary to treat these effects perturbatively, solving the equations of motion *before* EWSB and including the effects of EWSB through couplings. This approximation is justified since $v \ll m_1 \sim R'^{-1}$, with leading order corrections being $\mathcal{O}((vR')^2)$. Exactly the same apply for gauge bosons, where the Z and W masses can be computed in terms of $(vR')^2$ corrections, instead of solving the equations of motion with the exact boundary conditions.

2.2 Non-Custodial Models

Models based on a purely AdS₅ background and a minimal field content are strongly constrained by EWPT. In particular, large contributions to the parameter T can easily push the scale of new physics beyond the reach of the LHC [150]. This is easy to understand if we write the oblique parameters due to the KK physics as follows,

$$\begin{aligned}\hat{T} &= \frac{g'^2 v^2}{2} (\hat{\alpha} - 2\hat{\beta} + \hat{\gamma}), \\ \hat{S} &= g^2 v^2 (-\hat{\beta} + \hat{\gamma}), \\ W &= Y = \frac{g^2 v^2}{2} \hat{\gamma},\end{aligned}\tag{2.115}$$

where the coefficients $\hat{\alpha}, \hat{\beta}$ and $\hat{\gamma}$ – which will be defined below – are diagrammatically shown in Fig. 2.2. Due to the warp factor, the gauge boson KK modes are forced to be localized close to the IR brane, where the Higgs is also localized. The large overlap then makes the mixing between the gauge boson zero-mode and massive KK modes large (the red square in Fig. 2.2). The light fermions on the other hand are localized towards the UV brane and therefore their coupling to the gauge boson KK modes (the blue dot) is typically small. This is the reason for the usual enhancement of the \hat{T} parameter ($\hat{\alpha}$ is proportional to the gauge mixing squared) over the \hat{S} parameter, and of \hat{S} over W and Y .

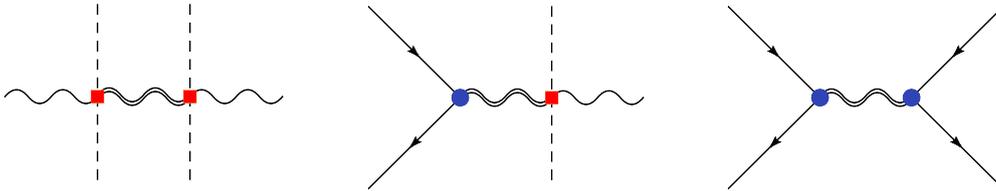


Figure 2.2: Contribution to the coefficients $\hat{\alpha}$, $\hat{\beta}$ and $\hat{\gamma}$ of Eq. (2.115). The double line represents the tower of massive gauge boson KK modes, the red squares the mixing between the gauge KK and zero-modes, and the blue dot the coupling of the light fermions to the gauge KK modes.

On the other hand, the large top mass requires the third generation $SU(2)_L$ quark doublet (as well as the top singlet) to be relatively close to the infrared (IR) brane. When the light generations are localized near the ultraviolet (UV) brane, this can lead to large corrections to the $Zb_L\bar{b}_L$ coupling, which also implies important restrictions.

A common solution to this problem is to enlarge the bulk gauge group and fermion content to accommodate a gauge custodial symmetry [110–115] protecting the T parameter and the $Zb_L\bar{b}_L$ coupling at the tree level. In these models, the S parameter –together with the one-loop fermion contributions to T and the $Zb_L\bar{b}_L$ coupling [102, 151], which are calculable in such models– imposes the strongest constraint. In the anarchic scenario, where all the Yukawa entries are of the same order, the new vector bosons should be heavier than $\mathcal{O}(3)$ TeV.² Another interesting possibility

²If one gives up on the anarchic assumption, the constraints can be significantly relaxed [152].

has been recently suggested [119–122], where a departure from pure AdS₅ near the IR brane substantially decreases the T parameter (and, although by a smaller amount, also the S parameter, as was previously observed in [153, 154]). In this case, the reduction of the T and S parameters is so effective that new vector bosons with masses below 1 TeV are compatible with the EWPT *without the custodial symmetry*.

Let us summarize the main results for the gravitational background and the bosonic field content, while referring the reader to [119–121] for full details. We will then introduce bulk fermions [1, 122], which were absent on the original setup [119–121].

The gravitational background is given by the metric

$$ds^2 = e^{-2A(y)} \eta_{\mu\nu} dx^\mu dx^\nu - dy^2, \quad (2.116)$$

with warp factor

$$A(y) = ky - \frac{1}{\nu^2} \log \left(1 - \frac{y}{y_s} \right). \quad (2.117)$$

We have chosen a non-conformally flat coordinate system to be as close as possible to the original reference and because this choice leads to simpler expressions. In the metric definition, $0 \leq y \leq y_1$ is the coordinate of the extra dimension with the UV and IR branes being localized at $y = 0$ and $y = y_1$ respectively. k is the curvature scale at the UV brane, of order of the Plank mass. We will chose y_s , the position of the singularity, such that it will be localized beyond the IR brane, i.e., $y_1 < y_s$. The gravitational parameters are therefore ν, y_1, y_s and k . However, instead of y_s we will use the value of the curvature radius at the IR brane, given in units of k

$$kL_1 = \frac{\nu^2 k (y_s - y_1)}{\sqrt{1 - 2\nu^2/5 + 2\nu^2 k (y_s - y_1) + \nu^4 k^2 (y_s - y_1)^2}}. \quad (2.118)$$

Requiring perturbativity of the gravitational expansion bounds its value by $kL_1 \gtrsim 0.2$ [119]. In addition, we fix the position of the IR brane y_1 such that the gravitational background generates the gauge hierarchy. We will simply set $A(y_1) = 35$, which determines y_1 .

2.2.1 Bulk Bosons

The bosonic content of the model consists of the SM gauge fields, with Neumann boundary conditions on both branes, and an EW scalar doublet, the Higgs. Other scalars involved in the gravitational background and the stabilization of the interbrane distance [119] are irrelevant for our purposes. The bulk gauge bosons can be expanded in KK modes (we focus on the μ component here)

$$A_\mu(x, y) = \frac{1}{\sqrt{y_1}} \sum_n f_n^V(y) A_\mu^{(n)}(x), \quad (2.119)$$

where the profiles satisfy

$$[\partial_y e^{-2A} \partial_y + m_n^2] f_n^V = 0, \quad \partial_y f_n^V|_{y=0, y_1} = 0, \quad (2.120)$$

(as mentioned before, we treat EWSB perturbatively), and are normalized according to

$$\frac{1}{y_1} \int_0^{y_1} dy f_n^V f_m^V = \delta_{nm}. \quad (2.121)$$

The boundary conditions fix the value of the KK masses. They are of the order of the effective IR scale

$$\tilde{k}_{\text{eff}} \equiv A'(y_1) e^{-A(y_1)}, \quad (2.122)$$

i.e. of order the warped down curvature at the IR brane. We show in Fig. 2.3 the mass of the first gauge KK mode, in units of \tilde{k}_{eff} , for different values of ν and kL_1 .

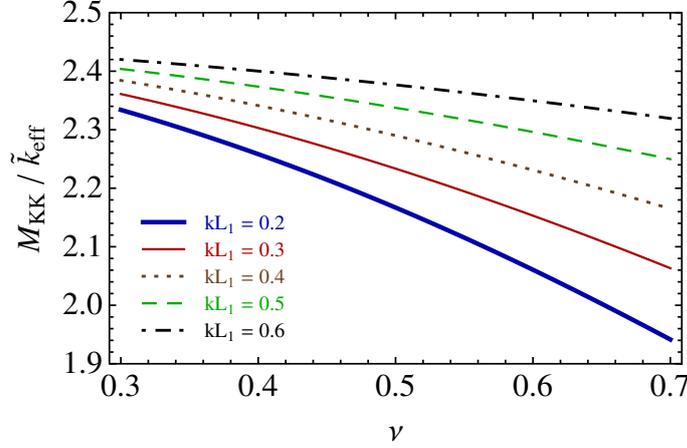


Figure 2.3: Mass of the first gauge KK mode in units of the effective IR scale \tilde{k}_{eff} , defined in Eq. (2.122), as a function of ν and for different values of kL_1 .

For the Higgs field we can write

$$H(x, y) = \frac{1}{\sqrt{2}} e^{i\chi(x, y)} \begin{pmatrix} 0 \\ h(y) + \xi(x, y) \end{pmatrix}, \quad (2.123)$$

where the Higgs KK expansion reads

$$\xi(x, y) = \frac{1}{\sqrt{y_1}} \sum_n f_n^\xi(y) \xi^{(n)}(x), \quad (2.124)$$

and the wavefunctions are normalized to

$$\frac{1}{y_1} \int_0^{y_1} dy e^{-2A} f_n^\xi f_m^\xi = \delta_{nm}. \quad (2.125)$$

Analogously to the RS case, for a light Higgs, we can assume that the Higgs vev is carried by the zero-mode, which has a profile

$$f_0^\xi(y) \approx N_h e^{aky}, \quad (2.126)$$

with N_h fixed by the normalization condition (2.125). Following [119] we trade a for

$$\delta \equiv \left| e^{-2(a-2)ky_s} k y_s [-2(a-2)ky_s]^{-1+\frac{4}{\nu^2}} \Gamma\left(1 - \frac{4}{\nu^2}, -2(a-2)k(y_s - y_1)\right) \right|, \quad (2.127)$$

which is a measure of how much fine-tuning in the 5D parameters we need to impose in order to preserve the Randall-Sundrum solution to the hierarchy problem.

2.2.2 Bulk Fermions

We introduce now bulk fermions in the model. The quadratic part of the action for bulk fermions reads

$$\mathcal{S} = \int d^4x dy e^{-4A} \bar{\psi} \left[e^A i \not{\partial} + (\partial_z - 2A') \gamma^5 - M \right] \psi, \quad (2.128)$$

where M is a 5D Dirac mass allowed by the symmetries. Following the same procedure as in previous sections, we expand the bulk fermions in KK modes

$$\psi_{L,R}(x, y) = \frac{1}{\sqrt{y_1}} \sum_n f_{L,R}^{(n)}(y) \psi_{L,R}^{(n)}(x), \quad (2.129)$$

where the KK profiles satisfy the following system of equations:

$$\begin{aligned} [\partial_y - (2A' + M)] f_R^{(n)} &= -e^A m_n f_L^{(n)}, \\ [\partial_y - (2A' - M)] f_L^{(n)} &= e^A m_n f_R^{(n)}, \end{aligned} \quad (2.130)$$

with the orthonormality conditions given by

$$\frac{1}{y_1} \int_0^{y_1} dy e^{-3A} f_L^{(n)} f_L^{(m)} = \frac{1}{y_1} \int_0^{y_1} dy e^{-3A} f_R^{(n)} f_R^{(m)} = \delta_{nm}. \quad (2.131)$$

As in the RS case, bulk fermions with a LH zero-mode are obtained by imposing Dirichlet boundary conditions for their right-handed RH chirality on both branes. The boundary conditions for the opposite, LH, chirality are fixed by the equations of motion. Similarly, bulk fermions with a RH zero-mode are obtained by imposing Dirichlet boundary conditions on their LH chirality. The LH (RH) massless profile of a $[++]$ ($[--]$) bulk fermion is given by

$$f_{L,R}^{(0)}(y) = N_0^{L,R} e^{2A \mp \int_0^y dy' M(y')}, \quad (2.132)$$

where $N_0^{L,R}$ is fixed by the normalization condition. In the following we will consider a constant bulk mass $M_i = c_i k$, where i denotes the fermion type.³

Unless we introduce y -dependent bulk masses as it was made in [122], there are no exactly flat fermion solutions in the present metric background, unlike for a pure AdS₅ background, $A_{RS}(y) = ky$, with a constant 5D Dirac mass defined by $c = 1/2$. However, the c parameter does control the localization of the fermion zero-modes, either towards the IR or UV brane. In particular, there is always a background-dependent value, $c_{1/2}$, such that for $c < c_{1/2}$, the (LH) fermion zero-mode is mostly IR localized, while for $c > c_{1/2}$ it is mostly UV localized. This value plays a role analogous to $c = 1/2$ in the pure AdS₅ background. In Fig. 2.4 we show the value of $c_{1/2}$, defined such that $e^{-\frac{3}{2}A(0)} f_0^L(0) = e^{-\frac{3}{2}A(y_1)} f_0^L(y_1)$, as a function of the input parameters ν and kL_1 .

Let us now discuss the couplings of the fermion zero-modes to the Higgs and gauge boson KK modes in this model. The gauge couplings are given by

$$\begin{aligned} \mathcal{L} &\supset g_5 \int dy e^{-3A} \bar{\psi} \mathcal{A} \psi = \sum_{mnr} \frac{g_5}{\sqrt{y_1}} \int dy e^{-3A} \frac{f_L^{(n)} f_L^{(m)} f_r^A}{y_1} \bar{\psi}_L^{(n)} \mathcal{A}^{(r)} \psi_L^{(m)} + (L \rightarrow R) \\ &\equiv \sum_{mnr} g_{nmr}^L \bar{\psi}_L^{(n)} \mathcal{A}^{(r)} \psi_L^{(m)} + (L \rightarrow R), \end{aligned} \quad (2.133)$$

whereas the Yukawa couplings can be computed from

$$\begin{aligned} \mathcal{L} &\supset Y_5 \int dy e^{-4A} \bar{Q}_L H U_R + (L \leftrightarrow R) \\ &= \sum_{mn} \frac{Y_5}{\sqrt{y_1}} \int dy e^{-4A} \frac{f_L^{Q(n)} f_\xi^{(0)} f_R^{U(m)}}{y_1} \bar{q}_L^{(n)} h u_R^{(m)} + (L \leftrightarrow R) + \dots \equiv \lambda_{mn}^{LR} \bar{q}_L^{(n)} h u_R^{(m)} + \dots, \end{aligned} \quad (2.134)$$

³In the limit in which $y_s \rightarrow y_1$ there could be problems of strong coupling similar to the ones present in soft-wall models [154], and a y -dependent mass term might be necessary [155] (see [156] for other realizations of flavor in soft-wall models).

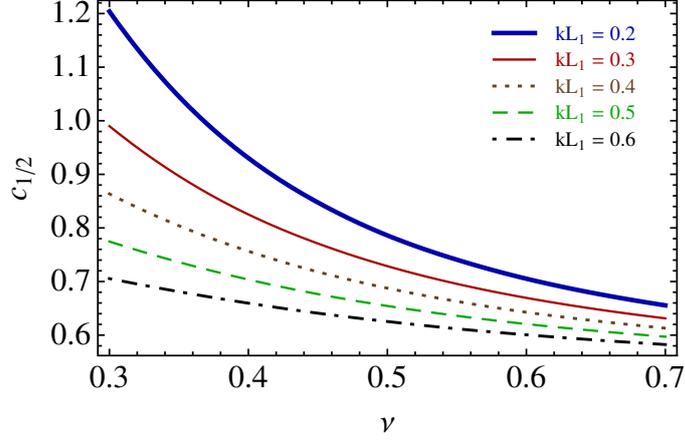


Figure 2.4: Value of the localization parameter, $c_{1/2}$, that makes a LH fermion zero-mode mostly delocalized, as a function of ν and for different values of kL_1 .

where we have defined $h \equiv \xi^{(0)}(x)$. The 5D gauge coupling can be fixed by matching the coupling of the gauge zero-mode to the observed 4D coupling. Assuming a tree-level matching this gives

$$g_5 = \sqrt{y_1} g_4. \quad (2.135)$$

For the 5D Yukawa coupling, Ref. [157] finds, based on NDA [158], that its maximum value is given by

$$Y_5 \leq Y_5^{\max} \approx \frac{4\pi}{\sqrt{3k}}, \quad (2.136)$$

which corresponds to strong coupling at a scale of the third KK level. We plot in the left panel of Fig. 2.5 the Yukawa coupling between the zero-modes of a $[++]$ fermion Q , and a $[--]$ fermion T , assuming $Y_5 = Y_5^{\max}$, as a function of a common localization parameter $c = c_Q = -c_T$. In the right panel we show the coupling of a LH fermion zero-mode to the first two gauge boson KK

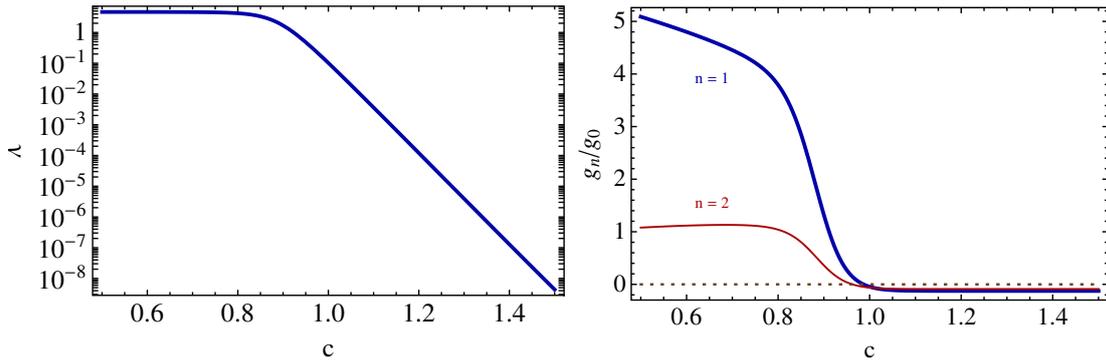


Figure 2.5: Left panel: Yukawa coupling, $\lambda \equiv \lambda_{00}^{LR}$, as a function of the bulk mass for $c_L = -c_R = c$ and a 5D Yukawa coupling that saturates the maximum value given in Eq. (2.136). Right panel: coupling of a LH fermion zero-mode to the first two gauge boson KK modes in units of $g_0 \equiv g_5/\sqrt{y_1}$. In both cases we have taken $\nu = 0.4$ and $kL_1 = 0.2$, which lead to maximally delocalized fermions for $c \approx 0.93$.

modes divided by the coupling to the gauge boson zero-mode (assuming tree level matching) as a function of c . We have chosen $\nu = 0.4$, and $kL_1 = 0.2$ in both plots. We see the change of behavior around $c_{1/2} \approx 0.93$, which corresponds to the most delocalized zero-mode fermion profile (see Fig. 2.4).

For $c \gtrsim c_{1/2}$, we see that the Yukawa coupling becomes exponentially suppressed. Furthermore, in the same region the coupling to the gauge boson KK modes becomes almost universal (i.e. independent of c). Thus, as for the pure AdS₅ case, the assumption that the light fermions are exactly localized on the UV brane is an excellent approximation (as far as EWPT are concerned) in these models.

2.2.3 Electroweak Constraints

If flavor is explained by means of localization in the extra dimension, the effects of NP in models with WED are almost universal and can therefore be encoded in the oblique parameters introduced in [82], with the most important exception being the couplings of the bottom quark. This can be most easily seen with holographic methods. However, the collider implications of these models are easier to understand if we discuss how the corrections are generated in the physical basis (i.e. the KK basis). A general discussion of EWPT in models with WED and the equivalence of different methods to compute them is given in [159]. Here we follow the equivalent notation in [119] to make the comparison easier. Let us start by studying the calculability of such effects in the present class of models.

As already emphasized, the present class of models does not have a custodial symmetry to protect the Peskin-Takeuchi T parameter, nor the corrections to certain gauge-fermion couplings. As a result, it is possible to write a term in the bulk that violates the custodial symmetry, $\mathcal{L}_5 \supset (\kappa/\Lambda^3) |H^\dagger D_M H|^2$, where we wrote the coefficient in units of the 5D cutoff, Λ . The dimensionless factor, κ , is UV sensitive. However, when the Higgs propagates in the bulk, the one-loop contributions are finite by power-counting. To see this, it is simplest to use a normalization where the gauge bosons, W_M , have mass dimension 1 [we write the kinetic term as $(-1/4g_5^2) W_{MN}^a W^{aMN}$]. Then, the contributing diagrams are simply proportional to g_5^4 or y_5^4 , where both the 5D (top) Yukawa coupling, y_5 , and the 5D gauge coupling have mass dimension $-1/2$. (We show in the upper-left corner of Fig. 2.6 an example diagram with a fermion loop.) It follows that the piece proportional to $\eta_{\mu\nu}$ in the loop integral has mass dimension -1 , and therefore it is IR dominated. Subtracting the zero-mode contribution, the remainder is controlled by the scale \tilde{k}_{eff} . At two-loop order, an example of which is shown in lower-left corner of Fig. 2.6, the diagram is *logarithmically* divergent by power counting.

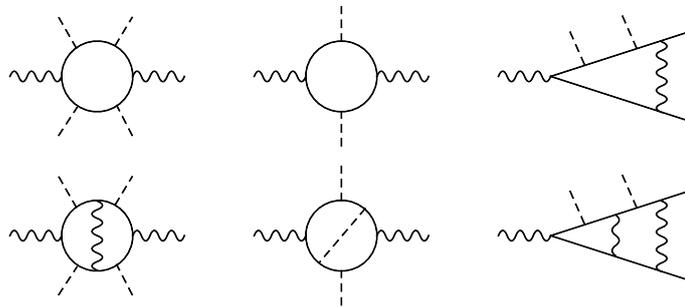


Figure 2.6: Examples of radiative corrections to the oblique parameters, as well as to the non-oblique vertex corrections. The most important contributions arise from the top KK tower in the loop. Upper row, left to right: one-loop contributions to T , S and δg_{b_L} , respectively. Lower row: examples of the corresponding two-loop contributions.

A similar point has been made in connection to the S -parameter when the Higgs is taken as a bulk field.⁴ The middle diagram in the upper row of Fig. 2.6 is finite, while at 2-loop order a *logarithmic* UV sensitivity is encountered (e.g. in the middle diagram of the lower row of Fig. 2.6), corresponding to the bulk operator $H^\dagger \sigma^a H W_{MN}^a B^{MN}$. Similar remarks apply to “vertex corrections” of the form $(H^\dagger D_M H)(\bar{\Psi} \Gamma^M \Psi)$ or $(H^\dagger \sigma^a D_M H)(\bar{\Psi} \Gamma^M \sigma^a \Psi)$. Examples of 1- and 2-loop contributions to these vertex corrections are shown in the right column of Fig. 2.6. We also note that operators localized on the branes (corresponding either to T , S or δg_{b_L}) can be induced only at three (and higher-order) loop order.

We conclude that just allowing the Higgs to propagate in the bulk can make the oblique parameters effectively calculable: the incalculable pieces associated with the 5D local operators above are suppressed compared to the finite, one-loop contribution roughly by M_{KK}/Λ . In the particular models studied here, the localization properties of the Higgs, to be discussed in the next subsection, imply that the couplings of the Higgs to the KK fermion or gauge states are suppressed compared to the situation in an AdS_5 background. In fact, for the favored region of parameter space such couplings are well in the perturbative regime (thus resembling more closely the case of flat rather than typical WED). However, although higher-order contributions due to Yukawa or weak gauge couplings can be expected to be further suppressed, there remains some uncertainty associated with higher order QCD contributions. As we will see in detail below, one of the effects of the departure from AdS_5 of the gravitational background is to push the KK modes closer to the IR brane. This effect increases the coupling among KK modes, thus reducing the scale of strong coupling in the QCD sector. This is reminiscent of the position dependent cut-off in soft-wall models [153, 154], and affects the EW observables at two-loop and higher order.⁵ Nevertheless, we find that the finite one-loop contributions to the EW observables—especially to T —can be significant, and therefore one should not neglect such loop effects. To get a concrete idea about their impact on the EW fit and the resulting bounds on the KK scale, we will assume that the QCD strong coupling scale is high enough to make the 5D description a reasonable approximation. Furthermore we will assume that 2-loop and higher-order QCD effects do not dramatically change the one-loop results. One should, however, keep in mind that QCD effects may not be negligible.

The Oblique Corrections at Tree Level

We perform now a detailed analysis of the EW precision constraints in the class of models without custodial symmetries under discussion. In this subsection we focus on the *oblique* analysis at *tree level* (which was already performed in [119]), and in the next one we take the most important non-oblique contribution into account, i.e. the correction to the $Z b_L \bar{b}_L$ coupling, as well as the one-loop contributions. This will allow us to better understand the impact of the various effects. Let us start with the gauge KK modes. The effects of NP can be classified in three types: corrections to the gauge boson self-energies, to fermion-gauge couplings and to four-fermion interactions. Each of these effects is characterized by the previously mentioned coefficients $\hat{\alpha}$, $\hat{\beta}$ and $\hat{\gamma}$, respectively. For the present case, only gauge bosons obeying Neumann boundary conditions on both branes are relevant, in which case one has [119]

$$\begin{aligned}\hat{\alpha} &= \int_0^{y_1} dy e^{2A(y)} \left(\Omega_h(y) - \frac{y}{y_1} \right)^2, \\ \hat{\beta} &= \int_0^{y_1} dy e^{2A(y)} \left(\Omega_h(y) - \frac{y}{y_1} \right) \left(\Omega_f(y) - \frac{y}{y_1} \right), \\ \hat{\gamma} &= \int_0^{y_1} dy e^{2A(y)} \left(\Omega_f(y) - \frac{y}{y_1} \right)^2.\end{aligned}\tag{2.137}$$

⁴K. Agashe, private communication. See also [152].

⁵A smaller hierarchy in the spirit of the Little RS model [160] would reduce the tension with the low QCD cut-off and increase the coupling of the KK gluon to light quarks, thus having an important impact on collider phenomenology.

The function $\Omega(y)$ is defined by⁶

$$\Omega_i(y) \equiv \frac{1}{y_1} \int_0^y d\tilde{y} \omega_i(\tilde{y}), \quad \omega_i(y) \equiv \begin{cases} e^{-2A(y)} f_{i,0}^2(y), & \text{scalars} \\ e^{-3A(y)} f_{i,0}^2(y), & \text{fermions} \end{cases}, \quad (2.138)$$

where $f_{i,0}(y)$ is the wave function for the scalar or fermion zero-modes (see previous sections). With our normalization we have $\Omega_i(y_1) = 1$. Besides of the oblique corrections due to the KK states given by Eq. (2.138), we also include the Higgs contribution to S and T , given by [84]

$$\Delta S = \frac{1}{2\pi} [g(m_h^2/m_Z^2) - g(m_{\text{ref}}^2/m_Z^2)], \quad (2.139)$$

$$\Delta T = -\frac{3}{16\pi c_W^2} [f(m_h^2/m_Z^2) - f(m_{\text{ref}}^2/m_Z^2)], \quad (2.140)$$

where

$$g(y) = \int_0^1 dx x(5x-3) \ln(1-x+xy), \quad (2.141)$$

$$f(y) = y \frac{\ln c_W^2 - \ln y}{c_W^2 - y} + \frac{\ln y}{c_W^2(1-y)}, \quad (2.142)$$

and we take $m_{\text{ref}} = 115$ GeV in the fit.

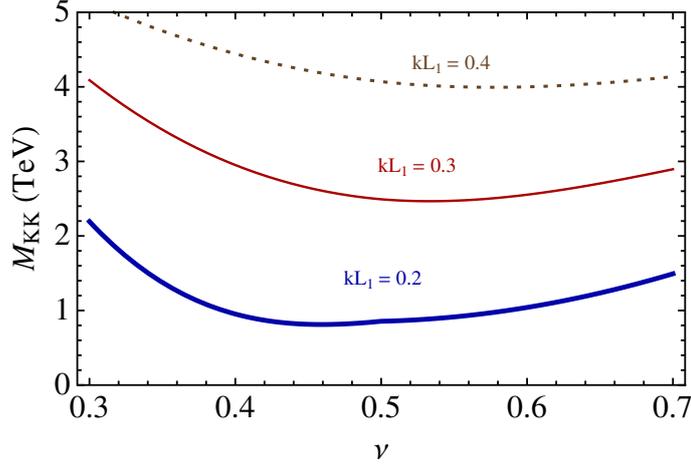


Figure 2.7: 95% CL lower bound on the mass of the first KK gauge boson, obtained from a *tree-level oblique* analysis. We assume UV localized fermions and different values of the input parameters ν and kL_1 . See text for details on the fit procedure.

We show in Fig. 2.7 the result of a fit to the oblique parameters when all fermions are assumed to live on the UV brane for different values of the input parameters ν and kL_1 . We have used an updated version of the code in [79], obtaining the bounds as follows. For fixed values of ν and kL_1 (i.e. for a fixed metric background), we compute the minimum of the χ^2 , including only the Z -pole observables,⁷ as a function of the Higgs mass (imposing the direct LEP bound of ≈ 114 GeV)

⁶The $\omega_i(y)$ are nothing but the (square of the) “physical wavefunction” profiles, i.e. the profiles with warp factors taken out, as dictated by dimensional analysis (which just redshift all mass scales appropriately).

⁷These are the 26 observables associated with the W mass (two measurements), the Z-line shape and lepton forward-backward asymmetries (8), heavy flavor (6), effective $\sin^2 \theta_W$ (2), and 8 leptonic/strange quark polarization asymmetries. We do not fit the SM parameters, but only those associated with the new KK physics.

and the value of the IR scale \tilde{k}_{eff} . We then fix the Higgs mass to its value at the minimum and compute the bound on \tilde{k}_{eff} by requiring $\Delta\chi^2 = 3.84$ (95% CL for one degree of freedom). The resulting value of the first gauge boson KK mode mass (see Fig. 2.3) is plotted as a function of ν for different values of kL_1 . We see that masses as light as ~ 1 TeV are allowed for $kL_1 = 0.2$ and $\nu \sim 0.45$. This plot reproduces the results presented in [119] up to small differences ($\lesssim 100$ GeV), due to the different fit procedure.

The departure from the AdS₅ background has several effects that go in the right direction to improve the EWPT. The first is that the KK gauge bosons are more strongly localized towards the IR brane whereas the Higgs, although localized towards the IR brane, reaches a maximum *before* the IR brane [the “physical” Higgs wavefunction is given by $\sqrt{\omega_h(y)} \approx e^{-A(y)} e^{aky}$, and the suppression near the IR brane arises from the nearby singularity in $A(y)$]. This reduces, sometimes dramatically, the gauge mixing through the Higgs vev, and therefore the contribution to the \hat{T} parameter (and somewhat less the \hat{S} parameter). This effect can be observed in Fig. 2.8, in which we show the “physical” profiles $\sqrt{\omega}$ of Eq. (2.138), for the Higgs, the first gauge KK mode, and for bulk fermion zero-modes with three different values of the bulk masses. The maximum of the Higgs profile before the IR brane is evident, together with the very strong localization of the first gauge KK mode, leading to a reduced value of the relevant overlap integral.

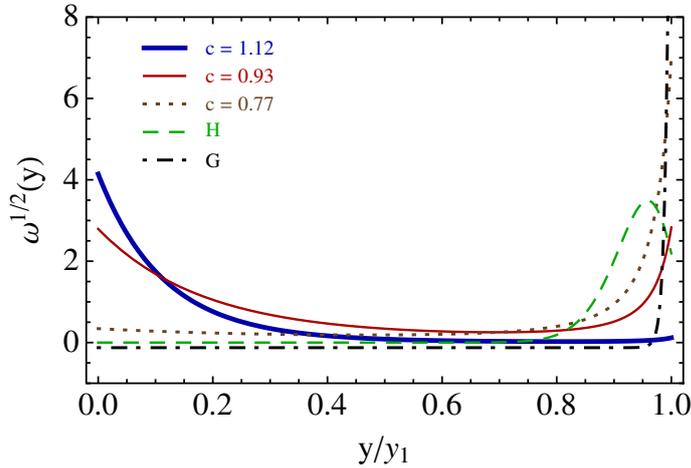


Figure 2.8: Fermion zero-mode, Higgs and first gauge KK mode profiles, $\sqrt{\omega}(y)$ for $\nu = 0.4$ and $kL_1 = 0.2$.

The second effect of the warp factor is that the coupling of UV localized fermions to gauge KK modes is reduced with respect to the standard AdS₅ case. This further reduces the \hat{S} parameter (but will also have a negative impact on collider searches). In Fig. 2.9 we show the value of the coupling of UV localized fermions to the first gauge boson KK mode (in units of $g_0 = g_5/\sqrt{y_1}$) for different values of ν and kL_1 . Only for small values of ν and large values of kL_1 does one approach the coupling of the AdS₅ background. Note that for the values preferred by the EWPT (see Fig. 2.7) this coupling is reduced to almost half the AdS₅ value.

The Effects of the Third Generation

Let us now consider the effect of the third quark generation. We consider three bulk fermion fields with the following quantum numbers under the $SU(2)_L \times U(1)_Y$ gauge group and BC

$$Q = (2, 1/6) \sim [++], \quad T = (1, 2/3) \sim [--], \quad B = (1, -1/3) \sim [--], \quad (2.143)$$

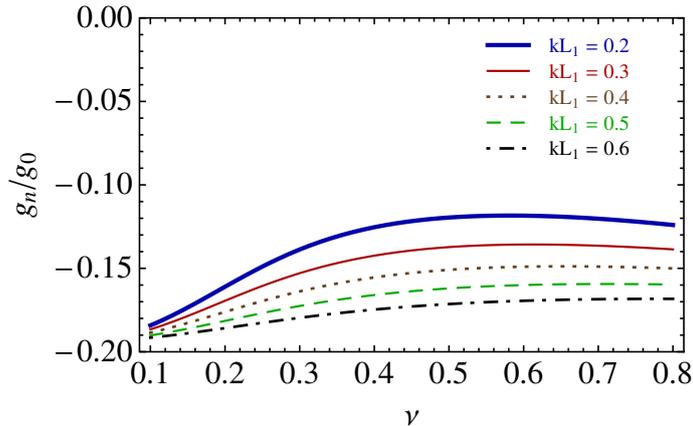


Figure 2.9: Couplings of UV localized fermions to the first-level KK gauge bosons, in units of the zero-mode gauge coupling. We show curves as a function of ν , and for different values of kL_1 .

with localization parameters c_Q , c_T and c_B , respectively. For fixed values of these localization parameters we can choose the 5D Yukawa couplings so that the top and bottom masses are reproduced. Due to the upper bound on Y_5 , the top mass cannot be generated if the Q and T zero-modes are far from the IR brane. The LH bottom, which is in the zero-mode of Q , can then receive large corrections to its couplings, from gauge and fermion KK modes. Anomalous contributions to the $Zb_L\bar{b}_L$ coupling can therefore impose stringent constraints in warped models without custodial protection. The general expression for the *tree-level* correction to the $Zb_L\bar{b}_L$ coupling induced by the gauge boson KK modes is given in [159]. For our model it reads

$$\delta g_{b_L} = -\frac{g^2 v^2}{2c_W^2} \left[\frac{g^2}{2} + \frac{g'^2}{6} \right] (\hat{\beta}_Q - \hat{\beta}_{UV}), \quad (2.144)$$

where the term proportional to $\hat{\beta}_{UV}$ corresponds to the universal part that is absorbed in the oblique parameters. To this we have to add the *tree-level* fermionic contribution, that we have computed exactly by diagonalizing numerically the KK fermion mass matrix, and computing the resulting coupling to the Z of the lightest mass eigenstate (the bottom quark). We will consider the one-loop effects separately.

In order to test the dependence of the constraints on the assumptions on the 5D Yukawa couplings we have taken the following benchmark scenarios. For each value of ν and kL_1 and each value of c_Q we fix c_T so that the top mass is reproduced (including the effect of the mixing with fermion KK modes) assuming that $Y_5^t = Y_5^{\max}$ (**scenario 1**). We note that, due to the maximum of the Higgs profile, there is a fixed value of c_T for which the overlap is maximal and therefore the 5D Yukawa coupling is minimal. Therefore, we also consider the case that Y_5^t is the minimal one for which it is possible to reproduce the correct top mass (**scenario 2**). Regarding the bottom sector, we consider three different scenarios by fixing the 5D bottom Yukawa to $Y_5^b = Y_5^t$ (**scenario a**), $Y_5^b = Y_5^t/5$ (**scenario b**), $Y_5^b = Y_5^t/10$ (**scenario c**). Scenario *a* assumes exact anarchy whereas in the other two we allow for deviations between different Yukawas.

We have studied the tree-level effect of third generation quarks on EWPT by performing a scan over ν and kL_1 . For each value of these parameters, we have computed the maximum value of c_Q that allows to generate the top mass (i.e. the furthest from the IR brane). We have then scanned over the values of c_Q smaller than this maximal value for the six different scenarios (1a, 1b, 1c, 2a, 2b, 2c) described above. The fit has been performed as in the case of the gauge contribution, described in the previous subsection, but including now the constraint from the $Zb_L\bar{b}_L$ coupling described above. Fixing c_Q and marginalizing over the Higgs mass, we find the

value of \tilde{k}_{eff} that gives $\Delta\chi^2 = 3.84$, corresponding to 95% CL for one degree of freedom. In all cases the preferred value of the Higgs mass is close to its current lower limit $m_h \approx 114$ GeV. We show in Fig. 2.10 a sample result for $\nu = 0.4$ and $kL_1 = 0.2$. We display, based on a tree-level analysis, the 95% CL lower bound on the mass of the first gauge KK mode as a function of c_Q for all six scenarios, and also the result of the fit when all fermions are localized on the UV brane as considered in [119] (horizontal line denoted by ST in the plot).

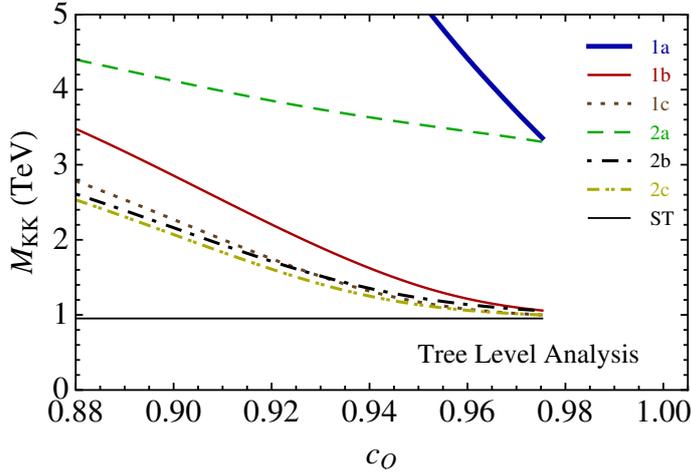


Figure 2.10: Tree-level 95% CL lower bound on the mass of the first gauge KK mode as a function of the localization of the LH top/bottom multiplet (c_Q) for the six scenarios discussed in the text. We fix $\nu = 0.4$ and $kL_1 = 0.2$. The lines end at the value of c_Q beyond which the top mass cannot be generated. For comparison we also show the result of the fit if the effects of third generation quarks are neglected (horizontal “ST” line). The maximal delocalization is obtained for $c \approx 0.93$ (see Fig. 2.4).

It is clear that the bound is very sensitive to the value of the localization of the LH top/bottom doublet as expected for a non-custodial model. The correction is smaller for a larger c_Q (the LH top/bottom further from the IR brane). The non-trivial result we find is that the top mass (just barely) allows c_Q to be large enough to make the corrections to the $Zb_L\bar{b}_L$ coupling negligible (the lines in the figure end at the point of c_Q beyond which the top mass cannot be generated). Unfortunately, loop effects change this conclusion, as discussed below. The other property that is clear from the plot is that exact anarchy (scenarios 1a and 2a) is extremely constrained by EWPT. The reason is that the Yukawa couplings in the bottom sector are very large and the mixing with the bottom KK modes induces very large corrections to the $Zb_L\bar{b}_L$ coupling. However, we see that a suppression in the 5D bottom Yukawa by a factor of 5 is already enough to get the bound on the scale of NP reasonably low. We have also checked that the $\bar{t}_R\gamma^\mu b_R W_\mu^+$ coupling is in these cases typically $\lesssim 10^{-4}$ (in units of $g/\sqrt{2}$) and should therefore cause no trouble with $b \rightarrow s\gamma$ constraints [161].

As mentioned previously, the one-loop contributions to T , S and δg_{b_L} are finite (while at two-loop order, they are logarithmically divergent). We have computed these one-loop effects using the methods described in [151], and show a numerical example in Fig. 2.11. Here we have taken a gravitational background with $\nu = 0.4$ and $kL_1 = 0.2$, and we have assumed scenario 2c defined above. Recall that scenarios 2 are such that the 5D Yukawa coupling is the minimal one that still allows to reproduce the top quark mass, for given c_Q . In this sense, these scenarios minimize the size of these one-loop effects, which are controlled by this coupling. We see in the figure that the one-loop contribution to the T parameter can be significant, and imposes an upper bound

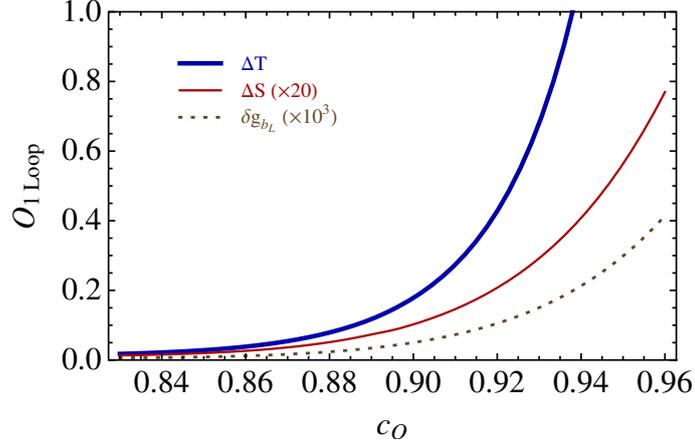


Figure 2.11: One-loop contribution to T , S and δg_{b_L} , as a function of c_Q , in scenario 2c (see text). We take $\nu = 0.4$ and $kL_1 = 0.2$.

on c_Q that is stronger than the one coming from the top mass itself. By contrast, the one-loop contributions to S and δg_{b_L} are relatively small (in the figure we show $20 \times S$ and $10^3 \times \delta g_{b_L}$). This constraint is in tension with the one due to the (tree-level) modification of the $Zb_L\bar{b}_L$ coupling. We show in the left panel of Fig. 2.12 the resulting lower bound on the KK gluon mass corresponding to **scenario 2c**. The thick solid (blue) line corresponds to the fit procedure used at tree-level, i.e. evaluating $\Delta\chi^2 = 3.84$ with a Higgs mass that minimizes the total χ^2 . However, we also show the bounds on the KK scale assuming other fixed values of the Higgs mass (as would be appropriate if a Higgs of such a mass was actually discovered). We see from the thick solid blue curve that –marginalizing over m_h – a lower 95% CL bound of $M_{\text{KK}} \approx 2.3$ TeV is found for $c_Q \approx 0.88$. We note that for this c_Q one has $\chi^2_{\text{min}}/\text{dof} = 25.6/24$ at $(m_h, M_{\text{KK}}) = (114 \text{ GeV}, 4.3 \text{ TeV})$, which gives a goodness-of-fit with 37% likelihood. This results mainly from a compromise between the (tree-level) δg_{b_L} and the one-loop contribution to T . However, the black dot-dashed line shows that

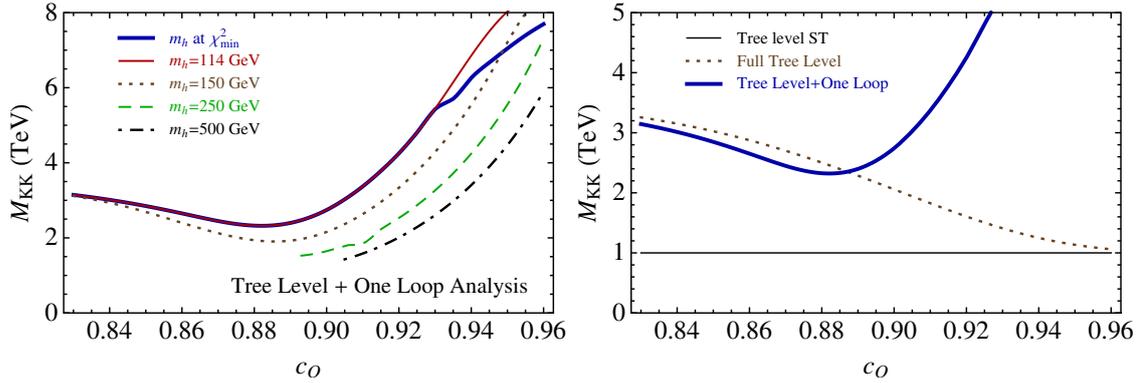


Figure 2.12: Left panel: 95% CL lower bound on the mass of the first gauge KK mode as a function of the localization of the LH top/bottom multiplet (c_Q) in scenario 2c, including one-loop effects. The different lines correspond to different values of m_h , with the one marked as “ m_h at χ^2_{min} ” corresponding to marginalization over m_h . The curves are terminated where the goodness-of-fit gives a 5% likelihood. Right panel: comparison of the tree-level oblique, full tree-level, and tree-level plus one-loop bounds on M_{KK} , assuming marginalization over m_h . In all cases, we fix $\nu = 0.4$ and $kL_1 = 0.2$.

for a heavier Higgs, with fixed $m_h = 500$ GeV, a KK gluon as light as 1.5 TeV (1.4 TeV) would be possible, which corresponds to the 95% CL contour about a best fit point with $\chi_{\min}^2/\text{dof} = 34/25$ ($\chi_{\min}^2/\text{dof} = 37.6/25$) leading to a 10% (5%) likelihood. Thus, it may be possible to have warped models with KK gluons around 1.5 TeV that fit the EW data reasonably well. As a summary plot that highlights the impact of the various contributions to the EW observables discussed above, we show in the right panel of Fig. 2.12 the bounds on the KK gluon mass, as a function of c_Q , for the EWPT fits at a) tree-level in the oblique approximation [thin solid black line], b) full tree-level [dotted brown line] and c) tree level plus one-loop [thick solid blue line]. In all cases we marginalize over m_h , although as just pointed out this may lead to an overly pessimistic conclusion in regards to how low M_{KK} could actually be. At any rate, it is clear from this figure that both the corrections to the $Zb_L\bar{b}_L$ coupling and the one-loop effects play an important role in determining the allowed M_{KK} .

We also point out that the models consistent with the EWPT up to one-loop order, which have a relatively low M_{KK} , always have KK fermion Yukawa couplings that are *perturbative*. For instance, at the minimum of the solid thick blue curve in Fig. 2.12, with $M_{\text{KK}} \approx 2.3$ TeV, the 4D Yukawa couplings of the form $h\bar{Q}_L^{(n)}t_R^{(n)}$ are all $\mathcal{O}(1)$, while the off-diagonal ones (i.e. coupling different KK levels) are much less than one (becoming smaller the further apart the masses of the two KK modes).⁸ This is a result of the suppression in overlap integrals associated with the non-trivial profile of the Higgs field, much as in the KK gauge/Higgs couplings illustrated in Fig. 2.8. Thus, higher order (divergent) effects involving additional powers of Yukawa couplings are expected to be suppressed. The most important effects that remain are associated with QCD higher-order corrections, as mentioned when we analyzed the calculability. Thus, the above results should be taken as an illustration of how light the KK resonances can reasonably be, as far as the EW precision constraints are concerned.

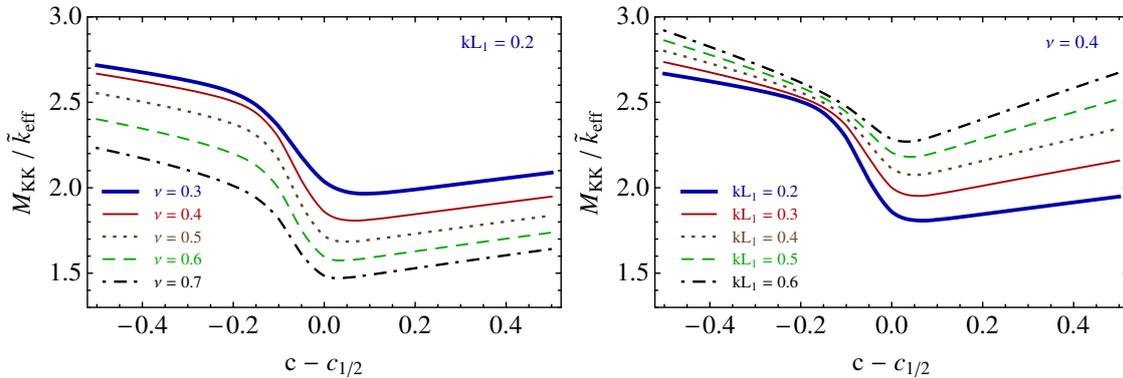


Figure 2.13: Mass of the first fermion KK mode for a $[++]$ field in units of \tilde{k}_{eff} as a function of its localization parameter (with respect to the mostly delocalized value) for values of $\nu = 0.3, 0.4, 0.5, 0.6, 0.7$ (top to bottom, left panel) and $kL_1 = 0.2, 0.3, 0.4, 0.5, 0.6$ (bottom to top, right panel).

These results have important implications for collider searches. First, the absence of custodial symmetry implies a quite minimal spectrum of massive modes. In particular, very light fermions [7, 8, 113, 131, 162], natural in custodial models are not expected in the model under study. We show in Fig. 2.13 the mass of the first fermion KK mode of a $[++]$ field as a function of the localization parameter c for different values of ν and kL_1 . These figures, together with Fig. 2.3 show that, in

⁸By contrast, scenarios 1 have diagonal 4D Yukawa couplings for the KK fermions of order 3–4, and always lead to a very large one-loop contribution to T , unless M_{KK} is above $\mathcal{O}(10)$ TeV. In such cases, higher-order contributions associated with the Yukawa interactions may not be suppressed, and can have a large impact on the EW analysis. Nevertheless, barring tuned cancellation between these and the UV contributions, one expects that the KK resonances will be out of the LHC reach in such scenarios.

some cases, the first KK gluon can decay into a top (or bottom) and a heavy fermion. Second, masses lighter than previously considered in models with WED (with semi-anarchic Yukawas) may be allowed by EWPT. This result is very sensitive to the localization of the third generation quarks which determine the coupling of the top and bottom quarks to the gauge KK modes, as well as the KK fermion Yukawa couplings. We show in Fig. 2.14 the couplings of the different quarks to the first KK gluon in units of $g_0 = g_5/\sqrt{y_1}$ for scenario 2, with $\nu = 0.4$ and $kL_1 = 0.2$. We see that the largest is the coupling to $t_R\bar{t}_R$, followed by $Q_L\bar{Q}_L$ and then to light quark pairs. Thus, the KK gluon decays dominantly into RH top pairs (or, perhaps, a channel involving one KK fermion and the associated zero-mode), bearing some resemblance to the scenario of Ref. [163]. However, the reduced couplings to the light quarks can make the discovery more challenging, for a given M_{KK} .

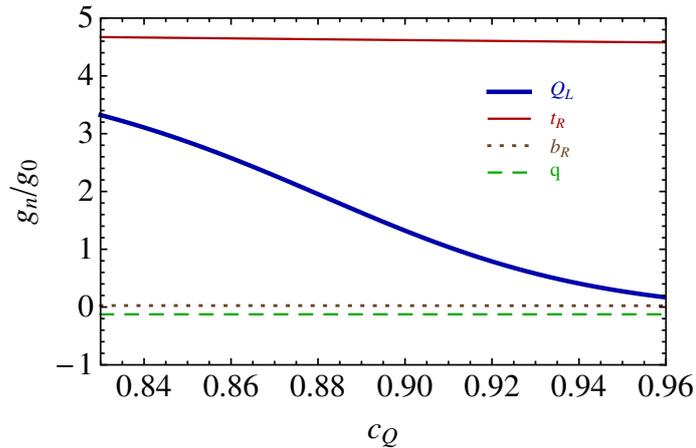


Figure 2.14: Couplings to the first gauge KK mode (in units of $g_0 = g_5/\sqrt{y_1}$) of the third generation LH quarks Q_L , RH top t_R , RH bottom b_R , and light quarks q , as a function of c_Q , for scenario 2 (sub-scenarios *a*, *b* and *c* give similar results for the couplings). We fix $\nu = 0.4$ and $kL_1 = 0.2$. The localization parameters c_T , c_B and the top and bottom masses have been fixed as described in the text. The b_R and q couplings are almost identical.

2.2.4 Phenomenological Implications

In what follows we will present the main collider implications of some selected points in parameter space. As we have seen in the previous section, the EW fit prefers models of type **2**, which always have the KK gluons relatively strongly coupled to t_R (see Figs. 2.12 and 2.14). Thus, the $t\bar{t}$ decay channel for the KK gluon is always dominant. To illustrate the expected signal at the LHC, we consider two models, as suggested by the analysis in the previous section.

The first one corresponds to scenario **2c** with $\nu = 0.4$, $kL_1 = 0.2$ and $c_Q = 0.88$. With $m_h = 114$ GeV, we find a $\chi^2/\text{dof} = 25.6/24$, giving a likelihood of 37%. This fit is only slightly worse than the SM one: the total χ^2 is slightly reduced, but there is one additional degree of freedom, corresponding to \tilde{k}_{eff} . The KK gluon mass is

$$M_{\text{KK}} \approx 2.3 \text{ TeV} \quad (95\% \text{ CL}) . \quad (2.145)$$

We also find that the first KK resonance of the third generation quark $SU(2)_L$ doublet has a mass $M_Q \approx 2.1$ TeV, while the first KK resonance of the bottom $SU(2)_L$ singlet has a mass $M_B \approx 1.85$ TeV. Both are sufficiently light for the decays $G^{(1)} \rightarrow Q_L^{(0)}\bar{Q}_L^{(1)}$ and $G^{(1)} \rightarrow b_R^{(0)}\bar{B}_R^{(1)}$

to be open. The corresponding couplings to fermion pairs are

$$g_{Q_L} \approx 1.95g_s, \quad g_{t_R} \approx 4.63g_s, \quad g_{b_R} \approx 0.02g_s, \quad g_q \approx -0.13g_s, \quad (2.146)$$

$$g_{q_L, Q_L^{(1)}} \approx 3.85g_s, \quad g_{b_R, B_R^{(1)}} \approx 1.15g_s, \quad (2.147)$$

where we omitted the superscripts for the zero modes, and the first line refers to SM fermion pairs. The first KK resonance of the top $SU(2)_L$ singlet is heavier than the KK gluon, so that this channel is kinematically closed. However, the first KK resonances of all the remaining SM fermions are lighter than the KK gluon, and are therefore open as decays of the form $G^{(1)} \rightarrow q^{(0)}q^{(1)}$. Nevertheless, the relevant couplings are all significantly smaller than g_s , so that these are somewhat rare decays that, in spite of the multiplicity, do not change appreciably the width of the KK gluon. With the above couplings, we find that $\Gamma_{G^{(1)}} \approx 710$ GeV, and that the KK gluon has the following branching fractions:

$$\text{BR}(G^{(1)} \rightarrow t\bar{t}) \approx 0.81, \quad \text{BR}(G^{(1)} \rightarrow b\bar{b}) \approx 0.12, \quad \text{BR}(G^{(1)} \rightarrow q\bar{q}) \approx 0.005, \quad (2.148)$$

$$\text{BR}(G^{(1)} \rightarrow t_L^{(1)}t) \approx 0.02, \quad \text{BR}(G^{(1)} \rightarrow b_L^{(1)}b) \approx 0.04, \quad \text{BR}(G^{(1)} \rightarrow b_R^{(1)}b) \approx 0.01, \quad (2.149)$$

where in the last line both conjugate processes (e.g. $G^{(1)} \rightarrow t_L^{(1)}\bar{t}$ and $G^{(1)} \rightarrow \bar{t}_L^{(1)}t$) are understood. The total $G^{(1)}$ production cross section is ~ 21 fb (~ 160 fb) at a center of mass energy of 7 TeV (14 TeV).

The second model has instead $c_Q = 0.906$ which, with $m_h = 500$ GeV, leads to $\chi^2/\text{dof} = 34/25$, giving a likelihood of 10% (still reasonably large). The KK gluon mass is now

$$M_{\text{KK}} \approx 1.5 \text{ TeV} \quad (95\% \text{ CL}), \quad (2.150)$$

while the first KK resonance of the third generation quark $SU(2)_L$ doublet has a mass $M_Q \approx 1.3$ TeV, and the first KK resonance of the bottom $SU(2)_L$ singlet has a mass $M_B \approx 1.2$ TeV. The corresponding couplings to fermion pairs are

$$g_{Q_L} \approx 1.17, \quad g_{t_R} \approx 4.62, \quad g_{b_R} \approx -0.03g_s, \quad g_q \approx -0.13g_s, \quad (2.151)$$

$$g_{q_L, Q_L^{(1)}} \approx 3.16g_s, \quad g_{b_R, B_R^{(1)}} \approx 1.15g_s. \quad (2.152)$$

Now we have $\Gamma_{G^{(1)}} \approx 390$ GeV and the following branching fractions:

$$\text{BR}(G^{(1)} \rightarrow t\bar{t}) = 0.83, \quad \text{BR}(G^{(1)} \rightarrow b\bar{b}) = 0.05, \quad \text{BR}(G^{(1)} \rightarrow q\bar{q}) = 0.005, \quad (2.153)$$

$$\text{BR}(G^{(1)} \rightarrow t_L^{(1)}t) \approx 0.03, \quad \text{BR}(G^{(1)} \rightarrow b_L^{(1)}b) \approx 0.06, \quad \text{BR}(G^{(1)} \rightarrow b_R^{(1)}b) \approx 0.02. \quad (2.154)$$

The total $G^{(1)}$ production cross section is ~ 0.2 pb (~ 1.3 pb) at a center of mass energy of 7 TeV (14 TeV).

The branching ratios in these models are relatively similar to the benchmark of Ref. [163], but with lighter masses and reduced couplings to the light quarks. Note, however, that the first model has a non-negligible branching fraction into bottom pairs, and that there are “exotic” channels involving a KK fermion with branching ratios at the few percent level (in the case of the third generation; for the first two generations the corresponding branching ratios are expected to be much smaller, although the precise values depend on the details of how flavor is implemented).

We have implemented these models in MADGRAPH/MADEVENT v4 [164], using PYTHIA 6 [165] for hadronization and showering and PGS4 [166] for detector simulation. We use the **CTEQ6L1** parton distribution function, with the QCD renormalization and factorization scales equal to the central m_T^2 of the event. We show in Fig. 2.15 the expected $t\bar{t}$ invariant mass distribution at the LHC, at the partonic level. The left (right) panel corresponds to the second (first)

model above at $\sqrt{s} = 7$ TeV ($\sqrt{s} = 14$ TeV). In both plots we represent the SM prediction with a red dotted line and the prediction of the model (including the interference with the SM $t\bar{t}$ contribution) in solid blue. Also, just to guide the eye, we show the contribution assuming only the KK gluon exchange as a purple dashed line. Although the lightest mass case shows a slight excess over background, these results suggest that extracting the signal will be challenging.

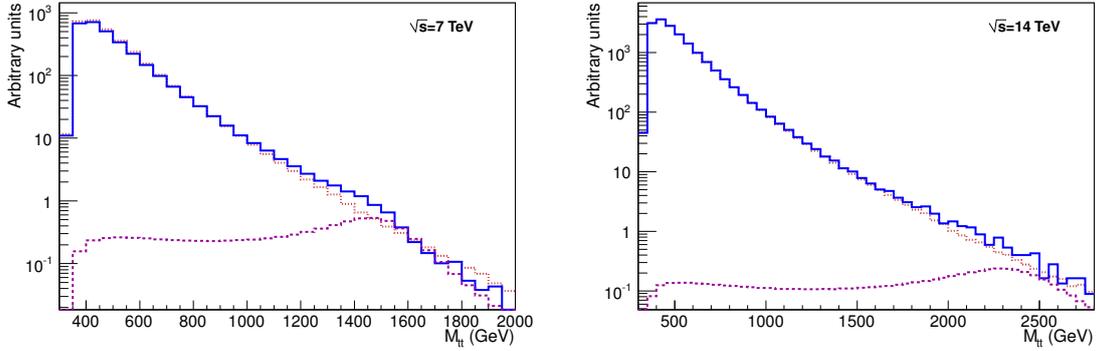


Figure 2.15: $t\bar{t}$ invariant mass distribution in the SM (red dotted), in the model with extra-dimensional physics (solid blue) and the contribution of just the KK gluon exchange (dashed purple). The left panel corresponds to a KK gluon with $M_{\text{KK}} \approx 1.5$ TeV and the couplings of Eqs. (2.151)-(2.152). The right panel corresponds to $M_{\text{KK}} \approx 2.3$ TeV and the couplings of Eqs. (2.146)-(2.147).

2.3 Gauge-Higgs Unification Models

As it was mentioned in the previous chapter, the main problem of how EWSB is realized in the SM is that a fundamental scalar develops a quadratic sensitive to any UV energy threshold. In other words, it is unnatural for a scalar to be much lighter than any other scale of the theory. In principle, one could naively argue that this is not a problem in the SM, since it is a renormalizable theory without any mass scale above the top mass. However, at some point, we should take into account gravity, which becomes strongly coupled at the Plank scale M_{Pl} . Moreover, even without resorting to gravity, we know that triviality and stability bounds [167] put, for almost every value of the Higgs mass, a UV cut-off above which EWSB becomes meaningless.

One way to alleviate this problem is finding a symmetry protecting the Higgs mass. This is the case, for instance, of GHU models, where the Higgs doublet is identified with the massless KK mode of the scalar component of some 5D gauge fields, $A_5^{\hat{a}}(x, z)$, $\hat{a} = 1, 2, 3, 4$. The 5D gauge symmetry prevents the Higgs to acquire a mass at the tree level, with one-loop corrections being finite and UV insensitive as they involve non-local contributions proportional to the interbrane distance [168]. Let us study in more detail the precise mechanism of EWSB in these models and the changes with respect to usual WED models.

Let us assume a WED compactified on an interval \mathcal{I} , with the following AdS₅ metric,

$$ds^2 = \left(\frac{R}{z}\right)^2 (dx^\mu dx^\nu \eta_{\mu\nu} - dz^2), \quad (2.155)$$

where $R \leq z \leq R'$ is the coordinate of the extra dimension, with R and R' the positions of the UV and IR branes, respectively. The bulk gauge group G is broken by the following boundary

conditions to the subgroups H_0 and H_1 on the UV and IR brane, respectively,

$$A_\mu^a(+,+), \quad T^a \in \text{Alg}\{H\}, \quad (2.156)$$

$$A_\mu^{\bar{a}}(+,-), \quad T^{\bar{a}} \in \text{Alg}\{H_0/H\}, \quad (2.157)$$

$$A_\mu^{\hat{a}}(-,+), \quad T^{\hat{a}} \in \text{Alg}\{H_1/H\}, \quad (2.158)$$

$$A_\mu^{\hat{a}}(-,-), \quad T^{\hat{a}} \in \text{Alg}\{G/(H_0 \cup H_1)\}, \quad (2.159)$$

where $H = H_0 \cap H_1$, and $+$ ($-$) denotes a Neumann (Dirichlet) boundary condition for the vector part of the 5D gauge boson, with A_5 having the opposite boundary conditions⁹ [134].

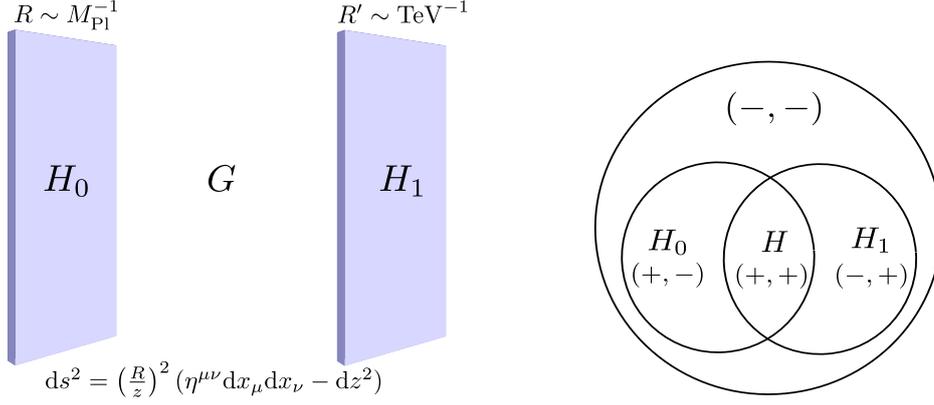


Figure 2.16: Left: Bulk gauge symmetry breaking on the different branes. Right: Boundary conditions for the vector component of the corresponding 5D gauge bosons.

According to this pattern of gauge symmetry breaking, the scalar component of the bulk gauge bosons corresponding to the generators $T^{\hat{a}} \in \text{Alg}\{G/(H_0 \cup H_1)\}$ satisfy Neumann boundary conditions, which allows the presence of a massless KK mode. If $\dim(G/(H_0 \cup H_1)) = 4$, we can, in principle, identify these zero modes with the Higgs doublet. In the unitary gauge, all the massive KK modes for the scalar components are gauged away, remaining just these zero modes $A_5^{(0)\hat{a}}(x)$ with profiles $f_0^{\hat{a}}(z)$ satisfying

$$\partial_z a(z) f_0^{\hat{a}}(z) = \frac{\kappa}{z}, \quad \partial_z a(z) f_0^{\hat{a}}(z)|_{z=R,R'} = 0, \quad (2.160)$$

or, equivalently,

$$\partial_z \left(\frac{f_0^{\hat{a}}(z)}{z} \right) = 0. \quad (2.161)$$

The solution is

$$f_0^{\hat{a}}(z) = \frac{z}{N^{\hat{a}}} = \sqrt{\frac{2/R}{1 - (R/R')^2}} \frac{z}{R'} \cong \sqrt{\frac{2}{R}} \frac{z}{R'}, \quad (2.162)$$

where $N^{\hat{a}}$ is obtained normalizing canonically the Higgs kinetic terms,

$$\left[\int_R^{R'} dz \left(\frac{R}{z} \right) \left(\frac{z}{N^{\hat{a}}} \right)^2 \right] \frac{1}{2} \partial_\mu A_5^{\hat{a}}(x) \partial^\mu A_5^{\hat{a}}(x) = \frac{1}{2} \partial_\mu A_5^{\hat{a}}(x) \partial^\mu A_5^{\hat{a}}(x). \quad (2.163)$$

⁹We will work in the unitary gauge, where this corresponds to the limits $v_{1,2} \rightarrow 0$ and ∞ , respectively.

As we have just seen, the Higgs doublet is a bulk field with profile $f_0^{\hat{a}}(z) = z/N^{\hat{a}}$. Nevertheless, in GHU models, we can perform a field redefinition, identical to a gauge transformation saving one brane, that locally removes the Higgs from the action except for this brane. In the new basis, the Higgs does not appear in the bulk action but only in a boundary condition, which can be easily implemented. We can therefore compute non-linear effects of the Higgs due to its Goldstone boson nature. For the sake of concreteness, let us consider the local transformation which removes the Higgs except at the IR brane,

$$\rho(z, v) = \exp \left[-ig_5 v T^{\hat{a}_0} \int_R^z ds \frac{s}{N^{\hat{a}_0}} \right], \quad (2.164)$$

where \hat{a}_0 is fixed to the $\text{Alg}\{G/(H_0 \cup H_1)\}$ component acquiring the Higgs vev and g_5 is the corresponding 5D gauge coupling. This transformation relates the solutions of the bulk gauge equations in the absence of Higgs vev, $f_n^\alpha(z, 0)$, with the ones arising in his presence [137],

$$f_n^\alpha(z, v) T^\alpha = \rho^{-1}(z, v) f_n^\alpha(z, 0) T^\alpha \rho(z, v), \quad \alpha = a, \bar{a}, \dot{a}, \hat{a}, \quad (2.165)$$

where

$$A_\mu^\alpha(x, z) = \sum_n f_n^\alpha(z, v) A_\mu^{(n)\alpha}(x), \quad (2.166)$$

and

$$[a(z)m_n^2 + \partial_z a(z)\partial_z] f_n^\alpha(z, 0) = 0. \quad (2.167)$$

The UV boundary conditions are the same for $f_n^\alpha(z, v)$ and $f_n^\alpha(z, 0)$, since $\rho(R, v) = 1$, but they differ on the IR brane, where $\rho(R', v)$ mixes different gauge profiles $f_n^\alpha(z, 0)$. Analogously, fermions will be transformed according with

$$f_{L,R}^{(n)k}(z, v) = A \rho A^{-1} f_{L,R}^{(n)k}(z, 0), \quad (2.168)$$

where A is a matrix taking into account possible changes of basis arising from different choices for $f_{L,R}^{(n)k}$ and T^α and

$$P_{L,R} \zeta_k(x, z) = \sum_n f_{L,R}^{(n)k}(z, v) \zeta_k^{(n)}(x), \quad (2.169)$$

with

$$[\mathcal{O}_{-c_k} \mathcal{O}_{c_k} + m_n^2] f_L^{(n)k}(z, 0) = 0, \quad (2.170)$$

$$[\mathcal{O}_{c_k} \mathcal{O}_{-c_k} + m_n^2] f_R^{(n)k}(z, 0) = 0. \quad (2.171)$$

In the same way, boundary conditions on the IR brane will mix different fermion profiles $f_{L,R}^{(n)k}(z, 0)$ (of both chiralities) through $\rho(R', v)$, with UV boundary conditions remaining the same.

Thanks to the 5D gauge symmetry, which forbids any possible tree-level potential for $A_5^{\hat{a}}(x, z)$, there is no tree-level mass for the Higgs doublet. Therefore, the Higgs mass arises radiatively at one loop from diagrams like Fig. 2.17 and, since it involves non-local contributions from one brane to the other, the result is finite and cut-off insensitive [133].

We can understand better this behavior using the AdS_5/CFT correspondence, which leads in this case to composite Higgs models [134, 135, 170]. In the dual picture of general AdS_5 models, a bulk gauge group G corresponds to a global symmetry group in a CFT. The breaking of this bulk gauge group by boundary conditions on the IR brane is described in the CFT as the SSB $G \rightarrow H_1$

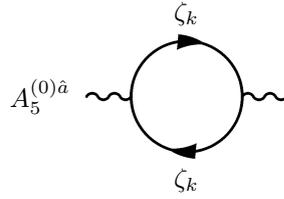


Figure 2.17: Fermion contribution to the one-loop Higgs mass in GHU models.

by strong dynamics, at the scale $\Lambda \sim R'^{-1} \sim \text{TeV}$. On the other hand, the symmetry breaking $G \rightarrow H_0$ on the UV brane is understood in the dual picture as the result of weakly gauging the subgroup H_0 at the Planck scale through the interaction with an elementary sector invariant under H_0 , which explicitly breaks the global symmetry G ,

$$\mathcal{L} = \mathcal{L}_{\text{CFT}} - \frac{1}{4} F_{\mu\nu}^\alpha F^{\mu\nu\alpha} + A_\mu^\alpha J^{\mu\alpha} + \varphi \cdot \mathcal{O}_\varphi, \quad \alpha = a, \bar{a}, \quad (2.172)$$

where φ represents any elementary field coupled to the CFT theory and coming in a representation of H_0 ; the dual transcription of any bulk field with $[+]$ boundary condition on the UV brane.

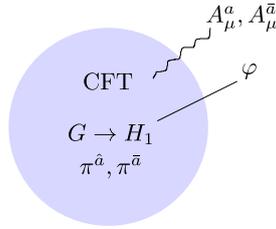
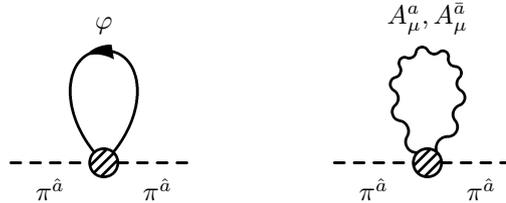


Figure 2.18: Schematic representation of the CFT interpretation of GHU models.

In principle, the SSB of G to the subgroup H_1 delivers $\dim(G/H_1)$ NGB, $\pi^{\hat{a}}, \pi^{\bar{a}}$. However, those corresponding to quotient group H_0/H , $\pi^{\bar{a}}$, are eaten by the external elementary gauge bosons $A_\mu^{\bar{a}}$ weakly coupled to the CFT. The remaining are pseudo NGB, which are massless at tree-level but acquire mass at one-loop through the interaction with the elementary sector, see Fig. 2.19, leading to

$$m_\pi^2 = m_h^2 \sim \frac{g_{\text{el}}^2}{16\pi^2} \Lambda^2, \quad (2.173)$$

where $g_{\text{el}} \ll 16\pi^2$. Therefore, analogously to what happens with pions in QCD, we can explain in this way the small hierarchy existing between the Higgs mass and the compositeness scale $\Lambda \sim \mathcal{O}(1)$ TeV.


 Figure 2.19: One-loop diagrams giving mass to the pseudo NGB $\pi^{\hat{a}}$ in the CFT.

2.4 Higgsless Models

As we have discussed, bulk gauge symmetries can be broken by boundary conditions in models with extra dimensions. We have also learned that it is possible to give masses to the different fermions through boundary mass terms modifying the original boundary conditions, with no need for a finite Higgs vev. Therefore, in the framework of models with extra dimensions, we could think of implementing EWSB in the same way, avoiding the introduction of a bulk or a boundary Higgs. The only two questions are whether such a model can replace the SM Higgs contribution to EWPT and to longitudinal gauge boson scattering. As we will see in a while, this is in fact possible up to some cut-off scale $\Lambda \lesssim \text{few TeV}$, where a more fundamental theory should complete the model.

Let us consider the elastic scattering of two equal KK modes $A_\mu^{(n)}(x)$, whose tree-level diagrams are shown in Fig. 2.20.

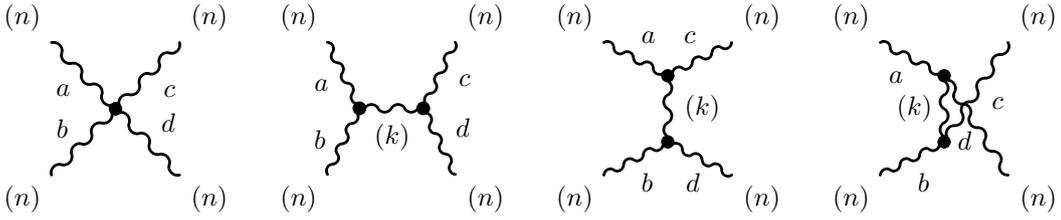


Figure 2.20: Tree-level diagrams contributing to the elastic scattering $A_\mu^{(n)a} + A_\mu^{(n)b} \rightarrow A_\mu^{(n)c} + A_\mu^{(n)d}$.

If we call E the incoming energy in the center of mass frame and m_n the mass of n 'th KK gauge mode (supposing that all the external KK modes in the process satisfy the same boundary conditions and, therefore, $m_{n,\alpha} = m_n$, with $\alpha = a, b, c, d$, being the the gauge index), the elastic scattering amplitude can be written as follows [124]

$$\mathcal{A} = \mathcal{A}^{(4)} \left(\frac{E}{m_n} \right)^4 + \mathcal{A}^{(2)} \left(\frac{E}{m_n} \right)^2 + \mathcal{A}^{(0)} + \mathcal{O}\left(\frac{m_n^2}{E^2}\right), \quad (2.174)$$

where the incoming and outgoing momentum vectors are

$$p_\mu = (E, 0, 0, \pm\sqrt{E^2 - m_n^2}), \quad \text{and} \quad p'_\mu = (E, \pm\sqrt{E^2 - m_n^2}s_\theta, 0, \pm\sqrt{E^2 - m_n^2}c_\theta), \quad (2.175)$$

respectively, and we have defined $s_\theta = \sin\theta$ and $c_\theta = \cos\theta$, with θ the scattering angle. The coefficients $\mathcal{A}^{(4)}$ and $\mathcal{A}^{(2)}$ read

$$\mathcal{A}^{(4)} = i \left((g_{nnnn}^{abcd})^2 - \sum_k (g_{nnk}^{abe})^2 \right) (f^{abe} f^{cde} (3 + 6c_\theta - c_\theta^2) + 2(3 - c_\theta^2) f^{ace} f^{bde}), \quad (2.176)$$

$$\begin{aligned} \mathcal{A}^{(2)} = & \frac{i}{m_n^2} f^{ace} f^{bde} \left(4(g_{nnnn}^{abcd})^2 m_n^2 - 3 \sum_k (g_{nnk}^{abe})^2 m_{k,e}^2 \right) - \frac{i}{2m_n^2} f^{abe} f^{cde} \left(4(g_{nnnn}^{abcd})^2 m_n^2 \right. \\ & \left. - 3 \sum_k (g_{nnk}^{abe})^2 m_{k,e}^2 + \left(12(g_{nnnn}^{abcd})^2 m_n^2 + \sum_k (g_{nnk}^{abe})^2 (3m_{k,e}^2 - 16m_n^2) \right) c_\theta \right), \end{aligned} \quad (2.177)$$

where we have used the cubic and quartic gauge couplings,

$$g_{nmk}^{abc} = g_5 \int_R^{R'} dz a(z) f_n^a(z) f_m^b(z) f_k^c(z), \quad (2.178)$$

$$(g_{nmkl}^{abcd})^2 = g_5^2 \int_R^{R'} dz a(z) f_n^a(z) f_m^b(z) f_k^c(z) f_l^d(z), \quad (2.179)$$

with g_5 the 5D gauge coupling. As mentioned before, in the above expressions we are assuming that all the incoming and outgoing gauge bosons satisfy the same boundary conditions, which means in particular that the n index is blind to the gauge one. The equation of motion for an arbitrary KK mode reads

$$[a(z)m_{k,\alpha} + \mathcal{O}(z)] f_k^\alpha(z) = 0, \quad \mathcal{O}(z) = \partial_z a(z) \partial_z. \quad (2.180)$$

If the boundary conditions are such that the operator $\mathcal{O}(z)$ is hermitian, i.e, $(f, \mathcal{O}(z)g) = (\mathcal{O}(z)f, g)$, for f and g solving the gauge bulk equation of motion and

$$(f, g) = \int_R^{R'} dz f^*(z)g(z), \quad (2.181)$$

the different eigenvectors satisfy orthonormality,

$$\int_R^{R'} dz a(z) f_k^\alpha(z) f_l^\alpha(z) = \delta_{kl}, \quad (2.182)$$

and completeness relations,

$$\sum_k a(z) f_k^\alpha(z) f_k^\alpha(z') = \delta(z - z'), \quad (2.183)$$

respectively. In particular, this last condition implies that

$$(g_{nnnn}^{abcd})^2 = \sum_k (g_{nnkk}^{abe})^2, \quad (2.184)$$

and therefore $\mathcal{A}^{(4)} = 0$.

Let us check that this is indeed the case. Integrating by parts twice, we obtain

$$\begin{aligned} (f, \mathcal{O}(z)g) &= \int_R^{R'} dz f^*(z) \partial_z a(z) \partial_z g(z) = a(z) f^*(z) \partial_z g(z) \Big|_R^{R'} - \int_R^{R'} dz a(z) \partial_z f^*(z) \partial_z g(z) \\ &= a(z) (f^*(z) \partial_z g(z) - \partial_z f^*(z) g(z)) \Big|_R^{R'} + (\mathcal{O}(z)f, g) = (\mathcal{O}(z)f, g), \end{aligned} \quad (2.185)$$

where, in the last step, we have used that the boundary term vanishes for $f(z)$ and $g(z)$ satisfying boundary conditions (2.58) and (2.59). In particular, if $[a(z)m_{k,\alpha} + \mathcal{O}(z)] f_k^\alpha(z) = 0$ and $[a(z)m_{l,\alpha} + \mathcal{O}(z)] f_l^\alpha(z) = 0$, then

$$\begin{aligned} (f_k^\alpha, \mathcal{O}(z) f_l^\alpha) &= -m_{l,\alpha} \int_R^{R'} dz a(z) f_k^{\alpha*}(z) f_l^\alpha(z), \\ (\mathcal{O}(z) f_k^\alpha, f_l^\alpha) &= -m_{k,\alpha} \int_R^{R'} dz a(z) f_k^{\alpha*}(z) f_l^\alpha(z). \end{aligned} \quad (2.186)$$

Thus, the hermiticity of $\mathcal{O}(z)$ leads to

$$(m_{k,\alpha} - m_{l,\alpha}) \int_R^{R'} dz a(z) f_k^{\alpha*}(z) f_l^\alpha(z) = 0 \implies \int_R^{R'} dz a(z) f_k^{\alpha*}(z) f_l^\alpha(z) = 0, \quad \forall k \neq l. \quad (2.187)$$

In general, as $f_k^\alpha(z)$ can be taken real, we can forget about the complex conjugate, obtaining the usual orthonormality relation

$$\int_R^{R'} dz a(z) f_k^\alpha(z) f_l^\alpha(z) = \delta_{kl}. \quad (2.188)$$

Finally, the orthonormality of eigenvectors will give the completeness relations leading to Eq. (2.184). This very equation allows us also to simplify the expression for $\mathcal{A}^{(2)}$,

$$\mathcal{A}^{(2)} = \frac{i}{m_n^2} \left(4 (g_{nnnn}^{abcd})^2 m_n^2 - 3 \sum_k (g_{nnk}^{abe})^2 m_{k,e}^2 \right) (f^{ace} f^{bde} - s_{\theta/2}^2 f^{abe} f^{cde}). \quad (2.189)$$

It can be shown [124] that

$$4 (g_{nnnn}^{abcd})^2 m_n^2 - 3 \sum_k (g_{nnk}^{abe})^2 m_{k,e}^2 = 0, \quad (2.190)$$

up to some boundary terms, which are also zero in the cases of Neumann or Dirichlet boundary conditions, i.e., $v_{1,2} \rightarrow 0$ or ∞ .

We have just seen that, thanks to the 5D gauge invariance, the contributions coming from terms growing with the energy in the elastic scattering amplitude cancel out, with no need of an extra scalar field. Nevertheless, that does not mean that the unitarity problem is automatically solved. In principle, $\mathcal{A}^{(0)}$ could be too big and spoil unitarity. This happens if R'^{-1} , which fixes the scale of the first KK modes, is too heavy and the contributions of the massive excitations regulating the elastic scattering arrive too late, when unitarity is already broken. As R and R' are related by the W mass, see Fig. 2.21-*left*, the mass of the first KK resonances can also be described in terms of the extra-dimensional curvature R . Looking at the right panel of the same figure we realize that, for $R \sim M_{\text{Pl}}^{-1}$, the first KK gauge excitations appear around 1.2 TeV, falling below the TeV for larger values of R . Even at ~ 1.2 TeV, the four-point vertices obtained after integrating out these states are enough to cancel the E^4 terms in the elastic scattering of longitudinal gauge bosons [125]. These same resonances also unitarize the E^2 contributions which otherwise would explode around 1.8 TeV.

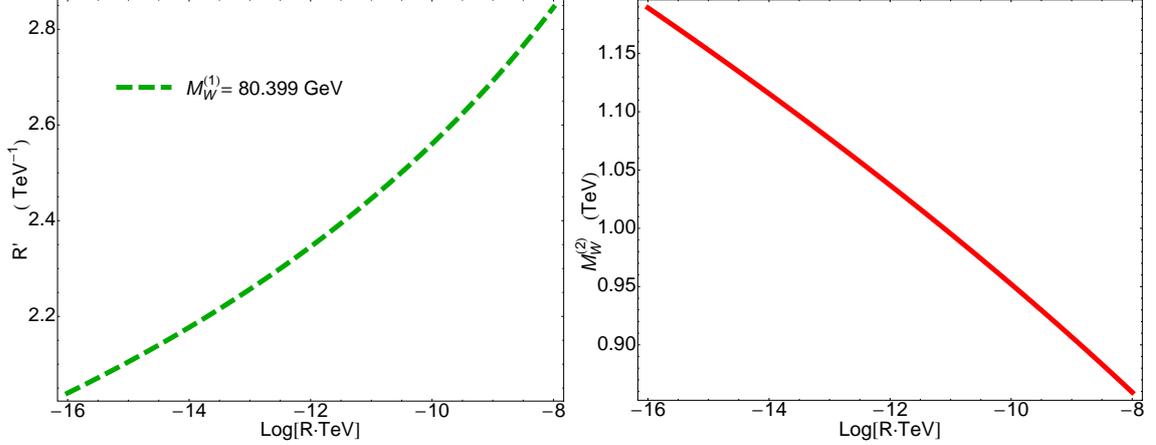


Figure 2.21: Left: In dashed green, contour plot for values of R and R' reproducing the observed W mass, in the Higgsless model introduced in [125]. Right: In the same model, $M_W^{(2)}$ mass in function of R , once $M_W^{(1)}$ is matched to $M_W = 80.399 \text{ GeV}$ by choosing the proper R value.

Other issue is related with the increasing number of KK modes in the model when the energy grows. This concerns the inelastic scattering amplitude, as we will find more and more possible final states as we increase the energy. Taking into account both effects [169], we get a cut-off scale Λ above which the theory is not longer valid. It can be shown that it is roughly given¹⁰ by the

¹⁰Up to a numerical factor $\sim 1/4$ according to Ref. [128].

naive dimensional analysis (NDA) cut-off [130], where perturbativity breaks down,

$$\Lambda_{\text{NDA}} \sim \frac{24\pi^3}{g_5^2} \frac{R}{R'} \sim \frac{12\pi^4}{g^2} \frac{M_W^{(1)2}}{M_W^{(2)}}. \quad (2.191)$$

In the above equation, $M_W^{(1)}$ is the mass of the first KK charged gauge boson, which will be matched to the observed W mass $M_W = 80.399$ GeV [44], while $M_W^{(2)}$ corresponds to the next KK excitation. According to this same equation, the smaller the mass $M_W^{(2)}$, the higher the cut-off scale Λ_{NDA} will be. Therefore, we can rise enough this scale by increasing R by several orders of magnitude. In principle, this will worsen the oblique corrections putting a bound on how much R can be augmented. However, values of R as large as 10^{-4} TeV $^{-1}$ are allowed, leading to resonances with masses of approximately 600 GeV [129].

In the next chapter we will introduce in more detail a realistic Higgsless model in WED and study the constraints coming from EWPT. We will see that it is possible to fulfill all of them in a custodial setup providing resonances below the TeV level.

3

Collider Implications of Top Compositeness

One of the primary goals of the LHC is the study of the precise mechanism of EWSB. Due to its large mass value, one could expect the top quark to play a major role in the understanding of this mechanism and to be somehow a bridge to any NP addressing the hierarchy problem. This is the case for instance in WED models, where the top quark is pushed towards the IR brane (where either the Higgs boson or the brane mass term giving mass to fermions in Higgsless models are localized), in order to reproduce its large mass. Since the KK excitations of gauge bosons and fermions are also localized towards the IR brane, its couplings with the top quark pair are naturally large. In the dual interpretation of AdS₅, that means that the top quark is partially composite, with sizable couplings with the CFT bound states. Thus, the top quark sector is an excellent place to look for NP. There are already hints of an anomaly in the $t\bar{t}$ forward-backward asymmetry $A^{t\bar{t}}$ at the Tevatron [171–174], which seems to point in this direction. However, other observables related to this measure as the total $t\bar{t}$ cross section or its invariant mass distribution are in very good agreement with the SM prediction, making an explanation of the anomaly in terms of NP challenging. There are also stringent constraints coming from dijet searches for new resonances or like-sign top pair production. Nevertheless, as we will prove in this chapter [2–4], light *axiguons* with large couplings to the quark sector and some of the extra vector-like quarks can still explain the observed asymmetry with no conflict with other Tevatron and LHC data. Interestingly enough, Higgsless models with WED naturally realize this scenario, providing all the necessary ingredients with no additional requirements. These vector-like excitations will be single produced with a SM quark, leading to different signatures according to their subsequent decays. In principle, they could decay into a EW gauge boson (W or Z) and a SM quark or produce the Higgs boson in addition to a SM fermion (if the Higgs exists). The decays into EW gauge bosons are always present and are a very promising discovery channel, leading to a quite interesting collider phenomenology. They are also rather model independent, unlike the Higgs case where, despite the recent LHC hints for its mass, we have by far more freedom and several different models can accommodate it. Thus, we will study in detail the collider signatures of a benchmark model in the first case, where the decays into the Higgs boson are absent. Nevertheless, in view of the recent *Higgs effort* the LHC community is going through and the very interesting collider signatures produced by Higgs decays, it is worth studying in some detail its collider searches for a particular class of models [5, 6]. First of all, we will start by introducing the mentioned $t\bar{t}$ forward-backward asymmetry $A^{t\bar{t}}$, as measured

by CDF and DØ, as well as the predicted SM value.

3.1 The $t\bar{t}$ Forward-Backward Asymmetry

The forward-backward asymmetry in top pair production is defined, in the $t\bar{t}$ rest frame, as follows

$$A^{t\bar{t}} = \frac{N(y_t^{t\bar{t}} > 0) - N(y_t^{t\bar{t}} < 0)}{N(y_t^{t\bar{t}} > 0) + N(y_t^{t\bar{t}} < 0)}, \quad y_t^{t\bar{t}} = \frac{1}{2} \ln \frac{E_t + p_t^z}{E_t - p_t^z}, \quad (3.1)$$

where $y_t^{t\bar{t}}$ is the top quark rapidity in the $t\bar{t}$ rest frame. Both experiments, CDF and DØ, use the *lepton+jets* topology, see Fig. 3.1, where one top quark decays leptonically ($t \rightarrow l\nu b$) while the other does it hadronically ($t \rightarrow q\bar{q}'b$).

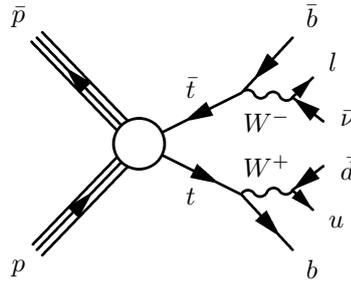


Figure 3.1: Lepton + jets topology used by CDF and DØ to define the $t\bar{t}$ forward-backward asymmetry $A^{t\bar{t}}$.

In the SM, such asymmetry arises at next to leading order (NLO) through the interference of the diagrams shown in Fig. 3.2. The interference of the tree-level and one-loop box diagrams shown above gives a positive contribution to $A^{t\bar{t}}$ while the interference of lower initial and final state radiation diagrams gives a contribution of the opposite sign.

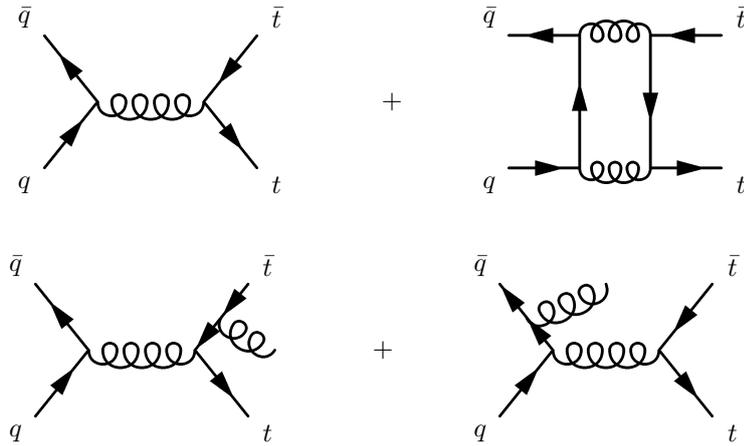


Figure 3.2: Above: Interference of the tree-level and one-loop box diagrams for $q\bar{q} \rightarrow t\bar{t}$. Below: Interference of initial and final state radiation diagrams in $q\bar{q} \rightarrow t\bar{t}j$.

The partonic prediction for the SM asymmetry at NLO computed by the event generator

POWHEG [176], reads in the $t\bar{t}$ rest frame [174]

$$A_{\text{SM}}^{t\bar{t}} = 0.066 \pm 0.020, \quad (3.2)$$

which shows a $\sim 2\sigma$ difference with the unfolded value obtained by CDF [174] using 8.7 fb^{-1} of $p\bar{p}$ collisions at $\sqrt{s} = 1.96 \text{ TeV}$,

$$A^{t\bar{t}} = 0.162 \pm 0.047. \quad (3.3)$$

These results are consistent with those measured at $D\bar{0}$, although the deviation observed in the latter is slightly smaller. In principle, in view of these numbers, it might seem that there is not a significance deviation from the SM prediction. However, CDF found a mass dependence on this asymmetry with larger deviations for higher invariant masses, as preferred by NP. Their results are shown in Table 3.1, where a $\sim 3\sigma$ difference can be observed for $M_{t\bar{t}} \geq 450 \text{ GeV}$. We can also see in Fig. 3.3, the invariance mass dependence plot for the CDF unfolded data and the SM NLO $t\bar{t}$ MC prediction.

	$A^{t\bar{t}}(M_{t\bar{t}} < 450 \text{ GeV})$	$A^{t\bar{t}}(M_{t\bar{t}} \geq 450 \text{ GeV})$
data	0.078 ± 0.054	0.296 ± 0.067
SM@NLO	0.047	0.100

Table 3.1: CDF results [174] for the $A^{t\bar{t}}$ forward-backward asymmetry for both the SM@NLO prediction and the unfolded data, for different regions of the $t\bar{t}$ invariant mass $M_{t\bar{t}}$.

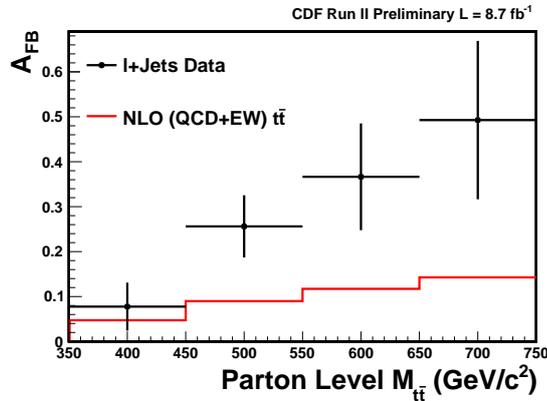


Figure 3.3: Invariant mass dependence of the $A^{t\bar{t}}$ forward-backward asymmetry for the SM@NLO $t\bar{t}$ and the CDF unfolded data for an integrated luminosity of 8.7 fb^{-1} , in the $t\bar{t}$ rest frame. Figure extracted from [174].

Unfortunately, as mentioned before, this deviation from the SM is not backed by other related observables, like the total $t\bar{t}$ cross section or the invariant mass distribution for top quark pairs or dijets. Nevertheless, as we will show later, there is still room for NP to explain the observed value for the forward-backward asymmetry. First of all, the large value measured at the Tevatron suggests that any NP behind it should be light. Moreover, as it must affect $t\bar{t}$ production while still being in agreement with its total cross section and invariant mass distribution, this NP should have axial couplings to either the top or the light quarks. In the case of a new massive gluon, the tree-level contribution to the forward-backward asymmetry is proportional to $-g_A^q g_A^t$ (with g_A^q

and g_A^t the axial components of the gauge couplings to the light quarks and the top, respectively), implying opposite-sign axial components of these gauge couplings to reproduce the positive value of the asymmetry. Finally, the large value observed for the asymmetry and the stringent constraints on contact interactions coming from dijet searches will naturally lead to small axial couplings to the light quarks and sizable couplings to one of the two top quiralities. We will show that all these ingredients, which can produce a large asymmetry while being consistent with other related observables, are naturally produced in the case of realistic Higgsless models.

3.2 A Realistic Higgsless Model

Let us consider a realistic Higgsless Model with flavor protection [131, 132]. As usual, the 4D Minkowski spacetime \mathcal{M}_4 is embedded in an slice of AdS_5 , with metric given by Eq. (2.2). The bulk gauge symmetry is $SU(3)_C \otimes SU(2)_L \otimes SU(2)_R \otimes U(1)_X$, broken by boundary conditions to $SU(3)_C \otimes SU(2)_L \otimes U(1)_Y$ on the UV brane and $SU(3)_C \otimes SU(2)_D \otimes U(1)_X$ on the IR.

If we denote by $G_M^\lambda, A_M^{La}, A_M^{Ra}$ and B_M the gauge bosons corresponding to $SU(3)_C, SU(2)_L, SU(2)_R$ and $U(1)_X$, respectively, with $\lambda = 1, 2, \dots, 8$, and $a = 1, 2, 3$, gauge indices, this breaking can be implemented, in the unitary gauge, with the following boundary conditions

$$\partial_z G_\mu^\lambda = \partial_z A_\mu^{La} = A_\mu^{R1,2} = 0, \quad \partial_z (g_{5R} B_\mu^{La} + \tilde{g}_5 A_\mu^{R3}) = 0, \quad \tilde{g}_5 B_\mu - g_{5R} A_\mu^{R3} = 0, \quad \text{at } z = R, \quad (3.4)$$

$$\partial_z G_\mu^\lambda = \partial_z (g_{5L} A_\mu^{La} + g_{5R} A_\mu^{Ra}) = 0, \quad g_{5L} A_\mu^{La} - g_{5R} A_\mu^{Ra} = 0, \quad \partial_z B_\mu = 0, \quad \text{at } z = R', \quad (3.5)$$

where g_{5L}, g_{5R} and \tilde{g}_5 are the 5D gauge couplings corresponding to $SU(2)_L, SU(2)_R$ and $U(1)_X$, respectively. Taking this into account, the KK expansion for the gauge bosons reads

$$G_\mu^\lambda(x, z) = \frac{1}{\sqrt{L}} g_\mu^\lambda(x) + \sum_{k=1}^{\infty} \psi_k^{(G)}(z) G_\mu^{(k)\lambda}(x), \quad (3.6)$$

$$B_\mu(x, z) = \frac{1}{\tilde{g}_5} a_0 A_\mu(x) + \sum_{k=1}^{\infty} \psi_k^{(B)}(z) Z_\mu^{(k)}(x), \quad (3.7)$$

$$A_\mu^{L3}(x, z) = \frac{1}{g_{5L}} a_0 A_\mu(x) + \sum_{k=1}^{\infty} \psi_k^{(L3)}(z) Z_\mu^{(k)}(x), \quad (3.8)$$

$$A_\mu^{R3}(x, z) = \frac{1}{g_{5R}} a_0 A_\mu(x) + \sum_{k=1}^{\infty} \psi_k^{(R3)}(z) Z_\mu^{(k)}(x), \quad (3.9)$$

$$A_\mu^{L\pm}(x, z) = \sum_{k=1}^{\infty} \psi_k^{(L\pm)}(z) W_\mu^{(k)\pm}(x), \quad (3.10)$$

$$A_\mu^{R\pm}(x, z) = \sum_{k=1}^{\infty} \psi_k^{(R\pm)}(z) W_\mu^{(k)\pm}(x), \quad (3.11)$$

where $g_\mu^\lambda(x)$ are the eight SM gluons, $A_\mu(x)$ is the photon and $Z_\mu^{(1)\pm}(x)$ and $W_\mu^{(1)\pm}(x)$ are the Z and W boson, respectively. The 5D profiles of the massless modes $g_\mu^\lambda(x)$ and $A_\mu(x)$ are flat, with constants obtained through canonical normalization of the respective kinetic term,

$$\frac{1}{a_0^2} = \left(\frac{1}{\tilde{g}_5^2} + \frac{1}{g_{5L}^2} + \frac{1}{g_{5R}^2} \right) L, \quad L = R \log \frac{R'}{R}. \quad (3.12)$$

As discussed in the previous chapter, in order to unitarize the elastic scattering of KK gauge bosons, the first KK level for the different gauge bosons must be below ~ 1 TeV scale. In particular, the first massive color octet, $G = G_\mu^{(1)\lambda}$, will have $m_G \lesssim 1$ TeV. To check EWPT we canonically

normalize the SM gauge fields and obtain, for a fixed value of R' , the parameters R , $g_{5L} = g_{5R}$ and \tilde{g}_5 in terms of the measured values of M_W , M_Z and the electromagnetic coupling $e(M_Z)$. We take the PDG's values [44], $M_W = 80.399$ GeV, $M_Z = 91.1876$ GeV and $e(M_Z) = \sqrt{4\pi}/128$. As the first KK gluon mass is given roughly by $m_G R' \sim 2.5$ we choose $R' = 2.5/0.850$ TeV $^{-1}$ obtaining $m_G = 0.848$ TeV.

Regarding fermions, we can consider that just the third quark generation is massive, neglecting the mass of the first two generations. They will live in $(2, 1)$ multiplets of $SU(2)_L \otimes SU(2)_R$ for the LH components and in $(1, 2)$ for the RH ones (they are all color triplets and have $Q_X = \frac{1}{6}$),

$$\Psi_l^k = \begin{pmatrix} u_l^k[+, +] \\ d_l^k[+, +] \end{pmatrix}, \quad \Psi_r^k = \begin{pmatrix} u_r^k[-, -] \\ d_r^k[-, -] \end{pmatrix}, \quad k = 1, 2. \quad (3.13)$$

Due to the absence of the brane mass terms required by massive fermions, the 5D profiles for the different light quarks will be given by the usual zero modes

$$f_{u_L, d_L}^{(0)k}(z) = \sqrt{\frac{1 - 2c_L}{R((R'/R)^{1-2c_L} - 1)}} \left(\frac{z}{R}\right)^{2-c_L}, \quad f_{u_R, d_R}^{(0)k}(z) = \sqrt{\frac{1 + 2c_R}{R((R'/R)^{1+2c_R} - 1)}} \left(\frac{z}{R}\right)^{2+c_R} \quad (3.14)$$

with $k = 1, 2$. In the above expressions, we have used that the flavor symmetry forces the localization of the two $(2, 1)$ multiplets to be the same and similarly for the $(1, 2)$ multiplets, meaning that $c_{\Psi_l^k} = c_L$ and $c_{\Psi_r^k} = c_R$, for $k = 1, 2$. The couplings to the Z boson are given by, see Fig. 3.4,

$$g_{q_L}^Z \bar{q}_L \gamma^\mu q_L Z_\mu = g_{5L} \mathcal{I}_l^{(L3)}(c_L) \bar{q}_L \left(T_L^3 + \frac{\tilde{g}_5 \mathcal{I}_l^{(B)}(c_L)}{g_{5L} \mathcal{I}_l^{(L3)}(c_L)} Y \right) \gamma^\mu q_L Z_\mu, \quad (3.15)$$

$$g_{q_R}^Z \bar{q}_R \gamma^\mu q_R Z_\mu = \bar{q}_R \left[\tilde{g}_5 \mathcal{I}_r^{(B)}(c_R) Y Z_\mu + \left(g_{5L} \mathcal{I}_r^{(R3)}(c_R) - \tilde{g}_5 \mathcal{I}_r^{(B)}(c_R) \right) T_R^3 \right] \gamma^\mu q_R Z_\mu, \quad (3.16)$$

where $q = u, d$ and

$$\mathcal{I}_l^X(c) = \sqrt{\frac{1 - 2c}{R((R'/R)^{1-2c} - 1)}} \int_R^{R'} dz \left(\frac{R}{z}\right)^{2c} \psi_1^{(X)}(z), \quad \mathcal{I}_r^X(c) = \mathcal{I}_l^X(-c). \quad (3.17)$$

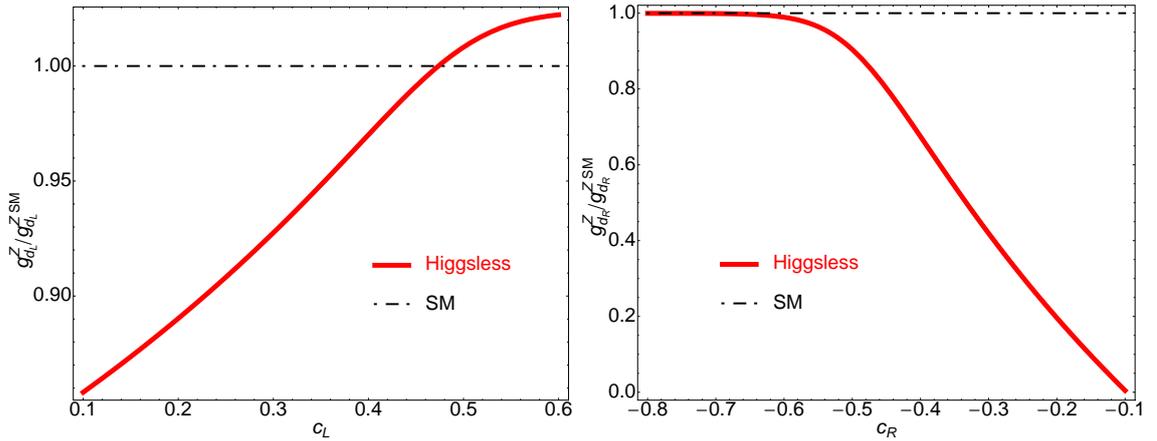


Figure 3.4: Left (right): Coupling of LH (RH) light down quarks to the Z boson, in the zero-mode approximation. In black dashed, the SM value.

Looking at Fig. 3.4 we can realize that, in order to fulfill constraints coming from EWPT, we need to localize the different chiralities of light generation quarks in opposite branes. As

the coupling $G\bar{q}q$ changes sign when the bulk mass parameter for light quarks pass through the conformal point (corresponding to $c_L = 0.5$ or $c_R = -0.5$), this will lead to opposite sign couplings for LH and RH quarks of the first two generations, see Fig. 3.5. In particular, choosing $c_L = 0.466$ and $c_R = -0.65$ we obtain the following shifts for the $Z\bar{d}d$ vertex

$$\delta g_{d_R}^Z/g_{d_R}^{Z SM} \sim -0.27\%, \quad \delta g_{d_R}^Z/g_{d_R}^{Z SM} \sim -0.30\%, \quad (3.18)$$

and similar deviations in the up sector. We consider these values reasonably compatible with EW precision data.¹ For these values of the bulk masses, the couplings to the KK gluon G are the following

$$g_R^q = -0.26g, \quad g_L^q = 0.19g. \quad (3.19)$$

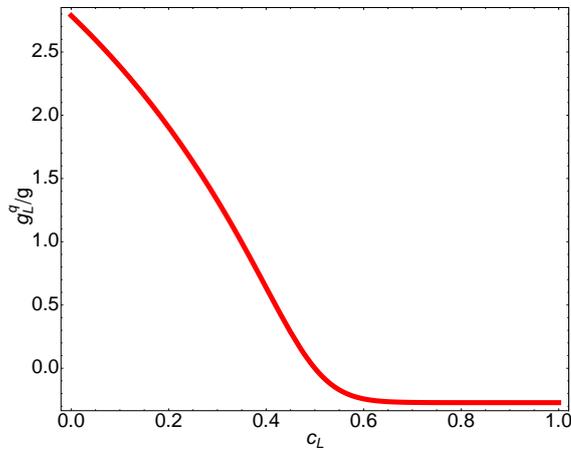


Figure 3.5: Coupling of LH light quarks to the first gluon excitation G , in the zero-mode approximation.

It is important to notice that the heavy gluon coupling to the light quarks tends to be almost purely axial and negative. Remarkably enough, this is just due to EWPT, having nothing to do with top data. However, we have to say that this is not a purely Higgsless behavior, being also present in the case of a finite Higgs vev, see Fig. 3.6. The special feature of Higgsless models is that, in order to unitarize the gauge boson elastic scattering, this massive gluon has to be *necessarily* light.

The third generation is in an almost custodially protected representation

$$\begin{aligned} \Psi_l^3 &= \begin{pmatrix} t_l[+, +] & X_l[-, +] \\ b_l[+, +] & T_l[-, +] \end{pmatrix} \sim (2, 2), & \Psi_r^3 &= \begin{pmatrix} X_r[+, -] \\ T_r[+, -] \\ b_r[-, -] \end{pmatrix} \sim (1, 3), \\ t_r[-, -] &\sim (1, 1). \end{aligned} \quad (3.20)$$

In this case all multiplets have $Q_X = \frac{2}{3}$ and the left and right columns of the bidoublet correspond to fields with $T_R^3 = \mp 1/2$ while the upper and lower components have $T_L^3 = \pm 1/2$. The boundary conditions for the third generation fields are changed on the IR brane due to the presence of the

¹It should be noted that higher dimensional operators could give a non-negligible contribution as could in general be needed to compensate for calculable one loop corrections in these models [177].

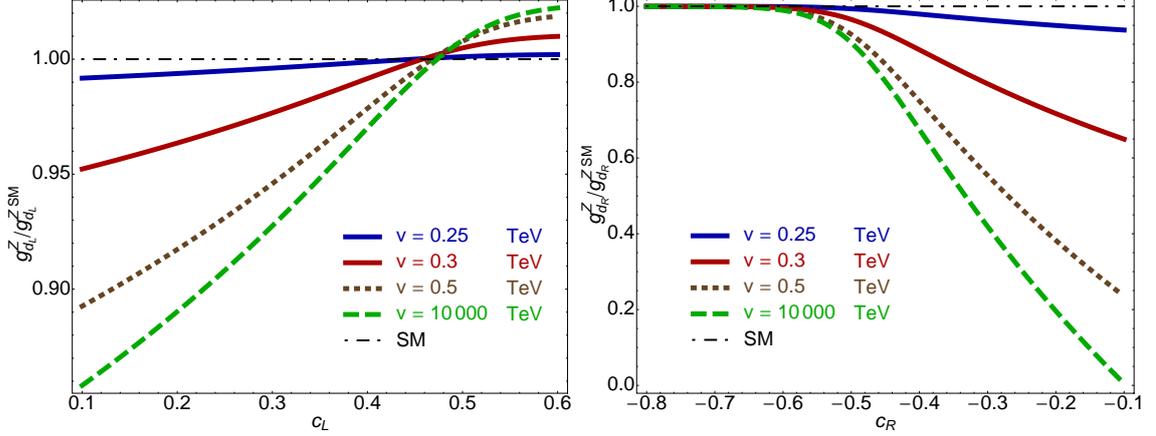


Figure 3.6: Left (right): Coupling of LH (RH) light down quarks to the Z boson, for different values of the Higgs vev. We have fixed R to the same value used in the realistic Higgsless model and, for each value of v , chosen R' and g_{5L} reproducing the W and Z mass. The case $v = 10000$ TeV can be identified with the Higgsless limit.

following localized mass terms

$$\begin{aligned}
 -\mathcal{S}_{IR} = & \int dx^4 \int_R^{R'} dz \left(\frac{R}{z}\right)^4 \delta(z - R') \left\{ M_3 \left[\frac{1}{\sqrt{2}} \psi_{T_r} (\chi_{t_l} + \chi_{T_l}) + \psi_{b_r} \chi_{b_l} + \psi_{X_r} \chi_{X_l} \right] \right. \\
 & \left. + \frac{M_1}{\sqrt{2}} \psi_{t_r} (\chi_{t_l} - \chi_{T_l}) \right\} + \text{h.c.} , \quad (3.21)
 \end{aligned}$$

where we denote with χ_Ψ ($\bar{\psi}_\Psi$) the LH (RH) component of field Ψ . These localized masses allow us to give a mass to the third generation of quarks and, as explained in [131], keep $Z\bar{b}_L b_L$ corrections under control. For each value of the bulk mass parameters $c_{\Psi_i^3}$, $c_{\Psi_r^3}$ and c_{t_r} , we fix M_1 and M_3 to reproduce the top and bottom masses, $m_t = 170$ GeV and $m_b = 4$ GeV. We find that the top mass cannot be generated, for any value of M_1 and M_3 , unless $c_{\Psi_i^3} \lesssim 0.35$. Thus, we take $c_{\Psi_i^3} = 0.35$.

Looking at the left side of Fig. 3.7, we can realize that – similarly to what happens in the usual WED case –, for fixed values of M_1 and M_3 , the more we localize the RH top towards the IR brane, the bigger is the top quark mass. However, in the Higgsless case, we can also fix the value of corresponding bulk mass parameter and increase the value of the brane localized masses, Fig. 3.7-right. We choose $c_{\Psi_i^3} = -0.677$ so that the corrections to the $Z\bar{b}b$ vertex are allowed by EWPT [178],

$$\delta g_{b_L}^Z / g_{b_L}^{Z SM} \sim -0.08\%, \quad \delta g_{b_R}^Z / g_{b_R}^{Z SM} \sim 2.5\%. \quad (3.22)$$

Besides, the $G\bar{t}_R t_R$ coupling is maximized for large values of c_{t_r} , saturating for $c_{t_r} \gtrsim 1$ as we can see in Fig. 3.8.

To avoid too large values for M_1 , we choose $c_{t_r} = 1.6$. With these values of the bulk masses for third generation quarks we obtain the following couplings to the first KK gluon G ,

$$g_L^t = +1.06g \quad g_R^t = 3.95g \quad (3.23)$$

$$g_L^b = +1.39g \quad g_R^b = -0.28g. \quad (3.24)$$

We can see that, in this model, both components of the top (LH and RH) are localized towards the IR brane. The localization is stronger for the RH component, resulting in large couplings to the KK gluon that are neither purely vector or purely axial, but with a positive and sizable axial component.

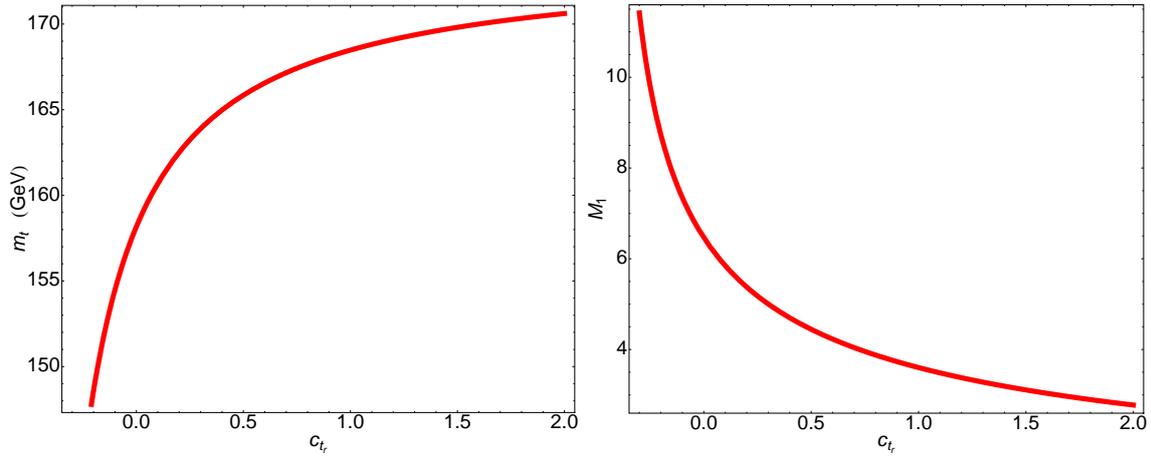


Figure 3.7: Left: Top quark mass dependence on c_{t_r} , with M_1 giving $m_t = 170$ GeV for $c_{t_r} = 1.6$. Right: M_1 value which reproduces the top quark mass in terms of c_{t_r} , once M_3 is fixed doing the same thing for the bottom quark. In both cases, we have chosen $c_{\Psi_l^3} = 0.35$ and $c_{\Psi_r^3} = -0.677$.

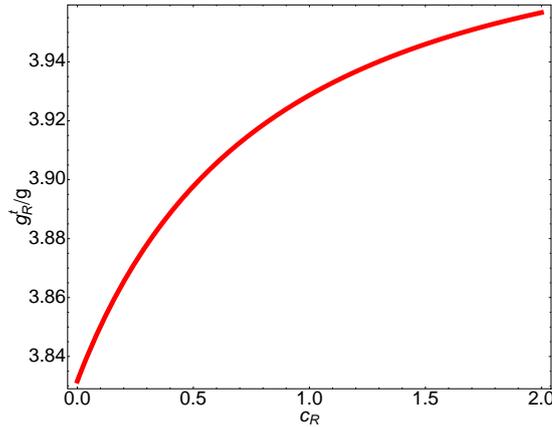


Figure 3.8: $G\bar{t}_R t_R$ coupling in terms of the bulk mass parameter c_{t_r} .

These features imply that Higgsless models naturally realize a light axigluon with large couplings to the third generation quarks, in particular with the RH top. The relatively large axial coupling of the top and light KK gluon mass make it possible to generate a sizable asymmetry without the need of large axial couplings for the light quarks. It is worth noticing that all these features are entirely imposed by constraints from EW precision data. Such axigluons have another unusual feature, namely, they do not decay into massless gluons. This can be easily understood from the orthogonality of their wave functions: the overlap between an initial massive mode and the two final (delocalized) gluons adds always to zero. The KK excitations are then far from being massive replicas of the standard zero mode, as often assumed in collider searches.

The realistic Higgsless model introduced in these lines is a small modification from the original one proposed in [131], which corresponds to a first gluon excitation with a mass $M_G = 714$ GeV and the following couplings

$$\begin{aligned} g_R^q &= g_R^b = -0.31 g, & g_L^q &= +0.17 g, \\ g_R^t &= +2.27 g, & g_L^t &= g_L^b = +1.93 g, \end{aligned} \quad (3.25)$$

resulting in a total width $\Gamma_G = 0.13 M_G$. In Fig. 3.9–*left* we plot the invariant mass distribution for this model using the luminosity (5.3 fb^{-1}) and the cuts described in [179]. The total number of $t\bar{t}$ pairs is almost a 60% higher than in the SM. In addition, the 275 events between 650 and 750 GeV form a clear peak that should have been observed in the analysis of the Tevatron data. For the simulations, we have used MADGRAPH/MADEVENT v4 [164], PYTHIA [165] for hadronization and showering and PGS4 [166] for detector simulation.

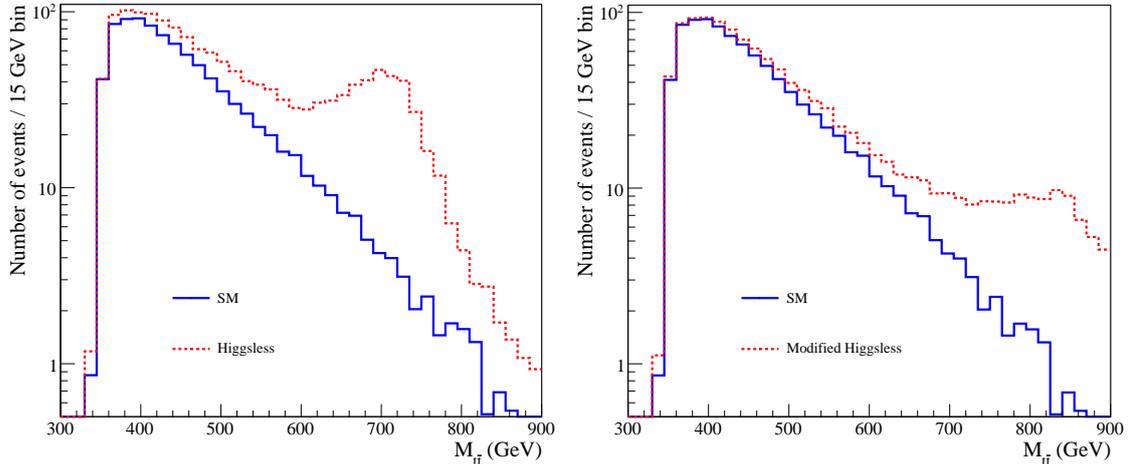


Figure 3.9: $M_{t\bar{t}}$ distribution at the Tevatron for Higgsless models. Left: original Higgsless model of Eq. (3.25); right: modified Higgsless model Eq. (3.26). In both cases the contribution in the Higgsless models is shown in dashed while the SM only contribution is shown in solid. We have considered a luminosity of 5.3 fb^{-1} .

The modified model, while still consistent with EW data, improves the agreement with Tevatron data with just slight changes. Let us use the following couplings for the simulations, very close to those presented in Eqs. (3.19) and (3.23-3.24),

$$\begin{aligned} g_R^q &= g_R^b = -0.25 g, & g_L^q &= +0.20 g, \\ g_R^t &= +4.00 g, & g_L^t &= g_L^b = +1.00 g. \end{aligned} \quad (3.26)$$

With this choice of parameters, the resonance has a width $\Gamma_G = 0.17 M_G$. We show in Fig. 3.9–*right* the invariant-mass distribution of the 1113 $t\bar{t}$ pairs that survive the cuts. At $M_{t\bar{t}} < 600$ GeV the model gives a 8% excess respect to the SM value, whereas at higher invariant masses we obtain 197 events versus 80 within the SM. This excess, together with the change in slope makes it likely that the model should have been seen in the Tevatron data, although only a detailed statistical analysis could state the confidence of the exclusion. Nevertheless it is clear that the slightly higher mass, the reduction in the vector component of the light-quark couplings, the enhancement of the top couplings and the increased width all go in the correct direction to hide the KK gluon in the invariant-mass distributions while increasing the agreement in the forward-backward asymmetry. The asymmetry for the original Higgsless model of Eq. (3.25) is very small, whereas we find for the modified model

$$A_{\#}^{t\bar{t}} \text{ mod} \approx \begin{cases} 0.04 & M_{t\bar{t}} < 450 \text{ GeV}; \\ 0.16 & M_{t\bar{t}} > 450 \text{ GeV}. \end{cases} \quad (3.27)$$

Adding the standard NLO contribution, of order $A_{NLO}^{t\bar{t}} \approx 0.09$ for $M_{t\bar{t}} > 450$ GeV, we obtain in the modified model a total asymmetry less than 2σ away from the measured value.

The realistic model presented in this section improves the agreement with the observed asymmetry, although still at the price of making the model likely visible in Tevatron data on the $t\bar{t}$

invariant-mass distribution. The crucial point is that these models provide in a natural way (all features are enforced by EW data, completely unrelated to the top physics we are discussing) a framework that realizes a light axigluon with the right couplings. Small variations of the model can easily further improve the agreement with the observed asymmetry without conflict with current data on the invariant-mass distribution. In particular, it is clear that making the RH top coupling a bit larger will increase the asymmetry and the width of the gluon resonance, thus suppressing the peak structure in the tail of the invariant mass distribution.

As an example, we have taken the following values of the couplings, with the same KK gluon mass,

$$\begin{aligned} g_R^q &= g_R^b = -0.25 g, & g_L^q &= +0.20 g, \\ g_R^t &= +6.00 g, & g_L^t &= g_L^b = +0.20 g. \end{aligned} \quad (3.28)$$

resulting in a width $\Gamma_G = 0.32 M_G$. We show in Fig. 3.10 the $t\bar{t}$ invariant mass distribution after cuts for the model and the SM contribution (left panel) and a particular MonteCarlo simulation with the collected luminosity to show that the differences are not statistically significant (right panel). The asymmetry is increased in this case to

$$A_{\cancel{H}}^{t\bar{t}} \approx \begin{cases} 0.07 & M_{t\bar{t}} < 450 \text{ GeV}; \\ 0.23 & M_{t\bar{t}} > 450 \text{ GeV}. \end{cases} \quad (3.29)$$

leaving the total asymmetry just 1.4σ below the observed value.

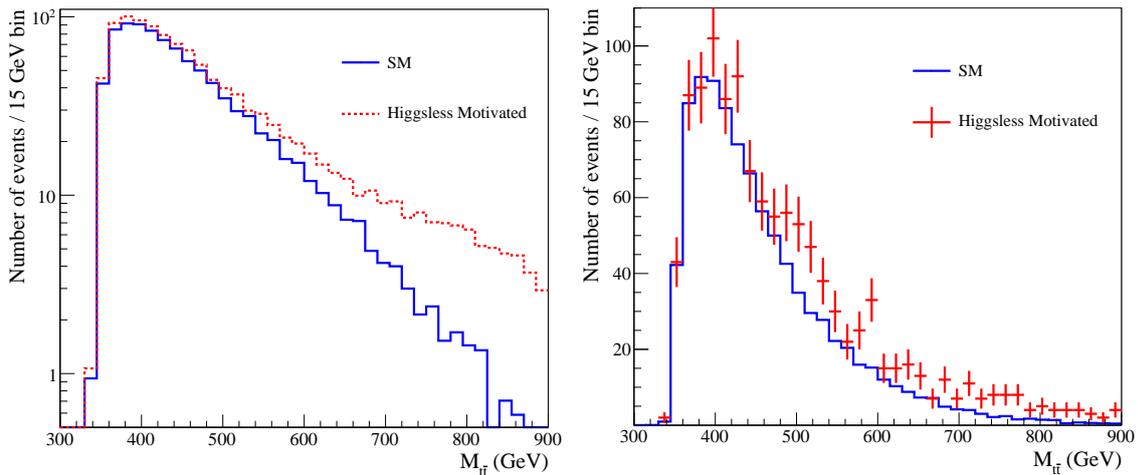


Figure 3.10: $M_{t\bar{t}}$ distribution at the Tevatron in the SM (solid) and in the Higgsless motivated model (dashed) for a luminosity of 5.3 fb^{-1} . On the right we plot a particular MonteCarlo simulation. The errors shown are statistical only.

3.3 Stealth Gluons

We have seen in the previous section that a light axigluon with large couplings to the top quark (especially to the RH chirality) can reduce significantly the deviation from the observed forward-backward asymmetry. However, there seems to be some tension with the data on $d\sigma/dM_{t\bar{t}}$ at $M_{t\bar{t}} \geq 600 \text{ GeV}$, near the gluon mass. This tension is weak at the 5.3 fb^{-1} Tevatron, but becomes more clear at the 4 fb^{-1} LHC, where the peak of the gluon resonance should be visible. One could

hope that an increase in the coupling g_R^t will increase the gluon width and smear out the peak. However, the fit does not improve because the total cross section also goes up with g_R^t and, most notably, the asymmetry $A^{t\bar{t}}$ seems to decrease.² This last effect can be understood because the gluon width appears in the denominator of the $t\bar{t}$ production amplitude, and larger values (similar to its mass) will suppress the effects of the massive gluon and thus the predicted asymmetry.

This tension can be weakened if new decay modes open at $\sqrt{\hat{s}} \sim 600$ GeV, producing heavy vector-like quarks $Q = Q, B, T$ in association with the SM ones,

$$G \rightarrow Q\bar{q}, \bar{Q}q, \quad G \rightarrow B\bar{b}, \bar{B}b, \quad G \rightarrow T\bar{t}, \bar{T}t, \quad (3.30)$$

where Q, B and T are massive vector-like excitations of the light generation quarks, b and t , respectively. Below those energies the process is irrelevant (it does not contribute to the imaginary part of the propagator), so the forward-backward asymmetry at 450 – 600 GeV is unchanged. At $M_{t\bar{t}} \geq 600$ GeV, in contrast, this decay channel will *dissolve* the peak with a non trivial increase of the number of $t\bar{t}$ pairs produced, requiring a detailed analysis to be observed. This scenario is very natural in WED or composite holographic models, where vector-like excitations with sizable couplings to the heavy gluons are always present.

In principle, these extra vector-like quarks could be also pair produced. However, away from the resonance, the interference terms of diagrams shown in Fig. 3.11 cancel, due to the axial couplings of the heavy gluon to the light quarks. Furthermore, the heavy gluon contribution is negligible with respect to the SM one at low energies while it is suppressed at high energies with a relative factor $\mathcal{O}(2-3)$ due to the additional energy dependence of the width. This means that pair production is roughly given by the SM contribution. Single heavy-quark production, on the other hand, is unsuppressed and opens kinematically at lower energies, appearing as a very promising mechanism unexplored in previous literature.

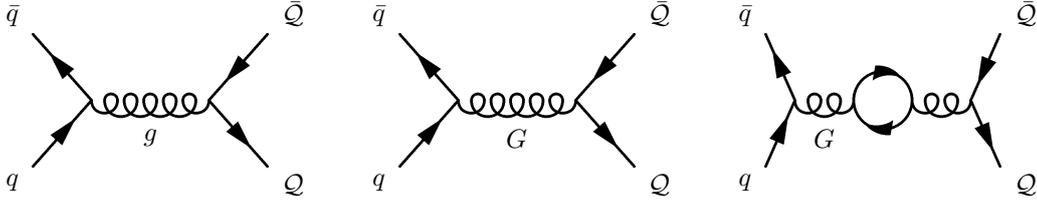


Figure 3.11: Main diagrams involved in pair production of vector-like excitations.

The large gluon width in this framework requires a proper treatment of energy-dependent effects. In particular, the new decay modes contribute to $\Gamma_G(s)$ in the following way

$$\Gamma_G^{\mathcal{Q}q}(\hat{s}) = \theta[\hat{s} - (m_q + m_Q)^2] \frac{g^2}{12\pi M_G} \left(1 - \frac{(m_q + m_Q)^2}{\hat{s}}\right)^{\frac{1}{2}} \left(1 - \frac{(m_q - m_Q)^2}{\hat{s}}\right)^{\frac{1}{2}} \times \left[\left(1 - \frac{m_q^2 + m_Q^2 + 6m_q m_Q}{2\hat{s}} - \frac{(m_Q^2 - m_q^2)^2}{2\hat{s}^2}\right) g_A^{\mathcal{Q}q^2} + \left(1 - \frac{m_q^2 + m_Q^2 - 6m_q m_Q}{2\hat{s}} - \frac{(m_Q^2 - m_q^2)^2}{2\hat{s}^2}\right) g_V^{\mathcal{Q}q^2} \right], \quad (3.31)$$

where $q = q, b, t$, with q denoting light quarks, and $g_{V,A}^{\mathcal{Q}q} = (g_R \pm g_L)/2$ are the vector and axial coupling of the massive gluon to Q and q , respectively.

²This is the main argument behind recent claims in the literature that heavier axigluons are favored over lighter ones [180, 181].

For the sake of definiteness, let us introduce a benchmark model reflecting all the relevant features. We consider a heavy gluon with mass $M_G = 850$ GeV and the following couplings

$$g_L^q = 0.3g_s \quad g_R^q = g_R^b = -0.3g_s \quad g_R^t = 4g_s \quad g_L^t = g_L^b = 0. \quad (3.32)$$

We consider also vector-like excitations of the SM quarks t_R, b_R and q_L , denoted by T, B and Q , respectively, with masses $M_T = 450$ GeV, $M_B = M_Q = 600$ GeV and couplings to G

$$g_R^{Tt} = 4g_s \quad g_R^{Bb} = 3.5g_s \quad g_L^{Qq} = 3.5g_s. \quad (3.33)$$

These values imply a total width $\Gamma_G(M_G^2) \approx 0.7 M_G$ and the following decay branching fractions

$$\text{BR}(G \rightarrow t\bar{t}) \approx 0.2, \quad \text{BR}(G \rightarrow T\bar{t}, t\bar{T}) \approx 0.24, \quad (3.34)$$

$$\text{BR}(G \rightarrow B\bar{b}, b\bar{B}) \approx 0.11, \quad \text{BR}(G \rightarrow Q\bar{q}, q\bar{Q}) \approx 0.44. \quad (3.35)$$

The benchmark model just defined has the advantage that all possible channels are present simultaneously. However, when studying the possible collider implications of this scenario we will also consider the extreme cases where just one G decay mode is present,

$$\text{Extreme } T \text{ model: } \quad g_R^{Tt} = 7.28 g_s, \quad g_R^{Bb} = g_L^{Qq} = 0, \quad (3.36)$$

$$\text{Extreme } B \text{ model: } \quad g_R^{Bb} = 9.36 g_s, \quad g_R^{Tt} = g_L^{Qq} = 0, \quad (3.37)$$

$$\text{Extreme } Q \text{ model: } \quad g_L^{Qq} = 4.68 g_s, \quad g_R^{Tt} = g_R^{Bb} = 0, \quad (3.38)$$

and all the other couplings unchanged. We have set the corresponding $g_{L,R}^{Qq}$ couplings to the required values to produce $\Gamma(M_G^2) \approx 0.7 M_G$, leading to too large values. Nevertheless, we just take these extreme models as limiting examples to get a clear idea of the LHC reach for these signatures, with realistic models lying somewhere in between the benchmark and the extreme cases. In all these cases the heavy gluon has a 20% branching ratio into $t\bar{t}$ and 80% into the new channel.

We will study the collider signatures of these vector-like excitations through single production. The final states we need to look for are the following (the conjugated processes are not explicitly shown but are included in our analysis):

(i) $W^+W^-b\bar{b}$, from

$$q\bar{q} \rightarrow G \rightarrow T\bar{t} \rightarrow (W^+b)W^-\bar{b} \quad (3.39)$$

and

$$q\bar{q} \rightarrow G \rightarrow B\bar{b} \rightarrow (W^-t)\bar{b} \rightarrow (W^-W^+b)\bar{b}. \quad (3.40)$$

(ii) $Zt\bar{t}$, from

$$q\bar{q} \rightarrow G \rightarrow T\bar{t} \rightarrow (Zt)\bar{t} \rightarrow (ZW^+b)W^-\bar{b}. \quad (3.41)$$

(iii) $Zb\bar{b}$, from

$$q\bar{q} \rightarrow G \rightarrow B\bar{b} \rightarrow (Zb)\bar{b}. \quad (3.42)$$

(iv) W +jets, from

$$q\bar{q} \rightarrow G \rightarrow Q\bar{q} \rightarrow (Wq')\bar{q} \quad (3.43)$$

(v) Z +jets, from

$$q\bar{q} \rightarrow G \rightarrow Q\bar{q} \rightarrow (Zq)\bar{q}. \quad (3.44)$$

Regarding the EW decay modes of heavy vector-like quarks, we have considered the branching ratios obtained in the large-mass limit of the usual Higgsless models,

$$\text{BR}(\mathcal{Q} \rightarrow Wq') = \frac{2}{3}, \quad \text{BR}(\mathcal{Q} \rightarrow Zq) = \frac{1}{3}. \quad (3.45)$$

We will mention later also some aspects of the collider phenomenology when Higgs decays are present.

For the phenomenological study of these models we have used MADGRAPH/MADEVENT v4 [164] (with the matrix element properly modified to include the energy dependence of the width), PYTHIA [165] for hadronization/showering effects and PGS4 [166] and DELPHES 1.9 [182] for detector simulation. In particular, for the benchmark model defined before, we obtain a partonic forward-backward asymmetry in agreement with the CDF and $D\emptyset$ measurements [171–173]

$$A^{t\bar{t}}(M_{t\bar{t}} \leq 450 \text{ GeV}) = 0.12, \quad A^{t\bar{t}}(M_{t\bar{t}} > 450 \text{ GeV}) = 0.33. \quad (3.46)$$

3.4 Third Generation Quark Excitations

3.4.1 $W^+W^-b\bar{b}$ Channel

This is the same final state as in $t\bar{t}$ production and arises when third generation vector-like excitations decay through a charged EW boson, see Fig. 3.12. This signal will be added to the extra

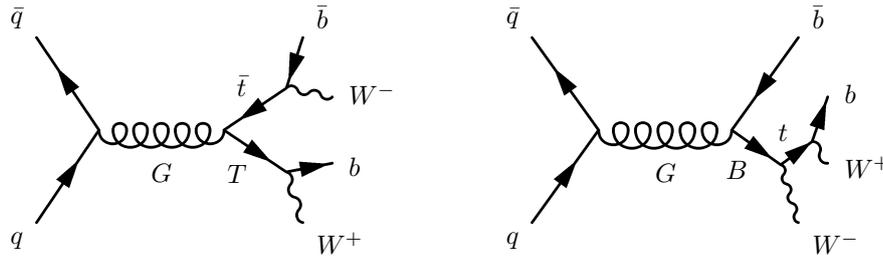


Figure 3.12: Left: Charged decay mode involving a third-generation quark excitation T and a top quark. Right: Diagram associated with the same final state but arising from the charged decay of a bottom quark and its vector-like excitation B . In both cases, the conjugated processes are not explicitly shown and should be added.

top-quark pairs coming from the massive gluon and also to the SM $t\bar{t}$ contribution. Therefore, it is crucial to be sure that there is no observable excess in $t\bar{t}$ or similar searches. We show in Fig. 3.13 the $M_{t\bar{t}}$ reconstructed distribution at the Tevatron for 5.3 fb^{-1} for the SM, the benchmark model and the extreme T case, following the analysis of [183]. We look for semileptonic decays of the W pair, reconstructing the neutrino momentum through the on-shell condition of the charged boson. The prediction for the extreme B model is very similar to the extreme T one while the extreme Q case lies below the benchmark model. The deviations from the SM are always below 2.5σ (assuming statistical errors only) and are smaller than 2σ for the benchmark and the extreme Q models.

Let us study now the effect of the new decay modes on LHC top-quark related searches. Measurements of the $t\bar{t}$ invariant mass distribution at the LHC have been reported in [184]. We have simulated the analysis in the first two works of this reference and studied the effect of the new channels together with the other new contributions to $t\bar{t}$ production. We show in Fig. 3.14 the results of these two analysis for a luminosity of 0.2 fb^{-1} (the third reference uses the dilepton channel and a larger data set, implying a very similar sensitivity). In both plots, we show the reconstructed signal for the SM, the benchmark model (with statistical error bars) and the extreme

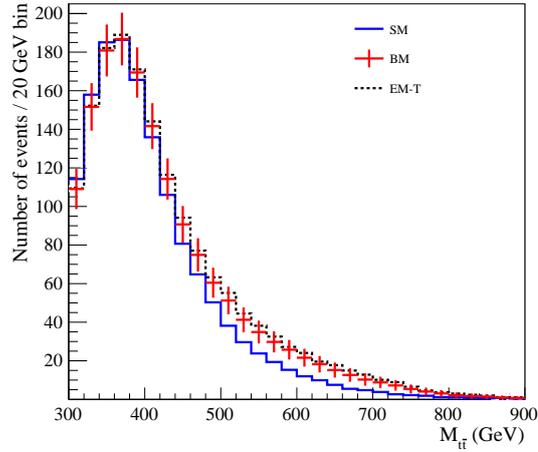


Figure 3.13: $M_{t\bar{t}}$ distribution at the Tevatron for 5.3 fb^{-1} in the SM (solid blue), the benchmark model (points with error bars) and the extreme T case (dashed black). We include the contribution from $T\bar{t}, t\bar{T}$ and $B\bar{b}, b\bar{B}$ when present.

T case. We have not plotted the results for the extreme B or Q models. In the first case, we obtain a prediction very similar to the extreme T one, while the extreme Q result is somewhere between the benchmark model and the SM. We have assumed a 10% uncertainty in the $t\bar{t}$ prediction, allowing a normalization factor (within this 10%) to correctly reproduce the three bins around the peak at $M_{t\bar{t}} \approx 500 \text{ GeV}$. We have used DELPHES for the ATLAS simulation of Fig. 3.14-left and PGS4 for the CMS prediction shown on the right panel. We observe a $\mathcal{O}(20\%)$ excess for invariant

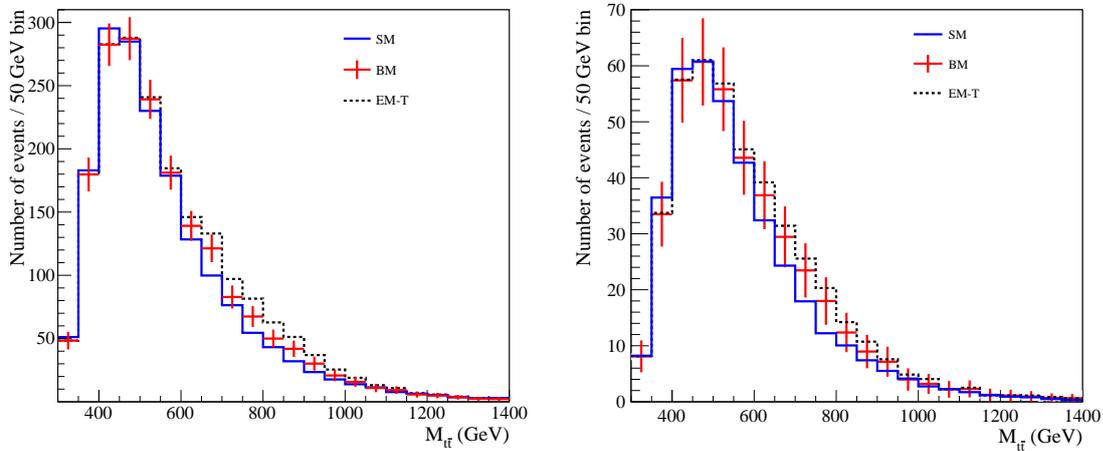


Figure 3.14: Left: Reconstructed $M_{t\bar{t}}$ distribution at the ATLAS detector for 0.2 fb^{-1} in the SM (solid blue), the benchmark model (points with error bars) and the extreme T model (dashed black). Right: $M_{t\bar{t}}$ distribution for the μ +jets channel (in the case of 4 or more jets with at least two b-tagged) at the CMS experiment for the same luminosity. We include the contribution from $T\bar{t}, t\bar{T}$ and $B\bar{b}, b\bar{B}$ when present.

masses in the range of 600–900 GeV for the extreme T and B models. This seems to be in the limit of the LHC reach for the considered luminosity. However, if we increase the luminosity to 4

fb^{-1} we observe 8 consecutive bins with differences above 3σ for the DELPHES simulation and 7 consecutive ones for the PGS prediction in the case of the extreme T model. Things are not so clear for the benchmark and extreme Q models. For example, in the 4 fb^{-1} PGS simulation, we find 3(2) consecutive bins more than 3σ away from the SM background for the benchmark (extreme Q) model, just including statistical errors. Therefore, one could expect in our model a 10% excess relative to the SM prediction in all the $M_{t\bar{t}}$ bins below 1 TeV, arising from $t\bar{t}$ pairs mediated by the gluon resonance G . Furthermore, the bins in the range of 600–900 GeV could be increased an additional 15% with $T\bar{t}$ and/or $B\bar{b}$ events reconstructed as $t\bar{t}$ pairs.

This is not the only LHC analysis which is sensitive to the new channels. Searches for a fourth generation of quarks produced as $T\bar{T}$ pairs [185] might probe the vector-like excitations present in these models. We have studied the impact of the new decay modes in these searches, following the CMS analysis. We show in Fig. 3.15 the results obtained for a luminosity of 0.821 fb^{-1} in the μ +jets channel for the SM, the benchmark model and the extreme T case. On the left panel we show the reconstructed H_T (defined as the scalar sum of the transverse momentum of the objects in the final state) while on Fig. 3.15-right we can see the reconstructed mass for the T quark, after imposing that the two legs of the process have the same invariant mass, i.e.,

$$m(\cancel{E}lb) = m(q\bar{q}b) = m_{\text{fit}}. \quad (3.47)$$

In both plots, the SM contribution is normalized with the same factor. The conclusions to be drawn are quite similar to the $t\bar{t}$ case, with the bigger deviation from the SM being given again by the extreme T model. We have also checked that pair production of T quarks is compatible with the bounds given in [185] and [186].

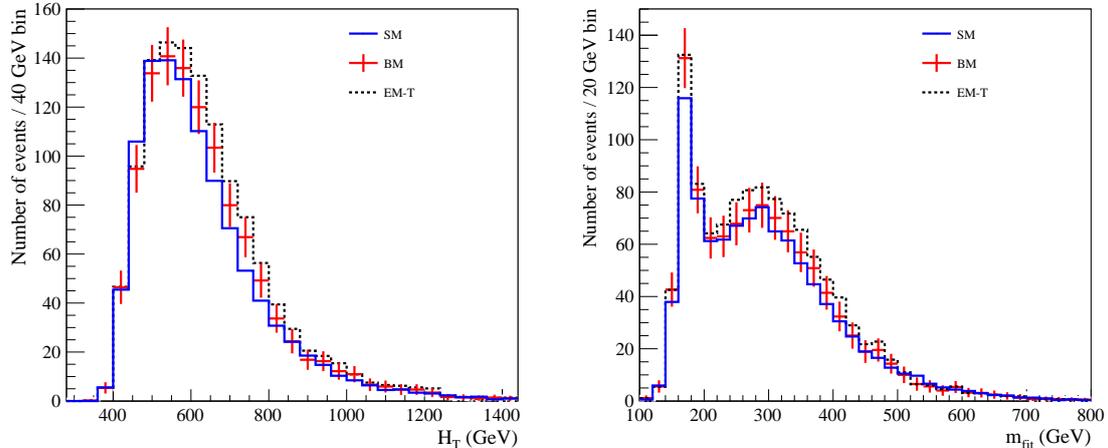


Figure 3.15: $T\bar{T}$ search at the LHC for 0.821 fb^{-1} . Left: H_T distribution. Right: m_{fit} distribution. In both cases we show the predictions in the SM (solid blue), in the benchmark model (data points with statistical errors) and in the extreme T case (dashed black). We include the contribution from $T\bar{t}$, $t\bar{T}$ and $B\bar{b}$, $b\bar{B}$ when present.

These results show that the model we have proposed to explain the large measured value of the $t\bar{t}$ forward-backward asymmetry is almost invisible at the Tevatron and the LHC, at least for the analyzed luminosities. This is due to two different reasons. On the one hand, we have the *stealth* gluon mechanism in the $t\bar{t}$ production, with the main contribution arising from the same diagrams as in Fig. 3.11 with the simple change $Q \rightarrow t$ in the final state. To understand better how the

stealth physics works, let us consider the $t\bar{t}$ amplitude, roughly given by

$$\mathcal{A} \propto \left| \frac{g_s^2}{\hat{s}} + \frac{g^q g^t}{\hat{s} - M_G^2 + iM_G \Gamma_G(\hat{s})} \right|^2. \quad (3.48)$$

First of all, and similarly to the case of vector-like quark pair production, the axial nature of the heavy gluon couplings to the light quarks suppresses the NP contribution to $t\bar{t}$ away from the resonance. The interference terms coming from the leading diagrams cancel due to the axial couplings of G to the light quarks. Besides, as mentioned previously, the heavy gluon mass suppress its contribution at low energies while at high energies it has an extra suppression factor $\mathcal{O}(2-3)$ due to the additional \hat{s} dependence of Γ_G . Therefore, when $|\hat{s} - M_G^2| \gg M_G \Gamma_G(\hat{s})$, we have just roughly the SM contribution. Secondly, when we are close to the resonance, the large gluon width suppresses the G contribution to the amplitude, making the gluon excitation very elusive. On the other hand, the $T\bar{t}$ and $B\bar{b}$ events are reconstructed as $t\bar{t}$ or $T\bar{T}$ pairs in analysis where it is customary to impose the same mass value for both legs, i.e.,

$$m(\cancel{E}lb) = m(q\bar{q}b) = m_t \quad \text{or} \quad m(\cancel{E}lb) = m(q\bar{q}b) = m_{\text{fit}}. \quad (3.49)$$

This leads to a poorer fit and a wider spread. In the case of $T\bar{t}$ events, we can solve this issue by reconstructing them as a t quark plus a T quark of arbitrary mass. Moreover, as these events only occur at high energies $M_{T\bar{t}} > M_T + m_t$, we can use the more stringent cuts used in the $T\bar{T}$ analysis [185] (we consider the μ +jets channel). Actually, we will impose a more severe cut for the hardest jet, $p_T \geq 200$ GeV, instead of the 120 GeV of that reference. To improve further the reconstruction, we will impose one of the reconstructed legs to be a 173 GeV t quark (using a χ^2 similar to the one used in the first reference of [184] and requiring $\chi^2 \leq 10$) and will plot the mass of the second leg in events of invariant mass above 600 GeV (Fig. 3.16, left panel) for SM and extreme T model simulations. We have normalized both plots to a luminosity of 4 fb^{-1} .

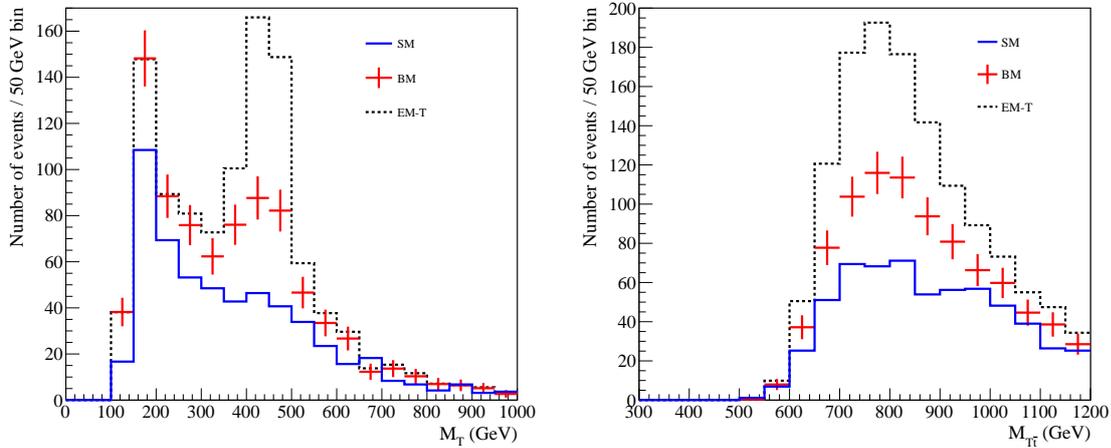


Figure 3.16: Left: Reconstructed M_T at the LHC. Right: Reconstruction of M_G . In both cases we have normalized the distributions to 4 fb^{-1} data and represent the results for the SM (solid blue), the benchmark model (data points with statistical errors) and the extreme T case (dashed black). Details of the reconstruction method can be found in the text.

We can see from the plot that there are three consecutive bins around $M_T = 450$ GeV with more than three sigma difference from the SM prediction even in the benchmark model. We obtain the

following total excess S of events over the SM background B around the peak (three bins between 350 and 500 GeV)

$$\frac{S}{\sqrt{B}} \approx \begin{cases} 8, & \text{Benchmark,} \\ 21, & \text{Extreme T.} \end{cases} \quad (3.50)$$

These numbers imply an impressive deviation for the extreme T model and even a possible evidence at the LHC for the benchmark one. Looking at the large excess predicted for the extreme T model, we can try to reconstruct the massive gluon peak. To this end, we drop the cut in the total invariant mass $M_{T\bar{t}}$ and plot it for the events with $M_T \geq 350$ GeV, Fig. 3.16-*right*. Even if the SM and the new physics model peak in the same region, there is a factor of $\sim 3(2)$ excess in the extreme T (benchmark) model.

Let us now consider the case of $B\bar{b}$ events, where we will use a slightly different strategy according to the distinct topology of the process, see Fig. 3.12-*right*. Now, it is no longer possible to reconstruct the heavy quark mass through a Wb pair. Instead, we need to collect both reconstructed W 's (one leptonic and the other hadronic) and one of the two bottom quarks present in the final state. We will use the same selection procedure of the previous analysis, with the cuts in [185] (muon channel) except for the p_T cut of the hardest jet, which is increased to 200 GeV, and a $\chi^2 \leq 10$ (again we use a similar χ^2 to the one used in the first reference of [184]) choosing the pairing reconstructing better a 173 GeV top quark. In Fig. 3.17, we plot the invariant mass of the reconstructed t quark plus the extra W for the benchmark and the extreme B models. We impose two different cuts in the total invariant mass distribution, $M_{B\bar{b}} > 600$ GeV and $M_{B\bar{b}} > 700$ GeV, and a luminosity of 4 fb^{-1} . As we can see from the picture, the reconstruction of the vector-like quark is far worse in this case than in the previous one, and a more sophisticated analysis would be needed to discriminate the signal from the background.

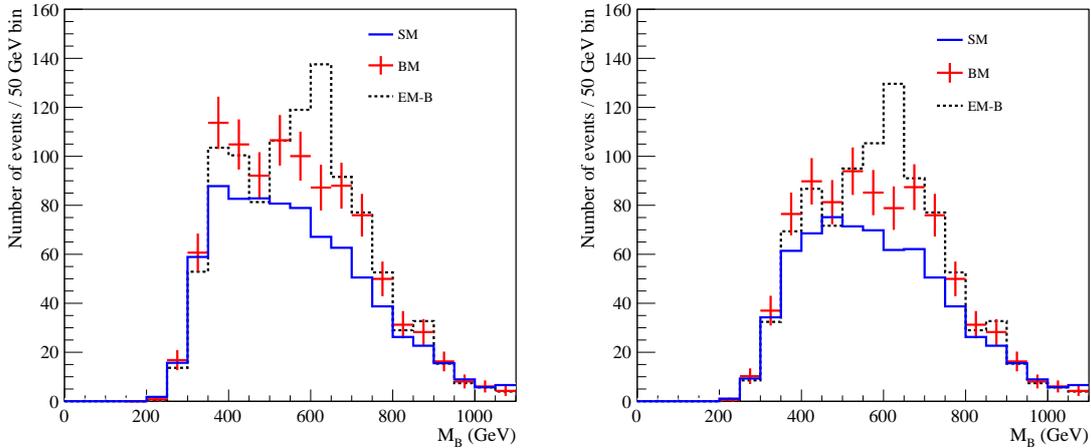


Figure 3.17: Reconstructed M_B at the LHC for 4 fb^{-1} in the SM (solid blue), the benchmark model (data points with errors) and the B case (dashed black). We consider the cuts $M_{B\bar{b}} > 600$ GeV (left) and $M_{B\bar{b}} > 700$ GeV (right). Details of the reconstruction method can be found in the text.

3.4.2 $Zt\bar{t}$ Channel

Let us consider now the neutral decay mode of the T vector-like quark, see Fig. 3.18. The final state associated with this process has a large multiplicity, which makes the reconstruction of the T quark problematic even with a very small SM background. Therefore, we will try better to

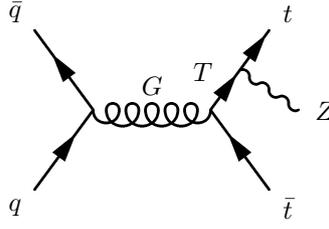


Figure 3.18: $Zt\bar{t}$ production mediated by the heavy gluon G and the vector-like excitation T . The conjugated process should be added.

reconstruct the total final state looking for the gluon excitation G . In order to do this, we consider a leptonic Z boson and a semileptonic $t\bar{t}$ pair. Therefore, we ask for (i) three charged leptons with $p_T \geq 25$ GeV, and at least two of them with the same flavor and opposite sign reconstructing the Z within 25 GeV; (ii) at least two b -tagged and at least two non- b -tagged jets with $p_T > 20$ and $|\eta| < 2.8$. As in the previous analysis, we reconstruct the neutrino momentum using the on-shell condition for a W . We take the two hardest jets and b -jets if there are more of them. We show in Fig. 3.19 the reconstructed total invariant mass obtained in this way. Looking at the results, we

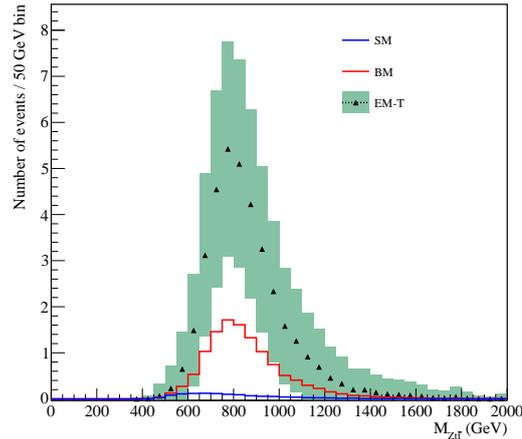


Figure 3.19: Reconstructed total invariant mass for the $Zt\bar{t}$ channel in the SM (solid blue), benchmark (solid red) and extreme T (data with statistical errors shown as a band) models for the $Zt\bar{t}$ analysis described in the text for the LHC with 4 fb^{-1} .

note that the extreme T model shows a clear peak (with ≈ 36 events and no expected background events) while the benchmark model gives a smaller deviation. A more sophisticated analysis is required to reconstruct the vector-like quark mass, using maybe some hint on its value from the charged decay channel previously considered.

3.4.3 $Zb\bar{b}$ Channel

Finally, we will study the neutral decay channel for the vector-like excitation of the bottom quark, which is given by the same diagrams as in Fig. 3.18 but changing $T \rightarrow B$. First of all, we will try to reconstruct the total invariant mass in the search of the heavy gluon. In the case of a leptonic Z , the SM irreducible background to this process is quite small, $\sigma(Zb\bar{b}) \approx 2 \text{ pb}$. On the other

hand, we can handle the background from final states with larger cross sections like $Z+jets$ and $t\bar{t}$ with a very simple set of cuts.³ To this end, we will require two same-flavor opposite-sign leptons with $p_T \geq 25$ GeV and reconstructing the Z boson in a range of 25 GeV, i.e., $|m_{l+l^-} - m_Z| \leq 25$ GeV. We will ask also for two b -tagged jets with $p_T \geq 20$ GeV and $|\eta| \leq 2.8$. We can reduce further the $t\bar{t}$ background imposing a veto on the missing energy $\cancel{E}_T \leq 40$ GeV. To reconstruct the B quark, we compute the invariant mass of the Z and the hardest of the two b -jets, since we expect the b quark coming from the vector-like excitation to be the hardest one, b_h . We show the reconstructed mass obtained following this procedure in Fig. 3.20-*left*, for the SM, the benchmark

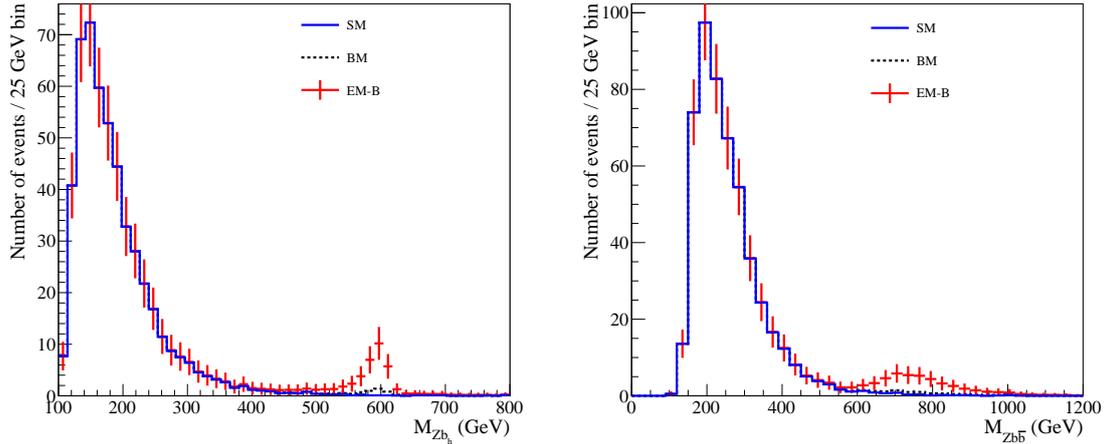


Figure 3.20: Left: reconstruction of M_{Zb_h} at the LHC. Right: reconstruction of $M_{zb\bar{b}}$ to show the heavy gluon mass. In both cases we have normalized the distributions to 4 fb^{-1} of data and have represented the SM with thick solid blue line, the benchmark model with thin solid red line and the extreme B case (data points with statistical errors).

model and the extreme B case. As we can see from the plot, the benchmark model would need a higher luminosity to be probed. On the other hand, the extreme B model, shows a distinct peak with a total number of ≈ 40 events at $M_{Zb_h} \approx M_B = 600$ GeV, versus ≈ 3 background events, leading to a statistical significance of

$$\frac{S}{\sqrt{B}} \approx 21, \quad (Zb\bar{b} \text{ for extreme } B). \quad (3.51)$$

We show also on Fig. 3.20-*right* the total invariant mass of the process, in an attempt to reconstruct the mass of the gluon resonance G . The large width of the heavy gluon makes the peak to pop up slightly before the actual gluon mass value. An approximate estimate of the excess observed above 600 GeV leads to

$$\frac{S}{\sqrt{B}} \approx \frac{38}{\sqrt{5}} = 17, \quad (M_G \text{ peak in } Zb\bar{b} \text{ for extreme } B). \quad (3.52)$$

These results show that the neutral channel is a very promising option to reconstruct the bottom like excitation and the heavy gluon. In addition, we could use the extra information obtained from the charged decays of the B quark studied before.

³For completeness, we have also checked that searches of $H \rightarrow ZZ \rightarrow Zb\bar{b}$ [187] or measurements of $Z + b$ cross-section [188] do not impose additional constraints on our model.

3.5 Light Quark Excitations

As we have seen in the previous section, vector-like excitations of light quarks do not leave an observable excess in $t\bar{t}$ or fourth generation $T\bar{T}$ searches. Indeed, models with predominant decays in these modes are a remarkable example of stealth NP [3]. Our goal in this section is to describe possible strategies to probe them. We will start by considering the neutral decays of these particles.

3.5.1 $Zq\bar{q}$ Channel

The SM irreducible background for Z plus ≥ 1 jets is 6 nb at the 7 TeV LHC, while the Zjj cross-section at the same center of mass energy is $\sim 1(1.8)$ pb for the benchmark (extreme Q) model. Thus, we need to impose stringent cuts to significantly reduce the background. As in the previous section, we will ask for a leptonic Z boson requiring two same-flavor, opposite charge leptons with $p_T \geq 25$ GeV that reconstruct the Z mass within 25 GeV. We require also two or more jets, with $p_T \geq 150$ GeV for the hardest one j_h . Again, as the jet coming from the decay of the Q quark will be typically harder than the other one, to reconstruct the vector-like excitation we compute the invariant mass of the Z boson plus the hardest jet, M_{Zj_h} , see Fig. 3.21. We can

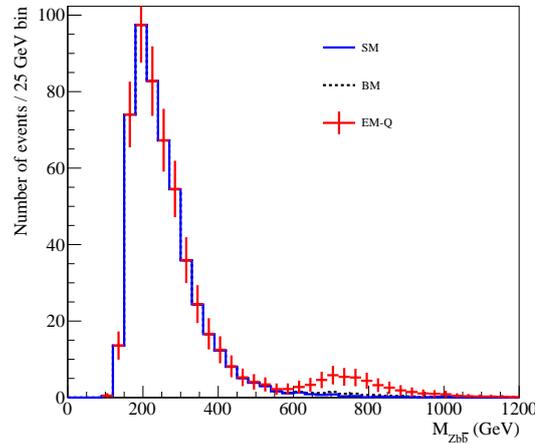


Figure 3.21: Result of the fit of the M_{Zj_h} distribution for the Zjj analysis described in the text for the SM (solid blue), extreme Q model (data points with statistical errors) and the fit to both distributions (dashed black). Simulations for the 7 TeV LHC with 4 fb^{-1} .

see from the plot that the benchmark model is out of the reach of this analysis. However, there is a distinct peak for the extreme Q model. After fitting the signal plus the background histogram to a Crystal Ball plus a Gaussian shape we obtain an excess of 170 events over the expected 540 background events in the region of two standard deviations around the center of the Gaussian. We get a statistical significance of 7σ with a best fit mass of $m_Q^{\text{fit}} = 590$ GeV, very close to the actual Q quark mass. We can conclude that, with a very simple set of cuts, we are able to probe a model which is in general quite difficult to see.

3.5.2 $Wq\bar{q}'$ Channel

Let us consider now the charged decay mode of these vector-like excitations. In this case, the SM irreducible background of W plus ≥ 1 jets at the 7 TeV LHC is 17 nb, whereas the Wjj cross-section for the benchmark and the extreme Q model are ~ 1.9 and 3.6 pb, respectively. As the jet arising from the decay of the Q quark is expected to be the hardest one, with a $p_T \sim M_Q$,

we impose a cut on this jet of $p_T \geq 150$ GeV in addition to the cuts defined in Ref. [189]. With this more stringent cut we can reduce the background to levels which allow us to see some NP evidence. We can see in Fig. 3.22 that for the extreme Q case, there are 6 bins departing more than 3σ from the standard background. The deviation for the benchmark model is smaller and a more detailed analysis should be done.

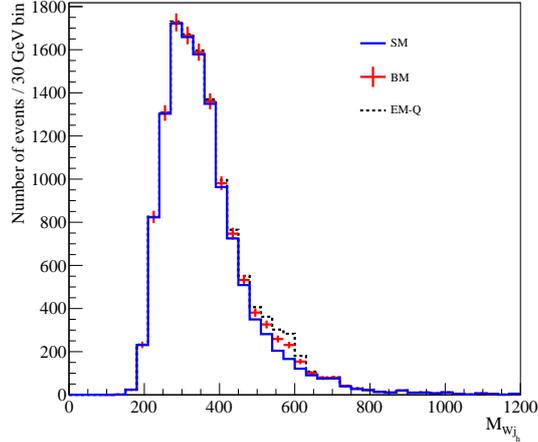


Figure 3.22: Transverse mass for the Wj_h system in the Wjj analysis described in the text for the SM (solid blue), benchmark model (data points with errors) and extreme Q model (dashed black). Search for the 7 TeV LHC with 4 fb^{-1} .

3.6 Higgs Decays

Until now, we have just considered decays of vector-like quarks into a EW gauge boson and a SM quark. As we have seen in the previous sections, these decay modes are quite model independent and a very promising discovery channel for the massive color-octet and the vector-like excitations. However, if the Higgs boson exists – as it seems considering the latest LHC results – a sizable fraction of the heavy fermion resonances will decay into a SM quark and the Higgs boson. Although it leads to very interesting collider signatures, a detailed study of its phenomenology is beyond the scope of this Thesis, we will describe Higgs decays in composite Higgs models [5,6]. In particular, we will consider a composite Higgs of 125 GeV arising from the two-site version of MCHM₅ [190,191]. Full details of the model can be found in [191]. Here we will just describe the features that are directly relevant for the Higgs production mechanism we want to study, namely the new massive gluons and vector-like quarks present in the spectrum. The relevant new vector-like quarks are, for each family, two EW doublets $Q_{1/6}$ and $Q_{7/6}$ of hypercharges 1/6 and 7/6, respectively and one singlet, \tilde{T} , of hypercharge 2/3

$$Q_{1/6}^{(i)} = \begin{pmatrix} T^{(i)} \\ B^{(i)} \end{pmatrix}, \quad Q_{7/6}^{(i)} = \begin{pmatrix} T_{5/3}^{(i)} \\ T_{2/3}^{(i)} \end{pmatrix}, \quad \tilde{T}^{(i)}, \quad (3.53)$$

with masses $M_{Q_{1/6}^{(i)}}$, $M_{Q_{7/6}^{(i)}}$, $M_{\tilde{T}^{(i)}}$. The masses of the new EW doublets are related through the compositeness degree of the standard LH doublets

$$M_{Q_{7/6}^{(i)}} = M_{Q_{1/6}^{(i)}} \cos \phi_q^{(i)}. \quad (3.54)$$

There is also a massive gluon in the spectrum, a color octet vector boson G , with mass M_G . We consider the anarchic scenario where the SM fermion mass hierarchies are explained in terms of the different degrees of compositeness of the SM fields. Due to the large masses of third generation quarks, and in particular to that of the top, the massive gluon couples mostly to the RH top, similarly to what happens in the benchmark model studied before. This leads also to sizable couplings of the massive gluon to the third generation quarks and its vector-like partners, with the relevant ones being

$$Gt_L T_L^{(3)}, \quad Gb_L B_L^{(3)}, \quad Gt_R \tilde{T}_R^{(3)}. \quad (3.55)$$

In particular, following the notation in [191], we take

$$Y_* = Y_{*U} = Y_{*D} = 3 = g_{*3}, \quad s_2 = 0.1, \quad s_u^{(1)} \ll s_u^{(2)} \ll s_u^{(3)} = 0.6, \quad (3.56)$$

and a Higgs degree of compositeness $\xi = 0.2$. The relatively large coupling in the composite sector, $g_{*3} = 3$, implies that the heavy resonances are strongly coupled to the heavy gluon. This large coupling and the large multiplicity imply a very large contribution to the heavy gluon width. We show in Fig. 3.23 the massive gluon width (left panel) and branching ratios (right panel) as a function of its mass for $M_F = M_{Q_{7/6}^{(3)}} = M_{\tilde{T}^{(3)}} = 1 \text{ TeV} \ll M^{(1,2)}$.

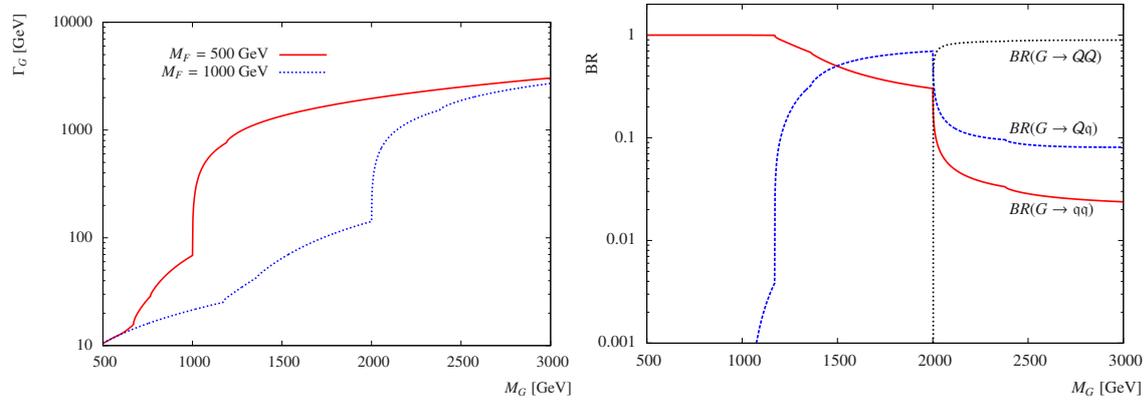


Figure 3.23: Left panel: massive gluon width as a function of its mass for the anarchic scenario with $M_F = 0.5$ and 1 TeV. Right panel: massive gluon branching fraction in two SM quarks (labeled qq), one SM and one heavy quark (Qq) and two heavy quarks (QQ), respectively.

Due to the extreme widths developed when the decays into two massive fermionic resonances open up, we restrict ourselves to the region of parameter space in which these decay modes are kinematically suppressed. Thus, in the following we fix

$$M^{(1,2)} \gg M_F = M_{Q_{7/6}^{(3)}} = M_{\tilde{T}^{(3)}} = M_G/2. \quad (3.57)$$

Naturalness arguments and the recent hints for a light Higgs might prefer lighter fermion resonances for the third generation [192, 193]. In these cases, if the heavy gluons are present, their width can easily exceed the perturbative limit. For instance, for our particular choice of parameters we get $\Gamma_G \gtrsim 0.9M_G$ for $M_F \lesssim 1 \text{ TeV}$. For these values of the vector-like quark masses, the leading decay channel is $G \rightarrow Q\bar{q} + q\bar{Q}$, with Q a vector-like excitation and q a SM quark. In the anarchic scenario the light SM quarks q are essentially elementary, leading to suppressed $GQ^{(1,2)}q$ couplings. Therefore, the main Higgs production mechanism is $G \rightarrow \mathcal{T}\bar{t} + \bar{\mathcal{T}}t$, with $\mathcal{T} = T^{(3)}$ and $\bar{\mathcal{T}} = \tilde{T}^{(3)}$, followed by the decay of the heavy quark into the Higgs boson and a top quark,

$$pp \rightarrow G \rightarrow \mathcal{T}\bar{t} + \bar{\mathcal{T}}t \rightarrow ht\bar{t}. \quad (3.58)$$

The corresponding cross sections depend on the coupling of G to the SM quarks, to $t\mathcal{T}$ and also on the branching fraction of the heavy quarks into a SM quark and the Higgs. The relevant such branching fractions are, in the limit of large masses [191]

$$\text{BR}(T^{(3)} \rightarrow t h) \approx 0.5, \quad \text{BR}(\tilde{T}^{(3)} \rightarrow t h) \approx 0.25. \quad (3.59)$$

Other channels either do not result in a Higgs or their production is strongly suppressed due to small degree of compositeness. We show in Fig. 3.24 the production cross section times branching ratio for $ht\bar{t}$.

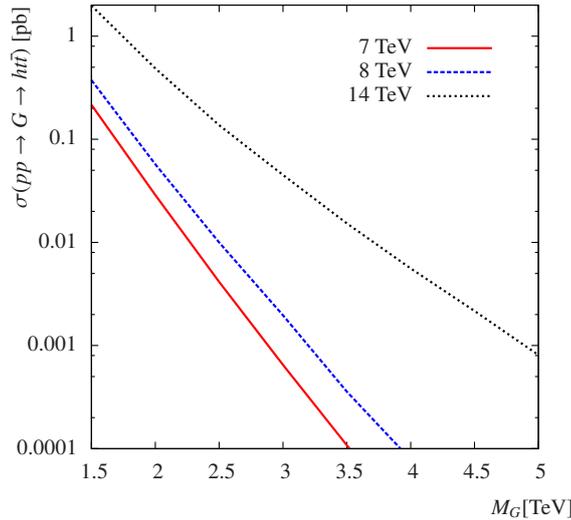


Figure 3.24: $ht\bar{t}$ production cross section in the model considered in the text, mediated by a color octet vector resonance with decay into a fermionic resonance and a top quark.

The very large multiplicity of the final state makes, in principle, full reconstruction rather complicated. We have considered three different configurations for the LHC parameters, namely 5 fb^{-1} integrated luminosity at $\sqrt{s} = 7 \text{ TeV}$, 20 fb^{-1} integrated luminosity at $\sqrt{s} = 8 \text{ TeV}$ and 100 fb^{-1} integrated luminosity at $\sqrt{s} = 14 \text{ TeV}$. The range of masses probed with the first two configurations (that we call the low energy phase) is quite different from the one probed by the high energy phase (the third option). Thus, the analysis are also different depending on the phase. In particular, as we describe below, the analysis channel in the high energy phase benefits from using boosted techniques.

3.6.1 Low Energy Phase

The mass range that can be probed at the LHC within the low energy phase ($\sqrt{s} = 7$ or 8 TeV) is relatively low. This means that the decay products are not extremely boosted. We have found that traditional analysis are more efficient probing this region of parameter space than analysis that use boosted techniques. Also, since we have the leptonic top decays to trigger on, we can afford to use the main Higgs decay channel, namely $b\bar{b}$, with a branching ratio $\text{BR}(h \rightarrow b\bar{b}) = 0.48$ for the choice of parameters of Eqs. (3.56) and (3.57). We are therefore interested in the following process

$$pp \rightarrow G \rightarrow \mathcal{T}\bar{t} + \bar{\mathcal{T}}t \rightarrow ht\bar{t} \rightarrow 4b + 2j + l + \cancel{E}_T. \quad (3.60)$$

We use as discriminating variable

$$S_T \equiv \sum_{j=1}^{n_j} p_T(j) + \sum_{l=1}^{n_l} p_T(l) + \cancel{E}_T, \quad (3.61)$$

where $n_{j,l}$ is the relevant number of jets or leptons (ordered according to their p_T), which depends on the analysis and will be specified below.

The main backgrounds are $t\bar{t}$ and $t\bar{t}b\bar{b}$. In order to reduce the number of background events to manageable values we impose the following initial cuts

- At least 4 jets, of which at least 3 must be tagged as b-jets.
- At least 1 isolated charged lepton.
- A cut on S_T (in this case we have $n_j = 4$ and $n_l = 1$) that depends on the test M_G we are considering

$$S_T > 0.9, 1.1, 1.5 \text{ TeV for } M_G = 1.5, 2, 2.5 \text{ TeV.} \quad (3.62)$$

M_G [TeV]	ϵ_s	$\epsilon_{t\bar{t}}$	$\epsilon_{t\bar{t}b\bar{b}}$
1.5	15.8	0.00652	0.514
2.0	13.69	0.00108	0.156
2.5	9.67	0.000292	0.0174
3.0	9.14	0.000292	0.0174

Table 3.2: Global efficiencies for the signal and relevant backgrounds as a function of M_G . All efficiencies are reported as per cent.

We show in Table 3.2, the global efficiencies for the signal and relevant backgrounds, as a function of M_G . We obtain the following statistical significances

$$\mathcal{S}(9.5, 3.3) = 4.0 \quad (\mathcal{L} = 5 \text{ fb}^{-1}, \sqrt{s} = 7 \text{ TeV}, M_G = 2 \text{ TeV}), \quad (3.63)$$

$$\mathcal{S}(77.2, 19.9) = 13.9 \quad (\mathcal{L} = 20 \text{ fb}^{-1}, \sqrt{s} = 8 \text{ TeV}, M_G = 2 \text{ TeV}), \quad (3.64)$$

defined as

$$\mathcal{S}(s, b) = \sqrt{2 \times \left[(s + b) \ln \left(1 + \frac{s}{b} \right) - s \right]}, \quad (3.65)$$

where s (b) is the number of signal (background) events after the corresponding cuts. As we will discuss below, current constraints from dijet contact interactions imply a bound $M_G \geq 2.5$ TeV for the benchmark model in the anarchy scenario. These values cannot be probed with the 7 TeV run but with $\sqrt{s} = 8$ TeV it should be possible to discover (exclude) it with 20 (5) fb^{-1} .

3.6.2 High Energy Phase

In the high energy phase, $\sqrt{s} = 14$ TeV, larger masses can be probed. In this case the decay products of G and \mathcal{T} are highly boosted and one can benefit from the use of boosted techniques. In this study we use a very simple technique, based on fat jet invariant masses [194–196]. The new set of cuts optimized for the larger masses probed are the following

- At least 3 jets, with a minimum of 2 b tags.
- At least 1 isolated charged lepton.
- All jets are then ordered according to their invariant mass and the first two jets are required to have invariant masses close to the top and Higgs mass, respectively, $|m_{j_1} - m_t| \leq 40$ GeV and $|m_{j_2} - m_h| \leq 40$ GeV (here $j_{1,2}$ are the jets with the largest and second largest invariant masses).

- A cut on S_T (in this case we have $n_j = 3$ and $n_l = 1$) that depends on the test M_G we are considering

$$S_T > 1.2, 1.5, 1.7, 2 \text{ TeV for } M_G = 2, 2.5, 3, \geq 3.5 \text{ TeV.} \quad (3.66)$$

M_G [TeV]	ϵ_s	$\epsilon_{t\bar{t}}$	$\epsilon_{t\bar{t}b\bar{b}}$
2.0	11.74	0.00265	0.1021
2.5	15.61	0.00095	0.0518
3.0	18.06	0.00054	0.0298
3.5	17.74	0.00027	0.0188
4	19.08	0.00027	0.0188
4.5	19.40	0.00027	0.0188

Table 3.3: Global efficiencies for the signal and relevant backgrounds as a function of M_G . All efficiencies are reported as per cent.

The results of these cuts on the main backgrounds and the signal are reported in Table 3.3 as a function of M_G . The corresponding statistical significance is

$$\mathcal{S}(828, 170) = 43 \quad (\mathcal{L} = 100 \text{ fb}^{-1}, \sqrt{s} = 14 \text{ TeV}, M_G = 3 \text{ TeV}). \quad (3.67)$$

3.6.3 Results

For the anarchic case we are considering, the bounds from dijet contact interactions depend only on g_{*3} . In particular, for the chosen value $g_{*3} = 3$ they imply a constant bound $M_G \geq 2.5$ TeV. This bound decreases as g_{*3} increases. For instance it becomes $M_G \geq 1.5$ TeV for $g_{*3} \approx 4.6$. Our main results are shown in Fig. 3.25 and can be summarized in the following points:

- Using the 2011 run, masses up to $M_G \approx 1.9 - 1.6$ TeV can be discovered in the region allowed by current constraints for $g_{*3} \gtrsim 4 - 5$. Exclusion bounds in the $M_G \sim 2.2 - 1.9$ TeV can be reached for $g_{*3} \sim 3 - 5$. These results assume $s_u \sim 0.5 - 0.7$ (notice that in the anarchy case this refers to the t_R degree of compositeness), outside this range, the reach decreases as shown in the left column of Fig. 3.25. The plot corresponding to this energy is not shown as it is quite similar to the one at $\sqrt{s} = 8$ TeV, only with the numbers reduced to match the results we have described.
- The expected 2012 run with 20 fb^{-1} at $\sqrt{s} = 8$ TeV can lead to a discovery in the region $M_G \sim 2.5 - 2$ TeV (and a similar exclusion with just 5 fb^{-1}) for $g_{*3} \sim 3 - 5$. Exclusion bounds in the $M_G \sim 2.8 - 2.4$ TeV region can be set, for $g_{*3} \sim 2.5 - 5$, with the same luminosity.
- Data with $\sqrt{s} = 14$ TeV can probe a much larger region of parameter space. Values up to $M_G \sim 4.3$ TeV can be discovered with 100 fb^{-1} and bounds up to 4.8 TeV can be set with the same luminosity.

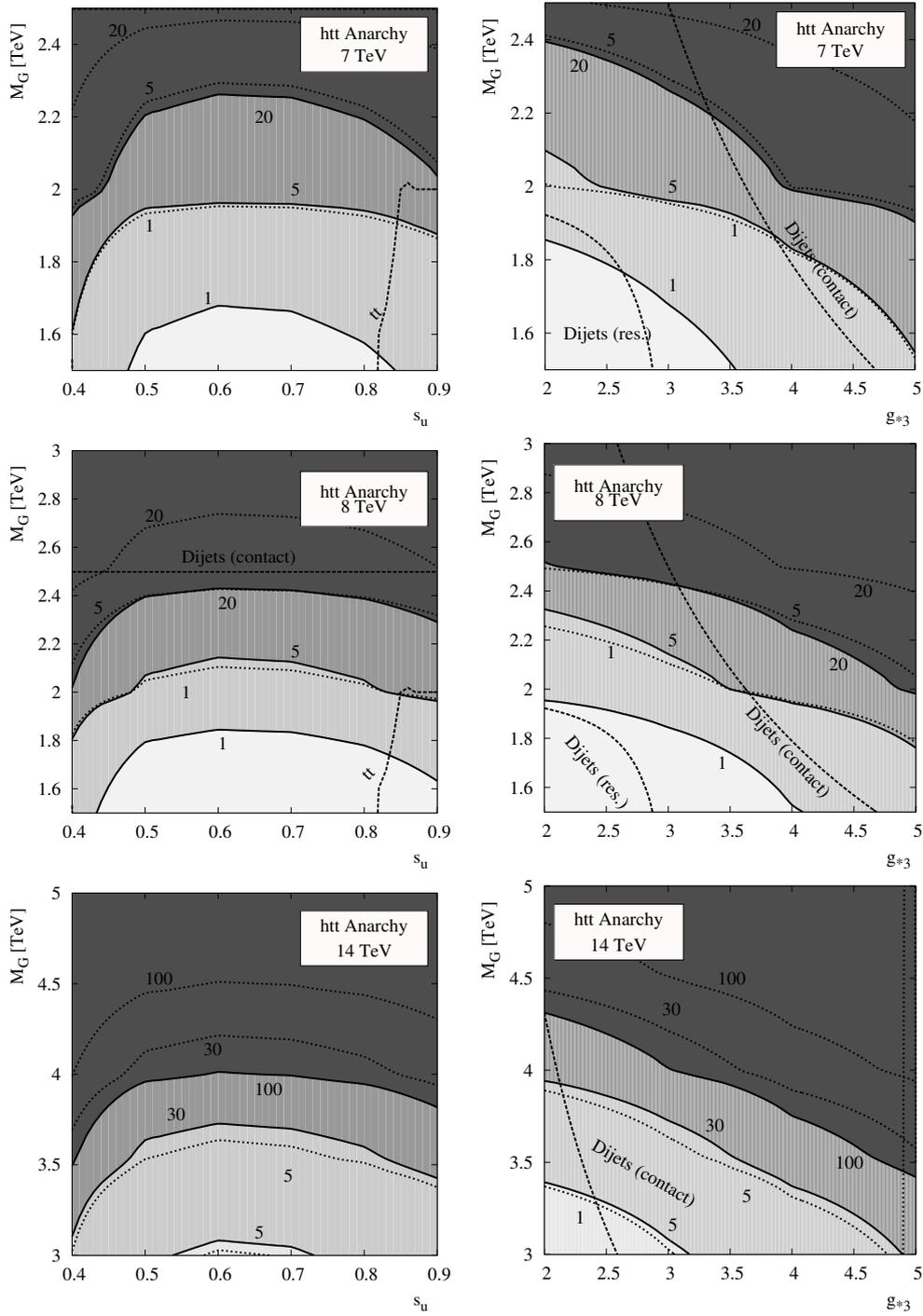


Figure 3.25: Contours of required luminosity for a 5σ discovery (bands and solid lines) and 95% exclusion limits (dotted lines) as a function of $s_u = s_u^{(3)}$ and M_G (left column) and g_{*3} and M_G (right column) for $\sqrt{s} = 7, 8$ and 14 TeV (first, second and third row, respectively). Current bounds are shown with dashed lines (the area below the dashed lines is excluded).

4

A Holographic Higgs Model of Lepton Masses and Mixings

As we have seen in Chapter 2, the AdS/CFT correspondence suggests that composite Higgs models are strongly coupled duals of models of GHU, which provide a calculable framework for the 4D conformal theory.¹ Most of the studies related to the 5D realization of composite Higgs models have only focused on the quark sector. In fact, although some of the first studies of bulk fermion phenomenology in models with WED were made with the leptonic sector in mind [96, 103, 199], not much progress has been made until quite recently. In particular, older proposals for models of lepton masses have, with few exceptions, not been updated to make them compatible with new, realistic models in WED. One possible reason is that the generation of Yukawa couplings by fermion splitting [200] seemed to naturally lead to a hierarchical pattern of fermion masses and mixing angles, like the one observed in the quark sector, but not to large mixing angles like those observed in the neutrino sector. This was shown not to be necessarily true [97], and a realization of neutrino masses within this framework and with a realistic dark matter candidate was presented in [98].

An alternative approach to differentiate the quark and lepton spectra is to assume a global symmetry acting on the leptonic sector. 4D models of neutrino masses with an A_4 symmetry [201, 202] can predict a tri-bimaximal (TBM) [203] pattern of lepton mixing to leading order, what can reproduce quite well the observed values [64, 235] after taking into account NLO corrections. This global symmetry can be also implemented in simple models with WED [100, 101].² Such a construction presents an advantage over 4D models since the mass hierarchy follows from wavefunction overlapping, geometrically realizing the required Frogatt-Nielsen mass generation in 4D models. Besides, it also improves other 5D models that solely rely on the former for it has an extra built-in flavor protection due to the discrete A_4 symmetry. Our goal is to extend this set-up to models of GHU, which are arguably the most natural models of EWSB in WED. We will show that, despite some subtleties related to the way fermions acquire non-trivial Yukawa couplings in GHU models [108], it is easy to find examples that naturally generate a realistic fermion spectrum also in the lepton sector.

¹See [190, 191, 197] for a discussion of composite Higgs models from the effective 4D point of view.

²Other symmetries that can simultaneously accommodate the pattern of quark and lepton mixing have been also considered in 5D contexts [101, 204] and in models compatible with an underlying GUT structure [205].

Two new features phenomenologically relevant come out from our analysis. First, due to an extra suppression of the leptonic Yukawa couplings implied by the A_4 symmetry, the τ lepton is typically more composite than one would naively expect from its mass. This makes new leptonic resonances at the EW scale a likely occurrence in these models. Besides, as they come in two almost degenerate doublets with hypercharges $-1/2$ and $-3/2$, respectively, and mainly couple to τ , they provide a very distinctive signature at LHC for they only decay through definite channels and into τ leptons. This structure is dictated by the same symmetry that protects the $Z\bar{b}_L b_L$ coupling in this type of models [111], which in the leptonic sector protects the SM lepton couplings despite the large new lepton couplings to τ [113]. Second, the A_4 symmetry together with the protecting mechanism above [114, 115] result in a double-layer flavor protection. Thus, LFV mediated by tree-level exchange of heavy modes is further suppressed, and typically below current experimental limits. The main constraints result from one-loop processes, like $\mu \rightarrow e\gamma$, which is close but quite often below the present experimental sensitivity, being then within the reach of future experiments.

4.1 The Model

We consider a 5D model in a slice of AdS_5 with metric given by Eq. (2.2), where $R \sim M_{\text{Pl}}^{-1}$ and $R' \sim \text{TeV}^{-1}$. Following [135], we assume an $SO(5) \otimes U(1)_X$ bulk gauge symmetry broken by boundary conditions to $SO(4) \otimes U(1)_X$ on the IR brane and to $SU(2)_L \otimes U(1)_Y$ on the UV brane. The bulk gauge fields read

$$\begin{aligned} L_\mu^a(+, +), & \quad B_\mu(+, +), & \quad C_\mu^{\hat{a}}(-, -), \\ R_\mu^b(-, +), & \quad Z'_\mu(-, +), \end{aligned} \quad (4.1)$$

where the superscripts $a = 1, 2, 3$, $b = 1, 2$ label the $SO(4)$ gauge bosons in explicit $SU(2)_L \otimes SU(2)_R$ notation, and

$$B_\mu = \frac{g_X R_\mu^3 + g_5 X_\mu}{\sqrt{g_5^2 + g_X^2}}, \quad Z'_\mu = \frac{g_5 R_\mu^3 - g_X X_\mu}{\sqrt{g_5^2 + g_X^2}}, \quad (4.2)$$

with g_5 and g_X the 5D $SO(5)$ and $U(1)_X$ gauge couplings, respectively. (The electric charge reads $Q = T_L^3 + Y = T_L^3 + T_R^3 + Q_X$ with this normalization.) Finally, $C_\mu^{\hat{a}}$, $\hat{a} = 1, \dots, 4$, are the gauge bosons corresponding to the $SO(5)/SO(4)$ coset space.

The gauge directions along $SO(5)/SO(4)$ are broken on both branes and there is a massless zero mode along the 5-th component,

$$C_5^{\hat{a}}(x, z) = \sqrt{\frac{2/R}{1 - (R/R')^2}} \frac{z}{R'} h^{\hat{a}}(x) + \dots \approx \sqrt{\frac{2}{R}} \frac{z}{R'} h^{\hat{a}}(x) + \dots, \quad (4.3)$$

where the dots denote massive modes. (We have chosen the normalization constant to obtain a canonically normalized scalar, and in the second equality we have used $R \ll R'$.) These four scalars transform as a $\mathbf{4}$ of $SO(4)$ and are identified with the SM Higgs. 5D gauge invariance guarantees that any potential generated for these scalars has to arise from non-local contributions and therefore, it is finite to all orders in perturbation theory [168].

Regarding the matter content of the model, there are several possibilities. We consider here all fermions to be in fundamental representations of $SO(5)$. Thus, four multiplets per family are required in order to have independent localizations for left and right-handed zero modes. This construction is parallel to the one giving rise to realistic composite Higgs models in the quark sector [198, 206, 225]; and as we will show, a similar matter content transforming non-trivially under a global A_4 symmetry generates the observed leptonic spectrum in a natural way, without conflict with present experimental data. Hence, there are four 5D fermion representations per

generation transforming as the fundamental $SO(5)$ representation $\mathbf{5}$, with boundary conditions

$$\begin{aligned}\zeta_1 &= \begin{pmatrix} \tilde{X}_1[-+] & \nu_1[++] \\ \tilde{\nu}_1[-+] & e_1[++] \end{pmatrix} \oplus \nu'_1[-+], & \zeta_2 &= \begin{pmatrix} \tilde{X}_2[+-] & \nu_2[+-] \\ \tilde{\nu}_2[+-] & e_2[+-] \end{pmatrix} \oplus \nu'_2[--], \\ \zeta_3 &= \begin{pmatrix} \nu_3[-+] & \tilde{e}_3[-+] \\ e_3[-+] & \tilde{Y}_3[-+] \end{pmatrix} \oplus e'_3[-+], & \zeta_\alpha &= \begin{pmatrix} \nu_\alpha[+-] & \tilde{e}_\alpha[+-] \\ e_\alpha[+-] & \tilde{Y}_\alpha[+-] \end{pmatrix} \oplus e'_\alpha[--],\end{aligned}\quad (4.4)$$

where $\zeta_{1,2}$ and $\zeta_{3,\alpha}$ have $U(1)_X$ charge 0 and -1 , respectively. Note that there are three copies for each $\zeta_{1,2,3}$ because there are three families, but only one ζ_α set with α running over the three lepton flavors e, μ, τ . We explicitly show the decomposition under $SU(2)_L \otimes SU(2)_R$, $\mathbf{5} = (\mathbf{2}, \mathbf{2}) \oplus (\mathbf{1}, \mathbf{1})$. The bi-doublet is represented by a 2×2 matrix with the $SU(2)_L$ rotation acting vertically and the $SU(2)_R$ one horizontally (*i.e.* the left and right columns correspond to fields with $T_R^3 = \pm 1/2$, whereas the upper and lower components have $T_L^3 = \pm 1/2$, respectively). The bi-doublets in $\zeta_{1,2}$ contain two $SU(2)_L$ doublets of hypercharge $\frac{1}{2}$ and $-\frac{1}{2}$, and those in $\zeta_{3,\alpha}$ two $SU(2)_L$ doublets of hypercharge $-\frac{1}{2}$ and $-\frac{3}{2}$, respectively. The corresponding electric charges read

$$Q(\nu.) = Q(\tilde{\nu}.) = Q(\nu'.) = 0, \quad Q(e.) = Q(e'.) = Q(\tilde{e}.) = -1, \quad Q(\tilde{X}.) = +1, \quad Q(\tilde{Y}.) = -2, \quad (4.5)$$

where the dot denotes all possible values of the corresponding subscript. The chosen boundary conditions allow for a LH zero mode transforming as an $SU(2)_L$ doublet with hypercharge $-1/2$ in ζ_1 , a RH singlet of charge -1 in ζ_α , and a RH neutral singlet in ζ_2 .

As usual in A_4 models, an extra global symmetry must be imposed to forbid dangerous operators. A discrete Z_8 group does the job in our case. Both global symmetries will be broken at the two branes by localized scalars transforming as gauge singlets, ϕ and η at the UV brane and ϕ' and η' at the IR one. The fermion and scalar transformation properties under $A_4 \otimes Z_8$ are gathered in Table 4.1. The three copies of $\zeta_{1,2,3}$ span the A_4 triplet representation, whereas each ζ_α transforms as one the three different A_4 one-dimensional representations (see Appendix A.1 for a summary of the A_4 representations).

	A_4	Z_8		A_4	Z_8
ζ_1	$\mathbf{3}$	1	$\phi(\text{UV})$	$\mathbf{3}$	4
ζ_2	$\mathbf{3}$	2	$\eta(\text{UV})$	$\mathbf{1}$	4
ζ_3	$\mathbf{3}$	1	$\phi'(\text{IR})$	$\mathbf{3}$	5
ζ_α	$\mathbf{1}, \mathbf{1}', \mathbf{1}''$	4	$\eta'(\text{IR})$	$\mathbf{1}$	7

Table 4.1: Bulk fermion (left) and localized scalar (right) quantum number assignments under the discrete group $A_4 \otimes Z_8$.

Once the matter content is fixed, we can write down the most general Lagrangian compatible with the symmetries. The bulk Lagrangian reads

$$\begin{aligned}\mathcal{L} = \int_R^{R'} dz a^4 \left\{ \bar{\zeta}_k \left[i\not{D} + \left(D_z + 2\frac{a'}{a} \right) \gamma^5 - aM_k \right] \zeta_k \right. \\ \left. + \bar{\zeta}_\alpha \left[i\not{D} + \left(D_z + 2\frac{a'}{a} \right) \gamma^5 - aM_\alpha \right] \zeta_\alpha \right\},\end{aligned}\quad (4.6)$$

where summation on repeated indices $k \in \{1, 2, 3\}$, $\alpha \in \{e, \mu, \tau\}$ is understood. $D_{\mu,z}$ are the gauge covariant derivatives and the bulk Dirac masses are conventionally parametrized in terms of the fundamental scale R ,

$$M_{k,\alpha} = \frac{c_{k,\alpha}}{R}. \quad (4.7)$$

Note that the A_4 symmetry implies a family independent bulk mass for ζ_k . The most general localized Lagrangians, excluding kinetic terms (discussed below), compatible with the boundary conditions, and local and global symmetries, can be written

$$\begin{aligned} -\mathcal{L}_{UV} &= \frac{x_\eta}{2\Lambda} \eta \bar{\nu}'_{2R} \nu'_{2R} + \frac{x_\nu}{2\Lambda} \phi \bar{\nu}'_{2R} \nu'_{2R} + x_l \bar{l}_{1L} l_{3R} + \text{h.c.} + \dots, \\ -\mathcal{L}_{IR} &= \left(\frac{R}{R'}\right)^4 \left\{ \frac{y_b^\alpha}{\Lambda'} \left[(\bar{l}_{3L} \phi')^\alpha l_{\alpha R} + (\tilde{l}_{3L} \phi')^\alpha \tilde{l}_{\alpha R} \right] + \frac{y_s^\alpha}{\Lambda'} (\bar{e}'_{3L} \phi')^\alpha e'_{\alpha R} \right. \\ &\quad \left. + \frac{y_b}{\Lambda'} \left[\eta' \bar{l}_{1L} l_{2R} + \eta' \tilde{l}_{1L} \tilde{l}_{2R} \right] + \frac{y_s}{\Lambda'} \eta' \bar{\nu}'_{1L} \nu'_{2R} \right\} + \text{h.c.} + \dots, \end{aligned} \quad (4.8)$$

where we have assumed that lepton number is only violated on the UV brane.³ l denotes the SM-like doublet and \tilde{l} stands for the other $SU(2)_L$ doublet within the given bi-doublet, whereas the dots correspond to higher dimensional operators. We have also introduced the LH and RH chirality projections $\zeta_{L,R} \equiv [(1 \mp \gamma^5)/2]\zeta$, recovering the standard 4D notation. Finally, $(\)^\alpha$, $\alpha = e, \mu, \tau$, are the $\mathbf{3} \otimes \mathbf{3}$ combinations transforming under A_4 as $\mathbf{1}, \mathbf{1}''$ and $\mathbf{1}'$, respectively.

As usually in these models, we shall assume that $A_4 \otimes Z_8$ is spontaneously broken by the boundary scalar vev

$$\langle \phi \rangle = (v, 0, 0), \quad \langle \eta \rangle = v_\eta, \quad \langle \phi' \rangle = (v', v', v') \quad \text{and} \quad \langle \eta' \rangle = v'_\eta, \quad (4.9)$$

resulting in the brane localized terms

$$\begin{aligned} -\mathcal{L}_{UV} &= \frac{1}{2} \bar{\nu}'_{2R} \theta_M \nu'_{2R} + x_l \bar{l}_{1L} l_{3R} + \text{h.c.} + \dots, \\ -\mathcal{L}_{IR} &= \left(\frac{R}{R'}\right)^4 \left\{ \sqrt{3} \frac{v'}{\Lambda'} \left[\bar{l}_{3L} \Omega \begin{pmatrix} y_b^e & 0 & 0 \\ 0 & y_b^\mu & 0 \\ 0 & 0 & y_b^\tau \end{pmatrix} l_R + [l_3, l \rightarrow \tilde{l}_3, \tilde{l}] + \bar{e}'_{3L} \Omega \begin{pmatrix} y_s^e & 0 & 0 \\ 0 & y_s^\mu & 0 \\ 0 & 0 & y_s^\tau \end{pmatrix} e'_R \right] \right. \\ &\quad \left. + y_b \frac{v'_\eta}{\Lambda'} [\bar{l}_{1L} l_{2R} + \tilde{l}_{1L} \tilde{l}_{2R}] + y_s \frac{v'_\eta}{\Lambda'} \bar{\nu}'_{1L} \nu'_{2R} \right\} + \text{h.c.} + \dots, \end{aligned} \quad (4.10)$$

with the Majorana mass matrix

$$\theta_M \equiv \begin{pmatrix} \frac{x_\eta v_\eta}{\Lambda} & 0 & 0 \\ 0 & \frac{x_\nu v_\eta}{\Lambda} & \frac{x_\nu v}{\Lambda} \\ 0 & \frac{x_\nu v}{\Lambda} & \frac{x_\eta v_\eta}{\Lambda} \end{pmatrix} = \begin{pmatrix} \epsilon_s & 0 & 0 \\ 0 & \epsilon_s & \epsilon_t \\ 0 & \epsilon_t & \epsilon_s \end{pmatrix}, \quad (4.11)$$

and the unitary matrix

$$\Omega \equiv \frac{1}{\sqrt{3}} \begin{pmatrix} 1 & 1 & 1 \\ 1 & \omega & \omega^2 \\ 1 & \omega^2 & \omega \end{pmatrix}, \quad \omega = e^{2\pi i/3}. \quad (4.12)$$

In order to simplify Eq. (4.10), we can rotate the matter fields

$$\zeta_k \rightarrow \Omega \zeta_k, \quad \forall k, \quad (4.13)$$

leaving the bulk Lagrangian \mathcal{L} invariant. However, the localized terms

$$\begin{aligned} -\mathcal{L}_{UV} &= \frac{1}{2} \bar{\nu}'_{2R} \hat{\theta}_M \nu'_{2R} + x_l \bar{l}_{1L} l_{3R} + \text{h.c.} + \dots, \\ -\mathcal{L}_{IR} &= \left(\frac{R}{R'}\right)^4 \left[\sqrt{3} \frac{v'}{\Lambda'} \left(y_b^\alpha \bar{l}_{3\alpha L} l_{\alpha R} + y_b^\alpha \tilde{l}_{3\alpha L} \tilde{l}_{\alpha R} + y_s^\alpha \bar{e}'_{3\alpha L} e'_{\alpha R} \right) \right. \\ &\quad \left. + y_b \frac{v'_\eta}{\Lambda'} (\bar{l}_{1L} l_{2R} + \tilde{l}_{1L} \tilde{l}_{2R}) + y_s \frac{v'_\eta}{\Lambda'} \bar{\nu}'_{1L} \nu'_{2R} \right] + \text{h.c.} + \dots, \end{aligned} \quad (4.14)$$

³This assumption, which corresponds to the strong sector preserving lepton number, can be obtained as an accidental symmetry by introducing, for instance, larger $SO(5)$ representations.

become diagonal in flavor space (the terms proportional to x_l and $y_{b,s}$ are actually flavor independent), except for the Majorana masses

$$\hat{\theta}_M \equiv \Omega \theta_M \Omega = \begin{pmatrix} \epsilon_s + \frac{2\epsilon_t}{3} & -\frac{\epsilon_t}{3} & -\frac{\epsilon_t}{3} \\ -\frac{\epsilon_t}{3} & \frac{2\epsilon_t}{3} & \epsilon_s - \frac{\epsilon_t}{3} \\ -\frac{\epsilon_t}{3} & \epsilon_s - \frac{\epsilon_t}{3} & \frac{2\epsilon_t}{3} \end{pmatrix}. \quad (4.15)$$

Dirichlet boundary conditions are modified in the presence of these boundary terms. Thus, on the UV brane

$$l_{1R} - x_l l_{3R} = 0, \quad l_{3L} + x_l^* l_{1L} = 0, \quad \nu'_{2L} + \hat{\theta}_M^\dagger \nu'_{2R} = 0, \quad (4.16)$$

and on the IR one

$$\begin{aligned} l_{3\alpha R} + \sqrt{3} \frac{v'}{\Lambda'} y_b^\alpha l_{\alpha R} &= 0, & \tilde{l}_{3\alpha R} + \sqrt{3} \frac{v'}{\Lambda'} y_b^\alpha \tilde{l}_{\alpha R} &= 0, & e'_{3\alpha R} + \sqrt{3} \frac{v'}{\Lambda'} y_s^\alpha e'_{\alpha R} &= 0, \\ l_{\alpha L} - \sqrt{3} \frac{v'}{\Lambda'} y_b^{\alpha*} l_{3\alpha L} &= 0, & \tilde{l}_{\alpha L} - \sqrt{3} \frac{v'}{\Lambda'} y_b^{\alpha*} \tilde{l}_{3\alpha L} &= 0, & e'_{\alpha L} - \sqrt{3} \frac{v'}{\Lambda'} y_s^{\alpha*} e'_{3\alpha L} &= 0, \\ l_{1R} + y_b \frac{v'_\eta}{\Lambda'} l_{2R} &= 0, & \tilde{l}_{1R} + y_b \frac{v'_\eta}{\Lambda'} \tilde{l}_{2R} &= 0, & \nu'_{1R} + y_s \frac{v'_\eta}{\Lambda'} \nu'_{2R} &= 0, \\ l_{2L} - y_b^* \frac{v'_\eta}{\Lambda'} l_{1L} &= 0, & \tilde{l}_{2L} - y_b^* \frac{v'_\eta}{\Lambda'} \tilde{l}_{1L} &= 0, & \nu'_{2L} - y_s^* \frac{v'_\eta}{\Lambda'} \nu'_{1L} &= 0. \end{aligned} \quad (4.17)$$

From these equations we observe that the lepton doublet zero mode is shared by all multiplets due to the non-zero values of x_l , y_b and y_b^α , whereas y_s splits the RH neutrino zero mode between ζ_1 and ζ_2 , and y_s^α splits the RH charge -1 singlet between ζ_3 and ζ_α . This splitting is crucial in models of GHU, since the Higgs being part of a gauge multiplet can only mix fermion fields within the same $SO(5)$ multiplet, coupling to them with the same (gauge) strength. The non-trivial flavor structure is then only due to the brane terms above. Thus, the only source of flavor violation in the rotated basis comes from $\hat{\theta}_M$ in Eq. (4.15), whose particular form will eventually lead to TBM mixing in the leptonic sector. This flavor universality is a welcome consequence of the A_4 symmetry, for it will also prevent flavor violating operators mediated by heavy KK gauge bosons to exceed current experimental bounds. This observation, which was made in simpler models with WED [100, 101], is maintained at this order in the more realistic models with GHU under study here. Incidentally, the extra fields required to complete the $SO(5)$ representations imply that simpler Z_2 or Z_3 symmetries are not suitable to banish operators violating this mixing pattern.

4.2 The Leptonic Spectrum

In order to find the lepton masses and mixings we have to solve the equations of motion derived from the bulk action with the boundary conditions in Eqs. (4.16) and (4.17). This can be actually carried out exactly in the case of GHU models because the Higgs, which is part of a higher-dimensional gauge field, can be eliminated from the bulk by a rotation in gauge space, thus reducing the Higgs effect to the modification of the boundary conditions. This is essential, for otherwise the Higgs would mix different multiplets in the bulk, and the corresponding equations of motion would be forbiddingly difficult to solve. Still, the large number of fields involved makes the solution of the full system technically challenging. An alternative approach is to perform a KK expansion without including the Higgs, and then to take into account its effects by diagonalizing the corresponding mass matrix. In this case one must include the Majorana masses not in the KK expansion but as a contribution to the mass matrix. Otherwise we would have to incorporate the effect of all physical modes up to the Majorana mass scale (which is $\sim R^{-1}$) in order to obtain an accurate enough approximation [199]. Furthermore, the leading contribution to the *light* neutrino masses and mixing angles can be obtained by simply considering the zero modes in the KK expansion (thus

including the *heavy* Majorana RH neutrinos), for heavier KK modes give a suppressed contribution. This so called zero mode approximation (ZMA) is convenient because of the transparent way the flavor structure leading to TBM mixing is realized. We will thus proceed in three steps, first we will compute the light lepton masses and mixing angles in the ZMA. Then, we will include the massive KK modes but still incorporating the localized Majorana masses and the Higgs effects in the mass matrix. Finally, we will take these into account considering the boundary conditions directly in the KK expansion.

The Yukawa couplings, being originally gauge couplings, are flavor diagonal and do not mix different 5D multiplets

$$\begin{aligned}\mathcal{L}_Y &= g_5 h^{\hat{a}}(x) \sqrt{\frac{2}{R}} \frac{1}{\sqrt{1-(R/R')^2}} \int_R^{R'} dz \left(\frac{R}{z}\right)^4 \frac{z}{R'} (\bar{\zeta}_k T_C^{\hat{a}} \Gamma^5 \zeta_k + \bar{\zeta}_\alpha T_C^{\hat{a}} \Gamma^5 \zeta_\alpha) \\ &= -i g_5 \tilde{v} \sqrt{\frac{2}{R}} \frac{1}{\sqrt{1-(R/R')^2}} \int_R^{R'} dz \left(\frac{R}{z}\right)^4 \frac{z}{R'} (\bar{\zeta}_{kL} T_C^4 \zeta_{kR} + \bar{\zeta}_{\alpha L} T_C^4 \zeta_{\alpha R}) + \text{h.c.},\end{aligned}\quad (4.18)$$

where we have used in the last equality $\Gamma^5 = -i\gamma^5$, and assumed that the Higgs takes a vev $\langle h^{\hat{a}} \rangle = \tilde{v} \delta^{\hat{a},4}$. Neglecting $R/R' \ll 1$ and inserting the expression for T_C^4 in Appendix A.2, we get the Yukawa Lagrangian from the bulk

$$\begin{aligned}\mathcal{L}_Y &= \frac{g_5 \tilde{v}}{2} \sqrt{\frac{2}{R}} \int_R^{R'} dz \left(\frac{R}{z}\right)^4 \frac{z}{R'} \left\{ \sum_{s=1,2} \left[\bar{\nu}'_{sL} (\nu_{sR} + \tilde{\nu}_{sR}) - (\bar{\nu}_{sL} + \tilde{\bar{\nu}}_{sL}) \nu'_{sR} \right] \right. \\ &\quad \left. + \sum_{s=3,\alpha} \left[\bar{e}'_{sL} (e_{sR} + \tilde{e}_{sR}) - (\bar{e}_{sL} + \tilde{\bar{e}}_{sL}) e'_{sR} \right] \right\} + \text{h.c.}\end{aligned}\quad (4.19)$$

4.2.1 Lepton Spectrum in the Zero Mode Approximation

In this section we only consider the leptonic zero modes. The localized Majorana masses and the Higgs couplings will be incorporated as mass terms to be diagonalized. The localized Dirac masses, on the other hand, have to be taken into account exactly. Since they mix different multiplets through the boundary conditions, the physical zero modes (the same will happen for massive modes) are split among all multiplets mixed by them. In particular, the LH lepton doublets live in all four multiplets. Note that as we do not include in the expansion the Majorana mass term, which is the only source of flavor violation, different generations do not mix. The properly normalized zero modes satisfying the corresponding boundary conditions read

$$l_{1\alpha L}(x, z) = \frac{1}{\sqrt{R'}} \left(\frac{z}{R}\right)^2 \left(\frac{z}{R'}\right)^{-c_1} \frac{f_{c_1}}{\sqrt{l_\alpha}} l_{\alpha L}(x) + \dots, \quad (4.20)$$

$$l_{2\alpha L}(x, z) = y_b^* \frac{v'_\eta}{\Lambda'} \frac{1}{\sqrt{R'}} \left(\frac{z}{R}\right)^2 \left(\frac{z}{R'}\right)^{-c_2} \frac{f_{c_1}}{\sqrt{l_\alpha}} l_{\alpha L}(x) + \dots, \quad (4.21)$$

$$l_{3\alpha L}(x, z) = -x_l^* \frac{1}{\sqrt{R'}} \left(\frac{R}{R'}\right)^{c_3-c_1} \left(\frac{z}{R}\right)^2 \left(\frac{z}{R'}\right)^{-c_3} \frac{f_{c_1}}{\sqrt{l_\alpha}} l_{\alpha L}(x) + \dots, \quad (4.22)$$

$$l_{\alpha L}(x, z) = -\sqrt{3} x_l^* \frac{v'}{\Lambda'} \frac{1}{\sqrt{R'}} \left(\frac{R}{R'}\right)^{c_3-c_1} \left(\frac{z}{R}\right)^2 \left(\frac{z}{R'}\right)^{-c_\alpha} y_b^* \frac{f_{c_1}}{\sqrt{l_\alpha}} l_{\alpha L}(x) + \dots, \quad (4.23)$$

where $\alpha = e, \mu, \tau$ denote the lepton flavor and $l_{1,2,3}(x, z)$, $l_\alpha(x, z)$ stand for the doublet component of hypercharge $-1/2$ within each $\zeta_{1,2,3,\alpha}$, respectively. Then, $l_\alpha(x)$ are the *physical* zero modes; and the dots correspond to heavy KK modes. The flavor dependent term takes the form

$$l_\alpha \equiv 1 + |y_b|^2 \frac{v'^2}{\Lambda'^2} \frac{f_{c_1}^2}{f_{c_2}^2} + |x_l|^2 \left(\frac{R}{R'}\right)^{2(c_3-c_1)} \left[\frac{f_{c_1}^2}{f_{c_3}^2} + |y_b^\alpha|^2 \frac{3v'^2}{\Lambda'^2} \frac{f_{c_1}^2}{f_{c_\alpha}^2} \right], \quad (4.24)$$

with

$$f_c \equiv \left[\frac{1-2c}{1-\left(\frac{R}{R'}\right)^{1-2c}} \right]^{\frac{1}{2}} \quad (4.25)$$

defined as usual. Eqs. (4.20-4.23) show that x_l governs the splitting of the LH lepton doublet zero mode between $\zeta_{1,2}$ and $\zeta_{3,\alpha}$. Similarly, the splitting between ζ_1 and ζ_2 and the one between ζ_3 and ζ_α are governed by y_b and y_b^α , respectively. Also note that for $c_3 > c_1$ the zero mode components along $\zeta_{3,\alpha}$ have an extra suppression proportional to $(R/R')^{c_3-c_1}$.

The RH charged lepton zero modes live in the $SO(4)$ singlet component of ζ_3 and ζ_α ,

$$e'_{3\alpha R}(x, z) = -\sqrt{3}y_s^\alpha \frac{v'}{\Lambda'} \frac{1}{\sqrt{R'}} \left(\frac{z}{R}\right)^2 \left(\frac{z}{R'}\right)^{c_3} \frac{f_{-c_\alpha}}{\sqrt{\rho_\alpha}} e_{\alpha R}(x) + \dots, \quad (4.26)$$

$$e'_{\alpha R}(x, z) = \frac{1}{\sqrt{R'}} \left(\frac{z}{R}\right)^2 \left(\frac{z}{R'}\right)^{c_\alpha} \frac{f_{-c_\alpha}}{\sqrt{\rho_\alpha}} e_{\alpha R}(x) + \dots, \quad (4.27)$$

with

$$\rho_\alpha \equiv 1 + |y_s^\alpha|^2 \frac{3v'^2}{\Lambda'^2} \frac{f_{-c_\alpha}^2}{f_{-c_3}^2}. \quad (4.28)$$

Finally, there are RH neutrino zero modes living in the $SO(4)$ singlet components of $\zeta_{1,2}$, which read

$$\nu'_{1\alpha R}(x, z) = -y_s \frac{v'_\eta}{\Lambda'} \frac{1}{\sqrt{R'}} \left(\frac{z}{R}\right)^2 \left(\frac{z}{R'}\right)^{c_1} \frac{f_{-c_2}}{\sqrt{\lambda}} \nu_{\alpha R}(x) + \dots, \quad (4.29)$$

$$\nu'_{2\alpha R}(x, z) = \frac{1}{\sqrt{R'}} \left(\frac{z}{R}\right)^2 \left(\frac{z}{R'}\right)^{c_2} \frac{f_{-c_2}}{\sqrt{\lambda}} \nu_{\alpha R}(x) + \dots, \quad (4.30)$$

with

$$\lambda \equiv 1 + |y_s|^2 \frac{v_\eta'^2}{\Lambda'^2} \frac{f_{-c_2}^2}{f_{-c_1}^2}. \quad (4.31)$$

Note that these profiles are not only flavor diagonal but flavor independent.

We can now insert the former expressions in the general Yukawa Lagrangian, Eq. (4.19), and get the corresponding zero mode mass term

$$-\mathcal{L}_Y = \bar{e}_L \mathcal{M}_D^e e_R + \bar{\nu}_L \mathcal{M}_D^\nu \nu_R + \text{h.c.}, \quad (4.32)$$

with

$$(\mathcal{M}_D^e)_{\alpha\beta} = \frac{\sqrt{3}g_5 \tilde{v} x_l}{2\sqrt{2}R} \frac{v'}{\Lambda'} \left(\frac{R}{R'}\right)^{c_3-c_1} (y_s^\alpha - y_b^\alpha) \frac{f_{c_1} f_{-c_\alpha}}{\sqrt{\iota_\alpha \rho_\alpha}} \delta_{\alpha\beta}, \quad (4.33)$$

$$(\mathcal{M}_D^\nu)_{\alpha\beta} = -\frac{g_5 \tilde{v} v'_\eta}{2\sqrt{2}R\Lambda'} (y_s - y_b) \frac{f_{c_1} f_{-c_2}}{\sqrt{\lambda \iota_\alpha}} \delta_{\alpha\beta}. \quad (4.34)$$

On the other hand, the UV brane term

$$-\mathcal{L}_M = \frac{1}{2} \bar{\nu}'_{2R} \hat{\theta}_M \nu'_{2R} \Big|_R + \text{h.c.} \quad (4.35)$$

gives a Majorana mass contribution to the three RH neutrinos, so that the total zero mode mass Lagrangian writes

$$-\mathcal{L}_m = \bar{e}_L \mathcal{M}_D^e e_R + \bar{\nu}_L \mathcal{M}_D^\nu \nu_R + \frac{1}{2} \bar{\nu}'_{2R} \mathcal{M}_M^\nu \nu'_R + \text{h.c.}, \quad (4.36)$$

with

$$\mathcal{M}_M^\nu \equiv \frac{f_{-c_2}^2}{\lambda R'} \left(\frac{R}{R'} \right)^{2c_2} \hat{\theta}_M. \quad (4.37)$$

Assuming $\lambda \approx 1$ and $R/R' \approx 10^{-16}$, the Majorana mass scale is in the range $(10^{-2} - 10^{-5})/R \approx 10^{17} - 10^{14}$ GeV for $-0.5 \leq c_2 \leq -0.35$. \mathcal{L}_m is already diagonal for charged leptons (see Eq. (4.33)). Furthermore, the localization parameters f_{-c_α} naturally explain a hierarchical pattern of charged lepton masses.⁴ The electron and muon masses are easily obtained with the corresponding zero modes localized towards the UV brane. The tau mass induces some tension that requires c_1 and c_3 to be relatively close to $1/2$, $c_{1,3} \lesssim 0.6$, and the RH tau to be somewhat localized towards the IR brane, $c_\tau \geq -1/2$. This tension is stronger the smaller the factor $(y_s^\alpha - y_b^\alpha)x_l v'/\Lambda'$ is. Note the v'/Λ' suppression due to the A_4 structure. This suppression makes the RH tau generically more composite ($c_\tau > -1/2$) than naively expected from its mass. What generically implies *light* leptonic resonances accessible at the LHC, as discussed in Section 4.4. The $c_3 - c_1$ difference also controls how the LH zero modes are split between the $\zeta_{1,2}$ and $\zeta_{3,\alpha}$ multiplets (see [206, 225] for a related discussion). This becomes essential to protect the τ (LFV) couplings to the Z when it is near the IR brane.

Let us now turn our attention to the neutrino sector. The matrix elements in Eq. (4.36) satisfy $\|\mathcal{M}_D^\nu\| \sim \mathcal{O}(\text{TeV}) \ll \|\mathcal{M}_M^\nu\| \lesssim \mathcal{O}(M_{\text{Pl}})$ for natural values of the model parameters. Then, integrating out the *heavy* RH neutrinos we obtain the standard see-saw type Majorana mass matrix for the LH neutrinos

$$\begin{aligned} \tilde{\mathcal{M}}^\nu &= -\mathcal{M}_D^\nu \mathcal{M}_M^\nu^{-1} (\mathcal{M}_D^\nu)^T \\ &= -\frac{\tilde{m}}{3} \begin{pmatrix} \frac{1}{\nu_e} \begin{bmatrix} \frac{1}{\epsilon_s} + \frac{2}{\epsilon_s + \epsilon_t} \\ \frac{1}{\sqrt{\nu_e \nu_\mu}} \begin{bmatrix} \frac{1}{\epsilon_s} - \frac{1}{\epsilon_s + \epsilon_t} \\ \frac{1}{\epsilon_s} - \frac{1}{\epsilon_s + \epsilon_t} \end{bmatrix} \\ \frac{1}{\sqrt{\nu_e \nu_\tau}} \begin{bmatrix} \frac{1}{\epsilon_s} - \frac{1}{\epsilon_s + \epsilon_t} \\ \frac{1}{\epsilon_s} - \frac{1}{\epsilon_s + \epsilon_t} \end{bmatrix} \end{bmatrix} & \frac{1}{\sqrt{\nu_e \nu_\mu}} \begin{bmatrix} \frac{1}{\epsilon_s} - \frac{1}{\epsilon_s + \epsilon_t} \\ \frac{1}{\nu_\mu} \begin{bmatrix} \frac{1}{\epsilon_s} - \frac{1}{\epsilon_s - \epsilon_t} - \frac{\epsilon_t}{\Delta} \\ \frac{1}{\epsilon_s} + \frac{1}{\epsilon_s - \epsilon_t} + \frac{\epsilon_s}{\Delta} \end{bmatrix} \\ \frac{1}{\sqrt{\nu_\mu \nu_\tau}} \begin{bmatrix} \frac{1}{\epsilon_s} + \frac{1}{\epsilon_s - \epsilon_t} + \frac{\epsilon_s}{\Delta} \\ \frac{1}{\nu_\tau} \begin{bmatrix} \frac{1}{\epsilon_s} - \frac{1}{\epsilon_s + \epsilon_t} \\ \frac{1}{\epsilon_s} + \frac{1}{\epsilon_s - \epsilon_t} + \frac{\epsilon_s}{\Delta} \end{bmatrix} \end{bmatrix} \end{pmatrix}, \end{aligned} \quad (4.38)$$

where we have defined $\Delta = \epsilon_s^2 - \epsilon_t^2$ and

$$\tilde{m} \equiv \frac{g_5^2 (y_s - y_b)^2 v_\eta'^2}{R} \tilde{v}^2 R' f_{c_1}^2 \left(\frac{R}{R'} \right)^{-2c_2} = g^2 \log \left(\frac{R'}{R} \right) \frac{(y_s - y_b)^2 v_\eta'^2}{8\Lambda'^2} \tilde{v}^2 R' f_{c_1}^2 \left(\frac{R}{R'} \right)^{-2c_2}. \quad (4.39)$$

In the last equality we have used the tree-level matching of the 5D and 4D gauge coupling constants (in the absence of brane kinetic terms)

$$g_5 = g \sqrt{R \log(R'/R)}, \quad (4.40)$$

with $g \approx 0.65$ the 4D $SU(2)_L$ coupling constant. If we choose $c_{1,3} \geq \frac{1}{2}$, $c_3 > c_\alpha$, we can take $\nu_\alpha \cong \nu$ independent of α and then

$$\tilde{\mathcal{M}}^\nu \cong -\frac{\tilde{m}}{3\nu} \begin{pmatrix} \frac{1}{\epsilon_s} + \frac{2}{\epsilon_s + \epsilon_t} & \frac{1}{\epsilon_s} - \frac{1}{\epsilon_s + \epsilon_t} & \frac{1}{\epsilon_s} - \frac{1}{\epsilon_s + \epsilon_t} \\ \frac{1}{\sqrt{\nu_e \nu_\mu}} \begin{bmatrix} \frac{1}{\epsilon_s} - \frac{1}{\epsilon_s + \epsilon_t} \\ \frac{1}{\epsilon_s} - \frac{1}{\epsilon_s + \epsilon_t} \end{bmatrix} & \frac{1}{\nu_\mu} \begin{bmatrix} \frac{1}{\epsilon_s} - \frac{1}{\epsilon_s - \epsilon_t} - \frac{\epsilon_t}{\Delta} \\ \frac{1}{\epsilon_s} + \frac{1}{\epsilon_s - \epsilon_t} + \frac{\epsilon_s}{\Delta} \end{bmatrix} & \frac{1}{\sqrt{\nu_\mu \nu_\tau}} \begin{bmatrix} \frac{1}{\epsilon_s} + \frac{1}{\epsilon_s - \epsilon_t} + \frac{\epsilon_s}{\Delta} \\ \frac{1}{\nu_\tau} \begin{bmatrix} \frac{1}{\epsilon_s} - \frac{1}{\epsilon_s + \epsilon_t} \\ \frac{1}{\epsilon_s} + \frac{1}{\epsilon_s - \epsilon_t} + \frac{\epsilon_s}{\Delta} \end{bmatrix} \end{bmatrix} \end{pmatrix}, \quad (4.41)$$

which can be diagonalized by the Harrison-Perkins-Scott matrix [203]

$$U_{\text{HPS}} = \begin{pmatrix} \sqrt{2/3} & 1/\sqrt{3} & 0 \\ -1/\sqrt{6} & 1/\sqrt{3} & -1/\sqrt{2} \\ -1/\sqrt{6} & 1/\sqrt{3} & 1/\sqrt{2} \end{pmatrix}. \quad (4.42)$$

⁴The A_4 symmetry forces the LH charged leptons to share a common localization thus naturally explaining why the mass hierarchy in this sector is smaller than the one in the charge $2/3$ quark sector [207].

Recall that the charged lepton sector is already diagonal in this basis and therefore, U_{HPS} gives the PMNS mixing matrix with the predicted TBM form. The resulting neutrino mass spectrum reads

$$U_{\text{HPS}}^T \tilde{\mathcal{M}}^\nu U_{\text{HPS}} = -\frac{\tilde{m}}{\iota} \begin{pmatrix} \frac{1}{\epsilon_s + \epsilon_t} & 0 & 0 \\ 0 & \frac{1}{\epsilon_s} & 0 \\ 0 & 0 & \frac{1}{\epsilon_t - \epsilon_s} \end{pmatrix}, \quad (4.43)$$

implying the neutrino mass-squared differences

$$\Delta m_{21}^2 \equiv |m_2|^2 - |m_1|^2 = \left| \frac{\tilde{m}}{\iota \epsilon_s} \right|^2 \left[1 - \frac{1}{(1+r)^2} \right], \quad (4.44)$$

$$\Delta m_{31}^2 \equiv |m_3|^2 - |m_1|^2 = \left| \frac{\tilde{m}}{\iota \epsilon_s} \right|^2 \left[\frac{4r}{(1-r^2)^2} \right], \quad (4.45)$$

where $r \equiv \epsilon_t/\epsilon_s$. From Eq. (4.44) we see that Δm_{21}^2 is positive, as conventionally assumed, for $r < -2$ or $r > 0$. (For $-2 < r < 0$ we would have to exchange the ordering of the first two neutrinos, thus ruining the TBM prediction.) Hence, the neutrino spectrum is normal ($\Delta m_{31}^2 > 0$) for $r > 0$ and inverted ($\Delta m_{31}^2 < 0$) for $r < -2$ (see Eq. (4.45)). There are three solutions to Eqs. (4.44) and (4.45) reproducing the observed mass-squared differences, $\Delta m_{21}^2 \approx 7.67 \times 10^{-5} \text{ eV}^2$ and $\Delta m_{31}^2 \approx 2.46 (-2.37) \times 10^{-3} \text{ eV}^2$ for normal (inverted) hierarchy [29], in the allowed r range,

$$r \approx -2.01, 0.79, 1.20. \quad (4.46)$$

The other solution $r \approx -1.99$ does not give the correct mixing pattern and is therefore ignored. However, both, the normal ($r = 0.79, 1.20$) and the inverted ($r = -2.01$) mass hierarchy, can be realized in these models, with similar phenomenology in either case. On the other hand, the correct scale of neutrino masses is easily obtained varying the localization parameter c_2 , which lies in the interval $-0.4 \lesssim c_2 \lesssim -0.2$ for $c_{1,3}$ values giving the τ mass and $|\epsilon_{t,s}| \sim \mathcal{O}(10^{-2} - 10^{-1})$.

These results receive three types of corrections. First, there are bulk lepton KK modes with masses $\sim \text{TeV}$ which mix with the zero modes. This mixing is small for leptons localized near the UV brane, and therefore the modifications they induce on the fermion masses and mixings are small too. However since the inter-generational mixing is large in the lepton sector, it is important to check that no large LFV is introduced. The second source of corrections is related to the perturbative treatment of the Higgs effects. This is justified for the scales allowed by EWPT, but in GHU models we can actually test how good this approximation is because in this case it is possible to get a solution to all orders in the Higgs vev. These two types of corrections, which do not significantly modify the picture drawn above, are studied in the next two subsections. Finally, we have only included the leading order $A_4 \otimes Z_8$ breaking terms. Higher orders, although suppressed by extra powers of $1/\Lambda^{(\prime)}$, could destabilize the TBM mixing pattern and introduce new sources of LFV. We will consider these higher order corrections in the following Section.

4.2.2 Inclusion of Massive Kaluza-Klein Modes

The lepton mass Lagrangian contains a Dirac part that includes the Yukawa Lagrangian plus the KK mass terms,

$$\begin{aligned} \mathcal{L}_D = \mathcal{L}_Y - \sum_{n \geq 1} \left[m_n^l \bar{l}_L^{(n)} l_R^{(n)} + m_n^{\tilde{l}} \bar{l}_{\frac{1}{2}L}^{\tilde{(n)}} \tilde{l}_{\frac{1}{2}L}^{(n)} \right. \\ \left. + m_n^{\tilde{l}'} \bar{l}_{-\frac{3}{2}L}^{\tilde{(n)}} \tilde{l}_{-\frac{3}{2}L}^{(n)} + m_n^{\nu'} \bar{\nu}_L^{\prime(n)} \nu_R^{\prime(n)} + m_n^{e'} \bar{e}_L^{\prime(n)} e_R^{\prime(n)} + \text{h.c.} \right], \end{aligned} \quad (4.47)$$

where the $SU(2)_L$ doublets with hypercharges $\frac{1}{2}$ and $-\frac{3}{2}$ are denoted by $\tilde{l}_{\frac{1}{2}}$ and $\tilde{l}_{-\frac{3}{2}}$, respectively, and the SM-like (hypercharge $-\frac{1}{2}$) doublets which participate from all $SO(5)$ multiplets by l . Obviously, \mathcal{L}_Y also includes Yukawa couplings with the massive KK modes. The Dirac mass Lagrangian can be written in matrix form

$$-\mathcal{L}_D = \bar{e}_L \mathcal{M}_D^e e_R + \bar{\nu}_L \mathcal{M}_D^\nu \nu_R + \sum_{n \geq 1} m_n^{\tilde{l}_{1/2}} \bar{\tilde{X}}_L^{(n)} \tilde{X}_R^{(n)} + \sum_{n \geq 1} m_n^{\tilde{l}_{-3/2}} \bar{\tilde{Y}}_L^{(n)} \tilde{Y}_R^{(n)} + \text{h.c.}, \quad (4.48)$$

where we have grouped together the charge -1 leptons into $e_{L,R}$ and the neutral ones into $\nu_{L,R}$.⁵ The UV brane term, Eq. (4.35), induces a Majorana mass term that now involves all KK modes of the RH neutrinos

$$-\mathcal{L}_M = \frac{1}{2} \bar{\nu}_R^c \mathcal{M}_M^\nu \nu_R + \text{h.c.} . \quad (4.49)$$

The mass Lagrangian is diagonal for the charge $+1$ and -2 sectors but not for the charge -1 and neutral ones. However, it is still true that it is family diagonal except for the terms involving the Majorana neutrino masses. Thus, although we have now to diagonalize the charged lepton mass term, this diagonalization does not mix different generations and then does not introduce flavor changing neutral currents (FCNC). The corresponding modification of the diagonal Z couplings is proportional to the charged lepton masses and therefore relatively small [208]. On the other hand, the neutrino mass matrix

$$\mathcal{M}^\nu = \begin{pmatrix} 0 & \mathcal{M}_D^\nu \\ (\mathcal{M}_D^\nu)^T & \mathcal{M}_M^\nu \end{pmatrix} \quad (4.50)$$

is not family diagonal, and the required rotation could in principle induce modifications of the TBM mixing and introduce dangerous non-diagonal couplings between the SM charged leptons and the neutrino KK modes of mass $\sim \text{TeV}$, implying large LFV processes at the loop level. We have numerically checked that neither of these two possibilities is actually realized. The inclusion of massive KK modes does not appreciably modify the TBM mixing pattern and furthermore, although there are non-negligible charged couplings between the SM charged leptons and the neutrino KK modes, they are, to an excellent approximation, family diagonal, *i.e.* if the coupling eN is sizable for some heavy N , then the couplings μN and τN are extremely suppressed. This can be easily understood observing that flavor violation (and also light neutrino masses and thus TBM mixing) is induced by the corresponding Majorana mass, which being localized at the UV brane is much larger than the TeV scale. (For a detailed discussion of the effect on neutrino masses and mixing see [199].)

4.2.3 Exact Higgs Treatment

GHU models like the one we are considering are among the best motivated models with WED, due to the extra protection of the Higgs potential. They are also interesting because they allow us to solve the bulk equations of motion in the presence of a bulk Higgs. We can perform a field redefinition identical to a gauge transformation which locally removes the Higgs from the action, except at one of the branes. Then, the Higgs does not enter in the bulk action for rotated fields but only as a boundary condition, which can be implemented numerically. We can, therefore, compute non-linear effects of the Higgs due to its Goldstone boson nature. These effects are typically small for the values of the KK scale allowed by EWPT, but this exact treatment will allow us to test our approximation. Besides, we can also include the UV localized Majorana masses as exact boundary conditions, instead of perturbatively.

⁵In this subsection we use the same calligraphic notation to denote matrices although they have a larger size here because they also include massive KK modes.

The field transformation that removes the Higgs locally except at the IR brane is identical to a gauge transformation with gauge parameter

$$\rho(z, \tilde{v}) = \exp \left[i \frac{\sqrt{2} g_5 \tilde{v} T_C^4}{\sqrt{R(R'^2 - R^2)}} \int_R^z dz' z' \right] \approx \exp \left[i g \tilde{v} T_C^4 \sqrt{\log(R'/R)/2} \left(\frac{z^2 - R^2}{R'} \right) \right]. \quad (4.51)$$

This is not an actual gauge transformation because this gauge parameter does not satisfy the corresponding boundary conditions, but it eliminates the Higgs boson locally except at the IR brane. The bulk action for the rotated fields

$$\zeta' = \rho \zeta \quad (4.52)$$

is then free of the Higgs vev \tilde{v} , and it can be solved analytically as we did before. The boundary conditions at the UV brane remain the same, since $\rho(R) = 1$. However, the boundary conditions at the IR brane in Eq. (4.17) apply to the original fields and when written in terms of the rotated ones, they will explicitly include the Higgs effects. Note that the physical modes will now participate from all multiplets, not only from those mixed by localized terms but from those mixed by the Higgs, too. This makes the corresponding boundary conditions much more challenging. Also note that, since we are imposing now as boundary conditions the UV localized Majorana masses, we necessarily have to deal with all three generations simultaneously in the neutrino expansion. For instance, once we impose the UV boundary conditions, the Higgs dependent IR boundary conditions give a system of 8 equations with 8 unknowns (per family) for the charge -1 leptons and two independent systems of 24 equations with 24 unknowns for the neutral ones (due to the Majorana boundary condition the three families mix and the corresponding system of 24 equations with 24 complex unknowns splits into real and imaginary parts, as discussed in Chapter 2). Requiring a non-trivial solution of the corresponding systems fixes the mass of the physical states and determines all unknowns in terms of one normalization constant, which is then fixed by the normalization condition involving all relevant multiplets. The exact expression for these boundary conditions are too large to be included here but we have checked that the masses of the charged and neutral leptons (for simplicity we have neglected inter-generational mixing) are in excellent agreement with those obtained with a perturbative treatment of Higgs and UV Majorana mass effects.

4.3 Higher Order Effects

We have seen in the previous section that a global A_4 symmetry can naturally explain the observed lepton masses and TBM neutrino mixing at leading order in the breaking of this discrete symmetry along the appropriate direction. The zero mode pattern remains almost unchanged when lepton KK modes or bulk Higgs effects are included. Furthermore, this global symmetry provides an extra level of flavor protection that makes the model compatible with experimental data despite the large number of new particles. The nearly exact realization of TBM mixing, the very precise cancellation of flavor violations and the τ mass preference for a not too small value of v'/Λ' (or alternatively a large degree of compositeness) must be also verified at higher orders in the global symmetry breaking. The structure of higher order contributions is greatly simplified because ϕ (ϕ') preserves a Z_2 (Z_3) subgroup of A_4 [108]. In practice, this means that

$$\langle \phi \rangle^3 \sim \langle \phi \rangle, \quad \langle \phi' \rangle^2 \sim 1 + \langle \phi' \rangle, \quad (4.53)$$

where \sim means that they have the same A_4 transformation properties. Hence, only operators with one or two powers of ϕ on the UV brane and operators with none or one power of ϕ' on the IR brane give rise to independent flavor structures. The allowed operators are further constrained by the Z_8 symmetry.

The Majorana neutrino masses on the UV brane already have terms with none and one power of ϕ , so the only new structure comes from operators with two powers of ϕ . The lowest order contribution compatible with Z_8 has of the form

$$\frac{\eta\phi^2}{\Lambda^3}\bar{\nu}'_{2R}{}^c\nu'_{2R} + \text{h.c.} \rightarrow \bar{\nu}'_{2R}{}^c \begin{pmatrix} \delta_1 + \delta_2 + \delta_3 & 0 & 0 \\ 0 & \delta_1 + \omega\delta_2 + \omega^2\delta_3 & 0 \\ 0 & 0 & \delta_1 + \omega^2\delta_2 + \omega\delta_3 \end{pmatrix} \nu'_{2R} + \text{h.c.}, \quad (4.54)$$

with $\delta_i \sim v_\eta v^2/\Lambda^3$ arbitrary. The boundary coupling between the ζ_1 and ζ_3 bi-doublets gets new structures from terms with one or two powers of ϕ . The latter gives a similar contribution to the previous one for neutrinos, whereas the former gives a 2 – 3 mixing,

$$\left[\frac{\eta\phi}{\Lambda^2} + \frac{\phi^2}{\Lambda^2} \right] \bar{l}_{1L} l_{3R} + \text{h.c.} \rightarrow \bar{l}_{1L} \begin{pmatrix} \rho_1 + \rho_2 + \rho_3 & 0 & 0 \\ 0 & \rho_1 + \omega\rho_2 + \omega^2\rho_3 & \gamma_1 \\ 0 & \gamma_2 & \rho_1 + \omega^2\rho_2 + \omega\rho_3 \end{pmatrix} l_{3R} + \text{h.c.}, \quad (4.55)$$

where $\rho_i \sim v^2/\Lambda^2$ and $\gamma_i \sim v_\eta v/\Lambda^2$.

Let us discuss now the terms on the IR brane. The leading term mixing ζ_1 with ζ_2 contains no power of ϕ' , so the only new structure corresponds to one factor of ϕ' . The first such term comes at order $1/\Lambda'^3$, due to the Z_8 symmetry. At this order we have

$$\begin{aligned} & \left[\frac{\eta'^{*2}\phi'}{\Lambda'^3} + \frac{\eta'|\phi'|^2}{\Lambda'^3} + \frac{\eta'^{*}\phi'^{\dagger 2}}{\Lambda'^3} \right] \left(\bar{l}_{1L} l_{2R} + \bar{l}_{1L} \tilde{l}_{2R} \right) + \text{h.c.} \\ & \rightarrow \bar{l}_{1L} \begin{pmatrix} \epsilon_1 & \epsilon_2 & \epsilon_3 \\ \epsilon_3 & \epsilon_1 & \epsilon_2 \\ \epsilon_2 & \epsilon_3 & \epsilon_1 \end{pmatrix} l_{2R} + [l_{1,2} \rightarrow \tilde{l}_{1,2}] + \text{h.c.}, \end{aligned} \quad (4.56)$$

where $\epsilon_1 \sim v'_\eta v'^2/\Lambda'^3$ and $\epsilon_{2,3}$ get contributions $\sim v'_\eta v'^2/\Lambda'^3$ and $\sim v'_\eta{}^2 v'/\Lambda'^3$, and similarly for $\bar{\nu}'_{1L}\nu'_{2R}$. Finally, the coupling between ζ_3 and ζ_α is not modified by higher order terms, because we already have a term with one power of ϕ' and the singlet contribution cannot result from a singlet structure under A_4 . No further structures are generated at higher orders.

Therefore the higher order effects in the A_4 breaking can be summarized, after the rotation $\zeta_k \rightarrow \Omega \zeta_k$ in Eq. (4.13), by the following replacements

$$\hat{\theta}_M \rightarrow \hat{\theta}_M + \begin{pmatrix} \delta_1 & \delta_3 & \delta_2 \\ \delta_3 & \delta_2 & \delta_1 \\ \delta_2 & \delta_1 & \delta_3 \end{pmatrix} \quad (4.57)$$

for the Majorana masses,

$$x_l \rightarrow x_l + X_l, \quad (4.58)$$

with

$$X_l = \Omega^\dagger \begin{pmatrix} \rho_1 + \rho_2 + \rho_3 & 0 & 0 \\ 0 & \rho_1 + \omega\rho_2 + \omega^2\rho_3 & \gamma_1 \\ 0 & \gamma_2 & \rho_1 + \omega^2\rho_2 + \omega\rho_3 \end{pmatrix} \Omega \quad (4.59)$$

for the mixing between the SM LH doublets in ζ_1 and ζ_3 , and

$$y_{b,s} \frac{v'}{\Lambda'} \rightarrow y_{b,s} \frac{v'}{\Lambda'} + \begin{pmatrix} \epsilon_1^{b,s} + \epsilon_2^{b,s} + \epsilon_3^{b,s} & 0 & 0 \\ 0 & \epsilon_1^{b,s} + \omega\epsilon_2^{b,s} + \omega^2\epsilon_3^{b,s} & 0 \\ 0 & 0 & \epsilon_1^{b,s} + \omega^2\epsilon_2^{b,s} + \omega\epsilon_3^{b,s} \end{pmatrix} \quad (4.60)$$

for the mixing between the bi-doublets or the singlets in ζ_1 and ζ_2 . The IR terms remain diagonal whereas the UV terms receive non-diagonal corrections. All three effects are a source of violation of TBM and the non-diagonal X_l a source of FCNC for the charged leptons. This implies some constraint on $v_{(\eta)}^{(\prime)}/\Lambda^{(\prime)}$ that will be discussed in the next section.

A comment on brane kinetic terms

We have neglected so far in our discussion the effect of brane kinetic terms (BKT). These are generated by quantum corrections and therefore cannot be set to zero at arbitrary scales [209]. The global symmetries of our model, however, strongly constrain them. In particular, all possible BKT are proportional to the identity at leading order in A_4 and Z_8 breaking, except those involving ζ_α fields, which are diagonal but flavor dependent. Corrections to this pattern are of order v^2/Λ^2 , where v and Λ stand here for any v, v_η, v', v'_η and Λ, Λ' , respectively. Since at leading order there is no flavor violation in the charged lepton sector, these flavor dependent (but diagonal) BKT do not generate FCNC. Once higher order terms are included, there is a small flavor violation in the charged lepton sector and therefore the flavor dependent BKT will induce FCNC. Higher order contributions to BKT breaking A_4 are also a potential source of flavor violation. However, the A_4 and Z_8 symmetries ensure that the v'^2/Λ'^2 corrections are diagonal. Therefore, their effect is subleading and we will disregard them here. Hence, we include higher order effects in the localized mass terms but not in the BKT. The effects of diagonal BKT are well-known (see for instance [210]). They do not change the functional dependence of the fermion zero modes and only affect their normalization. The ones leading to flavor violation are the BKTs for the RH component of the $SO(4)$ singlet in ζ_α (all the other ones are proportional to the identity, up to tiny corrections). The corresponding BKT can be written as

$$\delta S = \int d^4x dz a^4 \delta(z - R') R' \kappa^\alpha \bar{e}'_{\alpha R} i \not{D} e'_{\alpha R} + \dots, \quad (4.61)$$

where κ^α is a dimensionless coefficients parametrizing the BKTs. The fermion zero modes for the RH charge -1 leptons have the same functional form as in the absence of BKT, Eqs. (4.26) and (4.27), except for the normalization that is now

$$\rho_\alpha^{\text{BKT}} = \rho_\alpha + \kappa^\alpha f_{-c_\alpha}^2. \quad (4.62)$$

Note that $f_{-c}^2 \ll 1$ for $c \lesssim -0.4$ so this effect in the normalization can be only relevant for the tau lepton. A more significant effect regarding flavor is that the covariant derivative in Eq. (4.61) contains the KK expansion of the corresponding gauge bosons. This implies the following flavor dependent coupling of the fermion zero modes to the gauge boson KK modes

$$\delta S = \int d^4x \left[g \sqrt{R \log(R'/R)} \kappa^\alpha \frac{f_{-c_\alpha}^2}{\rho_\alpha^{\text{BKT}}} f_n^A(R') \right] \bar{e}_{\alpha R} \not{A}_n e_{\alpha R} + \dots, \quad (4.63)$$

which has to be added to the bulk contribution. We have used again the tree level matching of the coupling constant Eq. (4.40) and assumed a KK expansion of the gauge bosons

$$A_\mu(x, z) = \sum_n f_n^A(z) A_\mu^{(n)}(x), \quad (4.64)$$

with $A_\mu(x, z)$ a generic gauge field (we have left the group structure implicit). After the inclusion of higher order terms in the brane mass terms discussed in the previous section, the charged lepton sector is no longer flavor diagonal in the current eigenstate basis. The rotation of the RH charged leptons required to go to the physical basis will then induce flavor violating couplings to the gauge boson KK modes. Recall however that the charged lepton mass hierarchy is obtained by means of the localization of the RH charged lepton zero modes. This implies that the RH rotation to go to the physical mass is strongly hierarchical and therefore the FCNC induced by the BKT suppressed by the charged lepton masses. We have indeed numerically checked that BKTs do not impose any significant constraint in the model and we will therefore neglect them in the discussion about EW and flavor constraints in the next section.

4.4 Electroweak and Flavor Constraints

Once we have classified all possible higher order terms in the $A_4 \otimes Z_8$ breaking expansion, we can discuss their effects on the leptonic mixing, *i.e.* departures from TBM mixing, as well as LFV. All three new flavor structures, Eqs. (4.57-4.60), are a source of departure from TBM mixing; whereas LFV is mostly affected by Eq. (4.59). Given the large number of parameters in our model, it is difficult to establish detailed bounds on each one. However, there are some general tendencies that are easy to understand. We have performed a detailed scanning to test these tendencies. The main conclusion is that a large region of parameter space is allowed by all current EW and flavor data for an IR scale $1/R' = 1.5$ TeV, provided v/Λ is not too large ($\lesssim 0.1$) and the LH charged leptons are close to the UV brane ($c_{3,1} \gtrsim 0.5$). This conclusion might seem a bit surprising, given previous studies of LFV in models with WED [107]. The reason our model works so well regarding LFV is a combination of two types of flavor protection. The first one is the protection provided by the A_4 symmetry, which in simpler models with WED is enough to ensure agreement with experimental data [100,101]. In our case, due to the richer structure imposed by GHU models, this protection is not enough. This is where the second layer of flavor protection enters. Our model naturally falls in the optimal configuration discussed in [115]. The custodial symmetry, together with a LR symmetry originally proposed to protect the $Z\bar{b}_L b_L$ coupling [111], and the splitting of the SM fields in two separate sectors ($\zeta_{1,2}$ and $\zeta_{3,\alpha}$ in our case) reduce LFV in our model to values compatible with current data, despite the low scale of new physics.⁶

We must require for the model to be realistic that it satisfies all experimental constraints. We can classify them in four types: those from EWPT, which we will estimate requiring small deviations from the SM tree-level couplings; limits on LFV processes which can proceed at tree-level; bounds on LFV processes which are banished to higher orders; and constraints from neutrino oscillations. The first three types of restrictions are mainly related to the heavy spectrum, whereas the latter one depends more directly on the discrete flavor symmetry breaking. Thus, although it involves less precisely determined parameters, it does restrict the model. The following phenomenological analysis must be understood as an existence proof. A refined analysis, which is outside the scope of this Thesis, should consistently include all contributions to a given order. We have done this for tree-level processes, but not for one-loop contributions which have been only estimated with the typically larger amplitude barring, for instance, possible cancellations. On the other hand, we have not considered one-loop corrections to $Z\bar{e}\mu$ [211]. A detailed study of this type of constraints will be presented elsewhere, for they require a precise enough (numerical) treatment of fermion mixing to recover the proper behavior of the different contributions, and then of decoupling [212]. The restrictions we explicitly consider are:

- **Electroweak precision tests.** We have required the gauge couplings of the SM charged leptons to be in agreement with the SM prediction within 2 per mil accuracy [100,101], both for neutral $Z\bar{l}_\alpha l_\alpha$ and charged $W\bar{l}_\alpha \nu_\alpha$ currents. This is typically the present limit on the mixing of the EW gauge bosons with new resonances [44], and on the square of the SM lepton mixing with heavier vector-like fermions [213].
- **Tree-level LFV.** We have included the most relevant constraints following [107]. Explicitly, we have studied the decays $\mu \rightarrow e^- e^+ e^-$, $\tau \rightarrow \mu^- \mu^+ \mu^-$, $\tau \rightarrow e^- e^+ e^-$, $\tau \rightarrow \mu^- e^+ e^-$, $\tau \rightarrow \mu^- e^+ \mu^-$ and the $\mu - e$ nuclear conversion rate. The tri-lepton decays $l \rightarrow l_1 \bar{l}_2 l_3$ are mediated by LFV tree-level couplings to the physical Z gauge boson and its KK excitations. (The effects due to fermion mixing are negligible.)⁷ At low energies, these contributions can

⁶Recent analysis of LFV in 4D supersymmetric models with an A_4 symmetry can be found in [202].

⁷Higgs mediated contributions [214] are suppressed by the A_4 symmetry and the SM lepton masses, and then very small in this class of models.

be parametrized by the following effective Lagrangian,

$$-\mathcal{L}_{\text{eff}} = \frac{4G_F}{\sqrt{2}} \left[g_3^{\alpha\beta} \left(\bar{l}_R^\beta \gamma^\mu l_R^\alpha \right) \left(\bar{l}_R^\beta \gamma^\mu l_R^\beta \right) + g_4^{\alpha\beta} \left(\bar{l}_L^\beta \gamma^\mu l_L^\alpha \right) \left(\bar{l}_L^\beta \gamma^\mu l_L^\beta \right) \right. \\ \left. + g_5^{\alpha\beta} \left(\bar{l}_R^\beta \gamma^\mu l_R^\alpha \right) \left(\bar{l}_L^\beta \gamma^\mu l_L^\beta \right) + g_6^{\alpha\beta} \left(\bar{l}_L^\beta \gamma^\mu l_L^\alpha \right) \left(\bar{l}_R^\beta \gamma^\mu l_R^\beta \right) \right] + \text{h.c.}, \quad (4.65)$$

where $\alpha = e, \mu, \tau$. In terms of this effective Lagrangian, the branching ratios for these decays read

$$\begin{aligned} \text{BR}(\mu \rightarrow eee) &= 2 \left(|g_3^{\mu e}|^2 + |g_4^{\mu e}|^2 \right) + |g_5^{\mu e}|^2 + |g_6^{\mu e}|^2, \\ \text{BR}(\tau \rightarrow \mu\mu\mu) &= \{ 2 \left(|g_3^{\tau\mu}|^2 + |g_4^{\tau\mu}|^2 \right) + |g_5^{\tau\mu}|^2 + |g_6^{\tau\mu}|^2 \} \text{BR}(\tau \rightarrow e\nu\nu), \\ \text{BR}(\tau \rightarrow eee) &= \{ 2 \left(|g_3^{\tau e}|^2 + |g_4^{\tau e}|^2 \right) + |g_5^{\tau e}|^2 + |g_6^{\tau e}|^2 \} \text{BR}(\tau \rightarrow e\nu\nu), \\ \text{BR}(\tau \rightarrow ee\mu) &= \{ |g_3^{\tau\mu}|^2 + |g_4^{\tau\mu}|^2 + |g_5^{\tau\mu}|^2 + |g_6^{\tau\mu}|^2 \} \text{BR}(\tau \rightarrow e\nu\nu), \\ \text{BR}(\tau \rightarrow e\mu\mu) &= \{ |g_3^{\tau e}|^2 + |g_4^{\tau e}|^2 + |g_5^{\tau e}|^2 + |g_6^{\tau e}|^2 \} \text{BR}(\tau \rightarrow e\nu\nu). \end{aligned} \quad (4.66)$$

For the $\mu - e$ conversion rate we have applied the usual expression

$$B_{\text{conv}} = \frac{2p_e E_e G_F^2 m_\mu^3 \alpha^3 |F_q|^2 Z_{\text{eff}}^4 Q_N^2}{\pi^2 Z \Gamma_{\text{capt}}} \left[|g_R^{\mu e}|^2 + |g_L^{\mu e}|^2 \right], \quad (4.67)$$

where $g_{L,R}^{\mu e}$ are the corresponding off-diagonal $Z\bar{e}\mu$ couplings, G_F is the Fermi constant and α the QED coupling strength, while the other terms are atomic physics constants defined in [215]. We shall use the bounds in Ref. [216] for the tri-lepton decays and the titanium bound $B_{\text{conv}} < 6.1 \times 10^{-13}$ from the SINDRUM II experiment [91] for $\mu - e$ conversion.

- **One-loop LFV.** We have also considered the constraints on gauge boson [100, 101] and Higgs [107] mediated amplitudes for $\mu \rightarrow e\gamma$. The charged boson contributions to this branching ratio read

$$\text{BR}^{(G)}(\mu \rightarrow e\gamma) = \frac{3\alpha}{8\pi} \left[\left| \sum_V \sum_i U_{\mu i}^{VL*} U_{ei}^{VL} F_1 \left(\frac{m_i^2}{M_V^2} \right) \right|^2 + L \rightarrow R \right], \quad (4.68)$$

where V denotes the gauge boson running in the loop, including the W_L zero mode and its lightest KK excitation, and the first W_R KK mode (the charged gauge boson in $SU(2)_R$). The subscript i indicates the massive fermion running in the loop, and $U_{e,\mu i}^{VL,R}$ stand for the electron and muon couplings to the corresponding gauge boson and heavy lepton (in units of $g/\sqrt{2}$). Finally, the function F_1 is given by

$$F_1(z) = \frac{1}{6(1-z)^4} (10 - 43z + 78z^2 - 49z^3 + 4z^4 + 18z^3 \log z). \quad (4.69)$$

There is a comparable contribution from neutral gauge boson exchange, typically of opposite sign [217, 218]. The Higgs mediated branching ratio reads [107, 217]

$$\text{BR}^{(h)}(\mu \rightarrow e\gamma) = \frac{3\alpha}{8\pi} \left[\left| \sum_i \Lambda_{\bar{e}L i R} \Lambda_{\bar{i}L \mu R} \frac{\tilde{v}^2}{2m_\mu m_i} F_2 \left(\frac{m_h^2}{m_i^2} \right) \right|^2 + L \leftrightarrow R \right], \quad (4.70)$$

where Λ is the corresponding Yukawa matrix, $\tilde{v} \approx 246$ GeV,

$$F_2(x) = \frac{1}{(1-x)^3} (1 - 4x + 3x^2 - 2x^2 \log x), \quad (4.71)$$

and the sum runs over the leptonic KK modes. The contributions in Eqs. (4.68) and (4.70) are of similar order when the mixing between light (SM) and heavy (vector-like) leptons, which is encoded in U and Λ , respectively, is explicitly taken into account, despite the apparently large enhancement factor \tilde{v}/m_μ in the latter case [219]. We will use the current PDG limit $\text{BR}(\mu \rightarrow e\gamma) < 1.2 \times 10^{-11}$ [44], as well as the expected bound $\sim 10^{-13}$ from the on-going MEG experiment [89] in the quantitative discussion below.

- **PMNS matrix.** We shall take the constraints on the PMNS mixing matrix from [29]

$$|U|_{3\sigma} = \begin{pmatrix} 0.77 \rightarrow 0.86 & 0.50 \rightarrow 0.63 & 0.00 \rightarrow 0.22 \\ 0.22 \rightarrow 0.56 & 0.44 \rightarrow 0.73 & 0.57 \rightarrow 0.80 \\ 0.21 \rightarrow 0.55 & 0.40 \rightarrow 0.71 & 0.59 \rightarrow 0.82 \end{pmatrix}. \quad (4.72)$$

Let us discuss the scanning over the model parameters. Electroweak tests are generically satisfied for our choice of IR scale $1/R' = 1.5$ TeV, as expected for UV localized light fermions [102, 131, 151, 206, 225] (with partial protection of universality for Z couplings). The constraints from tree-level LFV are also typically mild, due to the double layer of flavor protection in our model. Among the processes considered only $\mu \rightarrow eee$ and $\mu-e$ conversion are close to current experimental limits. In our general scan up to $\sim 70\%$ and $\sim 51\%$ of the points pass the corresponding bounds, respectively.⁸ The main constraint turns out to arise from $\mu \rightarrow e\gamma$. In general the new contributions are smaller for smaller values of v/Λ and relatively large values of c_3 . On the other hand, the departure from TBM mixing is somewhat sensitive to the value of v'/Λ' , decreasing with this ratio. Thus, in the following we fix $v'/\Lambda' = 0.05$ to ensure a nearly correct neutrino mixing, passing $\sim 82\%$ of the points the PMNS test when varying the other parameters. These are randomly selected with $0 \leq v_\eta/\Lambda, v'_\eta/\Lambda' \leq 0.3$ and $c_3 \geq 0.5$. v/Λ is computed from Eq. (4.44). In Figure 4.1 we show the most restricting observables as a function of this ratio, together with the corresponding current experimental limit (solid line). These are $\mu \rightarrow eee$ (top-left panel), $\mu-e$ conversion in nuclei (top-right panel) and $\mu \rightarrow e\gamma$ (lower panels, with the full range of v/Λ on the left and only small v/Λ values on the right), for which we have also drawn the expected sensitivity from MEG (dashed line). The extra flavor protection of tree-level mediated processes in the top panels relative to the one-loop $\mu \rightarrow e\gamma$ decay can be clearly observed in the Figure. As we see, a large number of points passes the different tests for relatively small v/Λ values. If we restrict ourselves to $v/\Lambda \leq 0.05$, about 97% of the points pass the $\mu \rightarrow eee$ and $\mu-e$ conversion tests, whereas 61% satisfy the $\mu \rightarrow e\gamma$ bound (and only 28% the expected MEG sensitivity). We collect in Table 4.2 the percentage of points that satisfies all the experimental tests for different ranges of c_3 and v/Λ . Requiring $c_3 \geq 0.55$ and $v/\Lambda \leq 0.05$ we find that 91% of the points pass all current experimental constraints (53% if we include the projected MEG sensitivity on $\mu \rightarrow e\gamma$). For v/Λ small enough, all tree-level LFV effects are negligible, and the only (mild) constraint comes from $\mu \rightarrow e\gamma$. Note, however, that in our scans we have randomly selected order one values of the dimensionless couplings and fixed the global scale through the ratios $v_{(\eta)}^{(\prime)}/\Lambda^{(\prime)}$. The unbalanced sensitivity of $\mu \rightarrow e\gamma$ forces the global

Constraint		All tests	All tests + MEG
$c_3 \geq 0.5,$	$\frac{v}{\Lambda} \leq 0.05$	60%	28%
$c_3 \geq 0.55,$	$\frac{v}{\Lambda} \leq 0.15$	65%	31%
$c_3 \geq 0.55,$	$\frac{v}{\Lambda} \leq 0.05$	91%	53%

Table 4.2: Percentage of points that satisfy all experimental tests (including the projected MEG sensitivity on the last column) for different parameter intervals.

⁸ $\mu-e$ conversion can be within the reach of projected experiments, see [202].

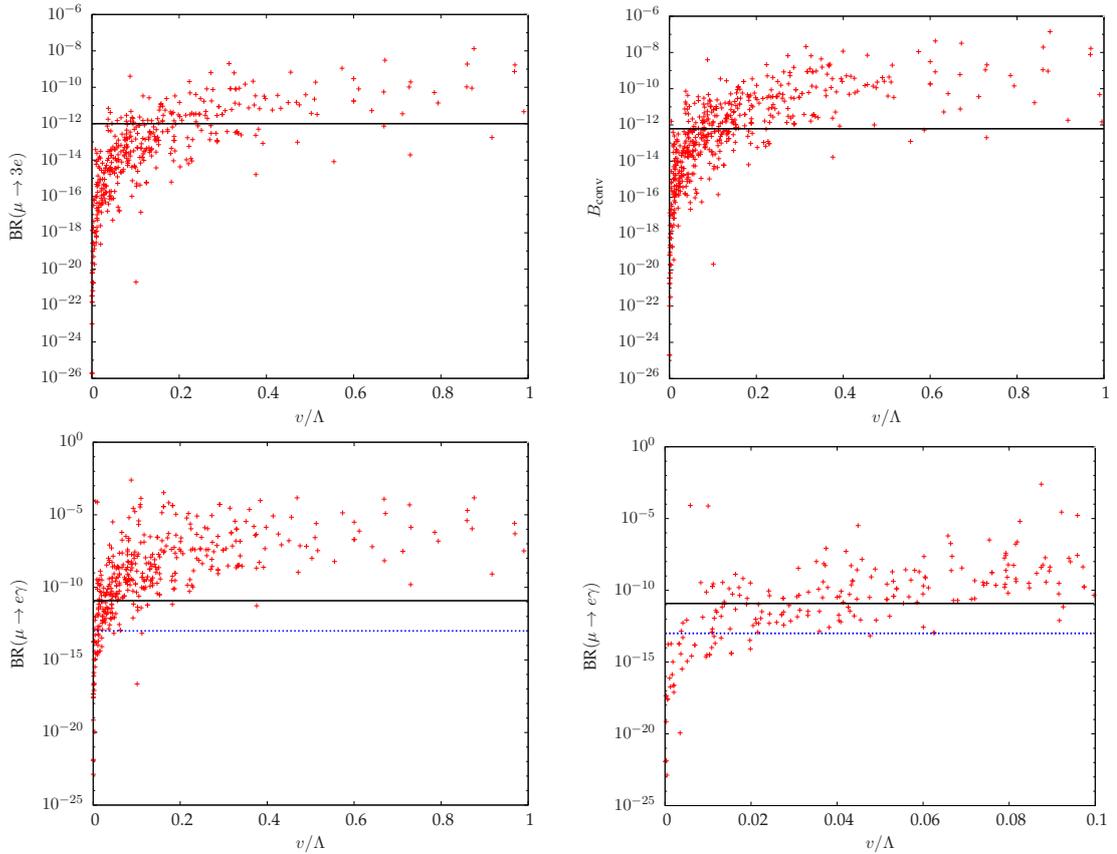


Figure 4.1: LFV branching ratios as a function of v/Λ for the scan described in the text. $\mu \rightarrow eee$ is plotted on the top-left panel, $\mu - e$ conversion in nuclei on the top-right one, and $\mu \rightarrow e\gamma$ on the two lower panels (any v/Λ value on the left panel and small v/Λ values on the right one). The horizontal lines correspond to the current experimental upper bound (solid) and future sensitivity (dashed).

scale to be small, and then all other effects are almost negligible, including deviations from TBM mixing. Of course, it is also possible that some couplings are accidentally larger than others, thus inducing sizable corrections to some observables without being excluded by the $\mu \rightarrow e\gamma$ limit. For example, if we set $v/\Lambda = 0.5$ and all the coefficients of higher dimensional operators equal to zero except $\delta_2 = 8$ (well below its NDA estimate $\delta \lesssim 4\pi^2 x_\eta$ if $x_\eta \sim 1$), we obtain

$$\sin \theta_{13} = 0.18, \quad (4.73)$$

with all other observables within experimental limits. Thus, in our construction sizable departures from TBM mixing can be still compatible in with all other experimental constraints (although some fine-tuning might be necessary for large departures).

Our analysis shows that, in general, small values of v/Λ and v'/Λ' are preferred by lepton mixing and LFV observables. We have already emphasized the correlation between v'/Λ' and c_τ (the smaller the former, the larger c_τ has to be in order to reproduce the τ mass, implying in turn a more composite τ_R). This has important consequences regarding the spectrum in our model as a larger c_τ value implies light modes. The structure is very generic in this class of models. There is a relatively light, almost degenerate bi-doublet (two charge -1 , one neutral and one charge -2 leptons) that mainly couples to τ_R . This bi-doublet mostly lives in ζ_τ (see Eq. (4.4)), which is

light due to the assigned twisted boundary conditions [220]. These four leptons, which are from the dual CFT standpoint the custodial symmetry partners of the composite state mixing with the elementary tau, can be very light and couple strongly to τ_R without being experimentally excluded because they are almost degenerate (see [113] for a discussion of this phenomenon in the quark sector). This degeneracy also dictates a very characteristic collider phenomenology as we discuss in the following.

4.5 Tau Custodians at the LHC

In the following, we investigate the LHC reach for these new leptonic resonances required by custodial symmetry, the tau custodians. They can be pair produced with EW strength through the exchange of a SM gauge boson, decaying almost exclusively into taus and a vector or scalar SM boson. This analysis is crucial because signatures with taus in the final state are typically deemed challenging and therefore not the first choice for new physics searches. Such a signature could however very well be the first hint, and maybe the only one for a while, of the explicit realization of the lepton spectrum in models of strong EWSB.⁹ Pair production of these new resonances with the taus subsequently decaying into leptons appears to be the cleanest, model independent channel for these searches. Assuming collinearity and no other source of missing energy we can fully reconstruct the two taus. Equality of the invariant mass of the two reconstructed new leptons then allows to reduce the background and reconstruct the custodian masses.

The relevant new matter content consists of two vector-like lepton doublets with hypercharges $-1/2$ and $-3/2$,

$$L_{1L,R}^{(0)} = \begin{pmatrix} N_{L,R}^{(0)} \\ E_{1L,R}^{(0)} \end{pmatrix} \sim (2)_{-\frac{1}{2}}, \quad L_{2L,R}^{(0)} = \begin{pmatrix} E_{2L,R}^{(0)} \\ Y_{L,R}^{(0)} \end{pmatrix} \sim (2)_{-\frac{3}{2}}, \quad (4.74)$$

respectively. The script (0) indicates the current basis. The pertinent part of the Yukawa and mass Lagrangian reads, in the basis with diagonal charged lepton Yukawa couplings,

$$\mathcal{L} = -\sqrt{2} \frac{m}{v} \bar{l}_L^{(0)} H \tau_R^{(0)} - \sqrt{2} \frac{m'}{v} [\bar{L}_{1L}^{(0)} H + \bar{L}_{2L}^{(0)} \tilde{H}] \tau_R^{(0)} - M [\bar{L}_{1L}^{(0)} L_{1R}^{(0)} + \bar{L}_{2L}^{(0)} L_{2R}^{(0)}] + \text{h.c.} + \dots, \quad (4.75)$$

where the dots denote kinetic terms and other terms in the Lagrangian not involving the new leptons. In the class of models we consider, the coupling to e , μ or any right-handed neutrino is negligible. After EWSB, the lepton mass matrix

$$\mathcal{M} = \begin{pmatrix} m & 0 & 0 \\ m' & M & 0 \\ m' & 0 & M \end{pmatrix} \quad (4.76)$$

is diagonalized with the usual bi-unitary rotations, $U_L^\dagger \mathcal{M} U_R = \mathcal{M}_{\text{diag}} = (m_\tau, m_{E_1}, m_{E_2})$, which in our case take the very simple form

$$U_{L,R} = \begin{pmatrix} c_{L,R} & 0 & s_{L,R} \\ -\frac{s_{L,R}}{\sqrt{2}} & \frac{1}{\sqrt{2}} & \frac{c_{L,R}}{\sqrt{2}} \\ -\frac{s_{L,R}}{\sqrt{2}} & -\frac{1}{\sqrt{2}} & \frac{c_{L,R}}{\sqrt{2}} \end{pmatrix}, \quad (4.77)$$

where $s_{L,R} \equiv \sin(\theta_{L,R})$, $c_{L,R} \equiv \cos(\theta_{L,R})$. All relevant physics can be parametrized in terms of m , m' and M . However, it is simpler to use as alternative parameters m_τ , s_R and M , where the latter two fully describe the model, with the left-handed mixing parameter

$$s_L = s_R \frac{m_\tau}{M}. \quad (4.78)$$

⁹This is an interesting example in which the mechanism of neutrino mass generation, despite having a large suppression scale, has testable consequences at the LHC.

In particular, assuming $M \geq 100$ GeV we have $s_L \leq 0.018$, $c_L \geq 0.9998$. (Thus $s_L \approx 0$, $c_L \approx 1$ is an excellent approximation.) The resulting physical spectrum consists of three degenerate leptons with mass M and charges 0, -1 and -2 , respectively

$$m_N = m_{E_1} = m_Y = M, \quad (4.79)$$

and a heavier charge -1 lepton with mass

$$m_{E_2} = \frac{M}{c_R} \sqrt{1 - s_R^2 \frac{m_\tau^2}{M^2}}. \quad (4.80)$$

In the physical basis the lepton couplings to the SM gauge bosons and to the Higgs can be written without loss of generality

$$\mathcal{L}^Z = \frac{g}{2c_W} \bar{\psi}_Q^i \gamma^\mu \left[X_{ij}^{QL} P_L + X_{ij}^{QR} P_R - 2s_W^2 Q \delta_{ij} \right] \psi_Q^j Z_\mu, \quad (4.81)$$

$$\mathcal{L}^W = \frac{g}{\sqrt{2}} \bar{\psi}_Q^i \gamma^\mu \left[V_{ij}^{QL} P_L + V_{ij}^{QR} P_R \right] \psi_{(Q-1)}^j W_\mu^+ + \text{h.c.}, \quad (4.82)$$

$$\mathcal{L}^h = -\frac{h}{\sqrt{2}} \bar{\psi}_Q^i Y_{ij}^Q P_R \psi_Q^j + \text{h.c.}, \quad (4.83)$$

where Q runs over the electric charges in the spectrum $(-2, -1, 0)$ and $P_{LR} = (1 \mp \gamma^5)/2$ are the chirality projectors. In our case, the neutral gauge couplings read

$$X_L^{(-1)} = \begin{pmatrix} -c_L^2 & s_L & -s_L c_L \\ s_L & 0 & -c_L \\ -s_L c_L & -c_L & -s_L^2 \end{pmatrix}, \quad X_R^{(-1)} = \begin{pmatrix} 0 & s_R & 0 \\ s_R & 0 & -c_R \\ 0 & -c_R & 0 \end{pmatrix}, \quad (4.84)$$

$$X_L^{(0)} = \begin{pmatrix} 1 & 0 \\ 0 & 1 \end{pmatrix}, \quad X_R^{(0)} = \begin{pmatrix} 0 & 0 \\ 0 & 1 \end{pmatrix}, \quad X_L^{(-2)} = X_R^{(-2)} = -1; \quad (4.85)$$

and the charged ones

$$V_L^{(0)} = \begin{pmatrix} c_L U_{33}^{PMNS} & 0 & s_L U_{33}^{PMNS} \\ -\frac{s_L}{\sqrt{2}} & \frac{1}{\sqrt{2}} & \frac{c_L}{\sqrt{2}} \end{pmatrix}, \quad V_R^{(0)} = \begin{pmatrix} 0 & 0 & 0 \\ -\frac{s_R}{\sqrt{2}} & \frac{1}{\sqrt{2}} & \frac{c_R}{\sqrt{2}} \end{pmatrix}, \quad (4.86)$$

$$V_L^{(-1)} = \begin{pmatrix} -\frac{s_L}{\sqrt{2}} & -\frac{1}{\sqrt{2}} & \frac{c_L}{\sqrt{2}} \end{pmatrix}^T, \quad V_R^{(-1)} = \begin{pmatrix} -\frac{s_R}{\sqrt{2}} & -\frac{1}{\sqrt{2}} & \frac{c_R}{\sqrt{2}} \end{pmatrix}^T, \quad (4.87)$$

where U_{33}^{PMNS} is the corresponding entry of the PMNS matrix. Finally, the corresponding Yukawa couplings read

$$vY^{(-1)} = \begin{pmatrix} c_R^2 m_\tau & 0 & s_R c_R m_\tau \\ 0 & 0 & 0 \\ s_R c_L M & 0 & \frac{s_R^2}{c_R} c_L M \end{pmatrix}. \quad (4.88)$$

Note that EW single production of these states in association with a tau lepton is proportional to $s_L \approx 0$ or s_R , and therefore very sensitive to the particular value of the latter. Pair production, on the other hand, is proportional to the electric charge, to $c_L \approx 1$ or to c_R , and then less sensitive to the precise value of s_R unless $s_R \gtrsim 0.5$. The three leptons with mass M always decay into a tau lepton and a SM gauge boson

$$N \rightarrow \tau W^+, \quad E_1 \rightarrow \tau Z, \quad Y \rightarrow \tau W^-, \quad (4.89)$$

whereas the heavier one always decays to a tau and a Higgs

$$E_2 \rightarrow \tau H, \quad (4.90)$$

provided $c_R \geq (1 + m_W/M)^{-1}$. For smaller c_R values the corresponding decay channels into another heavy lepton and a gauge or Higgs boson open up. This is an exciting possibility, since it allows for a richer phenomenology but requires a large mixing (for instance, $s_R \geq 0.5$ for $M \approx 720$ GeV). Mixing angles that large require a detailed analysis of indirect constraints to assess the phenomenological viability of the model and we defer it to a future publication. Hence, we restrict ourselves to the case in which all new leptons only decay to tau leptons and a SM scalar or vector boson.

New leptons can be singly produced in association with a tau or pair produced at the LHC. Single production, which may be relevant for the early LHC run $\mathcal{L} \sim 1 \text{ fb}^{-1}$ at $\sqrt{s} = 7$ TeV, is very sensitive to the values of the couplings in the model, as just stressed. The relatively light masses and large couplings that can be tested in this early run not only require an analysis of current EW constraints but a dedicated study of the LHC reach, which will be presented elsewhere. Pair production, on the other hand, is EW and model independent to a large extent. The two heavy leptons then decay into two taus and two SM bosons, which in turn will result in ten fermions in the final state. We are in the best position to beat the background if we consider fully leptonic tau decays. Besides, we will require a Z in the final state decaying into leptons for the same reason. Due to the relatively large mass of the heavy leptons, the two taus are largely boosted and therefore their decay products highly collimated. Assuming full collimation, we can completely reconstruct the two taus despite having four neutrinos in the final state if there is no further source of missing energy. Thus, we consider the following channels

$$pp \rightarrow \bar{E}_1 E_1 \rightarrow ZZ\bar{\tau}\tau, \quad pp \rightarrow \bar{E}_1 Y \rightarrow ZW^-\bar{\tau}\tau, \quad (4.91)$$

$$pp \rightarrow \bar{E}_1 E_2 \rightarrow ZH\bar{\tau}\tau, \quad pp \rightarrow \bar{E}_1 N \rightarrow ZW^+\bar{\tau}\tau, \quad (4.92)$$

together with the conjugated ones. The signature we are interested in is therefore

$$pp \rightarrow l^+ l^- l'^+ l''^- jj\cancel{E}_T, \quad \text{with } l, l', l'' = e, \mu. \quad (4.93)$$

Even though we have to pay an important price due to the leptonic branching ratios $\sim 0.6\%$ [$\text{BR}(Z \rightarrow l^+ l^-) \approx 6.6\%$, $\text{BR}(\tau \rightarrow l\cancel{E}_T) \approx 34\%$], the dramatic reduction of backgrounds overcomes this signal suppression. Besides the multilepton final state, the full reconstruction of the taus decaying leptonically and that the pair produced heavy leptons have the same mass allows us to further reduce the background down to an almost unobservable level.

4.6 Analysis

As explained in the previous section, we consider pair production of tau custodians for it is model independent. The corresponding branching ratios, together with the energy required to produce two heavy states makes the cross section too small to have a significant number of events in the early LHC run. We thus concentrate on the nominal energy $\sqrt{s} = 14$ TeV. The backgrounds we have considered are

$$Zt\bar{t} + n \text{ jets}, \quad \sigma = 39.6 \text{ fb}, \quad Zb\bar{b} + n \text{ jets}, \quad \sigma = 5.85 \text{ pb}, \quad (4.94)$$

$$ZZ + n \text{ jets}, \quad \sigma = 2.35 \text{ pb}, \quad ZW + n \text{ jets}, \quad \sigma = 1.76 \text{ pb}. \quad (4.95)$$

$$t\bar{t} + n \text{ jets}, \quad \sigma = 55 \text{ pb}, \quad ZWW + n \text{ jets}, \quad \sigma = 1.9 \text{ fb}, \quad (4.96)$$

where σ are the corresponding cross sections. One Z in all channels and both tops in the $t\bar{t}$ channel have been required to decay leptonically and the cross section reported includes the corresponding branching ratios and some minimal cuts. In all cases we have generated up to $n = 2$ jets at the partonic level with ALPGEN V2.13 [231], and used the PGS4 [166] fast detector simulation after passing the events through PYTHIA [165] for hadronization and showering (with the MLM matching algorithm). Our signal events are generated with MADGRAPH/MADEVENT v4 [164]

and taus are decayed with TAUOLA [232]. In all cases we have included initial and final state radiation but no pile-up effects. We show in Fig. 4.2 the signal production cross section, including the Z leptonic branching ratio but not decaying the tau leptons, as a function of the heavy mass M (and assuming a Higgs mass $m_h = 120$ GeV).

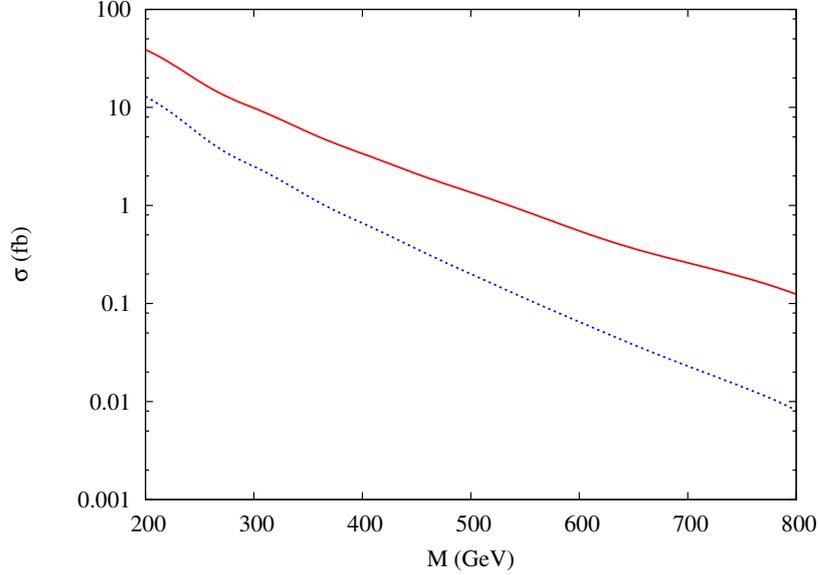


Figure 4.2: Heavy lepton pair production cross section (in fb) as a function of the heavy mass M . The dotted (solid) line corresponds to $\sqrt{s} = 7$ (14) TeV. The cross section includes the leptonic Z decay but not the tau decays, i.e. $pp \rightarrow l^+ l^- j j \tau^+ \tau^-$.

In order to reduce the background we have implemented the following cuts

- **Basic cuts.** We require at least two positively and two negatively charged isolated leptons (electrons or muons), two jets and missing energy with

$$p_T(l) \geq 10 \text{ GeV}, \quad p_T(j) \geq 20 \text{ GeV}, \quad \cancel{E}_T \geq 20 \text{ GeV}, \\ |\eta_l| \leq 2.5, \quad |\eta_j| \leq 5, \quad \Delta R_{jj} \geq 0.5, \quad \Delta R_{jl} \geq 0.5. \quad (4.97)$$

We keep the hardest four leptons and two jets if their multiplicity is larger.

- **Leptons.** We require two same flavour, opposite charge leptons to reconstruct a Z , and the other two not to be back to back (so that the two taus can be reconstructed assuming collinearity),

$$|M_{l+l^-} - M_Z| \leq 10 \text{ GeV}, \quad \cos(\phi_{l'+l''-}) \geq -0.95, \quad (4.98)$$

- **M_{jj} .** The two jets in our signal come from the decay of a SM boson. We therefore impose a cut on the invariant mass of the two jets

$$50 \text{ GeV} \leq M_{jj} \leq 150 \text{ GeV}. \quad (4.99)$$

- **τ reconstruction.** We use the two leptons not reconstructing the Z and the transverse missing energy to infer the tau four-momenta [233]. First, we assume all momenta in the tau

decays are aligned

$$p_i^{l'+} = x^+ p_i^{\tau^+}, \quad \not{p}_i^+ = (1 - x^+) p_i^{\tau^+}, \quad (4.100)$$

$$p_i^{l''-} = x^- p_i^{\tau^-}, \quad \not{p}_i^- = (1 - x^-) p_i^{\tau^-}, \quad (4.101)$$

where i stands for the spatial components x, y, z and \not{p}_i^\pm denotes the sum of the momenta of the neutrinos coming from the τ^\pm decay. x^\pm are the fraction of τ^\pm momentum taken by $l'^+, l''-$, respectively. They are fixed by momentum conservation in the transverse plane

$$x^+ = \frac{p_y^{l''-} p_x^{l'+} - p_x^{l''-} p_y^{l'+}}{\not{p}_x p_y^{l''-} - \not{p}_y p_x^{l''-} + p_y^{l''-} p_x^{l'+} - p_x^{l''-} p_y^{l'+}}, \quad (4.102)$$

$$x^- = \frac{p_y^{l''-} p_x^{l'+} - p_x^{l''-} p_y^{l'+}}{\not{p}_y p_x^{l'+} - \not{p}_x p_y^{l'+} + p_y^{l''-} p_x^{l'+} - p_x^{l''-} p_y^{l'+}}. \quad (4.103)$$

These lie between 0 and 1 if all transverse missing energy, measured with infinite precision, comes from collinear tau decays. Thus, we require $0 \leq x^\pm \leq 1$ and use them to reconstruct the τ^\pm four-momenta

$$p_i^{\tau^+} = \frac{p_i^{l'+}}{x^+}, \quad p_i^{\tau^-} = \frac{p_i^{l''-}}{x^-}, \quad i = x, y, z, \quad (4.104)$$

$$p_0^{\tau^\pm} = \sqrt{m_\tau^2 + \sum_{i=x,y,z} (p_i^{\tau^\pm})^2}. \quad (4.105)$$

- **Pair production.** We require the two reconstructed heavy leptons to have the same mass within 50 GeV,

$$|M_{L_1} - M_{L_2}| \leq 50 \text{ GeV}, \quad (4.106)$$

where M_{L_i} corresponds to the invariant mass of τ^\pm and either l^+l^- or jj . (We select the pairing giving the smaller difference.)

- **Mass reconstruction.** Finally we require the invariant mass of the τl^+l^- pairing to peak around a test mass within 50 GeV.

$$|M_{\tau l^+l^-} - M_{L_{\text{test}}}| \leq 50 \text{ GeV}. \quad (4.107)$$

We have applied the analysis described above to the signal, for different values of the custodian mass M , and to the background. In order to estimate the statistical significance of the result we use Eq. (3.65), where s and b are the number of signal and background events, respectively, after all cuts have been imposed [234]. We require a minimum number of 3 signal events and $\mathcal{S}(s, b) = 5$ for a 5σ discovery. An example of the efficiency of each cut on the signal and on the main backgrounds for two sample custodian masses $M = 200$ GeV and $M = 400$ GeV is shown in Table 4.3. The required luminosity for a 5σ discovery is 17 and 170 fb^{-1} , respectively. The corresponding luminosity as a function of the custodian masses is shown in Fig. 4.3. The expected reach after 30, 300 and 3000 fb^{-1} of integrated luminosity is $M \sim 240, 480$ and 720 GeV, respectively, for a 5σ discovery.

14 TeV	$M = 200$ GeV	$M = 400$ GeV	$Zt\bar{t}$		ZZ	
Basic	0.85	0.14	0.49		0.44	
Leptons	0.68 (81%)	0.11 (77%)	0.41 (84%)		0.41 (93%)	
M_{jj}	0.49 (72%)	0.063 (59%)	0.15 (37%)		0.13 (31%)	
Tau rec.	0.42 (86%)	0.057 (90%)	0.039 (26%)		0.052 (40%)	
Pair prod.	0.39 (91%)	0.045 (79%)	0.017 (44%)		0.032 (61%)	
Mass rec.	0.37 (96%)	0.041 (91%)	0.008 (48%)	0.0016 (9%)	0.016 (50%)	0.0018 (6%)

Table 4.3: Cross sections in fb (and corresponding efficiencies) after cuts for the signal and main backgrounds. The cuts are described in Eqs. (4.97-4.107). We show the results for two different values of the custodian masses $M = 200, 400$ GeV. The effect of the last cut on the background depends on the test mass as shown in the last row. The required luminosity to have a 5σ discovery, with 3 or more events, being $\mathcal{L} \approx 17, 170 \text{ fb}^{-1}$, respectively.

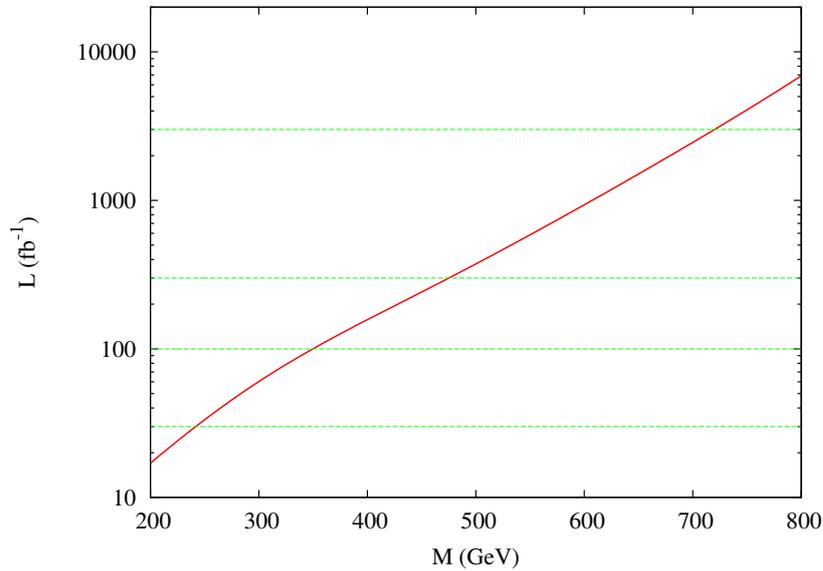


Figure 4.3: Luminosity required for a 5σ discovery at the LHC with $\sqrt{s} = 14$ TeV as a function of the custodian mass M .

4.7 Updated Results

Since the completion of this study, some bounds on LFV processes have been updated. In particular, we show in Table 4.4 the current limits on processes with new experimental results, together with the previous numbers. We can see that just one of the three most restricting flavor observables in our model have been updated, $\mu \rightarrow e\gamma$. As a consequence, these changes have a rather small impact on our results. As an example, we show in Table 4.5 the percentage of points of our previous scan satisfying all the experimental tests with current bounds for LFV processes. In order to compare, we also show the numbers for the outdated bounds.

Process	Used bound	Current bound
$\mu \rightarrow e\gamma$	1.2×10^{-11}	2.4×10^{-12}
$\tau \rightarrow \mu\mu\mu$	3.2×10^{-8}	2.1×10^{-8}
$\tau \rightarrow eee$	3.6×10^{-8}	2.7×10^{-8}
$\tau \rightarrow ee\mu$	2.0×10^{-8}	1.5×10^{-8}
$\tau \rightarrow e\mu\mu$	2.3×10^{-8}	1.7×10^{-8}

Table 4.4: Used and current bounds on some LFV processes.

Constraint	Old bounds	New bounds
$c_3 \geq 0.5, \frac{v}{\Lambda} \leq 0.05$	60%	51%
$c_3 \geq 0.55, \frac{v}{\Lambda} \leq 0.15$	65%	55%
$c_3 \geq 0.55, \frac{v}{\Lambda} \leq 0.05$	91%	88%

Table 4.5: Percentage of points that satisfy all experimental tests for old and current bounds on LFV processes.

Also, as mentioned in Chapter 1, recent results from Daya Bay experiment [58] have excluded the $\theta_{13} = 0$ hypothesis at 5.2σ , obtaining

$$\sin^2 2\theta_{13} = 0.092 \pm 0.016 \text{ (stat)} \pm 0.005 \text{ (syst)}. \quad (4.108)$$

In the same direction, the RENO experiment [59] have recently measured the θ_{13} mixing angle with a significance of 4.9σ , leading to

$$\sin^2 2\theta_{13} = 0.113 \pm 0.013 \text{ (stat)} \pm 0.019 \text{ (syst)}, \quad (4.109)$$

a value which is compatible with the previous one. The latest global fit takes into account measurements coming from both reactor experiments [235], and obtain at 3σ

$$0.0149 \text{ (0.0150)} < \sin^2 \theta_{13} < 0.0344 \text{ (0.0347)}, \quad (4.110)$$

for a normal (inverted) hierarchy. This strong evidence of a non-zero θ_{13} angle has triggered a small revolution in the field, leading to new attempts to produce such a large angle with the help of discrete symmetries [236–246]. Besides groups of small size as S_3, A_4, S_4 or D_4 , larger groups like $A_5, \Delta(54), \Delta(96)$ or $\Delta(384)$ have been proposed. As we have discussed previously, large values of θ_{13} can be accommodated in our model while still being compatible with all other experimental constraints. However, to this end, some fine-tuning might be needed, rendering the model less natural. We can understand this better by noting that the TBM pattern is produced at leading order by $Z_2 \otimes Z_2$ and Z_3 symmetries in the neutrino and the charged lepton sector, respectively. While one $Z_2 \subset Z_2 \otimes Z_2$ and the Z_3 symmetry groups are imposed by the alignment of the boundary scalars vev's, the extra Z_2 symmetry of the Klein group is accidental and arises at leading order from the absence of boundary scalar transforming under $\mathbf{1}'$ or $\mathbf{1}''$ [245]. Higher order corrections break this accidental Z_2 symmetry, leading to deviations from the original TBM mixing matrix. This behavior, which could be a drawback before the recent θ_{13} measurements, is now something precious to accommodate such a large mixing angle. However, as the breaking of the extra Z_2 symmetry by NLO terms increases, the rest of entries in the PMNS matrix also changes. This fact, together with the larger contributions to LFV processes induced by higher order corrections, introduce some tension with the desired value of the θ_{13} angle. One might consider changing to larger groups like $\Delta(96)$ or $\Delta(384)$, although it would require paying the price of a less minimal scenario.

Conclusions

The LHC is trying to disentangle the precise mechanism breaking the EW symmetry. Thanks to the big effort made by the LHC community we are about to find out whether the Higgs boson exists or not. Trying to solve the hierarchy problem (arising in the case of a fundamental Higgs), different models extend the SM including new particles at the TeV scale, which may be observable at the LHC. As third generation quarks and leptons feel more strongly the EW symmetry breaking than the rest of SM fermions, one could expect that any new physics fixing the hierarchy problem will leave its footprint especially on this sector. As we have seen in this Thesis, this is indeed the case in models with WED and their CFT duals. Moreover, the hints of an anomaly in the $t\bar{t}$ forward-backward asymmetry measured at the Tevatron seems to point in this direction. Throughout this Thesis, we have considered some of these BSM models, which describe alternative realizations of the EWSB, and studied in detail their collider phenomenology in connection with the third generation. Our main results can be summarized as follows:

- We have studied in Chapter 2 the effect of bulk fermions on EW precision observables in a non-custodial model with warped extra dimensions and a strong deviation from AdS₅ near the infrared brane [1]. We have found that reproducing the observed top quark mass can result in significant constraints from anomalous contributions to the $Zb_L\bar{b}_L$ coupling. In addition, we have seen that the one-loop corrections to the EW observables, which are finite in these scenarios, strongly restrict the allowed region of parameter space. In particular, a tension between the (tree-level) corrections to the $Zb_L\bar{b}_L$ coupling and the 1-loop contribution to the T -parameter, strongly constrains the localization of the quarks of the third generation and the resulting 95% CL bound on the KK scale. Nevertheless we have found that the KK gluons can be as light as 1.5 TeV if the Higgs is heavy. However, if the Higgs mass is allowed to float in the fit, one finds a 95% CL lower bound of $M_{\text{KK}} \approx 2.3$ TeV. Due to the strong localization of the gauge boson resonances towards the IR brane, KK gluons have smaller couplings to the light fermions, leading to a suppression in the production cross section. This can be compensated by the lower allowed mass of the gauge KK modes. However, we find that discovering such a resonance in the dominant $t\bar{t}$ channel is likely to be challenging. Boosted top techniques and a very detailed knowledge of the $t\bar{t}$ tail will likely be required to discover these modes.
- We have shown in Chapter 3 that a gluon resonance G of mass below 1 TeV could be the origin of the $t\bar{t}$ forward-backward asymmetry observed at the Tevatron provided that new decay modes $G \rightarrow \bar{q}Q$, with q a standard quark and Q its massive excitation, make G broad enough [2–4]. We consider all the different cases, with q the top, the bottom or a light quark, and dominant decay modes $Q \rightarrow Wq'$ or $Q \rightarrow Zq$. We show that current experimental searches are unable to probe the model, but that minimal departures from these analysis can explore a large region of its parameter space for the current LHC luminosity. This includes the challenging case with the new quarks decaying mostly into light quark flavors. In some channels not only the heavy quark but also the massive gluon can be reconstructed, which would establish the origin of the $t\bar{t}$ asymmetry. We have considered also the case of new vector-like excitations decaying into a Higgs boson and a SM quark in the framework of minimal composite Higgs models [5,6]. We have found that masses for new color octet vector

resonances up to 2.8 TeV can be probed with the 2011 and 2012 data sets. This enters the region currently preferred by EW precision constraints. With the energy upgrade to $\sqrt{s} = 14$ TeV, up to $M_G \sim 5$ TeV can be probed with 100 fb^{-1} .

- In Chapter 4 we have studied for the first time the implementation of a global A_4 symmetry in models of GHU [7]. Although LFV is generated at tree level, we have found that the global symmetry provides a strong enough flavor protection thanks to a subgroup of the custodial symmetry which naturally provides the necessary extra suppression. We have also investigated possible deviations from TBM (which is predicted at LO by the assumed discrete symmetry breaking) and the implications of EWPT, LFV and neutrino masses and mixing on the spectrum of new resonances. This requires a precise enough determination of the masses and mixings of particles spreaded by many orders of magnitude, making the numerical analysis rather challenging. The model is compatible with all those experimental constraints for new gauge boson masses $M_{KK} \gtrsim 3.5$ TeV, which could be accessible at the LHC. We have found that, in order to keep LFV below current (and expected) experimental bounds, the A_4 breaking has to be relatively small. This leads to an extra suppression on the lepton Yukawa couplings and a more composite τ_R . This in turn implies the existence of new leptonic resonances – the tau custodians – with masses of few hundreds of GeV and large couplings to τ_R . They come in a full almost degenerate $SU(2)_L \times SU(2)_R$ bi-doublet with a very distinctive phenomenology at the LHC.

We have shown that pair production of tau custodians provides a clean, model independent channel, that results in two taus and two gauge or Higgs bosons [8]. Requiring at least one Z decaying into electrons or muons, leptonic tau decays and no further source of missing energy, we end up with a final state with four charged leptons (electrons or muons), missing energy and two jets. The large number of leptons allows for a very efficient reduction of the main backgrounds. The relative large mass of the custodians results in highly boosted taus with very collimated decay products. Assuming complete collimation, we can fully reconstruct both taus, despite the presence of four neutrinos in the final state. The requirement of pair production of same mass objects then further enhances the signal, leading to a discovery reach for tau custodians at the LHC with $\sqrt{s} = 14$ TeV of $M = 240, 480$ and 720 GeV for a total integrated luminosity $\mathcal{L} = 30, 300, 3000 \text{ fb}^{-1}$, respectively.

In summary, we have studied the phenomenology of models with extra dimensions and its possible signals at LHC. In these SM extensions the main deviations from the minimal SM are expected to show up in processes involving the third family, what is also widely expected because it is the heaviest one. With this in mind we have worked out the phenomenological implications of the extra-dimensional models which can be probed at LHC in top processes. We have also constructed a definite model for leptons reproducing the observed spectrum and predicting a rather composite tau lepton with characteristic signatures at LHC.

Conclusiones

El LHC está tratando de determinar el mecanismo exacto de ruptura de la simetría electrodébil. Gracias al gran esfuerzo realizado por la comunidad estamos a punto de averiguar si el bosón de Higgs existe o no. En un intento por resolver el problema de las jerarquías (que surge en el caso de un Higgs fundamental), diferentes modelos extienden el Modelo Estándar con nuevas partículas a la escala del TeV, que podrían ser observables en el LHC. Como los quarks y los leptones de la tercera generación sienten con más fuerza que el resto de fermiones del Modelo Estándar la ruptura espontánea de simetría, podemos esperar que cualquier nueva física que resuelva el problema de las jerarquías deje su huella especialmente en este sector. Como hemos visto en esta Tesis, esto es cierto en los modelos con dimensiones extras curvas y en sus duales cuatro-dimensionales fuertemente acoplados. Por otro lado, los indicios de una anomalía en la asimetría angular de $t\bar{t}$ medidos en el Tevatron parecen apuntar en esa dirección. A lo largo de esta Tesis, hemos considerado algunos de estos modelos de física más allá del Modelo Estándar, que describen realizaciones alternativas de la ruptura espontánea de la simetría electrodébil, y estudiado en detalle su fenomenología en colisionadores en conexión con la tercera generación. Nuestros principales resultados pueden resumirse como sigue:

- Hemos estudiado en el Capítulo 2 el efecto de los fermiones cinco-dimensionales en los observables electrodébiles de precisión en un modelo no custodial con una dimensión extra curva y una fuerte desviación de AdS₅ cerca de la membrana infrarroja [1]. Hemos encontrado que reproducir la masa observada del quark *top* puede dar lugar a importantes restricciones por parte de contribuciones anómalas al acoplamiento $Zb_L\bar{b}_L$. Además, hemos visto que las correcciones a un lazo a los observables electrodébiles, que son finitas en estos escenarios, limitan fuertemente la región del espacio de parámetros permitida. En particular, la tensión entre las correcciones (a nivel árbol) al acoplamiento $Zb_L\bar{b}_L$ y la contribución a un lazo al parámetro T , restringe de manera importante la localización de los quarks de la tercera generación y la cota resultante para la escala de Kaluza-Klein. Sin embargo, hemos encontrado que los gluones de Kaluza-Klein pueden ser tan ligeros como 1.5 TeV, si el bosón de Higgs es pesado. Por contra, si permitimos que la masa del bosón de Higgs varíe en el ajuste, encontramos un límite inferior $M_{KK} \approx 2.3$ TeV con un nivel de confianza del 95%. Debido a la fuerte localización de las resonancias de los bosones de *gauge* hacia la membrana infrarroja, los gluones de Kaluza-Klein tienen menor acoplamiento a los fermiones ligeros, dando lugar a una menor sección eficaz de producción. Esto puede ser compensado por la menor masa permitida para los bosones de *gauge* de Kaluza-Klein. Sin embargo, encontramos que el descubrimiento de dicha resonancia en el canal dominante $t\bar{t}$ será desafiante. Técnicas de *tops* impulsados y un conocimiento muy detallado de la cola de $t\bar{t}$ serán probablemente necesarias para descubrir estos modos.
- Hemos demostrado en el Capítulo 3 que una resonancia gluónica G con masa por debajo de 1 TeV podría ser el origen de la asimetría angular de $t\bar{t}$ observada en el Tevatron siempre y cuando los nuevos modos de desintegración $G \rightarrow \bar{q}Q$, con q un quark estándar y Q su excitación masiva, hagan a G lo suficientemente ancha [2-4]. Consideramos todos los diferentes casos, con q el quark *top*, *bottom* o un quark ligero, y canales principales de desintegración $Q \rightarrow Wq'$ o $Q \rightarrow Zq$. Hemos mostrado que las búsquedas experimentales actuales son in-

capaces de descubrir el modelo, pero que modificaciones mínimas de estos análisis pueden explorar una gran región de su espacio de parámetros con la luminosidad actual del LHC. Esto incluye el desafiante caso en el que los nuevos quarks se desintegran mayormente en quarks de sabores ligeros. En algunos canales no sólo el quark pesado sino también el gluon masivo puede ser reconstruido, lo que establecería el origen de la asimetría de $t\bar{t}$. Hemos considerado también el caso en que los nuevos fermiones vectoriales se desintegran en un bosón de Higgs y un quark del Modelo Estándar en el marco de modelos minimales de Higgs compuesto [5, 6]. Hemos encontrado que masas de hasta 2.8 TeV para las nuevas resonancias gluónicas pueden ser sondeadas con los datos de 2011 y 2012. Esto entra en la región preferida actualmente por los datos de precisión electrodébil. Con la actualización de energía a $\sqrt{s} = 14$ TeV, hasta $M_G \sim 5$ TeV pueden estudiarse con 100 fb^{-1} .

- En el Capítulo 4 hemos estudiado por vez primera la implementación de una simetría global A_4 en modelos de unificación *gauge*-Higgs [7]. Aunque la violación de sabor leptónico se genera a nivel árbol, hemos encontrado que la simetría global otorga una fuerte protección gracias a un subgrupo de la simetría custodial que proporciona de forma natural la supresión adicional necesaria. También hemos investigado posibles desviaciones del patrón tri-bimaximal (que se predice a primer orden por la ruptura asumida de la simetría discreta) y las implicaciones de los tests de precisión electrodébil, la violación del sabor leptónico y las masas de los neutrinos y los ángulos de mezcla leptónicos en el espectro de nuevas resonancias. Esto requiere una determinación suficientemente precisa de las masas y las mezclas de partículas esparcidas en muchos órdenes de magnitud, haciendo del análisis numérico un interesante reto. El modelo es compatible con todas esas restricciones experimentales para masas de los nuevos bosones *gauge* $M_{KK} \gtrsim 3.5$ TeV, que podrían ser accesibles en el LHC. Hemos encontrado que, para mantener la violación de sabor leptónico por debajo de límites experimentales actuales (y esperados), la ruptura de A_4 tiene que ser relativamente pequeña. Esto conduce a una supresión adicional en los acoplamientos de Yukawa leptónicos y a un τ_R más compuesto. Esto implica a su vez la existencia de nuevas resonancias leptónicas - los custodios del tau - con masas de unos pocos cientos de GeV y grandes acoplamientos al τ_R . Vienen en un bidoblete de $SU(2)_L \times SU(2)_R$ casi degenerado con una fenomenología muy particular en el LHC.

Hemos demostrado que la producción de pares de custodios proporciona un canal limpio, independiente del modelo, dando lugar a dos taus y dos bosones de *gauge* o de Higgs [8]. Pidiendo que al menos una Z se desintegre en electrones o muones, desintegraciones leptónicas para los taus y ninguna fuente adicional de energía perdida, nos encontramos con un estado final con cuatro leptones cargados (electrones o muones), energía perdida y dos *jets*. El gran número de leptones permite una reducción muy eficiente de los principales fondos. La masa relativamente grande de los custodios resulta en taus altamente impulsados con productos de desintegración muy colimados. Suponiendo colimación completa, se puede reconstruir totalmente los dos taus, a pesar de la presencia de cuatro neutrinos en el estado final. Pidiendo además producción de pares de objetos con idéntica masa incrementamos aún más la señal, obteniendo un alcance para los custodios en el LHC con $\sqrt{s} = 14$ TeV de $M = 240, 480$ y 720 GeV para una luminosidad total integrada de $\mathcal{L} = 30, 300, 3000 \text{ fb}^{-1}$, respectivamente.

En resumen, hemos estudiado la fenomenología de los modelos con dimensiones adicionales y sus posibles señales en el LHC. En estas extensiones del Modelo Estándar, las principales desviaciones respecto al Modelo Estándar minimal se espera que aparezcan en procesos relacionados con la tercera familia, lo que también se espera por ser ésta la más pesada. Con esto en mente hemos estudiado las implicaciones fenomenológicas de los modelos extra-dimensionales que pueden ser observadas en el LHC a través del quark *top*. También hemos construido un modelo concreto para leptones que reproduce el espectro observado y predice un leptón tau más bien compuesto con señales características en el LHC.

A

Group Theory Summary

In this appendix we summarize the main group theory properties used in the text.

A.1 A_4 Representations

A_4 is the group of even permutations of four elements. It has twelve elements which can be written in terms of two generators, S and T , satisfying

$$S^2 = T^3 = (ST)^3 = \mathbf{1}. \quad (\text{A.1})$$

This discrete group has three inequivalent one-dimensional representations

$$\begin{aligned} \mathbf{1} : \quad & S = 1, \quad T = 1, \\ \mathbf{1}' : \quad & S = 1, \quad T = e^{i2\pi/3} = \omega, \\ \mathbf{1}'' : \quad & S = 1, \quad T = e^{i4\pi/3} = \omega^2, \end{aligned} \quad (\text{A.2})$$

and one three-dimensional irreducible representation, $\mathbf{3}$; being the Clebsch-Gordan series of their non-trivial products

$$\begin{aligned} \mathbf{1}' \times \mathbf{1}' &= \mathbf{1}'', \quad \mathbf{1}' \times \mathbf{1}'' = \mathbf{1}, \quad \mathbf{1}'' \times \mathbf{1}'' = \mathbf{1}', \\ \mathbf{1}' \times \mathbf{3} &= \mathbf{3}, \quad \mathbf{1}'' \times \mathbf{3} = \mathbf{3}, \\ \mathbf{3}_x \times \mathbf{3}_y &= \mathbf{3}_1 + \mathbf{3}_2 + \mathbf{1} + \mathbf{1}' + \mathbf{1}''. \end{aligned} \quad (\text{A.3})$$

In the basis where S is diagonal

$$S = \begin{pmatrix} 1 & 0 & 0 \\ 0 & -1 & 0 \\ 0 & 0 & -1 \end{pmatrix}, \quad T = \begin{pmatrix} 0 & 1 & 0 \\ 0 & 0 & 1 \\ 1 & 0 & 0 \end{pmatrix}, \quad (\text{A.4})$$

and the decomposition of $\mathbf{3}_x \times \mathbf{3}_y$ reads

$$\begin{aligned} \mathbf{1} &= x_1y_1 + x_2y_2 + x_3y_3, \\ \mathbf{1}' &= x_1y_1 + \omega^2x_2y_2 + \omega x_3y_3, \\ \mathbf{1}'' &= x_1y_1 + \omega x_2y_2 + \omega^2x_3y_3, \\ \mathbf{3}_1 &= (x_2y_3, x_3y_1, x_1y_2), \\ \mathbf{3}_2 &= (x_3y_2, x_1y_3, x_2y_1), \end{aligned} \quad (\text{A.5})$$

with $\mathbf{3}_x = (x_1, x_2, x_3)$ and $\mathbf{3}_y = (y_1, y_2, y_3)$.

A.2 $SO(5)$ Generators in the Fundamental Representation

The ten $SO(5)$ generators can be written in the fundamental representation (5)

$$\begin{aligned}
T_{L,ij}^a &= -\frac{i}{2} \left[\frac{1}{2} \epsilon^{abc} (\delta_i^b \delta_j^c - \delta_j^b \delta_i^c) + (\delta_i^a \delta_j^4 - \delta_j^a \delta_i^4) \right], & a = 1, 2, 3, \\
T_{R,ij}^a &= -\frac{i}{2} \left[\frac{1}{2} \epsilon^{abc} (\delta_i^b \delta_j^c - \delta_j^b \delta_i^c) - (\delta_i^a \delta_j^4 - \delta_j^a \delta_i^4) \right], & a = 1, 2, 3, \\
T_{C,ij}^{\hat{a}} &= -\frac{i}{\sqrt{2}} [\delta_i^{\hat{a}} \delta_j^5 - \delta_j^{\hat{a}} \delta_i^5], & \hat{a} = 1, 2, 3, 4.
\end{aligned} \tag{A.6}$$

They are normalized to $\text{Tr} T^\alpha T^\beta = \delta^{\alpha\beta}$. In this basis $\mathbf{5}$, which decomposes into $(\mathbf{2}, \mathbf{2}) \oplus (\mathbf{1}, \mathbf{1})$ under $SU(2)_L \times SU(2)_R$, reads

$$Q = \frac{1}{\sqrt{2}} \begin{pmatrix} q_{++} - q_{--} \\ iq_{++} + iq_{--} \\ -iq_{+-} + iq_{-+} \\ q_{+-} + q_{-+} \\ \sqrt{2}q_{00} \end{pmatrix}, \tag{A.7}$$

where the first (second) subscript $\pm, 0$ corresponds to $T_L^3 = \pm\frac{1}{2}, 0$ ($T_R^3 = \pm\frac{1}{2}, 0$), respectively.

List of figures

1.1	Solar neutrino flux predicted by the SSM [32]. Figure taken from John Bahcall's web site, [33].	16
1.2	Electron and muon/tau neutrino flux by SNO [41]. The intercept of these bands with the axes represent the $\pm 1\sigma$ uncertainties.	17
1.3	Global experimental constraints on the low energy solar P_{ee} . For the ${}^7\text{Be}$ point, the inner (red) error bars show the experimental uncertainty, while the outer (blue) error bars show the total (experimental + SSM) uncertainty. The remaining points were obtained following the procedure described in [43]. The green points are calculated without using the Borexino data. The LMA MSW prediction is also shown for comparison; the band defines the 1σ range of the mixing parameter estimate in [44], which does not include the current result. Figure extracted from [42].	17
1.4	The zenith angle distribution for fully-contained 1-ring events, multi-ring events, partially-contained events and upward muons from SK experiment [50]. The points show the data, box histograms show the non-oscillated MC events and the lines show the best-fit expectations for $\nu_\mu \leftrightarrow \nu_\tau$ oscillations with $\sin^2 2\theta_{23} = 1.00$ and $ \Delta m_{32}^2 = 2.1 \times 10^{-3} \text{ eV}^2$. The best-fit expectation is corrected by the 39 systematic error terms, while the correction is not made for the non-oscillated MC events. The height of the boxes shows the statistical error of the MC.	19
1.5	Ratio of the observed $\bar{\nu}_e$ spectrum to the expectation for no-oscillation versus L_0/E for the KamLAND data [55]. $L_0 = 180 \text{ km}$ is the flux-weighted average reactor baseline. The 2ν and 3ν histograms are the expected distributions based on the best-fit parameter values from the two- and three-flavor unbinned maximum-likelihood analysis of the KamLAND data.	20
1.6	Allowed regions projected in the $(\tan^2 \theta_{12}, \Delta m_{21}^2)$ plane, for solar and KamLAND data from (a) the two-flavor oscillation analysis ($\theta_{13} = 0$) and (b) the three-flavor oscillation analysis, where θ_{13} is a free parameter. The shaded regions are from the combined analysis of the solar and KamLAND data. The side panels show the $\Delta\chi^2$ profiles projected onto the $\tan^2 \theta_{12}$ and Δm_{21}^2 axes. Figure extracted from [55].	20
1.7	Left: Allowed regions from the solar and KamLAND data projected in the $(\tan^2 \theta_{12}, \sin^2 \theta_{13})$ plane for the three-flavor analysis. Right: $\Delta\chi^2$ -profiles projected onto the $\sin^2 \theta_{13}$ axis for different combinations of the oscillation data floating the undisplayed parameters $(\tan^2 \theta_{12}, \Delta m_{21}^2)$. Figure extracted from [55].	21
1.8	Normal and inverted hierarchy for the neutrino spectrum.	21
1.9	Confidence intervals for $\sin^2 2\theta_{13}$ for the normal mass hierarchy (upper) and inverted hierarchy (lower) as a function of the CP violation parameter δ_{CP} . The 90% CL upper limits from Double-CHOOZ and MINOS are shown by the dashed lines. The shaded regions show the T2K 68% and 90% CL intervals, and the solid line shows the T2K best fit. Figure extracted from [63].	23

1.10	Global 3ν analysis: Joint contours at 1, 2 and 3σ ($\Delta\chi^2 = 1, 4$ and 9) for couples of $\sin^2\theta_{ij}$ parameters, assuming old reactor neutrino fluxes. For new reactor fluxes, the best fits (and, to a large extent, also the contours) are shifted as indicated by the arrows [64].	24
1.11	CMS 95% CL upper limits on $\sigma/\sigma_{\text{SM}}$ for the SM Higgs boson hypothesis as a function of the Higgs boson mass in the range 110–600 GeV (left) and 110–145 GeV (right). The observed values as a function of mass are shown by the solid line. The dashed line indicates the expected median of results for the no Higgs hypothesis, while the green (dark) and yellow (light) bands indicate the ranges that are expected to contain 68% and 95% of all observed excursions from the median, respectively. Figure taken from [68].	28
1.12	Allowed values at 90, 99% CL of (\hat{S}, \hat{T}) (for generic W, Y) and of (W, Y) (for generic \hat{S}, \hat{T}) with $m_h = 115$ GeV. The dashed lines show the weaker constraints obtained by the EWPT alone. Figure extracted from [82].	32
2.1	Rearrangement of KK towers mixed up through boundary conditions. We represent the different KK eigenstates, with bigger values in the y-axis meaning bigger KK masses.	46
2.2	Contribution to the coefficients $\hat{\alpha}$, $\hat{\beta}$ and $\hat{\gamma}$ of Eq. (2.115). The double line represents the tower of massive gauge boson KK modes, the red squares the mixing between the gauge KK and zero-modes, and the blue dot the coupling of the light fermions to the gauge KK modes.	48
2.3	Mass of the first gauge KK mode in units of the effective IR scale \tilde{k}_{eff} , defined in Eq. (2.122), as a function of ν and for different values of kL_1	50
2.4	Value of the localization parameter, $c_{1/2}$, that makes a LH fermion zero-mode mostly delocalized, as a function of ν and for different values of kL_1	52
2.5	Left panel: Yukawa coupling, $\lambda \equiv \lambda_{00}^{LR}$, as a function of the bulk mass for $c_L = -c_R = c$ and a 5D Yukawa coupling that saturates the maximum value given in Eq. (2.136). Right panel: coupling of a LH fermion zero-mode to the first two gauge boson KK modes in units of $g_0 \equiv g_5/\sqrt{y_1}$. In both cases we have taken $\nu = 0.4$ and $kL_1 = 0.2$, which lead to maximally delocalized fermions for $c \approx 0.93$	52
2.6	Examples of radiative corrections to the oblique parameters, as well as to the non-oblique vertex corrections. The most important contributions arise from the top KK tower in the loop. Upper row, left to right: one-loop contributions to T , S and δg_{b_L} , respectively. Lower row: examples of the corresponding two-loop contributions.	53
2.7	95% CL lower bound on the mass of the first KK gauge boson, obtained from a <i>tree-level oblique</i> analysis. We assume UV localized fermions and different values of the input parameters ν and kL_1 . See text for details on the fit procedure.	55
2.8	Fermion zero-mode, Higgs and first gauge KK mode profiles, $\sqrt{\omega}(y)$ for $\nu = 0.4$ and $kL_1 = 0.2$	56
2.9	Couplings of UV localized fermions to the first-level KK gauge bosons, in units of the zero-mode gauge coupling. We show curves as a function of ν , and for different values of kL_1	57
2.10	Tree-level 95% CL lower bound on the mass of the first gauge KK mode as a function of the localization of the LH top/bottom multiplet (c_Q) for the six scenarios discussed in the text. We fix $\nu = 0.4$ and $kL_1 = 0.2$. The lines end at the value of c_Q beyond which the top mass cannot be generated. For comparison we also show the result of the fit if the effects of third generation quarks are neglected (horizontal “ST” line). The maximal delocalization is obtained for $c \approx 0.93$ (see Fig. 2.4).	58
2.11	One-loop contribution to T , S and δg_{b_L} , as a function of c_Q , in scenario 2c (see text). We take $\nu = 0.4$ and $kL_1 = 0.2$	59

2.12	Left panel: 95% CL lower bound on the mass of the first gauge KK mode as a function of the localization of the LH top/bottom multiplet (c_Q) in scenario 2c, including one-loop effects. The different lines correspond to different values of m_h , with the one marked as “ m_h at χ_{\min}^2 ” corresponding to marginalization over m_h . The curves are terminated where the goodness-of-fit gives a 5% likelihood. Right panel: comparison of the tree-level oblique, full tree-level, and tree-level plus one-loop bounds on M_{KK} , assuming marginalization over m_h . In all cases, we fix $\nu = 0.4$ and $kL_1 = 0.2$	59
2.13	Mass of the first fermion KK mode for a $[++]$ field in units of \tilde{k}_{eff} as a function of its localization parameter (with respect to the mostly delocalized value) for values of $\nu = 0.3, 0.4, 0.5, 0.6, 0.7$ (top to bottom, left panel) and $kL_1 = 0.2, 0.3, 0.4, 0.5, 0.6$ (bottom to top, right panel).	60
2.14	Couplings to the first gauge KK mode (in units of $g_0 = g_5/\sqrt{y_1}$) of the third generation LH quarks Q_L , RH top t_R , RH bottom b_R , and light quarks q , as a function of c_Q , for scenario 2 (sub-scenarios a, b and c give similar results for the couplings). We fix $\nu = 0.4$ and $kL_1 = 0.2$. The localization parameters c_T, c_B and the top and bottom masses have been fixed as described in the text. The b_R and q couplings are almost identical.	61
2.15	$t\bar{t}$ invariant mass distribution in the SM (red dotted), in the model with extra-dimensional physics (solid blue) and the contribution of just the KK gluon exchange (dashed purple). The left panel corresponds to a KK gluon with $M_{\text{KK}} \approx 1.5$ TeV and the couplings of Eqs. (2.151)-(2.152). The right panel corresponds to $M_{\text{KK}} \approx 2.3$ TeV and the couplings of Eqs. (2.146)-(2.147).	63
2.16	Left: Bulk gauge symmetry breaking on the different branes. Right: Boundary conditions for the vector component of the corresponding 5D gauge bosons.	64
2.17	Fermion contribution to the one-loop Higgs mass in GHU models.	66
2.18	Schematic representation of the CFT interpretation of GHU models.	66
2.19	One-loop diagrams giving mass to the pseudo NGB π^a in the CFT.	66
2.20	Tree-level diagrams contributing to the elastic scattering $A_\mu^{(n)a} + A_\mu^{(n)b} \rightarrow A_\mu^{(n)c} + A_\mu^{(n)d}$	67
2.21	Left: In dashed green, contour plot for values of R and R' reproducing the observed W mass, in the Higgsless model introduced in [125]. Right: In the same model, $M_W^{(2)}$ mass in function of R , once $M_W^{(1)}$ is matched to $M_W = 80.399$ GeV by choosing the proper R value.	69
3.1	Lepton + jets topology used by CDF and DØ to define the $t\bar{t}$ forward-backward asymmetry $A^{t\bar{t}}$	72
3.2	Above: Interference of the tree-level and one-loop box diagrams for $q\bar{q} \rightarrow t\bar{t}$. Below: Interference of initial and final state radiation diagrams in $q\bar{q} \rightarrow t\bar{t}j$	72
3.3	Invariant mass dependence of the $A^{t\bar{t}}$ forward-backward asymmetry for the SM@NLO $t\bar{t}$ and the CDF unfolded data for an integrated luminosity of 8.7 fb^{-1} , in the $t\bar{t}$ rest frame. Figure extracted from [174].	73
3.4	Left (right): Coupling of LH (RH) light down quarks to the Z boson, in the zero-mode approximation. In black dashed, the SM value.	75
3.5	Coupling of LH light quarks to the first gluon excitation G , in the zero-mode approximation.	76
3.6	Left (right): Coupling of LH (RH) light down quarks to the Z boson, for different values of the Higgs vev. We have fixed R to the same value used in the realistic Higgsless model and, for each value of v , chosen R' and g_{5_L} reproducing the W and Z mass. The case $v = 10000$ TeV can be identified with the Higgsless limit.	77

3.7	Left: Top quark mass dependence on c_{t_r} , with M_1 giving $m_t = 170$ GeV for $c_{t_r} = 1.6$. Right: M_1 value which reproduces the top quark mass in terms of c_{t_r} , once M_3 is fixed doing the same thing for the bottom quark. In both cases, we have chosen $c_{\Psi_3^+} = 0.35$ and $c_{\Psi_3^0} = -0.677$	78
3.8	$G_{\bar{t}RtR}$ coupling in terms of the bulk mass parameter c_{t_r}	78
3.9	$M_{t\bar{t}}$ distribution at the Tevatron for Higgsless models. Left: original Higgsless model of Eq. (3.25); right: modified Higgsless model Eq. (3.26). In both cases the contribution in the Higgsless models is shown in dashed while the SM only contribution is shown in solid. We have considered a luminosity of 5.3 fb^{-1}	79
3.10	$M_{t\bar{t}}$ distribution at the Tevatron in the SM (solid) and in the Higgsless motivated model (dashed) for a luminosity of 5.3 fb^{-1} . On the right we plot a particular Montecarlo simulation. The errors shown are statistical only.	80
3.11	Main diagrams involved in pair production of vector-like excitations.	81
3.12	Left: Charged decay mode involving a third-generation quark excitation T and a top quark. Right: Diagram associated with the same final state but arising from the charged decay of a bottom quark and its vector-like excitation B . In both cases, the conjugated processes are not explicitly shown and should be added.	83
3.13	$M_{t\bar{t}}$ distribution at the Tevatron for 5.3 fb^{-1} in the SM (solid blue), the benchmark model (points with error bars) and the extreme T case (dashed black). We include the contribution from $T\bar{t}, t\bar{T}$ and $B\bar{b}, b\bar{B}$ when present.	84
3.14	Left: Reconstructed $M_{t\bar{t}}$ distribution at the ATLAS detector for 0.2 fb^{-1} in the SM (solid blue), the benchmark model (points with error bars) and the extreme T model (dashed black). Right: $M_{t\bar{t}}$ distribution for the μ +jets channel (in the case of 4 or more jets with at least two b-tagged) at the CMS experiment for the same luminosity. We include the contribution from $T\bar{t}, t\bar{T}$ and $B\bar{b}, b\bar{B}$ when present.	84
3.15	$T\bar{T}$ search at the LHC for 0.821 fb^{-1} . Left: H_T distribution. Right: m_{fit} distribution. In both cases we show the predictions in the SM (solid blue), in the benchmark model (data points with statistical errors) and in the extreme T case (dashed black). We include the contribution from $T\bar{t}, t\bar{T}$ and $B\bar{b}, b\bar{B}$ when present.	85
3.16	Left: Reconstructed M_T at the LHC. Right: Reconstruction of M_G . In both cases we have normalized the distributions to 4 fb^{-1} data and represent the results for the SM (solid blue), the benchmark model (data points with statistical errors) and the extreme T case (dashed black). Details of the reconstruction method can be found in the text.	86
3.17	Reconstructed M_B at the LHC for 4 fb^{-1} in the SM (solid blue), the benchmark model (data points with errors) and the B case (dashed black). We consider the cuts $M_{B\bar{b}} > 600$ GeV (left) and $M_{B\bar{b}} > 700$ GeV (right). Details of the reconstruction method can be found in the text.	87
3.18	$Zt\bar{t}$ production mediated by the heavy gluon G and the vector-like excitation T . The conjugated process should be added.	88
3.19	Reconstructed total invariant mass for the $Zt\bar{t}$ channel in the SM (solid blue), benchmark (solid red) and extreme T (data with statistical errors shown as a band) models for the $Zt\bar{t}$ analysis described in the text for the LHC with 4 fb^{-1}	88
3.20	Left: reconstruction of M_{Zb_h} at the LHC. Right: reconstruction of $M_{zb\bar{b}}$ to show the heavy gluon mass. In both cases we have normalized the distributions to 4 fb^{-1} of data and have represented the SM with thick solid blue line, the benchmark model with thin solid red line and the extreme B case (data points with statistical errors).	89
3.21	Result of the fit of the M_{Zj_h} distribution for the Zjj analysis described in the text for the SM (solid blue), extreme Q model (data points with statistical errors) and the fit to both distributions (dashed black). Simulations for the 7 TeV LHC with 4 fb^{-1}	90

3.22	Transverse mass for the Wj_h system in the Wjj analysis described in the text for the SM (solid blue), benchmark model (data points with errors) and extreme Q model (dashed black). Search for the 7 TeV LHC with 4 fb^{-1}	91
3.23	Left panel: massive gluon width as a function of its mass for the anarchic scenario with $M_F = 0.5$ and 1 TeV. Right panel: massive gluon branching fraction in two SM quarks (labeled qq), one SM and one heavy quark (Qq) and two heavy quarks (QQ), respectively.	92
3.24	$ht\bar{t}$ production cross section in the model considered in the text, mediated by a color octet vector resonance with decay into a fermionic resonance and a top quark.	93
3.25	Contours of required luminosity for a 5σ discovery (bands and solid lines) and 95% exclusion limits (dotted lines) as a function of $s_u = s_u^{(3)}$ and M_G (left column) and g_{*3} and M_G (right column) for $\sqrt{s} = 7, 8$ and 14 TeV (first, second and third row, respectively). Current bounds are shown with dashed lines (the area below the dashed lines is excluded).	96
4.1	LFV branching ratios as a function of v/Λ for the scan described in the text. $\mu \rightarrow eee$ is plotted on the top-left panel, $\mu - e$ conversion in nuclei on the top-right one, and $\mu \rightarrow e\gamma$ on the two lower panels (any v/Λ value on the left panel and small v/Λ values on the right one). The horizontal lines correspond to the current experimental upper bound (solid) and future sensitivity (dashed).	113
4.2	Heavy lepton pair production cross section (in fb) as a function of the heavy mass M . The dotted (solid) line corresponds to $\sqrt{s} = 7$ (14) TeV. The cross section includes the leptonic Z decay but not the tau decays, i.e. $pp \rightarrow l^+l^-jj\tau^+\tau^-$	117
4.3	Luminosity required for a 5σ discovery at the LHC with $\sqrt{s} = 14$ TeV as a function of the custodian mass M	119

List of tables

1.1	Gauge quantum numbers and chirality of one generation of SM fermions.	9
1.2	Orders of magnitude of Δm^2 values which can be probed in different experiments. SBL (LBL) stands for <i>short (long) baseline</i> . Table taken from [29].	15
1.3	Results of the global 3ν oscillation analysis, in terms of best-fit values and allowed 1, 2 and 3σ ranges for the mass-mixing parameters, assuming old reactor neutrino fluxes. The corresponding best fits and ranges for the new reactor fluxes are shown in parentheses [64].	24
1.4	Principal Z pole observables and their SM predictions. The first $\bar{s}_\ell^2(A_{FB}^{(0,q)})$ value is the effective angle extracted from the hadronic charge asymmetry while the second is the combined lepton asymmetry from CDF [45] and D0 [46]. The three values of A_e are (i) from A_{LR} for hadronic final states [47]; (ii) from A_{LR} for leptonic final states and from polarized Bhabba scattering [48]; and (iii) from the angular distribution of the τ polarization. The two A_τ values are from SLD and the total τ polarization, respectively. Table extracted from [44].	27
1.5	Coefficients of the most general Lagrangian of new universal physics BSM. The expressions below are also valid when the normalization conditions, Eq. (1.86), have not been imposed. We also show the contribution to these coefficients from the corresponding dimension 6 operators. Table adapted from [82].	31
1.6	Fit to universal corrections to the SM [82].	32
1.7	Bounds on representative dimension-six $\Delta F = 2$ operators. Observables related to CP violation are separated from the CP conserving ones with semicolons. In the B_s system we only quote a bound on the absolute value of the NP amplitude derived from Δm_{B_s} , see Ref. [86].	34
1.8	Upper bounds at 90 % CL on some LFV processes with their corresponding references. μ^+ and τ^+ decay modes are charge conjugates of the modes above. B_{conv} is the branching ratio for $\mu - e$ conversion.	34
3.1	CDF results [174] for the $A^{t\bar{t}}$ forward-backward asymmetry for both the SM@NLO prediction and the unfolded data, for different regions of the $t\bar{t}$ invariant mass $M_{t\bar{t}}$	73
3.2	Global efficiencies for the signal and relevant backgrounds as a function of M_G . All efficiencies are reported as per cent.	94
3.3	Global efficiencies for the signal and relevant backgrounds as a function of M_G . All efficiencies are reported as per cent.	95
4.1	Bulk fermion (left) and localized scalar (right) quantum number assignments under the discrete group $A_4 \otimes Z_8$	99
4.2	Percentage of points that satisfy all experimental tests (including the projected MEG sensitivity on the last column) for different parameter intervals.	112

4.3	Cross sections in fb (and corresponding efficiencies) after cuts for the signal and main backgrounds. The cuts are described in Eqs. (4.97-4.107). We show the results for two different values of the custodian masses $M = 200, 400$ GeV. The effect of the last cut on the background depends on the test mass as shown in the last row. The required luminosity to have a 5σ discovery, with 3 or more events, being $\mathcal{L} \approx 17, 170 \text{ fb}^{-1}$, respectively.	119
4.4	Used and current bounds on some LFV processes.	120
4.5	Percentage of points that satisfy all experimental tests for old and current bounds on LFV processes.	120

Bibliography

- [1] A. Carmona, E. Ponton and J. Santiago, JHEP **10** (2011) 137 [arXiv:1107.1500 [hep-ph]].
- [2] R. Barcelo, A. Carmona, M. Masip and J. Santiago, Phys. Rev. D **84** (2011) 014024 [arXiv:1105.3333 [hep-ph]].
- [3] R. Barcelo, A. Carmona, M. Masip and J. Santiago, Phys. Lett. B **707** (2012) 88 [arXiv:1106.4054 [hep-ph]].
- [4] R. Barcelo, A. Carmona, M. Chala, M. Masip and J. Santiago, Nucl. Phys. B **857** (2012) 172 [arXiv:1110.5914 [hep-ph]].
- [5] G. Brooijmans, B. Gripaios, F. Moortgat, J. Santiago, P. Skands, D. Albornoz Vasquez, B. C. Allanach and A. Alloul *et al.*, arXiv:1203.1488 [hep-ph].
- [6] A. Carmona, M. Chala and J. Santiago, arXiv:1205.2378 [hep-ph].
- [7] F. del Aguila, A. Carmona and J. Santiago, JHEP **1008** (2010) 127 [arXiv:1001.5151 [hep-ph]].
- [8] F. del Aguila, A. Carmona and J. Santiago, Phys. Lett. B **695** (2011) 449 [arXiv:1007.4206 [hep-ph]].
- [9] A. Carmona and J. Santiago, arXiv:1110.5651 [hep-ph].
- [10] F. del Aguila, J. de Blas, A. Carmona and J. Santiago, Fortsch. Phys. **58** (2010) 675 [arXiv:1003.5799 [hep-ph]].
- [11] A. Badiou, *Court traité d'ontologie transitoire*, Éditions du Seuil, Paris, 1998.
- [12] S. L. Glashow, Nucl. Phys. **22** (1961) 579.
- [13] S. Weinberg, Phys. Rev. Lett. **19** (1967) 1264.
- [14] A. Salam, Conf. Proc. C **680519** (1968) 367.
- [15] P. W. Higgs, Phys. Lett. **12** (1964) 132.
- [16] F. Englert and R. Brout, Phys. Rev. Lett. **13** (1964) 321.
- [17] G. S. Guralnik, C. R. Hagen and T. W. B. Kibble, Phys. Rev. Lett. **13** (1964) 585.
- [18] T. W. B. Kibble, Phys. Rev. **155** (1967) 1554.
- [19] Y. Nambu, Phys. Rev. Lett. **4** (1960) 380.
- [20] J. Goldstone, Nuovo Cim. **19** (1961) 154.
- [21] S. L. Glashow, J. Iliopoulos and L. Maiani, Phys. Rev. D **2** (1970) 1285.
- [22] N. Cabibbo, Phys. Rev. Lett. **10** (1963) 531.

- [23] M. Kobayashi and T. Maskawa, *Prog. Theor. Phys.* **49** (1973) 652.
- [24] V. N. Gribov and B. Pontecorvo, *Phys. Lett. B* **28** (1969) 493.
- [25] B. Pontecorvo, *Sov. Phys. JETP* **6** (1957) 429 [*Zh. Eksp. Teor. Fiz.* **33** (1957) 549].
- [26] Z. Maki, M. Nakagawa and S. Sakata, *Prog. Theor. Phys.* **28** (1962) 870.
- [27] B. Pontecorvo, *Sov. Phys. JETP* **26** (1968) 984 [*Zh. Eksp. Teor. Fiz.* **53** (1967) 1717].
- [28] B. Kayser, *Eur. Phys. J. C* **15** (2000) 344.
- [29] M. C. Gonzalez-Garcia and M. Maltoni, *Phys. Rept.* **460** (2008) 1 [arXiv:0704.1800 [hep-ph]].
- [30] L. Wolfenstein, *Phys. Rev. D* **17** (1978) 2369.
- [31] S. P. Mikheev and A. Y. Smirnov, *Sov. J. Nucl. Phys.* **42** (1985) 913 [*Yad. Fiz.* **42** (1985) 1441].
- [32] J. N. Bahcall, A. M. Serenelli and S. Basu, *Astrophys. J.* **621** (2005) L85 [astro-ph/0412440].
- [33] <http://www.sns.ias.edu/~jnb/>
- [34] B. T. Cleveland, T. Daily, R. Davis, Jr., J. R. Distel, K. Lande, C. K. Lee, P. S. Wildenhain and J. Ullman, *Astrophys. J.* **496** (1998) 505.
- [35] W. Hampel *et al.* [GALLEX Collaboration], *Phys. Lett. B* **447** (1999) 127.
- [36] M. Altmann *et al.* [GNO Collaboration], *Phys. Lett. B* **616** (2005) 174 [hep-ex/0504037].
- [37] J. N. Abdurashitov *et al.* [SAGE Collaboration], *J. Exp. Theor. Phys.* **95** (2002) 181 [*Zh. Eksp. Teor. Fiz.* **122** (2002) 211] [astro-ph/0204245].
- [38] Y. Fukuda *et al.* [Kamiokande Collaboration], *Phys. Lett. B* **388** (1996) 397.
- [39] J. Hosaka *et al.* [Super-Kamiokande Collaboration], *Phys. Rev. D* **73** (2006) 112001 [hep-ex/0508053].
- [40] K. Abe *et al.* [Super-Kamiokande Collaboration], *Phys. Rev. D* **83** (2011) 052010 [arXiv:1010.0118 [hep-ex]].
- [41] B. Aharmim *et al.* [SNO Collaboration], *Phys. Rev. C* **75** (2007) 045502 [nucl-ex/0610020].
- [42] G. Bellini, J. Benziger, D. Bick, S. Bonetti, G. Bonfini, M. Buizza Avanzini, B. Caccianiga and L. Cadonati *et al.*, *Phys. Rev. Lett.* **107** (2011) 141302 [arXiv:1104.1816 [hep-ex]].
- [43] V. Barger, D. Marfatia and K. Whisnant, *Phys. Lett. B* **617** (2005) 78 [hep-ph/0501247].
- [44] K. Nakamura *et al.* [Particle Data Group Collaboration], *J. Phys. G* **37** (2010) 075021.
- [45] D. Acosta *et al.* [CDF Collaboration], *Phys. Rev. D* **71** (2005) 052002 [hep-ex/0411059].
- [46] V. M. Abazov *et al.* [D0 Collaboration], *Phys. Rev. Lett.* **101** (2008) 191801 [arXiv:0804.3220 [hep-ex]].
- [47] K. Abe *et al.* [SLD Collaboration], *Phys. Rev. Lett.* **84** (2000) 5945 [hep-ex/0004026].
- [48] K. Abe *et al.* [SLD Collaboration], *Phys. Rev. Lett.* **86** (2001) 1162 [hep-ex/0010015].
- [49] R. Becker-Szendy, C. B. Bratton, D. Casper, S. T. Dye, W. Gajewski, M. Goldhaber, T. J. Haines and P. Halverson *et al.*, *Phys. Rev. D* **46** (1992) 3720.

-
- [50] Y. Ashie *et al.* [Super-Kamiokande Collaboration], Phys. Rev. D **71**, 112005 (2005) [hep-ex/0501064].
- [51] G. Zacek *et al.* [CALTECH-SIN-TUM Collaboration], Phys. Rev. D **34** (1986) 2621.
- [52] G. S. Vidyakin, V. N. Vyrodov, Y. V. Kozlov, A. V. Martemyanov, V. P. Martemyanov, A. N. Odinokov, S. V. Sukhotin and V. G. Tarasenkov *et al.*, JETP Lett. **59** (1994) 390 [Pisma Zh. Eksp. Teor. Fiz. **59** (1994) 364].
- [53] M. Apollonio *et al.* [CHOOZ Collaboration], Phys. Lett. B **466** (1999) 415 [hep-ex/9907037].
- [54] A. Piepke [Palo Verde Collaboration], Prog. Part. Nucl. Phys. **48** (2002) 113.
- [55] A. Gando *et al.* [The KamLAND Collaboration], Phys. Rev. D **83** (2011) 052002 [arXiv:1009.4771 [hep-ex]].
- [56] S. M. Bilenky, D. Nicolo and S. T. Petcov, Phys. Lett. B **538** (2002) 77 [hep-ph/0112216].
- [57] Y. Abe *et al.* [DOUBLE-CHOOZ Collaboration], arXiv:1112.6353 [hep-ex].
- [58] F. P. An *et al.* [DAYA-BAY Collaboration], arXiv:1203.1669 [hep-ex].
- [59] J. K. Ahn *et al.* [RENO Collaboration], Phys. Rev. Lett. **108** (2012) 191802 [arXiv:1204.0626 [hep-ex]].
- [60] M. H. Ahn *et al.* [K2K Collaboration], Phys. Rev. D **74** (2006) 072003 [hep-ex/0606032], M. Yokoyama [K2K and T2K Collaboration],
- [61] P. Adamson *et al.* [MINOS Collaboration], Phys. Rev. Lett. **107** (2011) 181802 [arXiv:1108.0015 [hep-ex]].
- [62] K. Abe *et al.* [T2K Collaboration], Phys. Rev. Lett. **107** (2011) 041801 [arXiv:1106.2822 [hep-ex]].
- [63] D. Karlen, arXiv:1111.2397 [hep-ex].
- [64] G. L. Fogli, E. Lisi, A. Marrone, A. Palazzo and A. M. Rotunno, Phys. Rev. D **84** (2011) 053007 [arXiv:1106.6028 [hep-ph]].
- [65] C. H. Llewellyn Smith, Phys. Lett. B **46** (1973) 233; D. A. Dicus and V. S. Mathur, Phys. Rev. D **7** (1973) 3111; J. M. Cornwall, D. N. Levin and G. Tiktopoulos, Phys. Rev. D **10** (1974) 1145 [Erratum-ibid. D **11** (1975) 972]; B. W. Lee, C. Quigg and H. B. Thacker, Phys. Rev. D **16** (1977) 1519.
- [66] T. Aaltonen *et al.* [CDF Collaboration], arXiv:1203.0275 [hep-ex].
- [67] T. Aaltonen *et al.* [CDF and D0 Collaboration], [arXiv:1103.3233 [hep-ex]].
- [68] S. Chatrchyan *et al.* [CMS Collaboration], arXiv:1202.1488 [hep-ex].
- [69] G. Aad *et al.* [ATLAS Collaboration], arXiv:1202.1408 [hep-ex].
- [70] LEP Working Group for Higgs boson searches, R. Barate *et al.*, Phys. Lett. **B565**, 61 (2003), hep-ex/0306033.
- [71] S. Egli *et al.* [SINDRUM Collaboration], Phys. Lett. B **222** (1989) 533.
- [72] G. D. Barr *et al.* [NA31 Collaboration], Phys. Lett. B **235** (1990) 356.

- [73] M. S. Alam *et al.* [CLEO Collaboration], Phys. Rev. D **40** (1989) 712 [Erratum-ibid. D **40** (1989) 3790].
- [74] M. Sievertz *et al.* [CUSB Collaboration], Phys. Rev. Lett. **26** (1982) 717; J. Lee-Franzini *et al.* [CUSB Collaboration], Proc. Int. Conf. High Energy Phys., XXIVth, Munich, Aug. 4-10, 1988, p. 891. (1989)
- [75] S. Chang, R. Dermisek, J. F. Gunion, and N. Weiner, (2008), arXiv:0801.4554 [hep-ph].
- [76] C. Arzt, Phys. Lett. **B342**, 189 (1995), [hep-ph/9304230].
- [77] S. Weinberg, Phys. Rev. Lett. **43**, 1566 (1979); F. Wilczek and A. Zee, Phys. Rev. Lett. **43**, 1571 (1979); H. A. Weldon and A. Zee, Nucl. Phys. **B173**, 269 (1980).
- [78] W. Buchmuller and D. Wyler, Nucl. Phys. **B268**, 621 (1986).
- [79] Z. Han and W. Skiba, Phys. Rev. **D71**, 075009 (2005), hep-ph/0412166.
- [80] Z. Han, Phys. Rev. **D73**, 015005 (2006), hep-ph/0510125.
- [81] G. Cacciapaglia, C. Csaki, G. Marandella, and A. Strumia, Phys. Rev. **D74**, 033011 (2006), hep-ph/0604111.
- [82] R. Barbieri, A. Pomarol, R. Rattazzi, and A. Strumia, Nucl. Phys. **B703**, 127 (2004), hep-ph/0405040.
- [83] M. E. Peskin and T. Takeuchi, Phys. Rev. **D46**, 381 (1992).
- [84] M. J. G. Veltman, Acta Phys. Polon. **B8**, 475 (1977).
- [85] M. Bona *et al.* [UTfit Collaboration], JHEP **0803** (2008) 049 [arXiv:0707.0636 [hep-ph]].
- [86] G. Isidori, Y. Nir and G. Perez, Ann. Rev. Nucl. Part. Sci. **60** (2010) 355 [arXiv:1002.0900 [hep-ph]].
- [87] W. H. Bertl *et al.* [SINDRUM II Collaboration], Eur. Phys. J. C **47** (2006) 337; Y. Kuno, Nucl. Phys. Proc. Suppl. **149** (2005) 376.
- [88] D. Asner *et al.* [Heavy Flavor Averaging Group Collaboration], arXiv:1010.1589 [hep-ex].
- [89] A. Maki, AIP Conf. Proc. **981** (2008) 363.
- [90] J. Adam *et al.* [MEG Collaboration], Phys. Rev. Lett. **107** (2011) 171801 [arXiv:1107.5547 [hep-ex]].
- [91] P. Wintz, *Prepared for 29th International Conference on High-Energy Physics (ICHEP 98), Vancouver, Canada, 23-29 Jul 1998*
- [92] S. Žižek, Extracted from the film *Zizek!*, by Astra Taylor (2005).
- [93] L. Randall, R. Sundrum, Phys. Rev. Lett. **83** (1999) 3370-3373. [hep-ph/9905221]; Phys. Rev. Lett. **83** (1999) 4690-4693. [hep-th/9906064].
- [94] H. Davoudiasl, J. L. Hewett and T. G. Rizzo, Phys. Lett. B **473** (2000) 43 [hep-ph/9911262].
- [95] A. Pomarol, Phys. Lett. B **486** (2000) 153 [hep-ph/9911294].
- [96] Y. Grossman and M. Neubert, Phys. Lett. B **474** (2000) 361 [hep-ph/9912408].

-
- [97] K. Agashe, T. Okui and R. Sundrum, *Phys. Rev. Lett.* **102** (2009) 101801 [arXiv:0810.1277 [hep-ph]].
- [98] M. Carena, A. D. Medina, N. R. Shah and C. E. M. Wagner, *Phys. Rev. D* **79** (2009) 096010 [arXiv:0901.0609 [hep-ph]].
- [99] G. Altarelli and F. Feruglio, *Nucl. Phys. B* **720** (2005) 64 [hep-ph/0504165].
- [100] C. Csaki, C. Delaunay, C. Grojean and Y. Grossman, *JHEP* **0810** (2008) 055 [arXiv:0806.0356 [hep-ph]].
- [101] M. -C. Chen, K. T. Mahanthappa and F. Yu, *Phys. Rev. D* **81** (2010) 036004 [arXiv:0907.3963 [hep-ph]]. arXiv:0909.5472 [hep-ph].
- [102] M. S. Carena, E. Ponton, J. Santiago and C. E. M. Wagner, *Phys. Rev. D* **76** (2007) 035006 [hep-ph/0701055].
- [103] S. J. Huber and Q. Shafi, *Phys. Lett. B* **498** (2001) 256 [hep-ph/0010195]; *Phys. Lett. B* **512** (2001) 365 [arXiv:hep-ph/0104293]; *Phys. Lett. B* **544** (2002) 295 [arXiv:hep-ph/0205327]. S. J. Huber, *Nucl. Phys. B* **666** (2003) 269 [hep-ph/0303183].
- [104] G. Burdman, *Phys. Rev. D* **66** (2002) 076003 [hep-ph/0205329]; G. Burdman, *Phys. Lett. B* **590** (2004) 86 [hep-ph/0310144].
- [105] K. Agashe, G. Perez and A. Soni, *Phys. Rev. Lett.* **93** (2004) 201804 [hep-ph/0406101].
- [106] K. Agashe, G. Perez and A. Soni, *Phys. Rev. D* **71** (2005) 016002 [hep-ph/0408134].
- [107] K. Agashe, A. E. Blechman and F. Petriello, *Phys. Rev. D* **74** (2006) 053011 [hep-ph/0606021].
- [108] C. Csaki, A. Falkowski and A. Weiler, *JHEP* **0809** (2008) 008 [arXiv:0804.1954 [hep-ph]].
- [109] C. Csaki, Y. Grossman, P. Tanedo and Y. Tsai, *Phys. Rev. D* **83** (2011) 073002 [arXiv:1004.2037 [hep-ph]].
- [110] K. Agashe, A. Delgado, M. J. May and R. Sundrum, *JHEP* **0308** (2003) 050 [hep-ph/0308036].
- [111] K. Agashe, R. Contino, L. Da Rold and A. Pomarol, *Phys. Lett. B* **641** (2006) 62 [hep-ph/0605341].
- [112] A. Djouadi, G. Moreau and F. Richard, *Nucl. Phys. B* **773** (2007) 43 [hep-ph/0610173].
- [113] A. Atre, M. Carena, T. Han and J. Santiago, *Phys. Rev. D* **79** (2009) 054018 [arXiv:0806.3966 [hep-ph]].
- [114] M. Blanke, A. J. Buras, B. Duling, S. Gori and A. Weiler, *JHEP* **0903** (2009) 001 [arXiv:0809.1073 [hep-ph]]; M. Blanke, A. J. Buras, B. Duling, K. Gemmler and S. Gori, *JHEP* **0903** (2009) 108 [arXiv:0812.3803 [hep-ph]]; A. J. Buras, B. Duling and S. Gori, *JHEP* **0909** (2009) 076 [arXiv:0905.2318 [hep-ph]].
- [115] K. Agashe, arXiv:0902.2400 [hep-ph].
- [116] C. Csaki, A. Falkowski and A. Weiler, *Phys. Rev. D* **80** (2009) 016001 [arXiv:0806.3757 [hep-ph]].
- [117] M. S. Carena, E. Ponton, T. M. P. Tait and C. E. MWagner, *Phys. Rev. D* **67** (2003) 096006 [hep-ph/0212307].

- [118] F. del Aguila, M. Perez-Victoria and J. Santiago, *JHEP* **0302** (2003) 051 [hep-th/0302023].
- [119] J. A. Cabrer, G. von Gersdorff and M. Quiros, *Phys. Lett. B* **697** (2011) 208 [arXiv:1011.2205 [hep-ph]].
- [120] J. A. Cabrer, G. von Gersdorff and M. Quiros, *JHEP* **1105** (2011) 083 [arXiv:1103.1388 [hep-ph]].
- [121] J. A. Cabrer, G. von Gersdorff and M. Quiros, *Phys. Rev. D* **84**, 035024 (2011) [arXiv:1104.3149 [hep-ph]].
- [122] J. A. Cabrer, G. von Gersdorff and M. Quiros, *JHEP* **1201** (2012) 033 [arXiv:1110.3324 [hep-ph]].
- [123] R. Barbieri and A. Strumia, hep-ph/0007265.
- [124] C. Csaki, C. Grojean, H. Murayama, L. Pilo and J. Terning, *Phys. Rev. D* **69** (2004) 055006 [hep-ph/0305237].
- [125] C. Csaki, C. Grojean, L. Pilo and J. Terning, *Phys. Rev. Lett.* **92** (2004) 101802 [hep-ph/0308038];
- [126] C. Csaki, C. Grojean, J. Hubisz, Y. Shirman and J. Terning, *Phys. Rev. D* **70** (2004) 015012 [hep-ph/0310355];
- [127] G. Cacciapaglia, C. Csaki, C. Grojean and J. Terning, *Phys. Rev. D* **70** (2004) 075014 [hep-ph/0401160].
- [128] M. Papucci, “NDA and perturbativity in Higgsless models,” hep-ph/0408058.
- [129] G. Cacciapaglia, C. Csaki, C. Grojean and J. Terning, *Phys. Rev. D* **71** (2005) 035015 [hep-ph/0409126];
- [130] G. Cacciapaglia, C. Csaki, C. Grojean, M. Reece and J. Terning, *Phys. Rev. D* **72** (2005) 095018 [hep-ph/0505001].
- [131] G. Cacciapaglia, C. Csaki, G. Marandella and J. Terning, *Phys. Rev. D* **75** (2007) 015003 [hep-ph/0607146];
- [132] C. Csaki and D. Curtin, *Phys. Rev. D* **80** (2009) 015027 [arXiv:0904.2137 [hep-ph]].
- [133] G. von Gersdorff, N. Irges and M. Quiros, *Nucl. Phys. B* **635** (2002) 127 [hep-th/0204223].
G. von Gersdorff, N. Irges and M. Quiros, *Phys. Lett. B* **551** (2003) 351 [hep-ph/0210134].
C. Biggio and M. Quiros, *Nucl. Phys. B* **703** (2004) 199 [hep-ph/0407348].
- [134] R. Contino, Y. Nomura and A. Pomarol, *Nucl. Phys. B* **671** (2003) 148 [hep-ph/0306259];
- [135] K. Agashe, R. Contino and A. Pomarol, *Nucl. Phys. B* **719** (2005) 165 [hep-ph/0412089].
- [136] A. Falkowski, *Phys. Rev. D* **75** (2007) 025017 [hep-ph/0610336].
- [137] A. D. Medina, N. R. Shah and C. E. M. Wagner, *Phys. Rev. D* **76** (2007) 095010 [arXiv:0706.1281 [hep-ph]].
- [138] J. M. Maldacena, *Adv. Theor. Math. Phys.* **2** (1998) 231 [Int. J. Theor. Phys. **38** (1999) 1113] [hep-th/9711200]; S. S. Gubser, I. R. Klebanov and A. M. Polyakov, *Phys. Lett. B* **428** (1998) 105 [hep-th/9802109]; E. Witten, *Adv. Theor. Math. Phys.* **2** (1998) 253 [hep-th/9802150].
- [139] W. D. Goldberger and M. B. Wise, *Phys. Rev. Lett.* **83** (1999) 4922 [hep-ph/9907447].

-
- [140] O. DeWolfe, D. Z. Freedman, S. S. Gubser and A. Karch, Phys. Rev. D **62** (2000) 046008 [hep-th/9909134].
- [141] C. Csaki, M. L. Graesser and G. D. Kribs, Phys. Rev. D **63** (2001) 065002 [hep-th/0008151].
- [142] W. D. Goldberger and M. B. Wise, Phys. Lett. B **475** (2000) 275 [hep-ph/9911457].
- [143] G. F. Giudice, R. Rattazzi and J. D. Wells, Nucl. Phys. B **595** (2001) 250 [hep-ph/0002178].
- [144] T. G. Rizzo, JHEP **0206** (2002) 056 [hep-ph/0205242].
- [145] C. Csaki, J. Hubisz and S. J. Lee, Phys. Rev. D **76** (2007) 125015 [arXiv:0705.3844 [hep-ph]].
- [146] M. Toharia, Phys. Rev. D **79** (2009) 015009 [arXiv:0809.5245 [hep-ph]].
- [147] A. Azatov, M. Toharia and L. Zhu, Phys. Rev. D **80** (2009) 031701 [arXiv:0812.2489 [hep-ph]].
- [148] H. Davoudiasl, B. Lillie and T. G. Rizzo, JHEP **0608** (2006) 042 [hep-ph/0508279].
- [149] G. Cacciapaglia, C. Csaki, G. Marandella and J. Terning, JHEP **0702** (2007) 036 [hep-ph/0611358].
- [150] S. J. Huber, C. -A. Lee, Q. Shafi, Phys. Lett. **B531** (2002) 112-118. [hep-ph/0111465].
- [151] M. S. Carena, E. Pontón, J. Santiago and C. E. M. Wagner, Nucl. Phys. B **759** (2006) 202 [arXiv:hep-ph/0607106];
- [152] C. Delaunay, O. Gedalia, S. J. Lee, G. Perez, E. Pontón, Phys. Rev. **D83**, 115003 (2011). [arXiv:1007.0243 [hep-ph]]; C. Delaunay, O. Gedalia, S. J. Lee, G. Perez and E. Pontón, arXiv:1101.2902 [hep-ph].
- [153] A. Falkowski and M. Perez-Victoria, JHEP **0812** (2008) 107 [arXiv:0806.1737 [hep-ph]]; JHEP **0912** (2009) 061 [arXiv:0901.3777 [hep-ph]].
- [154] B. Batell, T. Gherghetta and D. Sword, Phys. Rev. D **78** (2008) 116011 [arXiv:0808.3977 [hep-ph]].
- [155] S. Mert Aybat and J. Santiago, Phys. Rev. D **80** (2009) 035005 [arXiv:0905.3032 [hep-ph]]; AIP Conf. Proc. **1200** (2010) 611 [arXiv:0909.3999 [hep-ph]].
- [156] T. Gherghetta and D. Sword, Phys. Rev. D **80** (2009) 065015 [arXiv:0907.3523 [hep-ph]]; A. Delgado and D. Diego, Phys. Rev. D **80** (2009) 024030 [arXiv:0905.1095 [hep-ph]]; M. Atkins and S. J. Huber, Phys. Rev. D **82** (2010) 056007 [arXiv:1002.5044 [hep-ph]].
- [157] K. Agashe, A. Azatov, L. Zhu, Phys. Rev. **D79**, 056006 (2009). [arXiv:0810.1016 [hep-ph]].
- [158] Z. Chacko, M. A. Luty and E. Pontón, JHEP **0007**, 036 (2000) [arXiv:hep-ph/9909248].
- [159] H. Davoudiasl, S. Gopalakrishna, E. Pontón, J. Santiago, New J. Phys. **12** (2010) 075011. [arXiv:0908.1968 [hep-ph]].
- [160] H. Davoudiasl, G. Perez, A. Soni, Phys. Lett. **B665** (2008) 67-71. [arXiv:0802.0203 [hep-ph]].
- [161] P. L. Cho, M. Misiak, Phys. Rev. **D49**, 5894-5903 (1994). [hep-ph/9310332]; K. Fujikawa, A. Yamada, Phys. Rev. **D49**, 5890-5893 (1994); G. Burdman, M. C. Gonzalez-Garcia, S. F. Novaes, Phys. Rev. **D61**, 114016 (2000). [hep-ph/9906329].

- [162] R. Contino and G. Servant, JHEP **0806** (2008) 026 [arXiv:0801.1679 [hep-ph]]; J. A. Aguilar-Saavedra, JHEP **0911** (2009) 030 [arXiv:0907.3155 [hep-ph]]; J. Mrazek and A. Wulzer, Phys. Rev. D **81** (2010) 075006 [arXiv:0909.3977 [hep-ph]]; G. Dissertori, E. Furlan, F. Moortgat, P. Nef, JHEP **1009** (2010) 019. [arXiv:1005.4414 [hep-ph]]; A. Atre, G. Azuelos, M. Carena, T. Han, E. Ozcan, J. Santiago, G. Unel, [arXiv:1102.1987 [hep-ph]].
- [163] K. Agashe, A. Belyaev, T. Krupovnickas, G. Perez and J. Virzi, Phys. Rev. D **77**, 015003 (2008) [arXiv:hep-ph/0612015]; B. Lillie, L. Randall and L. T. Wang, JHEP **0709**, 074 (2007) [arXiv:hep-ph/0701166]; B. Lillie, J. Shu and T. M. P. Tait, Phys. Rev. D **76**, 115016 (2007) [arXiv:0706.3960 [hep-ph]]. B. Lillie, L. Randall and L. T. Wang, JHEP **0709** (2007) 074 [arXiv:hep-ph/0701166]; A. Djouadi, G. Moreau, R. K. Singh, Nucl. Phys. **B797**, 1-26 (2008). [arXiv:0706.4191 [hep-ph]].
- [164] J. Alwall *et al.*, JHEP **0709** (2007) 028 [arXiv:0706.2334 [hep-ph]].
- [165] T. Sjostrand, S. Mrenna and P. Z. Skands, JHEP **0605** (2006) 026 [arXiv:hep-ph/0603175].
- [166] PGS4 <http://www.physics.ucdavis.edu/~conway/research/software/pgs/pgs4-general.htm>
- [167] C. F. Kolda and H. Murayama, JHEP **0007** (2000) 035 [hep-ph/0003170].
- [168] G. von Gersdorff, N. Irges and M. Quiros, arXiv:hep-ph/0206029.
- [169] D. A. Dicus and H. -J. He, Phys. Rev. D **71** (2005) 093009 [hep-ph/0409131].
- [170] D. B. Kaplan and H. Georgi, Phys. Lett. B **136** (1984) 183; D. B. Kaplan, H. Georgi and S. Dimopoulos, Phys. Lett. B **136** (1984) 187. S. Dimopoulos and J. Preskill, Nucl. Phys. B **199** (1982) 206.
- [171] V. M. Abazov *et al.* [D0 Collaboration], Phys. Rev. Lett. **100** (2008) 142002 [arXiv:0712.0851 [hep-ex]].
- [172] T. Aaltonen *et al.* [CDF Collaboration], Phys. Rev. Lett. **101** (2008) 202001 [arXiv:0806.2472 [hep-ex]].
- [173] T. Aaltonen *et al.* [CDF Collaboration], Phys. Rev. D **83** (2011) 112003 [arXiv:1101.0034 [hep-ex]].
- [174] T. Aaltonen *et al.* [CDF Collaboration], CDF Note 10807.
- [175] J. M. Campbell and R. K. Ellis, Phys. Rev. D **60** (1999) 113006 [hep-ph/9905386].
- [176] S. Frixione, P. Nason and C. Oleari, JHEP **0711** (2007) 070 [arXiv:0709.2092 [hep-ph]].
- [177] S. Matsuzaki, R. S. Chivukula, E. H. Simmons, M. Tanabashi, Phys. Rev. **D75**, 073002 (2007). [hep-ph/0607191]; R. S. Chivukula, E. H. Simmons, S. Matsuzaki, M. Tanabashi, Phys. Rev. **D75**, 075012 (2007). [hep-ph/0702218 [HEP-PH]]; S. Dawson, C. B. Jackson, Phys. Rev. **D76**, 015014 (2007). [hep-ph/0703299 [HEP-PH]]; Phys. Rev. **D79**, 013006 (2009). [arXiv:0810.5068 [hep-ph]]; T. Abe, R. S. Chivukula, N. D. Christensen, K. Hsieh, S. Matsuzaki, E. H. Simmons, M. Tanabashi, Phys. Rev. **D79**, 075016 (2009).
- [178] D. Choudhury, T. M. P. Tait, C. E. M. Wagner, Phys. Rev. **D65** (2002) 053002. [hep-ph/0109097]. [arXiv:0902.3910 [hep-ph]].
- [179] T. Aaltonen *et al.* [CDF Collaboration], [arXiv:1101.0034 [hep-ex]].

-
- [180] P. H. Frampton, S. L. Glashow, Phys. Lett. **B190** (1987) 157; L. M. Sehgal, M. Wanninger, Phys. Lett. **B200** (1988) 211; D. Choudhury, R. M. Godbole, R. K. Singh, K. Wagh, Phys. Lett. **B657** (2007) 69-76. [arXiv:0705.1499 [hep-ph]]; O. Antunano, J. H. Kuhn, G. Rodrigo, Phys. Rev. **D77** (2008) 014003. [arXiv:0709.1652 [hep-ph]]; A. Djouadi, G. Moreau, F. Richard, R. K. Singh, Phys. Rev. **D82** (2010) 071702. [arXiv:0906.0604 [hep-ph]]; P. Ferrario, G. Rodrigo, Phys. Rev. **D80** (2009) 051701. [arXiv:0906.5541 [hep-ph]]; P. H. Frampton, J. Shu, K. Wang, Phys. Lett. **B683**, 294-297 (2010). [arXiv:0911.2955 [hep-ph]]; Q. -H. Cao, D. McKeen, J. L. Rosner, G. Shaughnessy, C. E. M. Wagner, Phys. Rev. **D81** (2010) 114004. [arXiv:1003.3461 [hep-ph]]; D. Choudhury, R. M. Godbole, S. D. Rindani, P. Saha, [arXiv:1012.4750 [hep-ph]]; Y. Bai, J. L. Hewett, J. Kaplan, T. G. Rizzo, JHEP **1103** (2011) 003. [arXiv:1101.5203 [hep-ph]]; M. I. Gresham, I. -W. Kim, K. M. Zurek, [arXiv:1103.3501 [hep-ph]]; J. L. Hewett, J. Shelton, M. Spannowsky, T. M. P. Tait, M. Takeuchi, [arXiv:1103.4618 [hep-ph]]; U. Haisch and S. Westhoff, arXiv:1106.0529 [hep-ph].
- [181] A. Djouadi, G. Moreau and F. Richard, arXiv:1105.3158 [hep-ph].
- [182] S. Ovyn, X. Rouby, V. Lemaitre, [arXiv:0903.2225 [hep-ph]].
- [183] T. Aaltonen *et al.* [CDF Collaboration], Phys. Rev. D **77** (2008) 051102 [arXiv:0710.5335 [hep-ex]].
- [184] CMS Collaboration, note CMS PAS TOP-10-007; ATLAS Collaboration, note ATLAS-CONF-2011-087; note ATLAS-CONF-2011-123.
- [185] CMS Collaboration, note CMS PAS EXO-11-050; CMS PAS EXO-11-051; CMS PAS EXO-11-054.
- [186] CMS Collaboration, note CMS PAS EXO-11-005.
- [187] G. Aad *et al.* [ATLAS Collaboration], [arXiv:1108.5064 [hep-ex]].
- [188] ATLAS Collaboration, note CERN-PH-EP-2011-133.
- [189] ATLAS Collaboration, note ATLAS-CONF-2011-097.
- [190] R. Contino, T. Kramer, M. Son and R. Sundrum, JHEP **0705** (2007) 074 [hep-ph/0612180].
- [191] C. Bini, R. Contino and N. Vignaroli, JHEP **1201** (2012) 157 [arXiv:1110.6058 [hep-ph]].
- [192] O. Matsedonskyi, G. Panico and A. Wulzer, arXiv:1204.6333 [hep-ph].
- [193] M. Redi and A. Tesi, arXiv:1205.0232 [hep-ph].
- [194] W. Skiba and D. Tucker-Smith, Phys. Rev. D **75** (2007) 115010 [hep-ph/0701247].
- [195] B. Holdom, JHEP **0703** (2007) 063 [hep-ph/0702037 [HEP-PH]].
- [196] B. Holdom, JHEP **0708** (2007) 069 [arXiv:0705.1736 [hep-ph]].
- [197] G. F. Giudice, C. Grojean, A. Pomarol and R. Rattazzi, JHEP **0706** (2007) 045 [arXiv:hep-ph/0703164]; R. Barbieri, B. Bellazzini, V. S. Rychkov and A. Varagnolo, Phys. Rev. D **76** (2007) 115008 [arXiv:0706.0432 [hep-ph]]; B. Bellazzini, S. Pokorski, V. S. Rychkov and A. Varagnolo, JHEP **0811** (2008) 027 [arXiv:0805.2107 [hep-ph]]; P. Lodone, JHEP **0812** (2008) 029 [arXiv:0806.1472 [hep-ph]]; A. Pomarol and J. Serra, Phys. Rev. D **78** (2008) 074026 [arXiv:0806.3247 [hep-ph]]; M. Gillioz, arXiv:0806.3450 [hep-ph]; C. Anastasiou, E. Furlan and J. Santiago, arXiv:0901.2117 [hep-ph]; B. Gripaios, A. Pomarol, F. Riva and J. Serra, JHEP **0904** (2009) 070 [arXiv:0902.1483 [hep-ph]]. J. R. Espinosa, C. Grojean and M. Muhlleitner,

- JHEP **1005** (2010) 065 [arXiv:1003.3251 [hep-ph]]. N. Vignaroli, Nuovo Cim. C **34** (2011) 6 [arXiv:1107.4558 [hep-ph]]. A. Azatov and J. Galloway, Phys. Rev. D **85** (2012) 055013 [arXiv:1110.5646 [hep-ph]]. J. R. Espinosa, C. Grojean and M. Muhlleitner, arXiv:1202.1286 [hep-ph]. N. Vignaroli, arXiv:1204.0468 [hep-ph].
- [198] G. Panico, E. Ponton, J. Santiago and M. Serone, Phys. Rev. D **77** (2008) 115012 [arXiv:0801.1645 [hep-ph]].
- [199] S. J. Huber and Q. Shafi, Phys. Lett. B **583** (2004) 293 [arXiv:hep-ph/0309252].
- [200] N. Arkani-Hamed and M. Schmaltz, Phys. Rev. D **61** (2000) 033005 [arXiv:hep-ph/9903417].
- [201] E. Ma and G. Rajasekaran, Phys. Rev. D **64**, 113012 (2001) [arXiv:hep-ph/0106291]; K. S. Babu, E. Ma and J. W. F. Valle, Phys. Lett. B **552**, 207 (2003) [arXiv:hep-ph/0206292]; M. Hirsch, J. C. Romao, S. Skadhauge, J. W. F. Valle and A. Villanova del Moral, Phys. Rev. D **69**, 093006 (2004) [arXiv:hep-ph/0312265]; E. Ma, Phys. Rev. D **70**, 031901 (2004) [arXiv:hep-ph/0404199]; S. L. Chen, M. Frigerio and E. Ma, Nucl. Phys. B **724**, 423 (2005) [arXiv:hep-ph/0504181]; E. Ma, Phys. Rev. D **73**, 057304 (2006) [arXiv:hep-ph/0511133]; G. Altarelli and F. Feruglio, Nucl. Phys. B **741**, 215 (2006) [arXiv:hep-ph/0512103]; I. de Medeiros Varzielas, S. F. King and G. G. Ross, Phys. Lett. B **644**, 153 (2007) [arXiv:hep-ph/0512313]; X. G. F. He, Y. Y. F. Keum and R. R. Volkas, JHEP **0604**, 039 (2006) [arXiv:hep-ph/0601001]; B. Adhikary, B. Brahmachari, A. Ghosal, E. Ma and M. K. Parida, Phys. Lett. B **638**, 345 (2006) [arXiv:hep-ph/0603059]; L. Lavoura and H. Kuhbock, Mod. Phys. Lett. A **22**, 181 (2007) [arXiv:hep-ph/0610050]; S. F. King and M. Malinsky, Phys. Lett. B **645**, 351 (2007) [arXiv:hep-ph/0610250]; S. Morisi, M. Picariello and E. Torrente-Lujan, Phys. Rev. D **75**, 075015 (2007) [arXiv:hep-ph/0702034]; F. Yin, Phys. Rev. D **75**, 073010 (2007) [arXiv:0704.3827 [hep-ph]]; F. Bazzocchi, S. Kaneko and S. Morisi, JHEP **0803**, 063 (2008) [arXiv:0707.3032 [hep-ph]]; W. Grimus and H. Kuhbock, Phys. Rev. D **77**, 055008 (2008) [arXiv:0710.1585 [hep-ph]]; F. Bazzocchi, S. Morisi and M. Picariello, Phys. Lett. B **659**, 628 (2008) [arXiv:0710.2928 [hep-ph]]; M. Honda and M. Tanimoto, Prog. Theor. Phys. **119**, 583 (2008) [arXiv:0801.0181 [hep-ph]]; B. Brahmachari, S. Choubey and M. Mitra, Phys. Rev. D **77**, 073008 (2008) [Erratum-ibid. D **77**, 119901 (2008)] [arXiv:0801.3554 [hep-ph]]; G. Altarelli, F. Feruglio and C. Hagedorn, JHEP **0803**, 052 (2008) [arXiv:0802.0090 [hep-ph]]; F. Bazzocchi, S. Morisi, M. Picariello and E. Torrente-Lujan, J. Phys. G **36**, 015002 (2009) [arXiv:0802.1693 [hep-ph]]; B. Adhikary and A. Ghosal, Phys. Rev. D **78**, 073007 (2008) [arXiv:0803.3582 [hep-ph]]; Y. Lin, Nucl. Phys. B **813**, 91 (2009) [arXiv:0804.2867 [hep-ph]]; F. Bazzocchi, M. Frigerio and S. Morisi, Phys. Rev. D **78**, 116018 (2008) [arXiv:0809.3573 [hep-ph]]; S. Morisi, Phys. Rev. D **79**, 033008 (2009) [arXiv:0901.1080 [hep-ph]]; P. Ciafaloni, M. Picariello, E. Torrente-Lujan and A. Urbano, Phys. Rev. D **79**, 116010 (2009) [arXiv:0901.2236 [hep-ph]]; M. C. Chen and S. F. King, JHEP **0906**, 072 (2009) [arXiv:0903.0125 [hep-ph]]; G. C. Branco, R. Gonzalez Felipe, M. N. Rebelo and H. Serodio, Phys. Rev. D **79**, 093008 (2009) [arXiv:0904.3076 [hep-ph]]; A. Hayakawa, H. Ishimori, Y. Shimizu and M. Tanimoto, Phys. Lett. B **680**, 334 (2009) [arXiv:0904.3820 [hep-ph]]; G. Altarelli and D. Meloni, J. Phys. G **36**, 085005 (2009) [arXiv:0905.0620 [hep-ph]]; Y. Lin, Nucl. Phys. B **824**, 95 (2010) [arXiv:0905.3534 [hep-ph]]; C. Hagedorn, E. Molinaro and S. T. Petcov, JHEP **0909**, 115 (2009) [arXiv:0908.0240 [hep-ph]]; E. Ma, arXiv:0908.3165 [hep-ph]; T. J. Burrows and S. F. King, arXiv:0909.1433 [hep-ph]; A. Albaid, Phys. Rev. D **80**, 093002 (2009) [arXiv:0909.1762 [hep-ph]]; P. Ciafaloni, M. Picariello, E. Torrente-Lujan and A. Urbano, arXiv:0909.2553 [hep-ph]; F. Feruglio, C. Hagedorn and L. Merlo, arXiv:0910.4058; S. Morisi and E. Peinado, arXiv:0910.4389; J. Berger and Y. Grossman, arXiv:0910.4392 [hep-ph].
- [202] F. Feruglio, C. Hagedorn, Y. Lin and L. Merlo, Nucl. Phys. B **809**, 218 (2009) [arXiv:0807.3160 [hep-ph]]. C. Hagedorn, E. Molinaro and S. T. Petcov, arXiv:0911.3605;

- F. Feruglio, C. Hagedorn, Y. Lin and L. Merlo, arXiv:0911.3874; G. J. Ding and J. F. Liu, arXiv:0911.4799.
- [203] P. F. Harrison, D. H. Perkins and W. G. Scott, Phys. Lett. B **530**, 167 (2002) [arXiv:hep-ph/0202074].
- [204] F. Feruglio, C. Hagedorn, Y. Lin and L. Merlo, Nucl. Phys. B **775**, 120 (2007) [arXiv:hep-ph/0702194].
- [205] I. de Medeiros Varzielas and G. G. Ross, Nucl. Phys. B **733**, 31 (2006) [arXiv:hep-ph/0507176]; I. de Medeiros Varzielas, S. F. King and G. G. Ross, Phys. Lett. B **648**, 201 (2007) [arXiv:hep-ph/0607045].
- [206] R. Contino, L. Da Rold and A. Pomarol, Phys. Rev. D **75** (2007) 055014 [arXiv:hep-ph/0612048].
- [207] J. Santiago, JHEP **0812**, 046 (2008) [arXiv:0806.1230 [hep-ph]].
- [208] F. del Aguila and J. Santiago, Phys. Lett. B **493**, 175 (2000) [arXiv:hep-ph/0008143]; arXiv:hep-ph/0011143.
- [209] H. Georgi, A. K. Grant and G. Hailu, Phys. Lett. B **506**, 207 (2001) [arXiv:hep-ph/0012379]; M. S. Carena, T. M. P. Tait and C. E. M. Wagner, Acta Phys. Polon. B **33**, 2355 (2002) [arXiv:hep-ph/0207056].
- [210] H. Davoudiasl, J. L. Hewett and T. G. Rizzo, Phys. Rev. D **68**, 045002 (2003) [arXiv:hep-ph/0212279]; M. S. Carena, E. Ponton, T. M. P. Tait and C. E. M. Wagner, Phys. Rev. D **67**, 096006 (2003) [arXiv:hep-ph/0212307]; F. del Aguila, M. Perez-Victoria and J. Santiago, JHEP **0302**, 051 (2003) [arXiv:hep-th/0302023]; Acta Phys. Polon. B **34**, 5511 (2003) [arXiv:hep-ph/0310353]; JHEP **0610**, 056 (2006) [arXiv:hep-ph/0601222]; M. S. Carena, A. Delgado, E. Ponton, T. M. P. Tait and C. E. M. Wagner, Phys. Rev. D **68**, 035010 (2003) [arXiv:hep-ph/0305188]; Phys. Rev. D **71**, 015010 (2005) [arXiv:hep-ph/0410344].
- [211] D. Tommasini, G. Barenboim, J. Bernabeu and C. Jarlskog, Nucl. Phys. B **444**, 451 (1995) [arXiv:hep-ph/9503228]; J. I. Illana and T. Riemann, Phys. Rev. D **63**, 053004 (2001) [arXiv:hep-ph/0010193].
- [212] T. Appelquist and J. Carazzone, Phys. Rev. D **11**, 2856 (1975).
- [213] F. del Aguila, J. de Blas and M. Perez-Victoria, Phys. Rev. D **78**, 013010 (2008) [arXiv:0803.4008 [hep-ph]]; F. del Aguila, J. A. Aguilar-Saavedra and J. de Blas, Acta Phys. Polon. B **40**, 2901 (2009) [arXiv:0910.2720 [hep-ph]].
- [214] K. Agashe and R. Contino, Phys. Rev. D **80**, 075016 (2009) [arXiv:0906.1542 [hep-ph]]; A. Azatov, M. Toharia and L. Zhu, Phys. Rev. D **80**, 035016 (2009) [arXiv:0906.1990 [hep-ph]].
- [215] Y. Kuno and Y. Okada, Rev. Mod. Phys. **73** (2001) 151 [arXiv:hep-ph/9909265].
- [216] C. Amsler *et al.* [Particle Data Group], Phys. Lett. B **667**, 1 (2008).
- [217] F. del Aguila and M. J. Bowick, Phys. Lett. B **119**, 144 (1982).
- [218] M. Blanke, A. J. Buras, B. Duling, A. Poschenrieder and C. Tarantino, JHEP **0705**, 013 (2007) [arXiv:hep-ph/0702136]; T. Goto, Y. Okada and Y. Yamamoto, Phys. Lett. B **670**, 378 (2009) [arXiv:0809.4753 [hep-ph]]; F. del Aguila, J. I. Illana and M. D. Jenkins, JHEP **0901**, 080 (2009) [arXiv:0811.2891 [hep-ph]].

- [219] F. del Aguila and M. J. Bowick, Nucl. Phys. B **224**, 107 (1983); F. del Aguila, M. Perez-Victoria and J. Santiago, JHEP **0009**, 011 (2000) [arXiv:hep-ph/0007316];
- [220] F. Del Aguila and J. Santiago, JHEP **0203**, 010 (2002) [arXiv:hep-ph/0111047]; K. Agashe and G. Servant, JCAP **0502**, 002 (2005) [arXiv:hep-ph/0411254].
- [221] F. del Aguila, J. A. Aguilar-Saavedra and R. Pittau, JHEP **0710**, 047 (2007) [arXiv:hep-ph/0703261]; F. del Aguila and J. A. Aguilar-Saavedra, Nucl. Phys. B **813**, 22 (2009) [arXiv:0808.2468 [hep-ph]].
- [222] F. del Aguila, L. Ametller, G. L. Kane and J. Vidal, Nucl. Phys. B **334**, 1 (1990); J. A. Aguilar-Saavedra, Nucl. Phys. B **828**, 289 (2010) [arXiv:0905.2221 [hep-ph]].
- [223] K. Agashe, G. Perez and A. Soni, Phys. Rev. D **71**, 016002 (2005) [arXiv:hep-ph/0408134]; G. Moreau and J. I. Silva-Marcos, JHEP **0603**, 090 (2006) [arXiv:hep-ph/0602155]; S. Casagrande, F. Goertz, U. Haisch, M. Neubert and T. Pfoh, JHEP **0810**, 094 (2008) [arXiv:0807.4937 [hep-ph]]; M. Blanke, A. J. Buras, B. Duling, S. Gori and A. Weiler, JHEP **0903**, 001 (2009) [arXiv:0809.1073 [hep-ph]]; K. Agashe, A. Azatov and L. Zhu, Phys. Rev. D **79**, 056006 (2009) [arXiv:0810.1016 [hep-ph]]; M. E. Albrecht, M. Blanke, A. J. Buras, B. Duling and K. Gemmler, JHEP **0909**, 064 (2009) [arXiv:0903.2415 [hep-ph]]; M. Bauer, S. Casagrande, U. Haisch and M. Neubert, arXiv:0912.1625 [hep-ph].
- [224] G. Cacciapaglia, C. Csaki, J. Galloway, G. Marandella, J. Terning and A. Weiler, JHEP **0804** (2008) 006 [arXiv:0709.1714 [hep-ph]]; A. L. Fitzpatrick, G. Perez and L. Randall, arXiv:0710.1869 [hep-ph]; C. Cheung, A. L. Fitzpatrick and L. Randall, JHEP **0801** (2008) 069 [arXiv:0711.4421 [hep-th]]; M. C. Chen and H. B. Yu, arXiv:0804.2503 [hep-ph]; C. Csaki, A. Falkowski and A. Weiler, Phys. Rev. D **80**, 016001 (2009) [arXiv:0806.3757 [hep-ph]]; C. Csaki, G. Perez, Z. Surujon and A. Weiler, arXiv:0907.0474 [hep-ph].
- [225] M. Carena, A. D. Medina, B. Panes, N. R. Shah and C. E. M. Wagner, Phys. Rev. D **77**, 076003 (2008) [arXiv:0712.0095 [hep-ph]]; R. Contino and G. Servant, JHEP **0806**, 026 (2008) [arXiv:0801.1679 [hep-ph]]; J. A. Aguilar-Saavedra, arXiv:0907.3155 [hep-ph]; J. Mrazek and A. Wulzer, arXiv:0909.3977 [hep-ph].
- [226] K. Agashe, K. Blum, S. J. Lee and G. Perez, arXiv:0912.3070 [hep-ph].
- [227] G. Burdman, L. Da Rold and R. D. Matheus, arXiv:0912.5219 [hep-ph].
- [228] P. Sikivie, L. Susskind, M. B. Voloshin and V. I. Zakharov, Nucl. Phys. B **173** (1980) 189.
- [229] D. B. Kaplan, Nucl. Phys. B **365** (1991) 259.
- [230] M. E. Albrecht, M. Blanke, A. J. Buras, B. Duling and K. Gemmler, JHEP **0909** (2009) 064 [arXiv:0903.2415 [hep-ph]].
- [231] M. L. Mangano, M. Moretti, F. Piccinini, R. Pittau and A. D. Polosa, JHEP **0307** (2003) 001 [arXiv:hep-ph/0206293].
- [232] N. Davidson, G. Nanava, T. Przedzinski, E. Richter-Was and Z. Was, arXiv:1002.0543 [hep-ph].
- [233] D. L. Rainwater, D. Zeppenfeld and K. Hagiwara, Phys. Rev. D **59** (1999) 014037 [arXiv:hep-ph/9808468]; T. Plehn, D. L. Rainwater and D. Zeppenfeld, Phys. Rev. D **61** (2000) 093005 [arXiv:hep-ph/9911385].
- [234] G. L. Bayatian *et al.* [CMS Collaboration], J. Phys. G **34** (2007) 995.

- [235] G. L. Fogli, E. Lisi, A. Marrone, D. Montanino, A. Palazzo and A. M. Rotunno, arXiv:1205.5254 [hep-ph].
- [236] C. Hagedorn and M. Serone, JHEP **1202** (2012) 077 [arXiv:1110.4612 [hep-ph]].
- [237] G. -J. Ding, Nucl. Phys. B **862** (2012) 1 [arXiv:1201.3279 [hep-ph]].
- [238] S. Dev, R. R. Gautam and L. Singh, Phys. Lett. B **708** (2012) 284 [arXiv:1201.3755 [hep-ph]].
- [239] P. S. Bhupal Dev, B. Dutta, R. N. Mohapatra and M. Severson, arXiv:1202.4012 [hep-ph].
- [240] H. -J. He and X. -J. Xu, arXiv:1203.2908 [hep-ph].
- [241] D. Meloni, arXiv:1203.3126 [hep-ph].
- [242] Y. H. Ahn and S. K. Kang, arXiv:1203.4185 [hep-ph].
- [243] I. d. M. Varzielas and G. G. Ross, arXiv:1203.6636 [hep-ph].
- [244] C. Hagedorn and D. Meloni, arXiv:1204.0715 [hep-ph].
- [245] G. Altarelli, F. Feruglio, L. Merlo and E. Stamou, arXiv:1205.4670 [hep-ph].
- [246] G. Altarelli, F. Feruglio and L. Merlo, arXiv:1205.5133 [hep-ph].